FROM FOREST FLOORS TO PHARMACOLOGY: ELUCIDATING MILLIPEDE DEFENSIVE ALKALOIDS FOR DRUG DISCOVERY

Paige Banks

Dissertation submitted to the faculty of the Virginia Polytechnic Institute and State University in partial fulfillment of the requirements for the degree of

Doctor of Philosophy

In

Chemistry

Emily Mevers (Chair)

Kylie D. Allen

Emily C. Gentry

Andrew N. Lowell

February 17th, 2025

Blacksburg, VA

Keywords: Millipede defense, natural products, neuromodulators, terpenoid alkaloids

SCIENTIFIC ABSTRACT

Millipedes are some of the oldest animals on earth, evolving over 400 million years ago (mya). The subterclass, Colobognatha evolved 99 mya and are largely understudied compared to other classes of millipedes. Like most other millipede classes, Colobognatha possess repugnatorial glands, which store alkaloids as defensive compounds. However, they have also evolved unique characteristics that set them apart from all other millipedes, including distinct anatomy, group behavior, brood care, and the production of terpenoid alkaloids. Prior to 2020, only 11 alkaloids were known. Herein, a total of 25 new terpenoid alkaloids are reported coming from three different genera, all belonging to the same order. Key findings include the discovery of indolizine and quinolizidine alkaloids (e.g., hydrogosodesmine, homogosodesmine and homo-hydrogosodesmine) from the defensive secretions of various *Brachcybye* species (**Chapter 2**), the discovery of the ischnocybine alkaloids from the defensive secretions of *Ischnocybe plicata* (**Chapter 3**), and the discovery of the andrognathines and andrognathanols from the defensive secretions of *Andrognathus corticarius* (**Chapter 4**). The structure elucidation of each utilized modern techniques, including 2D NMR, HRMS, DFT, ECD, chemical synthesis, and Mosher's analysis. Many of these new alkaloids represent new natural product classes with carbon backbones that are unprecedented in the literature. Biological and ecological evaluation revealed the new alkaloids deter ants, a common predator to millipedes (**Chapter 3**), and this led to the discovery that a subset of the alkaloids potently binds to sigma-1 receptor (ischnocybine A: K_i 14 nM), while others bind to sigma-2 (homo-hydrogosodesmine hydrate: K_i 260 nM). Furthermore, ecology studies revealed that the alkaloid production is conserved over large geographical regions, accumulated as the millipedes gain segments and are actively secreted through the ozopores when physically agitated. These discoveries provide insights into a potential biosynthetic pathway

shared by all Platydesmida millipedes and support the hypothesis that alkaloid biosynthesis in this order is evolving toward greater simplicity.

GENERAL AUDIENCE ABSTRACT

Millipedes are some of the oldest animals and have been roaming Earth for over 400 million years. These small, soft-bodied creatures live beneath decaying debris on forest floors and defend themselves from predators using unique chemical secretions. This dissertation focuses on understanding the chemical composition of the defensive secretions of a remarkable group of millipedes, the Colobognatha, which are known for their unusual feeding habits and social behaviors. Through this research, a total of 25 new distinct compounds were discovered from defensive secretions of four different millipede species. A subset of these compounds was determined to bind to a neuroreceptor and therefore may be useful in the treatment of non-addictive pain, Parkinson's, and Alzheimer Disease. The summation of this work sheds light on the diversity of millipede defensive secretions and provides insights into how these intriguing compounds are made by the millipede, as well as how they have evolved over millennia. This work may potentially lead to new treatments to treat a variety of neurological diseases.

ACKNOWLEDGMENTS

Firstly, I would like to express gratitude to my advisor, Prof. Emily Mevers. It has been an absolute honor to work with you. Being your first graduate student has been a privilege, and together, we've navigated uncharted waters and grown tremendously. Having spent time both snorkeling for moon snail eggs and hiking coast to coast for millipedes, we have been through a lot together. This dissertation is as much yours as it is mine. Thank you for the countless hours, energy, and effort you've dedicated to teaching, mentoring, and guiding me into the scientist I am today.

I also thank the rest of my committee—Prof. Kylie Allen, Prof. Emily Gentry, and Prof. Andrew Lowell—for your guidance, encouragement, and feedback throughout my PhD journey. Your support has been instrumental in shaping both this work and my scientific growth.

A special acknowledgment to Prof. Tappey Jones for introducing our lab to the fascinating world of millipede defense compounds and trusting me to wrap up your final project. This dissertation would not have taken its unique shape without your contributions. Similarly, I am immensely grateful to Prof. Paul Marek for his expertise and generosity in teaching us how to find Colobognatha and for his assistance in paper preparations.

To the members of the Mevers lab—Benjamin Blackburn, Carla Menegatti, Karla Piedl, Lois Kyei, Arden Hatch, Rose Campbell, and Joe Barton—thank you for your camaraderie, feedback, and support throughout this journey. I am incredibly grateful to have shared this time with you. Your insights and encouragement have challenged me to grow as a scientist, and I am excited to see the amazing places your careers will take you.

To my undergraduate researchers—Caitlin Winner, Molly Simek, Erik Payne, Matty Zincone, and Amy Reuter—thank you for your hard work, curiosity, and patience as we navigated

research together. Caitlin, Molly, and Erik, you were the first to join me on this journey, and I am forever grateful for the learning experiences we shared. Amy, thank you for your dedication to the marine egg mass project. Matty, your passion, initiative, and enthusiasm have been integral to continuing our project. I am grateful for the opportunity to collaborate with each of you.

I owe immense gratitude to my wonderful wife, Lillian Banks. Your support over the past five years has been instrumental. From helping collect millipedes to providing me with the space and time to focus on my work, your patience and encouragement have been integral to my success. I truly could not have done this without you. In addition, I would like to acknowledge our dog, Millie Mae, she has been our constant. Whether lying quietly by my side during long writing sessions, her patience on hikes for collection, or providing much-needed breaks, she has been an unsung hero of this dissertation.

To my parents, thank you for always believing in me and encouraging me to pursue my dreams. Your support, even when faced with my science jargon, has meant the world to me. I appreciate your willingness to engage with my work, your confidence in my abilities, and willingness to collect millipedes.

Lastly, to my friends and family—many of whom are not in STEM—thank you for your encouragement and curiosity about my work, even when it seemed like gibberish. Your support and humor have kept me grounded over these years. A special thanks to those who joined me in millipede collecting—your willingness to flip countless logs, hike endless miles, and share in the adventure has been integral to this dissertation.

ATTRIBUTIONS

Chapter 2 is a reprint of a manuscript published in the *Journal of Chemical Ecology*. The manuscript has been modified for use in this dissertation with the following authors: Paige Banks, Emma M Funkhouser, Angie M Macias, Brian Lovett, Shelby Meador, Arden Hatch, H Martin Garraffo, Kaitie C Cartwright, Matt T Kasson, Paul E Marek, Tappey H Jones, Emily Mevers. All authors contributed to the study conception and design. The manuscript was written by Paige Banks, Emily Mevers and Tappey Jones. Angie Macias, Brian Lovett, and Paul Marek participated in the writing by commenting on various versions of the manuscript. The synthetic work described in the chapter was completed by Tappey Jones, Emma Funkhouser, Martin Garraffo and Kaitie Cartwright. Paige Banks and Emily Mevers completed the NMR, isolation and further characterization. Biological samples were collected by Angie Macias, Brian Lovett, Shelby Meador, Arden Hatch, Paul Marek and Matt Kasson.

Chapter 3 is a reprint of a manuscript published in the *Journal of Natural Products*. The manuscript has been modified for use in this dissertation, with the following authors: Carla Menegatti, Jared S. Wood, Paige Banks, Kenneth Knott, Jonathan S. Briganti, Anthony J. Briganti, Samuel V. G. McNally, Paul E. Marek, Anne M. Brown, Tappey H. Jones, R. Thomas Williamson and Emily Mevers. The manuscript was written by Emily Mevers and Carla Menegatti. Paige Banks, Paul Marek, Tappey Jones, Jared S. Wood, Thomas Williamson commented on various drafts of the manuscript. The initial isolation and characterization of the ischnocybines were completed by Carla Menegatti. Thomas Williamson and Jared S. Wood reacquired the NMR data, completed the DFT calculations, and confirmed the constitution of ischnocybines. Paige Banks performed the field work, completed the syntheses, much of the ecological studies, and completed the second isolation. Kenneth Knott assisted in DFT calculations. Jonathan Briganti, Anthony

Briganti and Anne Brown performed the molecular docking studies. Samuel McNally assisted in collection. Carla Menegatti, Jared S. Wood and Paige Banks all contributed equally as represented by being co-first authors.

Chapter 4 is a reprint of a manuscript submitted to *Journal of the American Chemical Society*. The manuscript has been modified for use in this dissertation, with the following authors: Paige Banks, Carla Menegatti, Lin Du, Kenneth Knott, Paul E Marek and Emily Mevers. Portions of discussion in the original publication have been moved to **Chapter 5**. The manuscript was written by Paige Banks and Emily Mevers and edited by all authors. Paige Banks performed the isolation and characterization of the compounds. Carla Menegatti assisted with millipede collection, and the syntheses of the andrognathanols. Lin Du and Kenneth Knott completed the DFT calculations. Paul Marek assisted in millipede collection and editing the manuscript.

TABLE OF CONTENTS

LIST OF FIGURES 5
LIST OF TABLES 6
LIST OF SCHEMES 7
LIST OF APPENDIX FIGURES 8
CHAPTER 1. EXPLORING NATURE'S CHEMISTS: MILLIPEDES, NATURAL PRODUCTS, AND THEIR ROLE IN DRUG DISCOVERY 20
1.1. INTRODUCTION 20
1.0.1. Contribution of Natural Products to Drug Discovery 20
1.0.2. Modern Sources of Natural Products 25
1.2. LEVERAGING MILLIPEDE SECRETIONS FOR THE DISCOVERY OF NEW NATURAL PRODUCTS 27
1.0.3. Millipede Evolution 27
1.0.4. Millipede Chemical Secretions 28
1.0.5. Colobognatha: The Alkaloid-Producing Subterclass 31
1.3. SUMMARY 34
1.4. RESEARCH OBJECTIVES 34
1.5. REFERENCES 37
CHAPTER 2. THE CHEMISTRY OF THE DEFENSIVE SECRETIONS OF THREE SPECIES OF MILLIPEDES IN THE GENUS *BRACHYCYBE* 48
2.0. ABSTRACT 48
2.1. INTRODUCTION 50
2.2. RESULTS 53
2.3. DISCUSSION 60
2.4. EXPERIMENTAL METHODS 62
2.4.1. General Experimental Procedures 62
2.4.2. Millipede Collections 63
2.4.3. General GCMS Method Used for All Analyses Described Below 64
2.4.4. GCMS Analysis of Collected Millipedes Crude Extracts 64
2.4.5. Chemical Derivatization of *Brachycybe petasata* and *B. producta* Crude Extracts 64
2.4.6. Synthesis of 2-(4-Methylpentyl)-quinolizidine (2.8) 65
2.4.7. Synthesis of Homogosodesmine (2.5) 66
2.4.8. Synthesis of 7-(4-Hydroxy-4-methylpentyl)-indolizidine (2.18) 67
2.4.9. Synthesis of 2-(4-Hydroxy-4-methylpentyl)-quinolizidine (2.19) 68

2.4.10. Extraction and Isolation of Homogosodesmine (2.5) and Homo-Hydrogosodesmine (2.6) from *B. producta* 69
2.5. ACKNOWLEDGEMENTS 69
2.6. REFERENCES 70
2.7. APPENDIX FIGURES 76
2.8. APPENDIX TABLES 108
CHAPTER 3. NEUROMODULATING ALKALOIDS FROM MILLIPEDE DEFENSIVE SECRETIONS 115
3.0. ABSTRACT 115
3.1. INTRODUCTION 117
3.2. RESULTS AND DISCUSSION 119
3.3. EXPERIMENTAL METHODS 132
3.3.1. General Experimental Procedures 132
3.3.2. Millipede Collections 132
3.3.3. Gas Chromatography Mass Spectrometry (GCMS) Analysis of Crude Mixture 133
3.3.4. Purification of Ischnocybine A-C and Ischnocybinone (3.1–3.4) 134
3.3.5. DFT & TD-DFT Results for All Configurations of Ischnocybine Compounds (3.1–3.4) 137
3.3.6. Prey Deterrent Assays 139
3.3.7. Relative Quantification of Ischnocybines (3.1–3.4) on Individual Millipedes 139
3.3.8. Mosher Esterification of Ischnocybine A Alcohol (3.6) 140
3.3.9. Chemical Derivatization of Ischnocybine C (3.4) and Electronic Circular Dichroism Analysis 140
3.3.10. Binding Assay for the Sigma-1 and -2 Receptors 141
3.3.11. Molecular Docking 142
3.4. DATA AVAILABILITY STATEMENT 143
3.5. ACKNOWLEDGEMENTS 143
3.6. REFERENCES 143
3.7. APPENDIX FIGURES 148
3.8. APPENDIX TABLES 177
CHAPTER 4. THE DISCOVERY OF COMPLEX HETEROCYCLES FROM MILLIPEDE SECRETIONS PROVIDES INSIGHTS INTO BIOSYNTHESIS AND EVOLUTION 199
4.0. ABSTRACT 199
4.1. INTRODUCTION 201

4.2. RESULTS AND DISCUSSION 203
4.2.1. CHEMICAL INVESTIGATIONS INTO DEFENSIVE SECRETIONS OF *ANDROGNATHUS CORTICARIUS* 203
4.2.2. COMPLETE STRUCTURAL ASSIGNMENT OF THE ANDROGNATHINES (4.1–4.6) 205
4.2.3. STRUCTURAL ASSIGNMENT OF THE ANDROGNATHANOLS (4.9–4.12) 209
4.2.4. MASS SPECTROMETRY-BASED STRUCTURE ELUCIDATION OF LOW ABUNDANT ANDROGNATHINES AND ANDROGNATHANOLS 212
4.2.5. ECOLOGICAL ROLE OF THE *A. CORTICARIUS* CHEMICAL SECRETIONS 213
4.2.6. BIOLOGICAL ACTIVITY OF THE ANDROGNATHINES AND ANDROGNATHANOLS 215
4.3. CONCLUSION 216
4.4. AUTHOR INFORMATION 217
4.5. FUNDING SOURCES 217
4.5.1. NOTES 217
4.6. ACKNOWLEDGMENTS 217
4.7. EXPERIMENTAL METHODS 218
4.7.1. GENERAL EXPERIMENTAL PROCEDURES 218
4.7.2. MILLIPEDE COLLECTIONS 218
4.7.3. EXTRACTION AND PURIFCATION OF THE ANDROGNATHINES AND ANDROGNATHANOLS FROM *A. CORTICARIUS* 219
4.7.4. HYDROGENATION AND HYDROLYSIS OF CRUDE MILLIPEDE EXTRACT. 228
4.7.5. ACETONIDE PROTECTION OF ANDROGNATHINE CORE (4.7) 228
4.7.6. ANDROGNATHINE BENZOATE (4.8) FOR ECD 229
4.7.7. GCMS ANALYSIS OF FATTY ACID COMPOSITION IN *A. CORTICARIUS* CRUDE EXTRACT 229
4.7.8. GCMS ANALYSIS OF FATTY ACID COMPOSITION IN ANDROGNATHANOL A (4.9) AND B (4.10) 230
4.7.9. DENSITY FUNCTIONAL THEORY (DFT) CALCULATION OF 1H AND 13C NMR 230
4.7.10. LCMS QUANTIFICATION OF ANDROGNATHANOLS AND ANDROGNATHINES 231
4.7.11. SIGMA-1 AND SIGMA-2 RECEPTOR ASSAY PROCEDURE FROM PSYCHOACTIVE DRUG SCREENING PROGRAM (PDSP) 232
4.8. REFERENCES 233
4.9. APPENDIX FIGURES 238
4.10. APPENDIX TABLES 269
CHAPTER 5. FUTURE PATHWAYS: INTEGRATING PHYLOGENETICS, BIOSYNTHESIS, AND ECOLOGY IN MILLIPEDE RESEARCH 284
5.1. INTRODUCTION 284

5.2. SUMMARY OF FINDINGS AND THEIR SIGNIFICANCE 285
5.2.1. OUR CURRENT UNDERSTANDING OF THE CHEMICAL DIVERSITY WITHIN COLOBOGNATHA DEFENSIVE SECRETIONS 285
5.2.2. INSIGHTS INTO THE BIOSYNTHETIC PATHWAY LEADING TO ALL PLATYDESMIDA TERPENOID ALKALOIDS 288
5.2.3. EVOLUTION OF TERPENOID ALKALOIDS BIOSYNTHETIC PATHWAY IN PLATYDESMIDA 292
5.2.4. ECOLOGICAL AND BIOMEDICAL IMPLICATIONS OF MILLIPEDE TERPENOID ALKALOIDS 295
5.3. FUTURE DIRECTIONS 297
5.3.1. ADVANCING MILLIPEDE PHYLOGENY THROUGH SEQUENCING 297
5.3.2. EXPANDING OUR UNDERSTANDING OF THE ECOLOGICAL ROLE OF THE MILLIPEDE ALKALOIDS 298
5.3.3. CONSERVATION IMPLICATIONS 299
5.4. CONCLUSION 299
5.5. REFERENCES 300

LIST OF FIGURES

FIGURE 1.1. CONTRIBUTIONS OF NATURAL PRODUCTS TO APPROVED SMALL MOLECULE DRUGS ... 22
FIGURE 1.2. IMPORTANT NATURAL PRODUCTS ... 23
FIGURE 1.3. NEW NATURAL PRODUCTS DISCOVERED PER YEAR COMPARED TO THEIR STRUCTURAL NOVELTY ... 25
FIGURE 1.4. TOXIC NATURAL PRODUCTS ISOLATED FROM SESSILE MARINE ORGANISMS ... 26
FIGURE 1.5. DEFENSIVE SECRETIONS BEING SECRETED FROM OZOPORE ... 29
FIGURE 1.6. MILLIPEDE DEFENSIVE SECRETION COMPOSITION AND PHYLOGENY ... 30
FIGURE 1.7. PICTURES OF COLOBOGNATHAN MILLIPEDES ... 32
FIGURE 1.8. ALKALOIDS PREVIOUSLY DESCRIBED FROM COLOBOGNATHA. ... 33
FIGURE 1.9. PLATYDESMIDA MILLIPEDE AND THEIR DEFENSE COMPOUNDS ... 36
FIGURE 2.1. GEOGRAPHIC DISTRIBUTION OF *BRACHYCYBE LECONTII* AND *B. ROSEA* ... 51
FIGURE 2.2. EXTRACTED ION CHROMATOGRAMS (EICS) OF THE UNREACTED *B. PRODUCTA* EXTRACT AND HYDROGENATION PRODUCT ... 56
FIGURE 3.3. MILLIPEDE PHYLOGENY ... 119
FIGURE 3.4. STRUCTURES OF NEW HETEROCYCLIC TERPENOID ALKALOIDS ... 121
FIGURE 3.5. KEY 2D NMR CORRELATIONS AND COUPLING CONSTANTS ... 124
FIGURE 3.6. STEREOCHEMISTRY OF ISCHNOCYBINE A AND C ... 125
FIGURE 3.7. *ISCHNOCYBE PLICATA* ECOLOGY ... 127
FIGURE 3.8. PDSP RESULTS AND Σ_1R BINDING ... 129
FIGURE 4.9. PLATYDESMIDA PHYLOGENY WITH CHEMISTRY DESCRIBED ... 202
FIGURE 4.10. ANDROGNATHINE AND ANDROGNATHANOL STRUCTURES ... 204
FIGURE 4.11. ANDROGNATHINE STEREOCHEMISTRY ... 208
FIGURE 4.12. ANDROGNATHANOL STEREOCHEMISTRY ... 211
FIGURE 4.13. ECOLOGICAL ROLES OF ANDROGNATHINES AND ANDROGNATHANOLS ... 215
FIGURE 5.14. STRUCTURES COMING FROM COLOBOGNATHAN MILLIPEDES ... 288
FIGURE 5.15. POTENTIAL BIOSYNTHETIC ROUTE FOR PRODUCTION OF DEFENSE COMPOUNDS FROM PLATYDESMIDA ... 290
FIGURE 5.16. MILLIPEDE PHYLOGENETIC TREE FOR SUBTERCLASS COLOBOGNATH ... 294
FIGURE 5.17. *A. CORTICARIUS* Y-TUBE CHOICE ASSAYS ... 297

LIST OF TABLES

TABLE 2.1. PERCENTAGE OF ALKALOID DETECTED IN DIFFERENT COLLECTIONS..... 54
TABLE 3.2. INHIBITION PERCENT AND K_I OF Σ_1R AND Σ_2R FOR **3.1**–**3.4**. 130
TABLE 5.3. MILLIPEDE SUBTERCLASS COLOBOGNATHA CHEMISTRY 286

LIST OF SCHEMES

SCHEME 2.1. SYNTHESIS OF HOMOGOSODESMINE 57
SCHEME 2.2. SYNTHESIS OF WATER ADDUCTS OF **2.4** AND **2.6** 58

LIST OF APPENDIX FIGURES

Figure 2.7.1. GCMS chromatogram and spectra of a representative *Brachycybe petaseta* extract 76

Figure 2.7.2. GCMS chromatogram and spectra of a representative *B. producta* extract. 77

Figure 2.7.3. GCMS chromatogram and spectra of a representative *B. rosea* extract 78

Figure 2.7.4. GCMS chromatogram and spectrum of a representative *B. lecontii* extract. 78

Figure 2.7.5. GCMS chromatogram and spectra of the reaction product of the hydrogenation of *B. petasata* extract 79

Figure 2.7.6. GCMS chromatogram and spectra of the reaction product of the hydrogenation of *B. producta* extract 80

Figure 2.7.7. GCMS chromatogram and spectrum of the synthesized 7-(4-methylpentyl)-indolizidine (**2.7**). 81

Figure 2.7.8. GCMS chromatogram and spectrum of the synthesized 2-(4-methylpentyl)-quinolizidine (**2.8**). 81

Figure 2.7.9. GCMS chromatogram and spectrum of the synthesized homogosodesmine (**2.5**). 82

Figure 2.7.10. GCMS chromatogram and spectrum of the synthesized **2.11.** 83

Figure 2.7.11. Numbering of compounds for NMR data tables. 84

Figure 2.7.12. ^{1}H NMR spectrum for synthetic homogosodesmine (**2.5**) 84

Figure 2.7.13. gHSQC for synthetic homogosodesmine (**2.5**) 85

Figure 2.7.14. H2BC for synthetic homogosodesmine (**2.5**) 85

Figure 2.7.15. HMBC for synthetic homogosodesmine (**2.5**) 86

Figure 2.7.16. dqfCOSY for synthetic homogosodesmine (**2.5**) 86

Figure 2.7.17. Hydration product from reaction of *B. petasata* 87

Figure 2.7.18. Fragmentation of **2.18** and **2.19**, the hydrate adducts of **2.4** and **2.6**, respectively. 87

Figure 2.7.19. Plausible fragmentation mechanism that leads to observed loss of 85 Da in both **2.4** and **2.6.** 87

Figure 2.7.20. GCMS chromatogram and spectrum of the synthesized **2.14.** 88

Figure 2.7.21. GCMS chromatogram and spectrum of the synthesized **2.15.** 89

Figure 2.7.22. GCMS chromatogram and spectrum of the synthesized **2.16.** 90

Figure 2.7.23. GCMS chromatogram and spectrum of the synthesized **2.17.** 91

Figure 2.7.24. GCMS chromatogram and spectrum of the synthesized **2.18.** 92

Figure 2.7.25. GCMS chromatogram and spectrum of the synthesized **2.19.** 93

Figure 2.7.26. Comparison of synthetic **2.18** with hydration of *B. petasata* extract 94

Figure 2.7.27. Comparison of synthetic **2.19** with hydration of *B. petasata* extract 95

Figure 2.7.28. ^{1}H NMR spectrum for compound **2.18** 96

Figure 2.7.29. gHSQC for compound **2.18** 96
Figure 2.7.30. H2BC for compound **2.18** 97
Figure 2.7.31. HMBC for compound **2.18** 97
Figure 2.7.32. dqfCOSY for compound **2.18** 98
Figure 2.7.33. easyROESY for compound **2.18** 98
Figure 2.7.34. ^{1}H NMR spectrum for compound **2.19** 99
Figure 2.7.35. gHSQC for compound **2.19** 99
Figure 2.7.36. H2BC for compound **2.19** 100
Figure 2.7.37. HMBC for compound **2.19** 100
Figure 2.7.38. dqfCOSY for compound **2.19** 101
Figure 2.7.39. easyROESY for compound **2.19** 101
Figure 2.7.40. ^{1}H NMR spectrum for hydrogosodesmine (**2.4**) 102
Figure 2.7.41. gHSQC for hydrogosodesmine (**2.4**) 102
Figure 2.7.42. H2BC for hydrogosodesmine (**2.4**) 103
Figure 2.7.43. HMBC for hydrogosodesmine (**2.4**) 103
Figure 2.7.44. easyROESY for hydrogosodesmine (**2.4**) 104
Figure 2.7.45. ^{1}H NMR spectrum for homo-hydrogosodesmine (**2.6**) 104
Figure 2.7.46. gHSQC for homo-hydrogosodesmine (**2.6**) 105
Figure 2.7.47. H2BC for homo-hydrogosodesmine (**2.6**) 105
Figure 2.7.48. HMBC for homo-hydrogosodesmine (**2.6**) 106
Figure 2.7.49. dqfCOSY for homo-hydrogosodesmine (**2.6**) 106
Figure 2.7.50. easyROESY for homo-hydrogosodesmine (**2.6**) 107
Figure 3.7.1. GCMS total ion chromatogram of the crude MeOH extract of the *Ischnocybe plicata* collections. 148
Figure 3.7.2. EIMS spectrum for ischnocybine A (**3.1**) 148
Figure 3.7.3. EIMS spectrum for ischnocybinone (**3.2**) 148
Figure 3.7.4. EIMS spectrum for ischnocybine B (**3.3**) 149
Figure 3.7.5. EIMS spectrum for ischnocybine C (**3.4**) 149
Figure 3.7.6. EIMS spectrum for hydrogenated ischnocybine A (**3.1**) 149
Figure 3.7.7. EIMS spectrum for hydrogenated ischnocybinone (**3.2**) 149
Figure 3.7.8. EIMS spectrum for hydrogenated ischnocybine B (**3.3**) 149
Figure 3.7.9. Chromatogram of base hydrolysis of *I. plicata* extract 150
Figure 3.7.10. EIMS spectrum for methanolysis adduct (peak 1) of ischnocybine A (**3.1**) 150
Figure 3.7.11. EIMS spectrum for methanolysis adduct (peak 5) of ischnocybinone (**3.2**) 150
Figure 3.7.12. EIMS spectrum for methanolysis adduct (peak 6) of ischnocybine B (**3.3**) 150

Figure 3.7.13. EIMS spectrum for methanolysis adduct (peak 3) of ischnocybine C (**3.4**)..... 150
Figure 3.7.14. EIMS spectrum for methoxylamine adduct of ischnocybinone (**3.2**)..... 151
Figure 3.7.15. HRESIMS spectrum of ischnocybine A (**3.1**)..... 151
Figure 3.7.16. HRESIMS spectrum of ischnocybinone (**3.2**) 152
Figure 3.7.17. HRESIMS spectrum of ischnocybine B (**3.3**)..... 152
Figure 3.7.18. HRESIMS $[M+H]^+$ spectrum of ischnocybine C (**3.4**)..... 153
Figure 3.7.19. ^{1}H NMR spectrum of ischnocybine A (**3.1**) 153
Figure 3.7.20. ^{13}C NMR spectrum of ischnocybine A (**3.1**) 154
Figure 3.7.21. Multiplicity-edited ^{1}H-^{13}C HSQC NMR spectrum of ischnocybine A (**3.1**) 154
Figure 3.7.22. COSY NMR spectrum of ischnocybine A (**3.1**) 155
Figure 3.7.23. ^{1}H-^{13}C HMBC NMR spectrum of ischnocybine A (**3.1**)..... 155
Figure 3.7.24. easyROESY NMR spectrum of ischnocybine A (**3.1**) 156
Figure 3.7.25. ^{1}H NMR spectrum of ischnocybinone (**3.2**)..... 156
Figure 3.7.26. ^{13}C NMR spectrum of ischnocybinone (**3.2**) 157
Figure 3.7.27. Multiplicity-edited ^{1}H-^{13}C HSQC NMR spectrum of ischnocybinone (**3.2**)..... 157
Figure 3.7.28. COSY NMR spectrum of ischnocybinone (**3.2**)..... 158
Figure 3.7.29. ^{1}H-^{13}C HMBC NMR spectrum of ischnocybinone (**3.2**) 158
Figure 3.7.30. easyROESY NMR spectrum of ischnocybinone (**3.2**) 159
Figure 3.7.31. ^{1}H NMR spectrum of ischnocybine B (**3.3**)..... 159
Figure 3.7.32. ^{13}C NMR spectrum of ischnocybine B (**3.3**)..... 160
Figure 3.7.33. Multiplicity-edited ^{1}H-^{13}C HSQC NMR spectrum of ischnocybine B (**3.3**)..... 160
Figure 3.7.34. COSY NMR spectrum of ischnocybine B (**3.3**) 161
Figure 3.7.35. ^{1}H-^{13}C HMBC NMR spectrum of ischnocybine B (**3.3**) 161
Figure 3.7.36. easyROESY NMR spectrum of ischnocybine B (**3.3**)..... 162
Figure 3.7.37. ^{1}H NMR spectrum of ischnocybine C (**3.4**)..... 162
Figure 3.7.38. ^{13}C NMR spectrum of ischnocybine C (**3.4**)..... 163
Figure 3.7.39. Multiplicity-edited ^{1}H-^{13}C HSQC NMR spectrum of ischnocybine C (**3.4**)..... 163
Figure 3.7.40. COSY NMR spectrum of ischnocybine C (**3.4**) 164
Figure 3.7.41. ^{1}H-^{13}C HMBC NMR spectrum of ischnocybine C (**3.4**) 164
Figure 3.7.42. easyROESY NMR spectrum of ischnocybine C (**3.4**)..... 165
Figure 3.7.43. ^{1}H NMR spectrum of ischnocybine A alcohol (**3.6**) 165
Figure 3.7.44. Multiplicity-edited ^{1}H-^{13}C HSQC NMR spectrum of ischnocybine A alcohol (**3.6**) 166
Figure 3.7.45. dqfCOSY NMR spectrum of ischnocybine A alcohol (**3.6**) 166
Figure 3.7.46. ^{1}H-^{13}C HMBC NMR spectrum of ischnocybine A alcohol (**3.6**)..... 167

Figure 3.7.47. easyROESY NMR spectrum of ischnocybine A alcohol (**3.6**) 167
Figure 3.7.48. H2BC NMR spectrum of ischnocybine A alcohol (**3.6**) 168
Figure 3.7.49. Mosher's analysis of ischnocybine A (**3.1**) 168
Figure 3.7.50. All preliminary PDSP data graphed 169
Figure 3.7.51. Sigma-1 and Sigma-2 binding curves for Compound **3.6** 170
Figure 3.7.52. NE-100 docked into the agonist σ_1R. 170
Figure 3.7.53. Pentazocine docked into the antagonist σ_1R 171
Figure 3.7.54. Redocking of pentazocine and NE-100 into agonist and antagonist σ_1R structures 172
Figure 3.7.55. Ischnocybine A-SSR (**3.1**) docked into the agonist σ_1R 173
Figure 3.7.56. Ischnocybine B-RRSR (**3.3**) docked into the agonist σ_1R 174
Figure 3.7.57. Ischnocybine C-SRSSS (**3.4**) docked into the agonist σ_1R 175
Figure 3.7.58. Ischnocybinone-RSR (**3.2**) docked into the agonist σ_1R 176
Figure 4.9.1. ^{1}H NMR spectra for andrognathine A (**4.1**) 238
Figure 4.9.2. gHSQC NMR spectra for andrognathine A (**4.1**) 238
Figure 4.9.3. H2BC NMR spectra for andrognathine A (**4.1**) 239
Figure 4.9.4. HMBC NMR spectra for andrognathine A (**4.1**) 239
Figure 4.9.5. easyROESY NMR spectra for andrognathine A (**4.1**) 240
Figure 4.9.6. dqfCOSY NMR spectra for andrognathine A (**4.1**) 240
Figure 4.9.7. ^{1}H NMR spectra for andrognathine B (**4.2**) 241
Figure 4.9.8. gHSQC NMR spectra for andrognathine B (**4.2**) 241
Figure 4.9.9. H2BC NMR spectra for andrognathine B (**4.2**) 242
Figure 4.9.10. HMBC NMR spectra for andrognathine B (**4.2**) 242
Figure 4.9.11. easyROESY NMR spectra for andrognathine B (**4.2**) 243
Figure 4.9.12. dqfCOSY NMR spectra for andrognathine B (**4.2**) 243
Figure 4.9.13. ^{1}H NMR spectra for andrognathine C (**4.3**) 244
Figure 4.9.14. gHSQC NMR spectra for andrognathine C (**4.3**) 244
Figure 4.9.15. H2BC NMR spectra for andrognathine C (**4.3**) 245
Figure 4.9.16. HMBC NMR spectra for andrognathine C (**4.3**) 245
Figure 4.9.17. easyROESY NMR spectra for andrognathine C (**4.3**) 246
Figure 4.9.18. dqfCOSY NMR spectra for andrognathine C (**4.3**) 246
Figure 4.9.19. ^{1}H NMR spectra for andrognathine D (**4.4**) 247
Figure 4.9.20. gHSQC NMR spectra for andrognathine D (**4.4**) 247
Figure 4.9.21. H2BC NMR spectra for andrognathine D (**4.4**) 248
Figure 4.9.22. HMBC NMR spectra for andrognathine D (**4.4**) 248

Figure 4.9.23. COSY NMR spectra for andrognathine D (**4.4**) 249
Figure 4.9.24. ^{1}H NMR spectra for andrognathine E (**4.5**) 249
Figure 4.9.25. gHSQC NMR spectra for andrognathine E (**4.5**) 250
Figure 4.9.26. H2BC NMR spectra for andrognathine E (**4.5**) 250
Figure 4.9.27. HMBC NMR spectra for andrognathine E (**4.5**) 251
Figure 4.9.28. COSY NMR spectra for andrognathine E (**4.5**) 251
Figure 4.9.29. ^{1}H NMR spectra for andrognathine F (**4.6**) 252
Figure 4.9.30. gHSQC NMR spectra for andrognathine F (**4.6**) 252
Figure 4.9.31. HMBC NMR spectra for andrognathine F (**4.6**) 253
Figure 4.9.32. ^{1}H NMR spectra for andrognathine acetonide (**4.7**) 253
Figure 4.9.33. gHSQC NMR spectra for andrognathine acetonide (**4.7**) 254
Figure 4.9.34. H2BC NMR spectra for andrognathine acetonide (**4.7**) 254
Figure 4.9.35. HMBC NMR spectra for andrognathine acetonide (**4.7**) 255
Figure 4.9.36. easyROESY NMR spectra for andrognathine acetonide (**4.7**) 255
Figure 4.9.37. COSY NMR spectra for andrognathine acetonide (**4.7**) 256
Figure 4.9.38. ^{1}H NMR spectra for andrognathanol A (**4.9**) 256
Figure 4.9.39. gHSQC NMR spectra for andrognathanol A (**4.9**) 257
Figure 4.9.40. H2BC NMR spectra for andrognathanol A (**4.9**) 257
Figure 4.9.41. HMBC NMR spectra for andrognathanol A (**4.9**) 258
Figure 4.9.42. easyROESY NMR spectra for andrognathanol A (**4.9**) 258
Figure 4.9.43. dqfCOSY NMR spectra for andrognathanol A (**4.9**) 259
Figure 4.9.44. ^{1}H NMR spectra for andrognathanol B (**4.10**) 259
Figure 4.9.45. gHSQC NMR spectra for andrognathanol B (**4.10**) 260
Figure 4.9.46. H2BC NMR spectra for andrognathanol B (**4.10**) 260
Figure 4.9.47. HMBC NMR spectra for andrognathanol B (**4.10**) 261
Figure 4.9.48. easyROESY NMR spectra for andrognathanol B (**4.10**) 261
Figure 4.9.49. dqfCOSY NMR spectra for andrognathanol B (**4.10**) 262
Figure 4.9.50. ^{1}H NMR spectra for andrognathanol C (**4.11**) 262
Figure 4.9.51. gHSQC NMR spectra for andrognathanol C (**4.11**) 263
Figure 4.9.52. H2BC NMR spectra for andrognathanol C (**4.11**) 263
Figure 4.9.53. HMBC NMR spectra for andrognathanol C (**4.11**) 264
Figure 4.9.54. easyROESY NMR spectra for andrognathanol C (**4.11**) 264
Figure 4.9.55. dqfCOSY NMR spectra for andrognathanol C (**4.11**) 265
Figure 4.9.56. ^{1}H NMR spectra for andrognathanol D (**4.12**) 265

Figure 4.9.57. gHSQC NMR spectra for andrognathanol D (**4.12**) 266
Figure 4.9.58. H2BC NMR spectra for andrognathanol D (**4.12**)..... 266
Figure 4.9.59. HMBC NMR spectra for andrognathanol D (**4.12**)..... 267
Figure 4.9.60. Ester side chain reactions..... 267
Figure 4.9.61. σ_1R Binding 268
Figure 4.9.62. σ_2R Binding 268

LIST OF APPENDIX TABLES

Table 2.8.1. NMR Spectroscopy Data for Synthetic Homogosodesmine (**2.5**)..... 108
Table 2.8.2. NMR Spectroscopy Data for Synthetic *Syn*-Isomer of **2.18**..... 109
Table 2.8.3. NMR Spectroscopy Data for Synthetic *Anti*-Isomer of **2.18**.....110
Table 2.8.4. NMR Spectroscopy Data for Synthetic *Syn*-Isomer of **2.19**.....111
Table 2.8.5. NMR Spectroscopy Data for Synthetic *Anti*-Isomer of **2.19**.....112
Table 2.8.6. NMR Spectroscopy Data for Natural Hydrogosodesmine (**2.4**) 113
Table 2.8.7. NMR Spectroscopy Data for Natural Homo-Hydrogosodesmine (**2.6**) 114
Table 3.8.1. NMR Spectroscopy Data for Ischnocybine A (**3.1**)..... 177
Table 3.8.2. NMR Spectroscopy Data for Ischnocybinone (**3.2**) 178
Table 3.8.3. NMR Spectroscopy Data for Ischnocybine B (**3.3**)..... 179
Table 3.8.4. NMR Spectroscopy Data for Ischnocybine C (**3.4**)..... 180
Table 3.8.5. ^{13}C NMR Chemical Shifts Predictions for Ischnocybine A (**3.1**) 181
Table 3.8.6. ^{1}H NMR Chemical Shifts Predictions for Ischnocybine A (**3.1**) 182
Table 3.8.7. ^{13}C NMR Chemical Shifts Predictions for Ischnocybinone (**3.2**)..... 183
Table 3.8.8. ^{1}H NMR Chemical Shift Predictions for Ischnocybinone (**3.2**) 184
Table 3.8.9. ^{13}C NMR Chemical Shifts Predictions for Ischnocybine B (**3.3**) 185
Table 3.8.10. ^{1}H NMR Chemical Shift Predictions for Ischnocybine B (**3.3**)..... 186
Table 3.8.11. ^{13}C NMR Chemical Shifts Predictions for Ischnocybine C (**3.4**) 187
Table 3.8.12. ^{13}C NMR Chemical Shifts Predictions for Ischnocybine C (**3.4**) (cont.)..... 188
Table 3.8.13. ^{1}H NMR Chemical Shift Predictions for Ischnocybine C (**3.4**)..... 189
Table 3.8.14. ^{1}H NMR Chemical Shift Predictions for Ischnocybine C (**3.4**) (cont.) 190
Table 3.8.15. NMR Spectroscopy Data for Ischnocybine A Alcohol (**3.6**) 191
Table 3.8.16. Isolated quantity of ischnocybines from 300 individual *Ischnocybe plicata* 191
Table 3.8.17. *I. plicata* Length Versus Alkaloid Study..... 192
Table 3.8.18. Primary Binding Assay (Inhibition %) 193
Table 3.8.19. Inhibitor Constant (K_i) for Compounds **3.1–3.4**..... 198
Table 3.8.20. MM/GBSA Calculated Predicted Free Energy of Binding 198
Table 4.7.1. *Andrognathus corticarius* Collections 219
Table 4.10.2. NMR Spectroscopy Data for Andrognathine A (**4.1**) 269
Table 4.10.3. NMR Spectroscopy Data for Andrognathine B (**4.2**) 270
Table 4.10.4. NMR Spectroscopy Data for Andrognathine C (**4.3**) 271
Table 4.10.5. NMR Spectroscopy Data for Andrognathine D (**4.4**)..... 272
Table 4.10.6. NMR Spectroscopy Data for Andrognathine E (**4.5**) 273

Table 4.10.7. NMR Spectroscopy Data for Andrognathine F (**4.6**)..... 274
Table 4.10.8. NMR Spectroscopy Data for Andrognathine Acetonide (**4.7**)..... 275
Table 4.10.9. Comparison of Experimental and Calculated Chemical Shifts for **4.7**..... 276
Table 4.10.10. NMR Spectroscopy Data for Andrognathanol A (**4.9**) 277
Table 4.10.11. NMR Spectroscopy Data for Andrognathanol B (**4.10**) 278
Table 4.10.12. NMR Spectroscopy Data for Andrognathanol C (**4.11**) 279
Table 4.10.13. NMR Spectroscopy Data for Andrognathanol D (**4.12**)..... 280
Table 4.10.14. *A. corticarius* Length Versus Average Peak Area Study..... 281
Table 4.10.15. σ_1R Binding 282
Table 4.10.16. σ_2R Binding 282
Table 4.10.17. Nav1.5 Human Sodium Ion Channel Cell Based APC LeadHunter Assay..... 283
Table 4.10.18. Nav1.8 Human Sodium Ion Channel Cell Based APC LeadHunter Assay..... 283

LIST OF ABBREVIATIONS

mg	Milligram
mL	Milliliter
μL	Microliter
mol	Mole
mmol	Millimole
μmol	Micromole
nM	Nanomolar
ppm	Parts Per Million
μm	Micrometer
Da	Dalton
atm	Atmosphere (Pressure)
h	Hours
min	Minutes
°C	Degrees Celsius
MHz	Megahertz
m/z	Mass-to-Charge Ratio
MF	Molecular Formula
DoU	Degrees of Unsaturation
δ_C	Carbon Chemical Shift (NMR)
δ_H	Proton Chemical Shift (NMR)
K_i	Inhibition Constant
LTQ	Linear Trap Quadrupole

EDCI	1-Ethyl-3-(3-Dimethylaminopropyl)Carbodiimide
DMF	Dimethylformamide
DBU	1,8-Diazabicyclo[5.4.0]undec-7-ene
MTPA	α-Methoxy-α-trifluoromethylphenylacetic acid
MeOH	Methanol
MeCN	Acetonitrile
DMSO	Dimethyl Sulfoxide
EtOH	Ethanol
THF	Tetrahydrofuran
EtOAc	Ethyl Acetate
HCl	Hydrochloric Acid
NaOH	Sodium Hydroxide
LiCl	Lithium Chloride
$LiAlH_4$	Lithium Aluminium Hydride
K_2CO_3	Potassium Carbonate
PtO_2	Platinum(IV) Oxide
Pd/C	Palladium on Carbon
MeMgCl	Methylmagnesium Chloride
FA	Formic Acid
BPC	Base Peak Chromatogram
DMAP	4-Dimethylaminopyridine
GCMS	Gas Chromatography Mass Spectrometry
EI	Electron Ionization

LR-LCMS	Low Resolution Liquid Chromatography Mass Spectrometry
HR-LCMS	High Resolution Liquid Chromatography Mass Spectrometry
HRESIMS	High Resolution Electrospray Ionization Mass Spectrometry
EIMS	Electron Ionization Mass Spectrometry
RP-HPLC	Reverse-Phase High Performance Liquid Chromatography
EIC	Extracted Ion Chromatogram
HRMS	High Resolution Mass Spectrometry
q-TOF	Quadrupole Time-of-Flight
FID	Free Induction Decay
NMR	Nuclear Magnetic Resonance
ROE	Rotating Frame Overhauser Enhancement
dqfCOSY	Double-Quantum Filtered Correlation Spectroscopy
gHSQC	Gradient Heteronuclear Single Quantum Coherence
H2BC	Heteronuclear 2-Bond Correlation
HMBC	Heteronuclear Multiple Bond Correlation
easyROESY	Efficient Adiabatic Symmetrized Rotating Frame Overhauser Enhancement Spectroscopy
ECD	Electronic Circular Dichroism
RMSD	Root Mean Standard Deviation
MAE	Mean Absolute Error
NUS	Non-Uniform Sampling
DFT	Density Functional Theory
TD	Time Dependent

DNA	Deoxyribonucleic Acid
SAR	Structure-Activity Relationship
PDSP	Psychoactive Drug Screening Program
$Na_v1.5$	Voltage-Gated Sodium Channel 1.5
$Na_v1.8$	Voltage-Gated Sodium Channel 1.8
σ_1R	Sigma-1 Receptor
σ_2R	Sigma-2 Receptor
UV	Ultraviolet
LD_{50}	Lethal Dose 50%
N_2	Nitrogen Gas

Chapter 1.

Exploring Nature's Chemists: Millipedes, Natural Products, and Their Role in Drug Discovery

1.1. Introduction

Microbes, animals, and plants are unparalleled chemists, synthesizing natural products, which serve as chemical weapons, pheromones, metal scavengers, or signaling agents.[1] However, these molecules have also played an integral role in drug development for generations.[2] In nature, the competition for nutrients often drives the production of natural products in order to gain a competitive advantage, such as those used by plants or microbes to defend themselves against predators.[3-5] Nature is continuously investing valuable resources into producing these complex natural products, developing new ones and participating in the ever-evolving chemical arms race between herbivores and plants, or between microbes and antibiotic resistant-pathogens.[6,7] Natural products are also commonly called secondary metabolites. Secondary metabolites are not deemed essential for survival, but are not merely by-products of metabolism; they provide a competitive advantage to the producing organism.[8] These compounds enable organisms to obtain nutrients, deter predation, or signal danger to nearby species, thereby enhancing their chances of survival. By studying the interactions between organisms, we can unlock biomedical applications through their natural products, paving the way for new drug discoveries while deepening our understanding of ecological roles and strategies in chemical warfare and survival.

1.0.1. Contribution of Natural Products to Drug Discovery

The earliest recorded use of natural products as medicines comes from ancient clay cuneiform tablets, where remedies were described for various ailments, including colds, and inflammation.[9] Although some treatments were documented, many were passed down orally,

making it challenging to identify all medicinal plants used historically. Many of these treatments are still in use today in the form of herbal treatments or clinically approved drugs upon identification of the active ingredients.[9] These treatments are commonly in the form of tree oils, such as *Cedrus species* (cedar), *Cupressus sempervirens* (cypress), *Glycyrrhiza glabra* (licorice), *Commiphora species* (myrrh), and *Papaver somniferum* (poppy juice).[10] An example of one of these discoveries is the discovery of morphine (**1.1**), the first alkaloid discovered (1805) from *P. somniferum*, which possesses analgesic properties. This discovery was followed by discovery of related alkaloids from opium, with many classified as poisons due to their toxic properties.[11] In addition to plants, animal extracts have also contributed significantly to traditional medicines.[12,13] For instance, in Traditional Korean Medicine, arthropods like centipedes, silk moth larvae, and scorpions were and are still used to treat conditions such as arthritis, stroke, and pain.[12] Understanding the active ingredients within traditional medicines has laid the foundation for the field of natural products chemistry and is this area is still an active field of research.[14]

Today, natural products make up nearly 70% of all FDA approved drugs, including the natural product themselves, natural product mimics, or contain the pharmacophore of a natural product (**Figure 1.1**).[2] The impact of natural products on drug development is even more significant when analyzing the small molecule drugs used to treat microbial infections (67%) and cancer (83%).[2] This is unsurprising, as natural systems frequently produce toxic compounds, including venoms and poisons. However, the prominence of these compounds in drug discovery is also influenced by the methodologies employed to identify them (discussed later). Traditionally, many drugs originated from chemical studies of herbs, plants, and berries guided by traditional knowledge. More recently, marine organisms (e.g., sponges, tunicates, and cyanobacteria) and microorganisms have emerged as prolific sources of complex natural products.[15] From the marine

environment alone, thirteen compounds are currently approved for use in humans, while many more are in the pipeline.[16]

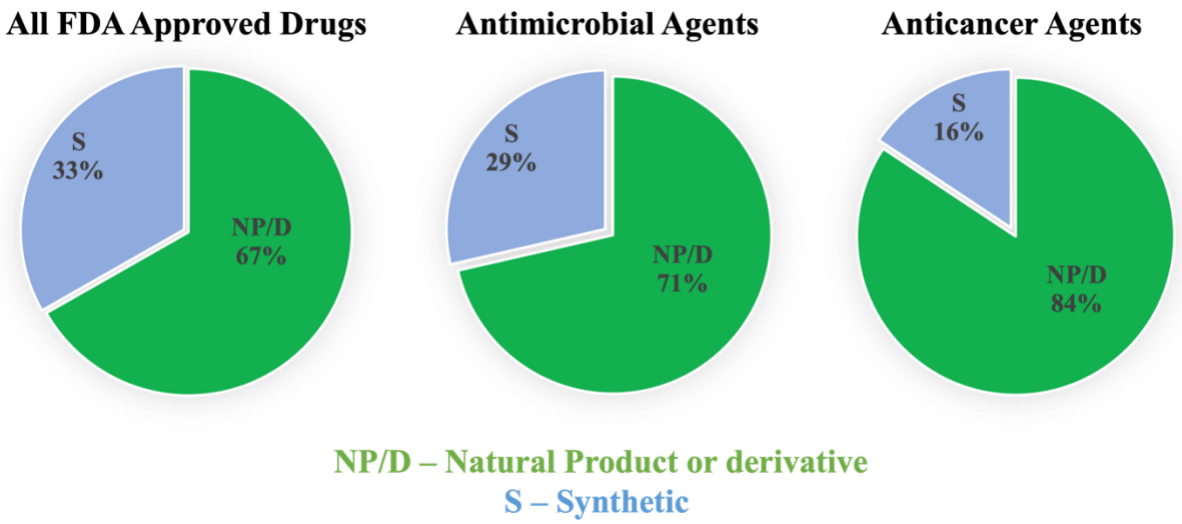

Figure 1.1. Contributions of natural products to approved small molecule drugs (image modified from Newman and Cragg (2020)).

The field of natural products chemistry began to flourish in the 1940s and 1950s, during what has now been termed "golden age of antibiotics", when penicillin (**1.2**) and vancomycin (**1.3**) were among the pivotal discoveries made during this period.[17] The breakthroughs were primarily sourced from terrestrial soil microorganisms, and were made possible due to bioactivity-guided isolation, also known as the Waksman platform.[10,18,19] Bioassay-guided isolation is a technique whereby a desired activity drives the purification process. For example, crude mixtures are processed using various chromatography techniques, and the refined fractions are screened for a desired activity. This process is repeated until an active component(s) have been identified. Bioassay-guided isolation excels at identifying toxic natural products (e.g., antibiotics and anticancer agents) due to the ease of the assay with a kill or no kill readout. Using this method has led to significant discoveries, such as identifying many of the successful drug scaffolds used in the clinic today, including antibiotics [e.g., **1.2**, daptomycin (**1.4**), and rifamycin (**1.5**)], antifungal

agents [e.g., echinocandin (**1.6**), amphotericin B (**1.7**)] and anticancer agents [e.g., taxol (**1.8**), Ceflatonin (**1.9**)] (**Figure 1.2**).[17,20-23]

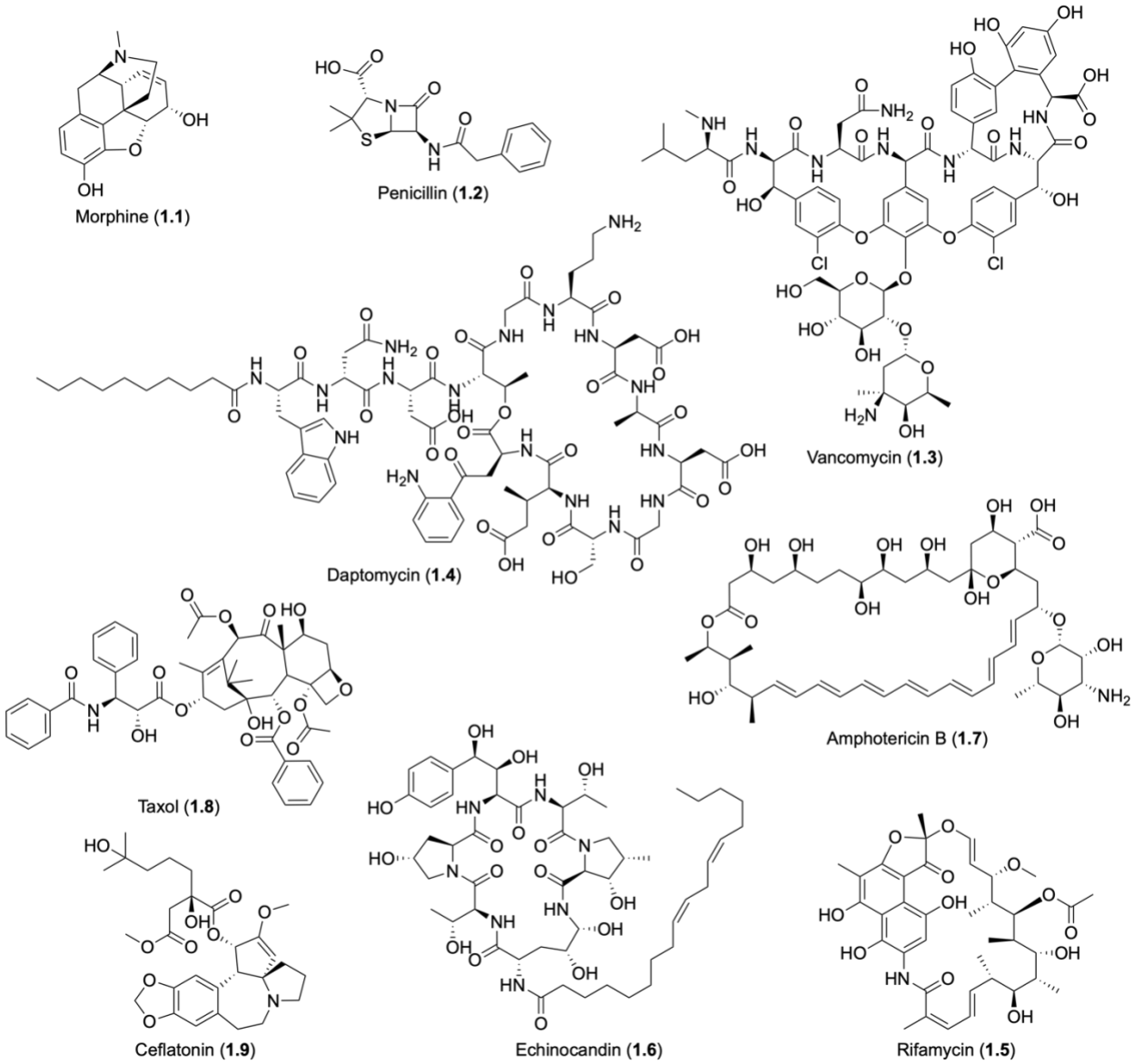

Figure 1.2. Important natural products, including analgesic [morphine (**1.1**)],[11] antibiotics [penicillin (**1.2**) , vancomycin (**1.3**), daptomycin (**1.4**), and rifamycin (**1.5**)],[17,24] antifungal agents [echinocandin (**1.6**) and amphotericin B (**1.7**)][20,21] and anticancer agents [taxol (**1.8**) and ceflatonin (**1.9**)].[22,23]

Although natural products have historically been a great source of bioactive molecules, the repeat discovery of metabolites has hampered recent discovery efforts and resulted in very few new drug candidates over the past 40 years. This 'innovation gap' is particularly noticeable for the discovery of new antibiotics where only eleven drugs were developed based on the discovery of a natural product.[25] It is believed that much of the 'low-hanging fruit' was found during "the Golden Age of Antibiotics", challenging the discovery new natural products.[26] Rediscovery is a persistent challenge in the field of natural products.[27] While new compounds are still being found, the rate of rediscovery—where compounds with similar structures to previously known ones are isolated—has been increasing. As seen in **Figure 1.3**, although the rate of discovery of new compounds has increased, the structural uniqueness of these compounds (based on the Tanimoto score) has decreased to about 10% of new compounds possessing a Tanimoto score of less than 0.4.[27] To combat this problem, we are using the functional roles of the compounds in nature to drive our discovery. We are also looking to find new natural products and avoid rediscovery by exploring new sources.[28] The continuation of natural products research is essential for the future development of drug discovery, especially for diseases with unmet needs, such as antibiotic-resistant infections and neurodegenerative diseases.[29]

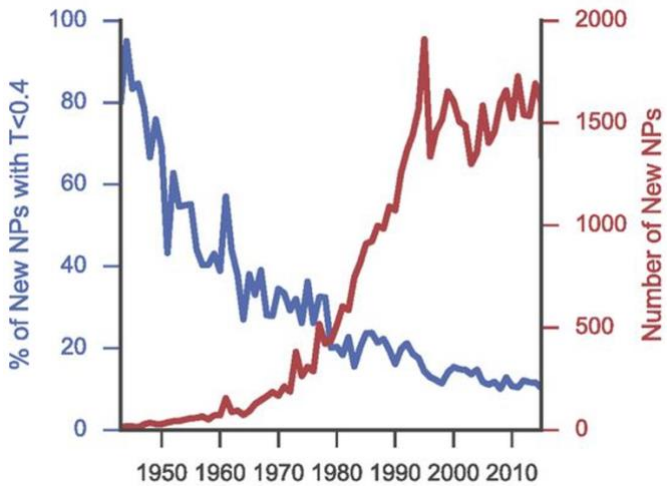

Figure 1.3. New natural products discovered per year compared to their structural novelty. In blue, the percent of new natural products with a Tanimoto score less than 0.4 each year, compared to the number of new natural products shown in red for each year. [Graph adapted from Pye*, et al.* (2017)].

1.0.2. Modern Sources of Natural Products

Historical efforts to discover natural products have revealed the ecological niche is a good predictor of the type of natural product they may produce and their potential biological activity.[30] One of the best examples highlighting this is the fact that nearly all approved antibiotics were first discovered from terrestrial microorganisms.[31] Over the past 80 years, microorganisms have been shown to be prolific producers of antimicrobial natural products, and this is believed to be a result of the intense competition between microbes to obtain limited nutrients.[3] However, this is not limited to microorganisms. Toxic natural products are commonly found in sessile or slow-moving organisms that lack other physical mechanisms (e.g., external shell or fast movement) to evade predators. Sessile marine organisms (e.g., sponges, tunicates, shell-less snails, and cyanobacteria) have been shown to protect themselves from predation using toxic natural products.[32] This includes some of the most complex and toxic natural products yet to be discovered, such as brevetoxin

(**1.10**), saxitoxin (**1.11**), and tetrodotoxin (**1.12**).[33] It has become clear that many toxin-producing organisms use aposematism (bright colors to signal toxicity) and are found in Amazon and neotropics (e.g., poison dart frogs and coral snakes).[34,35]

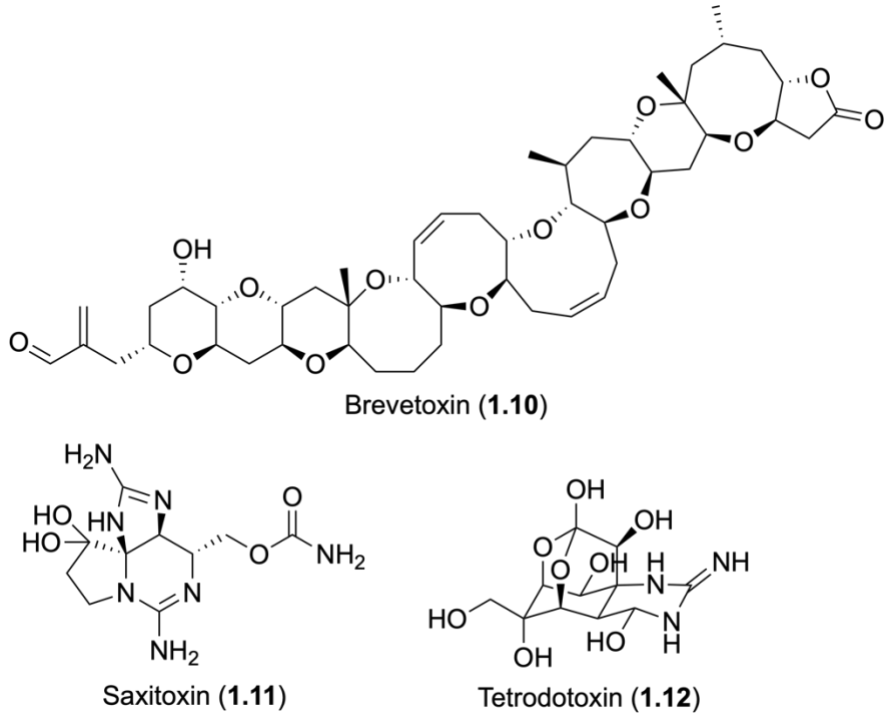

Figure 1.4. Toxic natural products isolated from sessile marine organisms.[32]

Although sessile and slow-moving soft bodied organisms have been shown to be a prolific source of bioactive natural products, the eukaryotic organism is rarely the producer of the natural product.[32] Many of these organisms, particularly marine animals, the true producer of the natural product are a symbiotic microorganism.[32] In fact, eukaryotes have evolved over time to depend on bacteria for various nutritional and defensive functions.[36] This includes obtaining vitamin B12—an essential nutrient—from microbial symbionts, as well as sponges deriving up to 50% of their energy from photosynthetically fixed carbon provided by cyanobacteria.[37,38] In addition to harboring microbial symbionts, both terrestrial and marine animals are known to acquire their defensive natural products through their diet.[39-41] For example, poison dart frogs in both the

Amazon and Neotropics have been found to sequester defensive compounds from the consumption of millipedes, specifically *Rhinotus purpureus*.[39]

The shift in effort to discover new natural products—from using traditional medicine to a ecology driven approach—has led to the discovery of truly novel natural products possessing intriguing bioactive compounds with promising therapeutic potential.[42] This includes the discovery of the roseobacticides, small molecule modulator produced by the bacteria *Phaeobacter gallaeciensis*. These compounds were discovered when observing the dynamic relationship between *P. gallaeciensis* and a microphytoplankton, *Emiliania huxleyi*. Initially, these two microbes live harmoniously together. The algae, *E. huxleyi*, produces food for the bacteria while the bacteria produce a growth promoter and antibiotic allowing both microbes to flourish. Then this relationship turns toxic and the algae releases an elicitor which stimulates the bacteria to switch production, using the same precursors from the mutualistic phase to produce the roseobacticides, in turn killing the algae.[43] This approach extends beyond the discovery of antibiotic and anticancer agents by examining how potential predators react to these compounds. One example is the identification of siphonazole, a natural product with antiplasmodial (malaria-preventative) properties.[44] Siphonazole was isolated from *Herpetosiphon* sp. and was discovered due to the genetic diversity within the genus, particularly the divergence in highly conserved regions of ribosomal RNA.[44]

1.2. Leveraging Millipede Secretions for the Discovery of New Natural Products

1.0.3. Millipede Evolution

Arthropods (Phylum: Arthropoda) are an incredibly diverse animal phylum and they are found in nearly every ecosystem (air, land, marine and freshwater ecosystems).[45] Rough estimates suggest arthropods account for over 80% of all known living animal species, totaling more than 5

million, which is more than all other animal phyla combined.[45,46] Millipedes (class: Diplopoda) is the largest class within the Arthropoda phylum, and are one of the oldest land animals on earth. Fossils near Bathgate, West Lothian, Scotland confirm their presence, dating back to the Lower Carboniferous period, around 323 mya.[47] Millipedes were among the first animals to breathe oxygen, evolving alongside marine myriapods, and were fully adapted to life on land 45 million years before vertebrates.[48] Since then, millipedes have evolved into 145 families classes, with more than 12,000 species of millipedes currently described, but there are more than 80,000 species hypothesized to exist worldwide.[49] Millipedes are commonly found in moist, dark organic rich environments, such as under tree debris on the forest floor. They are also nocturnal, making it difficult to observe them in their natural environment.[50] Therefore, many basic biology questions still remain for millipedes, such as diet, reproduction patterns, phylogeny, and their true ecological role.

1.0.4. Millipede Chemical Secretions

Millipedes are slow moving soft-bodied organisms, and as such, they are reliant on a consortium of protective mechanisms for survival. In part, millipedes gain some protection by living under woody debris, making them harder to spot, they will also roll in to a coil to evade predators, while some millipedes also have spines that have sharp spikes.[51] In addition, many millipedes are brightly colored, which indicates they are also chemically defended. In fact, early fossils confirm the ancient evolution of millipedes to deploy chemical defenses with the presence of specialized glands, called ozopores.[47] The ozopores are located bilaterally along the sides of the millipede at the end of their paranotal (**Figure 1.5**).[51] The structure contains a vesicle used to store the defense compounds until needed, a valve muscle is responsible for releasing the secretions upon disturbance to fend off predators. The ancient nature of millipedes has allowed for many

millennia of evolution to hone its chemical defense mechanisms, leading to diverse suite of potent defensive compounds.[52]

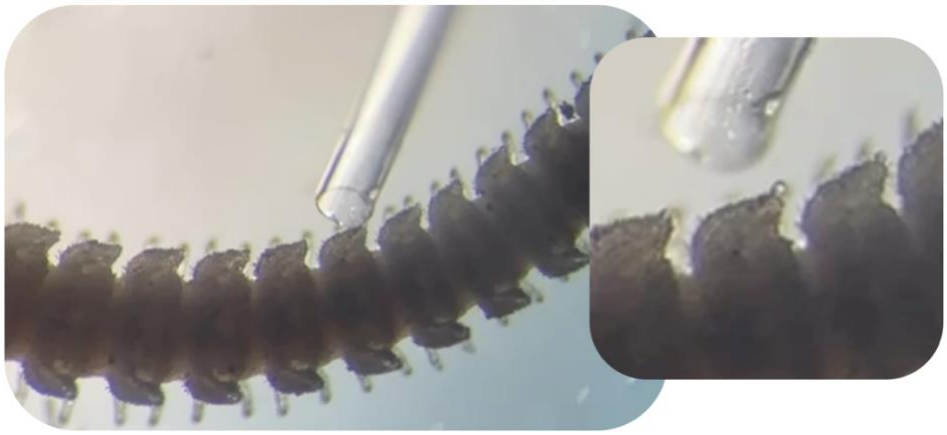

Figure 1.5. Defensive secretions being secreted from ozopore of *Andrognathus corticarius* upon agitation.

Chemical agents are employed by eleven of 16 millipede orders and these agents quite structurally diverse, including hydrogen cyanide, oxidized aromatics, quinazoline alkaloids, and terpenoid alkaloids (**Figure 1.6**).[52,53] Interestingly, the types of defensive compounds used by millipedes align with their phylogenetic relationships, with different chemical classes being produced by distinct millipede families. For example, the Julida order is known to produce oxidized aromatics-based defensive agents, such as benzoquinone, while the Polydesmida order produces primarily cyanogenic agents. The quinazoline alkaloids are produced by millipedes within the order Glomerida, and the terpenoid alkaloids are produced by millipedes belonging to the subterclass Colobognatha. (**Figure 1.6**)[52] From the 1960's to 2000, research on millipede defensive compounds grew substantially, but focused primarily on the hydrogen cyanide and oxidized aromatic producers, as these millipedes are some of the largest and most common ones. During this time, it was shown that millipedes secrete these agents are produced by the millipedes, and are actively secreted through the ozopores to fend off predators.[54]

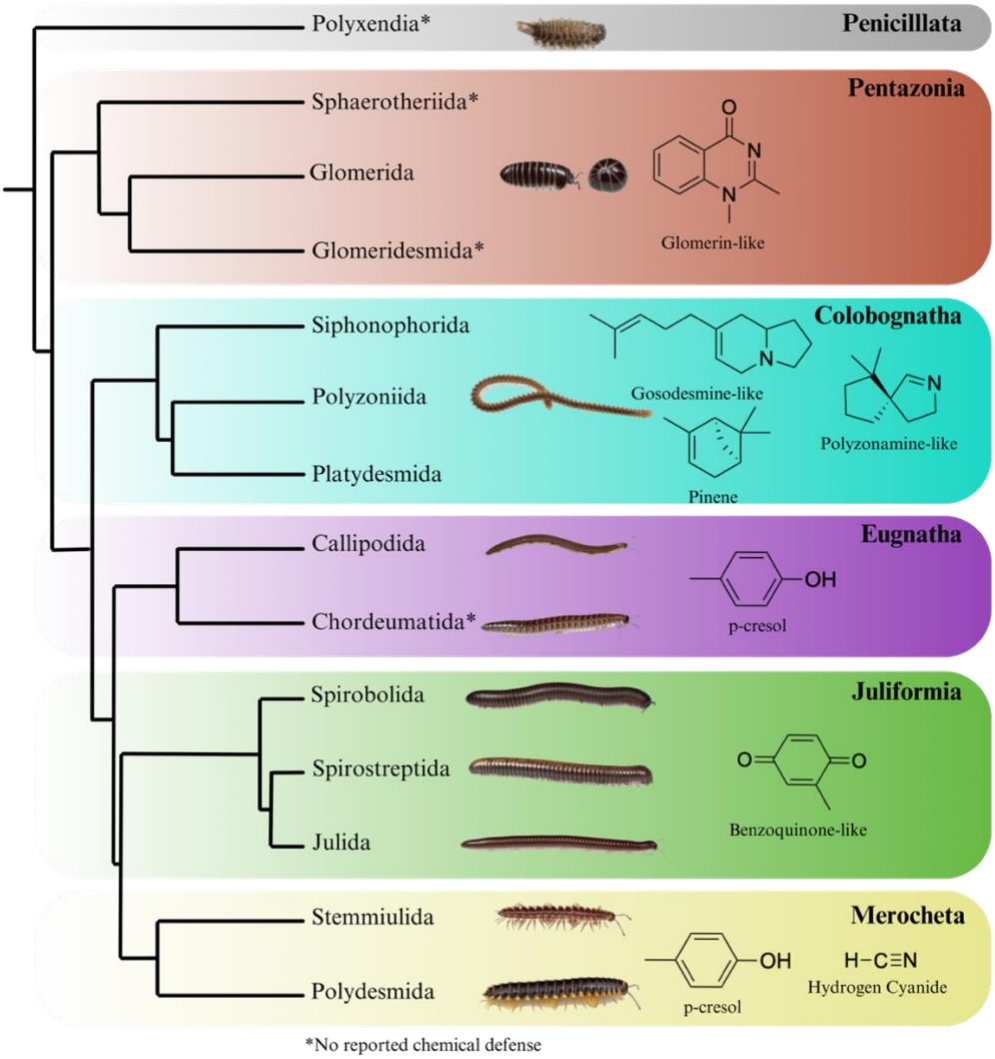

Figure 1.6. Millipede defensive secretion composition and phylogeny. Penicilllata do not contain ozopores, nor do they produce any defense compounds.[51] Pentazonia produce glomerin-like defenses.[55] Colobognatha produce monoterpenes and terpenoid alkaloids.[56-58] Eugnatha produce p-cresol.[59] Juliformia produce benzoquinones.[60] Merocheta produce hydrogen cyanide and phenolic compounds.[61] [Figure adapted from Rodriguez*, et al.* (2018)]

1.0.5. Colobognatha: The Alkaloid-Producing Subterclass

All terpenoid alkaloids are produced by a single subterclass, Colobognatha, which possess unique features that are absent in other millipede classes, such suctorial feeding mechanisms and brood care behavior. The subterclass is made up of four orders of millipedes, Platydesmida, Polyzoniida, Siphonocryptida, Siphonophorida.[62] They are found across North and South America, Europe and Asia, with some sightings in Africa and Australia.[63] Many Colobognatha feed specifically on fungus that is found on the underside of decaying logs and display social characteristics as they are commonly found in groups of greater than 100. It is currently unknown how these large aggregations form as the millipedes lack eyes.[62,64] Finally, Colobognatha species tend to be cryptic as they are significantly smaller (~1-3 cm) than other classes and are rarely found on the forest floor. Therefore, they have historically been understudied, with basic biological questions still unanswered, such as mating patterns, seasonality, range of species, number of species, and the ecological role of the defensive secretions. However, their defense compounds are known to be sequestered by animals for their own use as poison dart frogs in Madagascar and the Neotropics have been known to consume *R. purpureus* and sequester the defense compounds for use themselves.[39]

Figure 1.7. Pictures of Colobognathan millipedes. **A.** *Ischnocybe plicata*, **B.** *Platydesmus* sp. from Central America, **C.** *R. purpureus* with liquid alkaloid droplet on sixth segment. **D**. *Petaserpes* sp. (Photos by Paul Marek CC BY)

Chemically, the terpenoid alkaloids are the most intriguing, yet least studied of all the chemical defensive agents. The first terpenoid alkaloid was described by Smolanoff*, et al.* (1975) whom discovered the spirocyclic alkaloid, polyzonamine (**1.13**), from the glands of *Polyzonium rosalbum*. Several other terpenoid alkaloids related to polyzonamine were described shortly thereafter, namely nitropolyzonamine (**1.14**) and *O*-methyloxime 236 (**1.15**).[57,65] In 2000, buzonamine (1.**16**), β-pinene (**1.17**), and limonene (**1.18**) were described from the secretions of *Buzonimum crassipies*, a millipede native to coastal California. Deoxybuzonamine (**1.19**) was isolated and characterized from *Brachycybe lecontii*.[66] Buzonamine (1.**16**) and deoxybuzonamine (**1.19**) are structurally distinct terpenoid alkaloids, consisting of a 5,6,6-fused heterocyclic system.[58,66] Finally, in 2020, gosodesmine (**1.20**) was described from *Gosodesmus claremontus*, a

millipede native to California.[67] Compound **1.20** contains an indolizidine system and represents a third distinct terpenoid alkaloid scaffold.[68] Each of these are also known to produce α-pinene (**1.21**), **1.17** or both.[51] Although all Colobognatha defensive secretions appear to incorporate a mono-terpene, these compounds are structurally interesting due to their unprecedented structures, including the incorporation of a number of stereocenters and numerous predicted post-modifications (e.g., oxidations and nitrations).[69]

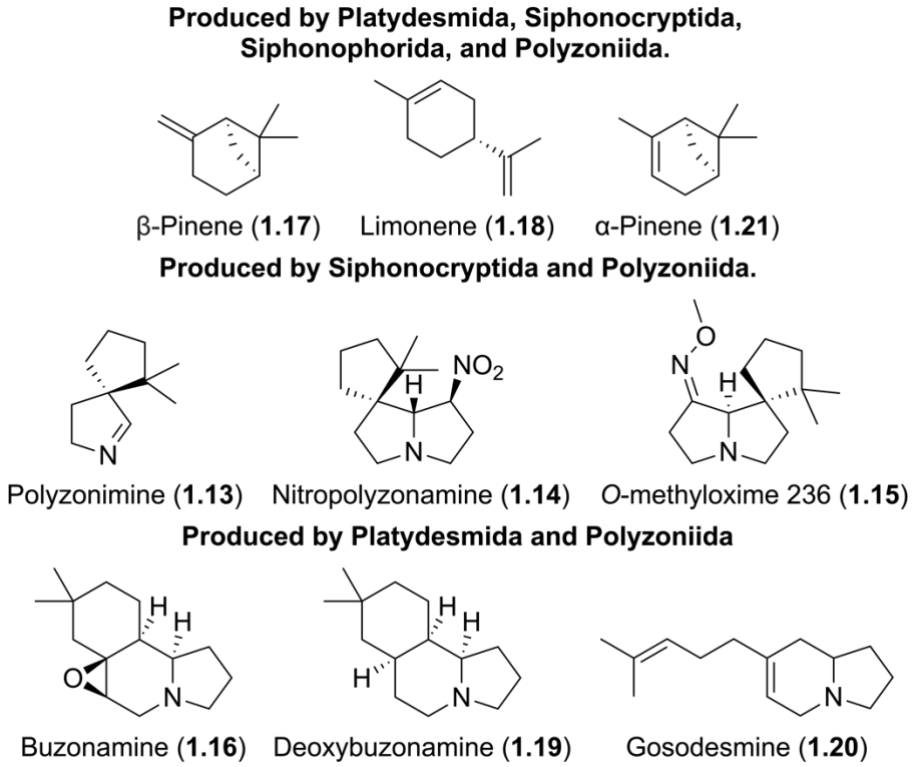

Figure 1.8. Alkaloids previously described from Colobognatha.

The millipede terpenoid alkaloids are widely believed to serve a defensive role, i.e. deters predation or microbial growth, the Colobognatha millipedes are significantly less studied than the other systems.[51] Recently, it has been hypothesized that these molecules may also be functioning as pheromones, i.e., intra-species communication to assist in forming the large aggregations, as this is similar to other systems.[51] For example, ants, also arthropods, are known to use chemical cues to establish territories, identify mates, or signal distress.[70,71] Similarly, millipedes may use

their secretions to communicate within their colonies or to alert others of impending threats, in addition to the defense they provide.[72] None of the Colobognatha alkaloids have been evaluated for functions beyond simply defensive roles.

1.3. Summary

The discovery of truly novel natural products is essential to repopulate the drug pipeline for diseases with unmet needs. Ecology-driven natural product discovery has proven to lead to new bioactive molecules. Millipedes are soft-bodied animals and have been shown to be a source of bioactive compounds but severely underexplored with less than 10% of the documented species being chemically investigated. Furthermore, as environmental pressures lead to the loss of biodiversity, the importance of discovering new natural products from underexplored ecosystems, such as the millipedes found within Colobognatha, become increasingly urgent. Regardless, these organisms have been shown to produce structurally diverse natural products, ranging from hydrogen cyanide to highly functionalized terpenoid alkaloids. However, very few studies have focused on molecular targets or biomedical applications.[51] Exploring these untapped ecological niches not only holds immense potential for addressing biomedical challenges but also emphasizes the need for conservation efforts to preserve biodiversity.

1.4. Research Objectives

This dissertation research has focused on investigating unstudied Colobognatha species, focusing particularly on the characterization of new natural products within the secretions, with the hope to expand upon our current understanding of Colobognatha millipedes. In addition, as new natural products were discovered, studies into their ecological function and medicinal potential were further investigated. The central hypothesis guiding this work is that the compounds in the secretions of Colobognatha millipedes serve dual roles as both chemical defense

mechanisms against predators and as pheromones for intra-species communication. Although none of the previously identified terpenoid alkaloids have been fully evaluated in receptor assays, we hypothesized that these compounds may have neuroactive properties based on the reported behaviors of predator exposed to the secretions.[54,55,73,74]

Within this dissertation, the detailed chemistry of Colobognatha will be discussed, with key findings including: 1) the discovery of homogosodesmine (**1.22**), homo-hydrogosodesmine (**1.23**), hydrogosodesmine (**1.24**) and previously discovered gosodesmine (**1.20**) from secretion glands of *Brachycybe petesata* and *B. producta* (the focus of **Chapter 2**), 2) the discovery of ischnocybines A–C (**1.25**, **1.26** and **1.27**) and ischnocybinone (**1.28**) from the secretions glands of *Ischnocybe plicata* (the focus of **Chapter 3**), and 3) the discovery of andrognathines (**1.29**) and andrognathanols (**1.30**) from *Andrognathus corticarius* (the focus of **Chapter 4**).[75-77] These discoveries followed the same general format. Millipedes were collected from their habitats, and extracted using methanol, leaving the millipede intact. The extract was then analyzed by HR-LCMS to identify the compounds, and new natural products were purified using HPLC then planar structures were determined by 2D NMR. When possible (**Chapter 3** and **Chapter 4**), absolute configurations were determined through chemical derivation. Purified compounds were then evaluated in a range of ecological and biological assays, including predator, pheromone, or psychoactive drug screening assays.

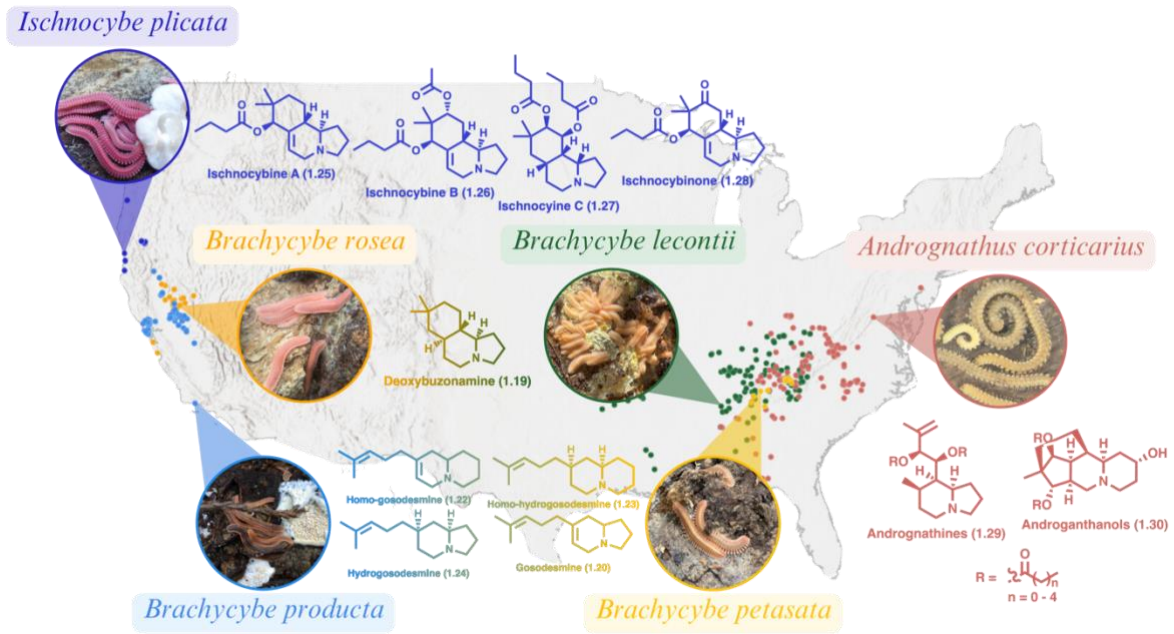

Figure 1.9. Platydesmida millipede and their defense compounds discovered within this dissertation.

We tested our hypothesis that the millipedes use their secretions for defense (**Chapter 3** and **Chapter 4**) and as pheromones (**Chapter 4**). Purified compounds that were screened against ants, a likely common predator, appeared to neurologically impair the ants, thus supporting these molecules serve a defensive role.[76] This observation led to the evaluation of a subset of the purified secretions in a broad range of neuroreceptors through collaboration with the Psychoactive Drug Screening Program (PDSP) at UNC Chapel Hill. The ischnocybines, specifically ischnocybine A (**1.25**), potently (K_i 14 nM) and selectively binds the sigma-1 receptor (σ_1R) over the sigma-2 receptor (σ_2R), with the andrognathines much less active against σ_1R (K_i 840 nM) and the andrognathanols completely inactive against both receptors. Interestingly, the hydrate of homo-hydrogosodesmine (**Chapter 2**) shows inverse selectivity compared to ischnocybine A (σ_1R: K_i 840 nM; σ_2R: K_i 260 nM).[76,77] Finally, a subset of the new alkaloids was evaluated against two sodium channels, Nav1.8 and Nav1.5 but all were inactive. This is the first report of a molecular

target for any of the terpenoid alkaloids and has potential implication in the development of drugs to treat neurological disorders.

The pharmacological potential of millipede-derived natural products has far-reaching implications for drug discovery, especially given their distinct and complex structures. Compounds like the ischnocybines, which have demonstrated selective binding to the σ_1R, represent promising candidates for the treatment of neurodegenerative diseases, such as Alzheimer's disease and Parkinson's disease, as well as for pain management.[78] Additionally, there is a growing interest in alternative pain management strategies, which makes the exploration of millipede secretions particularly timely.

Finally, the terpenoid alkaloids discovered from millipedes represent an underexplored avenue for natural product chemistry. Their unique structures, with unprecedented stereochemical complexity, offer insights into their biosynthetic pathways. The discoveries detailed in this dissertation underscore the untapped potential of millipede secretions in addressing challenges in neurodegenerative diseases, pain management, and beyond. Future studies with ecological, chemical, and pharmacological perspectives will be crucial in exploring these resources.

1.5. References

(1) Demain, A. L.; Fang, A. The Natural Functions of Secondary Metabolites. *Advances in Biochemical Engineering/Biotechnology* **2000**, *69*, 1-39. DOI: 10.1007/3-540-44964-7_1.

(2) Newman, D. J.; Cragg, G. M. Natural Products as Sources of New Drugs over the Nearly Four Decades from 01/1981 to 09/2019. *Journal of Natural Products* **2020**, *83* (3), 770-803. DOI: 10.1021/acs.jnatprod.9b01285.

(3) Hibbing, M. E.; Fuqua, C.; Parsek, M. R.; Peterson, S. B. Bacterial competition: surviving and thriving in the microbial jungle. *Nature Reviews Microbiology* **2010**, *8* (1), 15-25. DOI: 10.1038/nrmicro2259.

(4) Ji, H.-F.; Li, X.-J.; Zhang, H.-Y. Natural products and drug discovery. Can thousands of years of ancient medical knowledge lead us to new and powerful drug combinations in the fight against cancer and dementia? *European Molecular Biology Organization Reports* **2009**, *10* (3). DOI: 10.1038/embor.2009.12.

(5) Koehn, F. E.; Carter, G. T. The evolving role of natural products in drug discovery. *Nature Reviews Drug Discovery* **2005**, *4* (3). DOI: 10.1038/nrd1657.

(6) Kariñho-Betancourt, E. Coevolution: Plant-herbivore interactions and secondary metabolites of plants. Springer International Publishing, 2019; pp 1-31.

(7) Davies, J.; Davies, D. Origins and Evolution of Antibiotic Resistance. *Microbiology and Molecular Biology Reviews* **2010**, *74* (3), 417-433. DOI: 10.1128/mmbr.00016-10.

(8) Gerald, B. F.; James, G. B. Biologically Active Secondary Metabolites from the Fungi. *Microbiology Spectrum* **2016**, *4* (6), 10.1128/microbiolspec.funk-0009-2016. DOI: 10.1128/microbiolspec.funk-0009-2016.

(9) Dias, D. A.; Urban, S.; Roessner, U. A historical overview of natural products in drug discovery. *Metabolites* **2012**, *2* (2), 303-336. DOI: 10.3390/metabo2020303.

(10) Cragg, G. M.; Newman, D. J. Natural products: A continuing source of novel drug leads. *Biochimica et Biophysica Acta* **2013**, *1830* (6), 3670-3695. DOI: 10.1016/j.bbagen.2013.02.008.

(11) Krishnamurti, C.; Rao, S. C. The isolation of morphine by Serturner. *Indian Journal of Anaesthesia* **2016**, *60* (11). DOI: 10.4103/0019-5049.193696.

(12) Pemberton, R. W. Insects and other arthropods used as drugs in Korean traditional medicine. *Journal of Ethnopharmacology* **1999**, *65* (3), 207-216. DOI: 10.1016/s0378-8741(98)00209-8.

(13) Alves, R. R. N.; Rosa, I. L.; Albuquerque, U. P.; Cunningham, A. B. Medicine from the Wild: An Overview of the Use and Trade of Animal Pro. *Animals in Traditional Folk Medicine* **2013**. DOI: 10.1007/978-3-642-29026-8_3.

(14) Cox, P. A.; Balick, M. J. The Ethnobotanical Approach to Drug Discovery. *Scientific American* **1994**, *270* (6), 82-87.

(15) Fullbeck, M.; Michalsky, E.; Dunkel, M.; Preissner, R. Natural products: sources and databases. *Natural product reports* **2006**, *23* (3), 347-356. DOI: 10.1039/b513504b.

(16) Cappello, E.; Nieri, P. From Life in the Sea to the Clinic: The Marine Drugs Approved and under Clinical Trial. *Life* **2021**, *11* (12). DOI: 10.3390/life11121390.

(17) Davies, J. Where have All the Antibiotics Gone? *Canadian Journal of Infectious Diseases and Medical Microbiology* **2006**, *17* (5), 287-290. DOI: 10.1155/2006/707296.

(18) Phillipson, J. D. Natural-Products as Drugs. *Transactions of the Royal Society of Tropical Medicine and Hygiene* **1994**, *88*, 17-19. DOI: Doi 10.1016/0035-9203(94)90464-2.

(19) Lewis, K. The Science of Antibiotic Discovery. *Cell* **2020**, *181* (1). DOI: 10.1016/j.cell.2020.02.056.

(20) Cacho, R. A.; Jiang, W.; Chooi, Y.-H.; Walsh, C. T.; Tang, Y. Identification and Characterization of the Echinocandin B Biosynthetic Gene Cluster from Emericella rugulosa NRRL 11440. *Journal of the American Chemical Society* **2012**, *134* (40), 16781-16790. DOI: 10.1021/ja307220z.

(21) Cereghetti, D. M.; Carreira, E. M. Amphotericin B: 50 Years of Chemistry and Biochemistry. *Synthesis* **2006**, *2006* (06), 0914-0942. DOI: 10.1055/s-2006-926368.

(22) Kingston, D. G. I.; Samranayake, G.; Ivey, C. A. The Chemistry of Taxol, a Clinically Useful Anticancer Agent. *Journal of Natural Products* **1990**, *53* (1), 1-12. DOI: 10.1021/np50067a001.

(23) Lü, S.; Wang, J. Homoharringtonine and omacetaxine for myeloid hematological malignancies. *Journal of Hematology and Oncology* **2014**, *7* (1), 2. DOI: 10.1186/1756-8722-7-2.

(24) Chin, Y. W.; Balunas, M. J.; Chai, H. B.; Kinghorn, A. D. Drug discovery from natural sources. *American Association of Pharmaceutical Scientists Journal* **2006**, *8* (2), E239-253. DOI: 10.1007/BF02854894.

(25) Walsh, C. Where will new antibiotics come from? *Nature Reviews Microbiology* **2003**, *1* (1), 65-70. DOI: 10.1038/nrmicro727.

(26) Wright, P. M.; Seiple, I. B.; Myers, A. G. The Evolving Role of Chemical Synthesis in Antibacterial Drug Discovery. *Angewandte Chemie International Edition* **2014**, *53* (34). DOI: 10.1002/anie.201310843.

(27) Pye, C.; Bertin, M.; Lokey, R.; Gerwick, W.; Linington, R. Retrospective analysis of natural products provides insights for future discovery trends. *Proceedings of the National Academy of Sciences* **2017**, *114* (22). DOI: 10.1073/pnas.1614680114.

(28) Fukuda, T. T. H.; Cassilly, C. D.; Gerdt, J. P.; Henke, M. T.; Helfrich, E. J. N.; Mevers, E. Research Tales from the Clardy Laboratory: Function-Driven Natural Product Discovery. *Journal of Natural Products* **2020**, *83* (3). DOI: 10.1021/acs.jnatprod.9b01086.

(29) Sairazi, N. S. M.; Sirajudeen, K. N. S. Natural Products and Their Bioactive Compounds: Neuroprotective Potentials against Neurodegenerative Diseases. *Evidence-Based Complementary and Alternative Medicine* **2020**, *2020*. DOI: 10.1155/2020/6565396.

(30) Wright, G. D. Unlocking the potential of natural products in drug discovery. *Microbial Biotechnology* **2019**, *12* (1). DOI: 10.1111/1751-7915.13351.

(31) Hutchings, M. I.; Truman, A. W.; Wilkinson, B. Antibiotics: past, present and future. *Current Opinion in Microbiology* **2019**, *51*. DOI: 10.1016/j.mib.2019.10.008.

(32) Santos, J. D.; Vitorino, I.; Reyes, F.; Vicente, F.; Lage, O. M. From Ocean to Medicine: Pharmaceutical Applications of Metabolites from Marine Bacteria. *Antibiotics (Basel)* **2020**, *9* (8). DOI: 10.3390/antibiotics9080455.

(33) Blunt, J.; Buckingham, J.; Munro, M. Taxonomy and Marine Natural Products Research. *Handbook of Marine Natural Products* **2012**. DOI: 10.1007/978-90-481-3834-0_1.

(34) Bandaranayake, W. M. The nature and role of pigments of marine invertebrates. *Natural product reports* **2006**, *23* (2), 223-255. DOI: 10.1039/b307612c.

(35) Bohlen, C. J.; Chesler, A. T.; Sharif-Naeini, R.; Medzihradszky, K. F.; Zhou, S.; King, D.; Sanchez, E. E.; Burlingame, A. L.; Basbaum, A. I.; Julius, D. A heteromeric Texas coral snake toxin targets acid-sensing ion channels to produce pain. *Nature* **2011**, *479* (7373), 410-414. DOI: 10.1038/nature10607.

(36) Soucy, S. M.; Huang, J.; Gogarten, J. P. Horizontal gene transfer: building the web of life. *Nature Reviews Genetics* **2015**, *16* (8), 472-482. DOI: 10.1038/nrg3962.

(37) Martens, J. H.; Barg, H.; Warren, M. J.; Jahn, D. Microbial production of vitamin B12. *Applied Microbiology and Biotechnology* **2002**, *58* (3), 275-285. DOI: 10.1007/s00253-001-0902-7.

(38) Webster, N. S.; Taylor, M. W. Marine sponges and their microbial symbionts: love and other relationships. *Environmental Microbiology* **2012**, *14* (2). DOI: 10.1111/j.1462-2920.2011.02460.x.

(39) Clark, V. C.; Raxworthy, C. J.; Rakotomalala, V.; Sierwald, P.; Fisher, B. L. Convergent evolution of chemical defense in poison frogs and arthropod prey between Madagascar and the

Neotropics. *Proceedings of the National Academy of Sciences* **2005**, *102* (33), 11617-11622. DOI: 10.1073/pnas.0503502102.

(40) Pawlik, J. R.; Kernan, M. R.; Molinski, T. F.; Harper, M. K.; Faulkner, D. J. Defensive chemicals of the Spanisch dancer nudibranch Hexabranchus sanguineus and its egg ribbons: macrolides derived from a sponge diet. *Journal of Experimental Marine Biology and Ecology* **1988**, *119* (2). DOI: 10.1016/0022-0981(88)90225-0.

(41) Tan, L. T. Impact of Marine Chemical Ecology Research on the Discovery and Development of New Pharmaceuticals. *Marine Drugs* **2023**, *21* (3). DOI: 10.3390/md21030174.

(42) Adnani, N.; Rajski, S. R.; Bugni, T. S. Symbiosis-inspired approaches to antibiotic discovery. *Natural product reports* **2017**, *34* (7). DOI: 10.1039/c7np00009j.

(43) Seyedsayamdost, M. R.; Carr, G.; Kolter, R.; Clardy, J. Roseobacticides: small molecule modulators of an algal-bacterial symbiosis. *Journal of the American Chemical Society* **2011**, *133* (45), 18343-18349. DOI: 10.1021/ja207172s.

(44) Nett, M.; Erol, Ö.; Kehraus, S.; Köck, M.; Krick, A.; Eguereva, E.; Neu, E.; König, G. M. Siphonazole, an Unusual Metabolite from Herpetosiphon sp. *Angewandte Chemie International Edition* **2006**, *45* (23). DOI: 10.1002/anie.200504525.

(45) Mans, D. R. Exploring the global animal biodiversity in the search for new drugs – Spiders, scorpions, horseshoe crabs, sea spiders, centipedes, and millipedes. *Journal of Translational Science* **2017**. DOI: 10.15761/JTS.1000197.

(46) Ødegaard, F. How many species of arthropods? Erwin's estimate revised. *Biological Journal of the Linnean Society* **2000**, *71* (4). DOI: 10.1111/j.1095-8312.2000.tb01279.x.

(47) Shear, W. A. Myriapodous arthropods from the Viséan of East Kirkton, West Lothian, Scotland. *Earth and Environmental Science Transactions of the Royal Society of Edinburgh* **1993**, *84* (3-4), 309-316. DOI: 10.1017/S026359330000612X.

(48) Marek, P. E.; Shear, W. A. Myriapods. *Current Biology* **2022**, *32* (23). DOI: 10.1016/j.cub.2022.09.058.

(49) Golovatch, S.; Kime, R. Millipede (Diplopoda) distributions: a review. *Soil Organisms* **2009**, *81*.

(50) Cloudsley-Thompson, J. On the responses to environmental stimuli, and the sensory physiology of Millipedes (Diplopoda). *Proceedings of the Zoological Society of London* **1951**, *121* (2). DOI: 10.1111/j.1096-3642.1951.tb00795.x.

(51) Shear, W. A. The chemical defenses of millipedes (diplopoda): Biochemistry, physiology and ecology. *Biochemical Systematics and Ecology* **2015**, *61*, 78-117. DOI: 10.1016/j.bse.2015.04.033.

(52) Rodriguez, J.; Jones, T. H.; Sierwald, P.; Marek, P. E.; Shear, W. A.; Brewer, M. S.; Kocot, K. M.; Bond, J. E. Step-wise evolution of complex chemical defenses in millipedes: a phylogenomic approach. *Scientific Reports* **2018**, *8* (1), 3209. DOI: 10.1038/s41598-018-19996-6.

(53) Sierwald, P.; Bond, J. E. Current Status of the Myriapod Class Diplopoda (Millipedes): Taxonomic Diversity and Phylogeny. *Annual Review of Entomology* **2007**, *52* (Volume 52, 2007), 401-420. DOI: 10.1146/annurev.ento.52.111805.090210.

(54) Eisner, T.; Alsop, D.; Hicks, K.; Meinwald, J. Defensive Secretions of Millipeds. In *Arthropod Venoms*, Bettini, S. Ed.; Springer Berlin Heidelberg, 1978; pp 41-72.

(55) Shear, W.; Jones, T.; Wesener, T. Glomerin and homoglomerin from the North American pill millipede Onomeris sinuata (Loomis, 1943) (Diplopoda, Pentazonia, Glomeridae). *International Journal of Myriapodology* **2011**, *4*. DOI: 10.3897/ijm.4.1105.

(56) Smolanoff, J.; Kluge, A. F.; Meinwald, J.; McPhail, A.; Miller, R. W.; Hicks, K.; Eisner, T. Polyzonimine: A Novel Terpenoid Insect Repellent Produced by a Milliped. *Science* **1975**, *188* (4189), 734-736. DOI: doi:10.1126/science.1124395.

(57) Meinwald, J.; Smolanoff, J.; McPhail, A. T.; Miller, R. W.; Eisner, T.; Hicks, K. Nitropolyzonamine: A spirocyclic nitro compound from the defensive glands of a milliped (polyzonium rosalbum). *Tetrahedron Letters* **1975**, *16* (28). DOI: 10.1016/0040-4039(75)80013-X.

(58) Wood, W. F.; Hanke, F. J.; Kubo, I.; Carroll, J. A.; Crews, P. Buzonamine, a new alkaloid from the defensive secretion of the millipede, Buzonium crassipes. *Biochemical Systematics and Ecology* **2000**, *28* (4), 305-312. DOI: 10.1016/S0305-1978(99)00068-X.

(59) Eisner, H.; Eisner, T.; Hurst, J. Hydrogen cyanide and benzaldehyde produced by millipedes. *Chemistry and Industry* **1963**, (3), 124-125.

(60) Weatherston, J.; Tyrrell, D.; Percy, J. E. Long chain alcohol acetates in the defensive secretion of the millipede Blaniulus guttulatus. *Chemistry and Physics of Lipids* **1971**, *7* (1), 98-100. DOI: 10.1016/0009-3084(71)90023-5.

(61) Duffield, R. M.; Blum, M. S.; Brand, J. M. Guaicol in the Defensive Secretions of Polydesmid Millipedes. *Annals of the Entomological Society of America* **1974**, *67* (5), 821-822. DOI: 10.1093/aesa/67.5.821.

(62) Moritz, L.; Blanke, A.; Hammel, J. U.; Wesener, T. First steps toward suctorial feeding in millipedes: Comparative morphology of the head of the Platydesmida (Diplopoda: Colobognatha). *Invertebrate Biology* **2021**, *140* (2), e12312. DOI: 10.1111/ivb.12312.

(63) Golovatch, S.; Evsyukov, A.; Reip, H. S. Colobognatha millipedes in the Caucasus (Diplopoda: Polyzoniida, Platydesmida, Siphonocryptida). *Zootaxa* **2015**, *3972* (2). DOI: 10.11646/zootaxa.3972.2.6.

(64) Macias, A. M.; Marek, P. E.; Morrissey, E. M.; Brewer, M. S.; Short, D. P. G.; Stauder, C. M.; Wickert, K. L.; Berger, M. C.; Metheny, A. M.; Stajich, J. E.; et al. Diversity and function of fungi associated with the fungivorous millipede, Brachycybe lecontii. *Fungal Ecology* **2019**, *41*, 187-197. DOI: 10.1016/j.funeco.2019.06.006.

(65) Roper, H. Ergebnisse chemisch-analytischer Untersuchungen der Wehrsekrete von Spirostreptiden, Spiroboliden und Juliden (Diplopoda), von Peripatopsis (Onychophora) und von Polyzonium (Diplopoda, Colobognatha). *Abhandlungen und Verhandlungen* **1978**.

(66) Jones, T. H.; Harrison, D. P.; Menegatti, C.; Mevers, E.; Knott, K.; Marek, P.; Hennen, D. A.; Kasson, M. T.; Macias, A. M.; Lovett, B.; et al. Deoxybuzonamine Isomers from the Millipede Brachycybe lecontii (Platydesmida: Andrognathidae). *Journal of Natural Products* **2022**, *85* (4), 1134-1140. DOI: 10.1021/acs.jnatprod.2c00077.

(67) Buckett, J. S.; Gardner, M. R. A Review of the Genus Gosodesmus Chamberlin, with the Synonymy of Eucybe Chamberlin (Diplopoda: Platydesmida: Andrognathidae). *Journal of the New York Entomological Society* **1969**, *77* (1), 40-50.

(68) Hassler, M. F.; Harrison, D. P.; Jones, T. H.; Richart, C. H.; Saporito, R. A. Gosodesmine, a 7-Substituted Hexahydroindolizine from the Millipede Gosodesmus claremontus. *Journal of Natural Products* **2020**, *83* (9). DOI: 10.1021/acs.jnatprod.0c00722.

(69) Dewick, P. *Medicinal Natural Products*; 2009. DOI: 10.1002/9780470742761.

(70) Zhu, J.; Iannucci, A.; Dani, F. R.; Knoll, W.; Pelosi, P. Lipocalins in Arthropod Chemical Communication. *Genome Biology and Evolution* **2021**, *13* (6). DOI: 10.1093/gbe/evab091.

(71) Adams, R. M. M.; Wells, R. L.; Yanoviak, S. P.; Frost, C. J.; Fox, E. G. P. Interspecific Eavesdropping on Ant Chemical Communication. *Frontiers in Ecology and Evolution* **2020**, *8*. DOI: 10.3389/fevo.2020.00024.

(72) Stankovic, S.; Dimkic, I.; Vujisic, L.; Pavkovic-Lucic, S.; Jovanovic, Z.; Stevic, T.; Sofrenic, I.; Mitic, B.; Tomic, V. Chemical Defence in a Millipede: Evaluation and Characterization of Antimicrobial Activity of the Defensive Secretion from Pachyiulus hungaricus (Karsch, 1881) (Diplopoda, Julida, Julidae). *Public Library of Science One* **2016**, *11* (12). DOI: 10.1371/journal.pone.0167249.

(73) Carrel, J. E.; Eisner, T.; Carrel, J. E.; Eisner, T. Spider sedation induced by defensive chemicals of milliped prey. *Proceedings of the National Academy of Sciences* **1984**, *81* (3). DOI: 10.1073/pnas.81.3.806.

(74) Hash, J. M.; Millar, J. G.; Heraty, J. M.; Harwood, J. F.; Brown, B. V. Millipede Defensive Compounds Are a Double-Edged Sword: Natural History of the Millipede-Parasitic Genus Myriophora Brown (Diptera: Phoridae). *Journal of Chemical Ecology* **2017**, *43* (2), 198-206. DOI: 10.1007/s10886-016-0815-7.

(75) Banks, P.; Funkhouser, E. M.; Macias, A. M.; Lovett, B.; Meador, S.; Hatch, A.; Garraffo, H. M.; Cartwright, K. C.; Kasson, M. T.; Marek, P. E.; et al. The Chemistry of the Defensive Secretions of Three Species of Millipedes in the Genus Brachycybe. *Journal of Chemical Ecology* **2024**, *50* (9), 478-488. DOI: 10.1007/s10886-024-01518-6.

(76) Menegatti, C.; Wood, J. S.; Banks, P.; Knott, K.; Briganti, J. S.; Briganti, A. J.; McNally, S. V. G.; Marek, P. E.; Brown, A. M.; Jones, T. H.; et al. Neuromodulating Alkaloids from Millipede Defensive Secretions. *Journal of Natural Products* **2024**. DOI: 10.1021/acs.jnatprod.4c01162.

(77) Banks, P.; Menegatti, C.; Knott, K.; Marek, P.; Mevers, E. Chemical Diversity of Millipede Defensive Alkaloids Provides Insights into their Evolutionary History. **2025**. DOI: 10.26434/chemrxiv-2025-tdt3n.

(78) Nguyen, L.; Lucke-Wolds, B. P.; Mookerjee, S.; Kaushal, N.; Matsumoto, R. R. Sigma-1 Receptors and Neurodegenerative Diseases: Towards a Hypothesis of Sigma-1 Receptors as Amplifiers of Neurodegeneration and Neuroprotection. *Advances in experimental medicine and biology* **2017**, *964*. DOI: 10.1007/978-3-319-50174-1_10.

Chapter 2.

The Chemistry of the Defensive Secretions of Three Species of Millipedes in the Genus *Brachycybe*

Paige Banks[1], Emma M Funkhouser[2], Angie M Macias[3], Brian Lovett[4], Shelby Meador[3], Arden Hatch[1], H Martin Garraffo[5,6], Kaitie C Cartwright[2], Matt T Kasson[3], Paul E Marek[7], Tappey H Jones[2], Emily Mevers[1]

1. Department of Chemistry, Virginia Tech, Blacksburg, VA, 24061, USA.
2. Department of Chemistry, Virginia Military Institute, Lexington, VA, 24450, USA.
3. Division of Plant and Soil Sciences, West Virginia University, Morgantown, WV, 26506, USA.
4. Emerging Pests and Pathogens Research Unit, USDA ARS, Ithaca, NY, 14853, USA.
5. National Institute of Diabetes and Digestive and Kidney Diseases, National Institutes of Health, Bethesda, MD, 20892, USA.
6. National Institute of Standards and Technology, Gaithersburg, MD, 20899, USA.
7. Department of Entomology, Virginia Tech, Blacksburg, VA, 24061, USA.

2.0. Abstract

Millipedes have long been known to produce a diverse array of chemical defense agents that deter predation. These compounds, or their precursors, are stored in high concentration within glands (ozadenes) and are released upon disturbance. The subterclass Colobognatha contains four orders of millipedes, all of which are known to produce terpenoid alkaloids—spare the Siphonophorida that produce terpenes. Although these compounds represent some of the most structurally intriguing millipede-derived natural products, they are the least studied class of millipede defensive secretions. Here, we describe the chemistry of millipede defensive secretions from three species of *Brachycybe*: *B. producta*, *B. petasata*, and *B. rosea*. Chemical investigations

using mass spectrometry-based metabolomics, chemical synthesis, and 2D NMR led to the identification of five alkaloids, three of which are new to the literature. All identified compounds are monoterpene alkaloids with the new compounds representing indolizidine (i.e. hydrogosodesmine) and quinolizidine alkaloids (i.e. homogosodesmine and homo-hydrogosodesmine). The chemical diversity of these compounds tracks the known species phylogeny of this genus, rather than the geographical proximity of the species. The indolizidines and quinolizidines are produced by non-sympatric sister species, *B. producta* and *B. petasata*, while deoxybuzonamine is produced by another set of non-sympatric sister species, *B. rosea* and *B. lecontii*. The fidelity between the chemical diversity and phylogeny strongly suggests that millipedes generate these complex defensive agents *de novo* and begins to provide insights into the evolution of their biochemical pathways.

2.1. Introduction

Millipedes (class: Diplopoda) produce a myriad of defensive chemicals, including hydrogen cyanide, oxidized aromatics (e.g., benzoquinones), and alkaloids (e.g., quinazolinone and terpene alkaloids).[1] These compounds are stored in high concentrations in ozadenes (or rapidly generated from biological inert precursors) and the millipedes release the defensive agents when disturbed.[2,3] Some other millipedes use chemical secretions for defense against parasites and microbes, protection during the process of molting, and crypsis and background matching.[4-8] 385-million-year-old Devonian fossil millipedes show the first evidence of chemical defenses on land from the presence of ozopores (openings of the ozadenes) that line the length of the fossilized body.[9] Plausible origins of chemical defenses in millipedes are even older and their exclusive presence in the subclass Chilognatha indicates a Silurian origin 426 million years ago.[10] The evolutionary development of millipede defense glands appears similar to other arthropods in which cuticular invaginations became lined with glands to produce chemicals. Over evolutionary time, glands diversified into three or four types: (1) bilateral single-chambered glands of Juliformia and Nematophora, (2) median Y-shaped glands of Glomerida, and (3) bilateral bipartite glands of Polydesmida.[1,11] The defense glands of *Brachycybe lecontii* were described as long slender tubes, indicative of a fourth gland morphotype.[2,12] However, later authors showed that the gland architecture of *B. lecontii* is tear-drop-shaped and more voluminous than previously described and consists of a single chamber (akin to a type 1 glands) containing the defense secretions connected to a duct leading from the ozadene to the ozopore.[13] Bipartite and Y-shaped glands are ostensibly derived from single-chambered glands, but gland morphotype is known from a limited set of taxa, and a fully resolved phylogeny of millipedes with representatives of each order is not yet available as a context to address questions about gland morphological evolution.

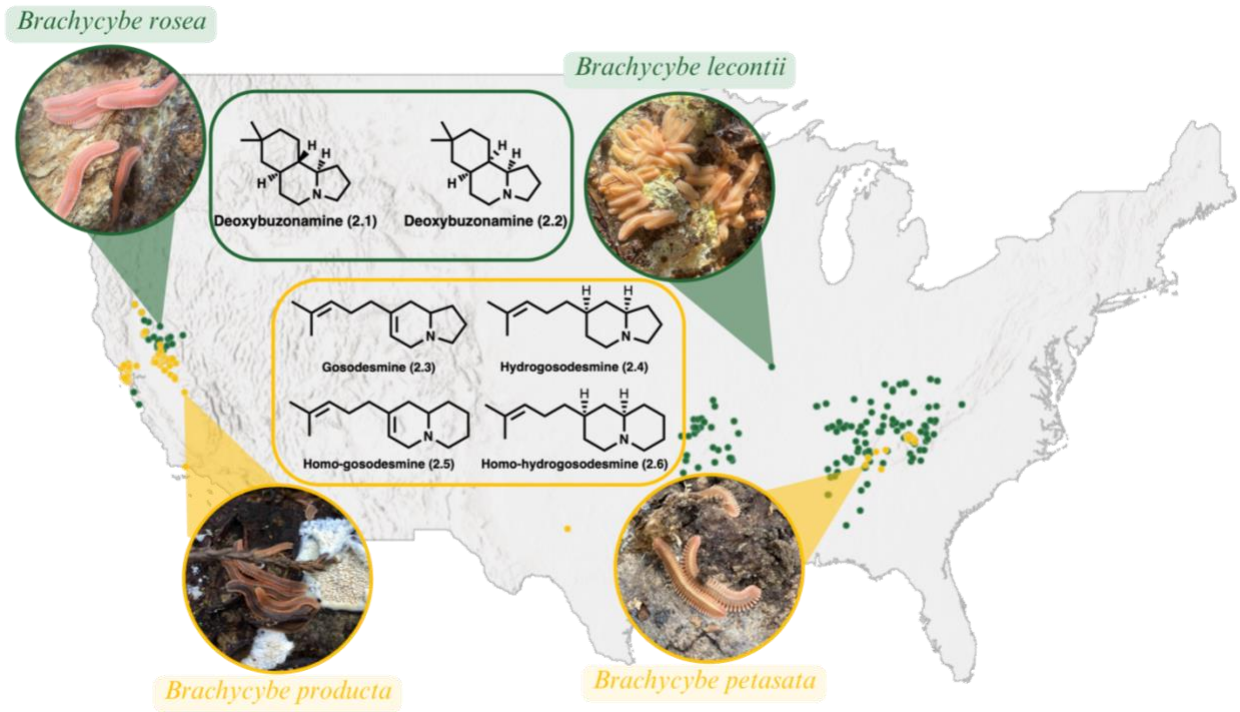

Figure 2.1. Geographic distribution of *Brachycybe lecontii* and *B. rosea*, with their associated defensive agents, deoxybuzonamine isomers (**2.1** and **2.2**) and *B. producta* and *B. petasata*, with their defensive agents gosodesmine (**2.3**), hydrogosodesmine (**2.4**), homogosodesmine (**2.5**) and homo-hydrogosodesmine (**2.6**).

Of the known defensive chemicals, the alkaloids are the most structurally intriguing and least studied. Structurally, these compounds can be classified into two groups: the quinazolinone alkaloids (e.g., glomerin and homoglomerin) and terpenoid alkaloids (e.g., polyzonimine and buzonamine).[14-16] The quinazolinone alkaloids are produced by pill millipedes from the order Glomerida and appear to be derived from benzoic acid (shikimate pathway) and hydrogen cyanide.[17] Therefore, these structures represent a hybrid between the oxidized aromatic and hydrogen cyanide products, making them pseudoalkaloids. Conversely, the terpenoid alkaloids are produced by a single subterclass, the Colobognatha (fungus-feeding millipedes). This subterclass is composed of four orders (Platydesmida, Polyzoniida, Siphonocryptida and Siphonophorida) and

all are known to produce simple monoterpenes (pinenes and limonene), along with various heterocyclic terpenoid alkaloids [**Figure 2.1**; e.g. deoxybuzonamines (**2.1** and **2.2**), and gosodesmine (**2.3**)].[1,18,19] However, the terpenoid alkaloids can be further separated into two structural classes, the spirocyclic (e.g., polyzonimine and nitropolyzonamine) and heterocyclic alkaloids (e.g., buzonamine and gosodesmine).[14,15,18,20] Both classes incorporate a monoterpene, as evident by the *gem*-dimethyl moiety. For the heterocyclic alkaloids, the nitrogen is likely derived from an amino acid, either proline or ornithine, making these metabolites true alkaloids.[17] Although the alkaloids are less studied than the other classes of defensive secretions, there are recent reports describing new compounds representing both the heterocyclic and spirocyclic families of alkaloids. This includes the discovery of deoxybuzonamine isomers and acetylated 3-hydroxynitropolyzonamine.[19,21] Interestingly, the spirocyclic alkaloids are known to be sequestered by neotropical frogs for defensive purposes.[22]

Members of the millipede order Platydesmida have intriguing qualities, such as egg brooding, and other quasisocial traits, and are almost exclusively associated with various fungal taxa, which some consume in unusual circular social aggregations called pinwheels.[13,23] All of the species of the Platydesmida with characterized chemical secretions, and its evolutionary sister Polyzoniida,[10] have disparate heterocyclic terpenoid alkaloids, including *B. lecontii* from the eastern U.S. that produces compounds **2.1** and **2.2**, and *Gosodesmus claremontus* from California and Oregon that produces **2.3** (**Figure 2.1**).[18,19] Interestingly, co-occurrence of species from the same genera does not correlate with phylogenetic relationship. For example, *B. lecontii* is sympatric with *B. petasata*, but *B. lecontii's* closest evolutionary sister is *B. nodulosa*, endemic to Japan.[24] To date, it is unknown how the chemical diversity of the defensive secretions relates to the reported phylogenetic relationship. Herein, we investigated the composition of the defensive

secretions of three unstudied species of *Brachycybe*—*B. petasata*, *B. producta*, and *B. rosea*—to gain a better understanding of the relationship between phylogeny and defensive secretions.

2.2. Results

Initial examination of methanol extracts from the collections of millipedes revealed that *B. petasata* and *B. producta* produce four alkaloids, while *B. rosea* has only one alkaloid that is dissimilar from the other two millipedes (**Table 2.1**, **Figure 2.7.1**–**Figure 2.7.3**). There is a bit of variability in the abundance of some of the alkaloids, but this is likely resulting from the size of the collections. The sole alkaloid peak in the *B. rosea* extracts matched both the retention time (17.7 min) and fragmentation of one of the previously identified deoxybuzonamine isomers (**2.1**) originally isolated from *B. lecontii* (**Figure 2.7.5**).[19] The major components in the *B. petasata* and *B. lecontii* extracts were separated by 14 Da [*B. petasata* - M^+ 205 (**2.3**) and 219 (**2.5**); *B. producta* - M^+ 207 (**2.4**) and 221 (**2.6**)] and the difference between the major components of the distinct millipede species was 2 Da. In *B. petasata* extracts, the first eluting alkaloid (M^+ 205) had an identical mass spectrum and retention time with an authentic sample of gosodesmine (**2.3**).[18] The other major alkaloids had no matches to known natural products; however, analysis of their fragmentation suggested they were structurally related to **2.3**.

Table 2.1. Percentage of alkaloid detected in different collections

Collection/ site	Species	M^+ (compound)/Retention index				
		207 (**2.1**)/ 1419	205 (**2.3**)/ 1414	207 (**2.4**)/ 1446	219 (**2.5**)/ 1518	221 (**2.6**)/ 1550
MTK-GA-21-BPE13	*B. petasata*	n.d.	48	n.d.	49	trace
PEM-2021-007	*B. petasata*	n.d.	21	trace	19	59
PEM-2021-008	*B. petasata*	n.d.	7	37	49	20
MTK-CA-21-05	*B. producta*	n.d.	1.5	52	trace	48
MTK-CA-21-06	*B. producta*	n.d.	trace	43	trace	57
AH-CA-23-11	*B. producta*	n.d.	15	34	trace	51
MTK-CA-21-12	*B. rosea*	100	n.d.	n.d.	n.d.	n.d.
MTK-CA-21-13	*B. rosea*	100	n.d.	n.d.	n.d.	n.d.
MTK-CA-21-03	*B. rosea*	100	n.d.	n.d.	n.d.	n.d.
Dickson Co., TN[1]	*B. lecontii*	100	n.d.	n.d.	n.d.	n.d.

[1]Previously reported (Jones et al. 2022), trace = < 1% area, n.d. = not detected

To understand the structural features of the new metabolites, the crude extracts were chemically derivatized and then analyzed by GCMS. First, it was hypothesized that the mass difference of 2 Da between the major compounds in *B. petasata* (**2.3** and **2.5**) and *B. producta* (**2.4**

and **2.6**) is indicative of a loss of a degree of unsaturation—either the elimination of one of the olefins or a loss of one of the rings. The former is a typical post-modification event therefore this was believed to be more likely. So, a small aliquot of representative samples of each crude extract were treated with hydrogenation conditions to reduce all olefins. Subsequent GCMS analysis revealed the presence of the same two saturated amines in both derivatized crude extracts, including the known 7-(4-methylpentyl)-indolizidine (**2.7**) and a metabolite that was 14 mass units larger (**Figure 2.7.5** and **Figure 2.7.6**). We suspected the larger metabolite was likely 2-(4-methylpentyl)-quinolizidine (**2.8**). Synthesis of **2.8** was accomplished using a similar approach to the method previously reported for **2.7** but started from 2-quinolizidone. The synthetic material possessed the same GC fragmentation and retention time, thus confirming the carbon skeleton of the three new analogs, **2.4–2.6** (**Figure 2.7.7** and **Figure 2.7.8**).[18,19] Compounds **2.3** and **2.4** incorporate indolizidine rings, and **2.5** and **2.6** incorporate quinolizidine rings (**Figure 2.2**).

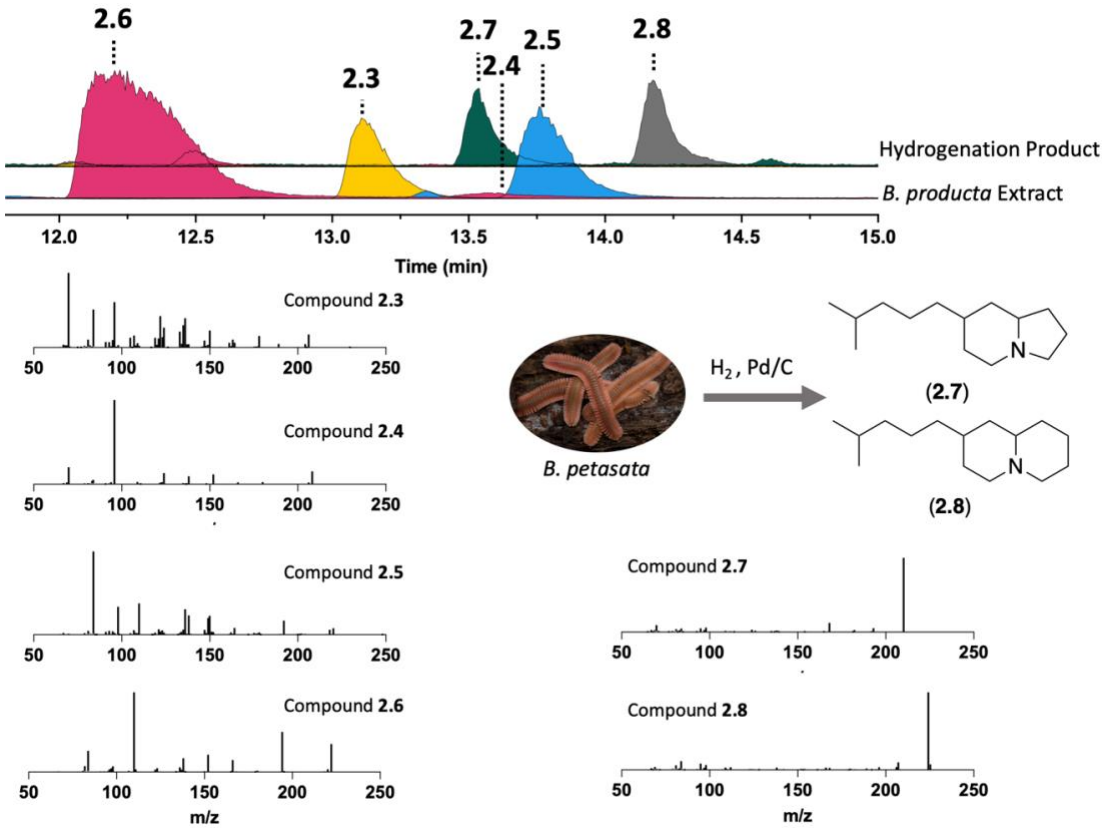

Figure 2.2. Extracted ion chromatograms (EICs) of the unreacted *B. producta* extract and hydrogenation product. Bottom chromatogram contains EICs of **2.3**–**2.6** (206, 208, 220, and 222 *m/z*) (PEM 2021-007), while the top chromatogram contains the same EICs plus **2.7** and **2.8** (210 and 224 *m/z*). The ion counts for the EICs associated with the crude extract were divided by an order of magnitude to scale to the hydrogenation reaction mixture. Spectra below chromatograms are LTQ tandem MS fragmentation patterns (35 eV) for compounds **2.3–2.8**.

Compound **2.5** was hypothesized to be structurally similar to **2.3** but contains a quinolizidine ring rather than indolizidine. To confirm this, we attempted a total synthesis (**Scheme 2.1**), which began by carbodiimide coupling of 6-methyl-1-(piperidin-2-yl)hept-5-en-2-one (**2.9**) with diethylphosphonoacetic acid to yield **2.10**.[25] This was followed by an intramolecular Horner-Wadsworth-Emmons cyclization that cleanly provided 2-(4-methylpent-3-en-1-yl)-7,8,9,9a-tetrahydro-1*H*-quinolizin-4(6*H*)-one (**2.11**).[26] Subsequent treatment with lithium aluminum

hydride to reduce the lactam gave what was predicted to be **2.5**, which we have named homogosodesmine. GCMS comparison of the synthetically derived material with the crude extract confirmed the structure of **2.5** as both the mass spectrum and GC retention time matched (**Figure 2.7.12–Figure 2.7.16**; **Table 2.8.1**). Additionally, catalytic hydrogenation of a sample of synthetic **2.5** provided a mixture of isomers of **2.8** whose mass spectra and GC retention times were identical to those obtained from the hydrogenation of the millipede extracts.

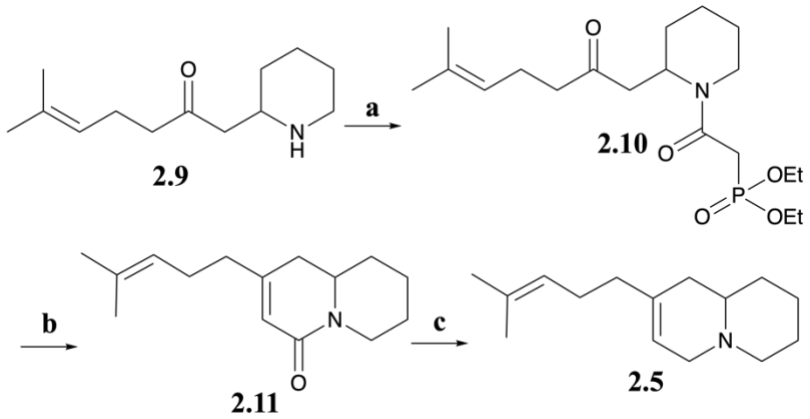

Scheme 2.1. Synthesis of homogosodesmine (**2.5**). 6-methyl-1-(piperidin-2-yl)hept-5-en-2-one (**2.9**) a) EDCI, diethylphosphono acetic acid, DMF, 16 h, rt yields, **2.10**; b) DBU, LiCl, MeCN, 16 h, rt, yields 2-(4-methylpent-3-en-1-yl)-7,8,9,9a-tetrahydro-1*H*-quinolizin-4(6*H*)-one (**2.11**); c) $LiAlH_4$, diethyl ether, 3 h, rt, yields **2.5**.

Compounds **2.4** and **2.6** are close structural analogs of **2.3** and **2.5**, respectively, but based on the hydrogenation experiment they have only one olefin. Both alkaloids showed a loss of 85 Da in their mass spectra, which is typical of a loss of C_6H_{13}. This loss was observed in the mass spectra of **2.7** and **2.8** and represented the loss of the saturated side chain from the heterocyclic core, so initially we hypothesized that the olefin was within the ring systems. Fortuitously, treatment of a portion of the crude extract with dilute HCl (aq) and subsequent neutralization resulted in the addition of water (**Figure 2.7.17**). The mass spectra of the hydrate adduct showed a loss of methyl (15 Da), intense ions for the loss of C_3H_7O fragment (59 Da) as well as the

corresponding fragment at 59 *m/z* that would be expected from a dimethyl tertiary alcohol (**Figure 2.7.18**). Thus, indicating that the olefin in **2.4** and **2.6** is on the sidechain opposed to within the bicyclic system. Since *B. petasata* produces all four analogs, they are likely the product of the same biosynthetic pathway with the olefins installed at the same position. Therefore, we hypothesized that the sole olefin in **2.4** and **2.6** was most likely between C-11 and C-12. The observed loss of 85 Da in **2.3** and **2.5** is hypothesized to result from a radical rearrangement that shifts the olefin to the bicyclic system (**Figure 2.7.19**).

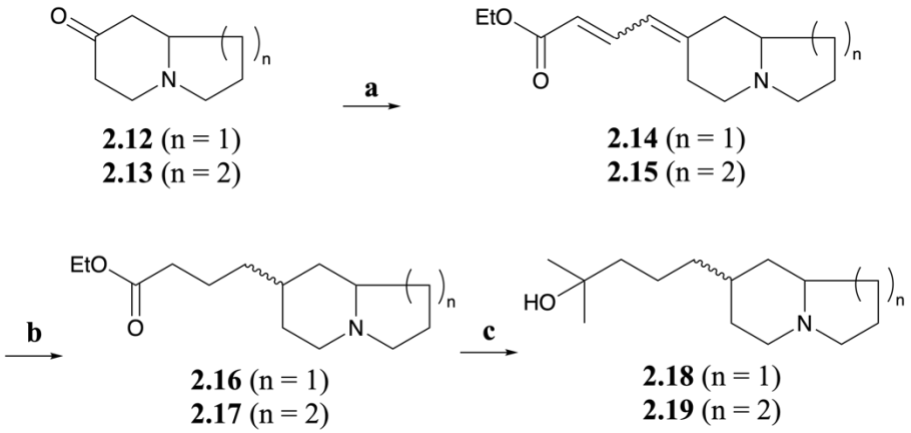

Scheme 2.2. Synthesis of water adducts of **2.4** and **2.6**. Starting with **2.12** and **2.13** a) triethyl-4-phosphonocrotonate, THF, 0 °C to rt, 16 h, yields **2.14** and **2.15**; b) 10% Pd/C, EtOH, 3 atm, 45 min, rt, yields **2.16** and **2.17**; c) MeMgCl, THF, 16 h, rt, yields **2.18** and **2.19**.

To confirm these hypotheses, total syntheses were attempted to produce both the hydrate adducts of **2.4** and **2.6** from 8-indolizidone and 2-quinolizidone, respectively (**Scheme 2.2**). First, **2.12** and **2.13** were reacted with triethylphosphonocrotonate via a Horner-Wadsworth-Emmons reaction to form **2.14** and **2.15** (**Figure 2.7.20** and **Figure 2.7.21**). Followed by hydrogenation, forming **2.16** and **2.17**. Crude reaction mixtures were subsequently hydrogenated and treated with excess methyl magnesium chloride to yield hydroxy indolizidine (**2.18**) and hydroxy quinolizidine (**2.19**) (**Figure 2.7.22–Figure 2.7.25**).[27] Both product mixtures consisted of a 3:1 mixture of

diastereomers, and the mass spectrum and retention time of the major (first eluting isomer) matched those of the hydrated natural alkaloids (**Figure 2.7.26** and **Figure 2.7.27**). Unfortunately, we were unable to separate the diastereomers using a range of LC methods and columns, so the products were analyzed by 2D NMR as mixtures (**Figure 2.7.28**–**Figure 2.7.39**; **Table 2.8.2–Table 2.8.5**). This led to complete assignments of both isomers for **2.18** and **2.19**, with the major isomer in both samples exhibiting a clear ROESY correlation between the two stereogenic methines, indicating a *syn* orientation. This was supported by the lack of a ROESY correlation between the same methines for the minor isomer (*anti* orientation).

In November 2023, we made a fortuitous collection of *B. producta* and this material was successfully used to isolate small quantities of both the hydro-analogs, **2.4** and **2.6**. Approximately 30 millipedes were extracted in methanol, and analysis of the crude extract by LCMS revealed both **2.4** and **2.6** as major components, while **2.3** and **2.5** were not present. RP-HPLC purification led to less than 0.5 mg of both **2.4** and **2.6**. Analysis of both compounds by 2D NMR confirmed their planar structures (**Table 2.8.6** and **Table 2.8.7**, **Figure 2.7.40**—**Figure 2.7.50**). In addition, a clear ROESY correlation was observed between H-3 and H-5 indicating a *syn* relationship between the methines. Assigning the absolute stereoconfiguration will require an enantiopure total synthesis of all four natural metabolites.

This investigation describes the chemistry of the defensive secretions from three previously unstudied species of *Brachycybe* millipedes, two of which are sister species (*B. petasata* and *B. producta*), and another closely related species (*B. rosea*). Although the sister species are non-sympatric—*B. petasata* is found on the East Coast and *B. producta* is found on the West Coast of the U.S.—both produce the same bicyclic monoterpene alkaloids (**2.3–2.6**). Their secretions consist of two indolizidines [gosodesmine (**2.3**) and hydrogosodesmine (**2.4**)] and their

quinolizidine homologs [homogosodesmine (**2.5**) and homo-hydrogosodesmine (**2.6**)], marking the first time a quinolizidine-containing natural product has been isolated from a millipede. In addition, the presence of indolizidine and quinolizidine concomitants in the millipede secretions is reminiscent of the pumiliotoxins (indolizidines) and homopumiliotoxins (quinolizidines) that are found within the skin of poison dart frogs. Although originally discovered from studies of poison dart frogs, it has since been determined that the frogs acquire these defensive agents from their arthropod diet, particularly oribatid mites.[28-30] The pumiliotoxins are believed to serve as defensive metabolites as they exhibit potent toxicity against mice, with LD_{50} of 20 to 50 μg.[30,31]

2.3. Discussion

While the chemical identity of these alkaloids has been elucidated, their ecological function and the evolution of their biosynthesis remains unclear. The volume, concentration, and apparent effect on the millipedes' predators, such as ants (rapid motor incapacitation), strongly implies a strong deterrent effect.[3,32,33] In support of a defensive role, many millipedes, including those producing alkaloids, secrete visible secretions from their ozopores (openings of the ozadenes, defense glands) when physically disturbed.[34] This includes the secretion of a white, milk-like substance when collected with forceps (field observations). In addition, there are a few examples of the alkaloids themselves deterring predation experimentally. For example, **2.1** has been shown to reduce the rate of attack by *Formica* ants when experimentally applied to mealworms, and polyzonimine produced by *Petaserpes rosalbus*, is known to act as an insect repellent at concentrations as low as 100 nM.[15,20] Thus, existing literature strongly supports a defensive role of the terpenoid alkaloid secretions. However, Shear (2015) raised the possibility that some of these compounds may also act as pheromones facilitating aggregation, as some members of the subterclass Colobognatha are social millipedes and are known to form aggregates on the

undersides of decaying logs.[1] Moreover, there are examples of high viscosity "sticky" components of secretions in Glomerida, Chordeumatida, and Siphonophorida.[3-5,32,33] The functions of these are unclear, but functional hypotheses have been made such as clinging to stones, an antipredatory or antiparasite role, or a soil-shedding mechanism to allow efficient burrowing.[5]

To date, sixteen terpenoid alkaloids have been isolated from ten genera of millipedes, all within the subterclass Colobognatha—spare Siphonophorida that produces monoterpenes.[1,21] The chemical diversity of the alkaloids varies across the millipede phylogeny where the monoterpene alkaloids (**2.1–2.6**, and buzonamine) are produced by species of millipedes within two orders, Platydesmida and Polyzoniida, and spiro-alkaloids, such as polyzonimine, are found within Siphonocryptida and Polyzoniida. The buzonamine, indolizidine and quinolizidine monoterpene alkaloids appear to each consist of a monoterpene and pyrrolidine or piperidine but have undergone different cyclization steps. Further analysis of the monoterpene alkaloids, the bicyclic analogs (**2.3–2.6**) have only been isolated from two genera of millipedes, all belonging to Platydesmida, while the tricyclic monoterpenes have been isolated from genera representing both Platydesmida and Polyzoniida. Through this study, we have discovered that this tight relationship between phylogeny and chemical diversity holds true down to sister species. Despite *B. lecontii* and *B. petasata* both being known from the eastern U.S., even co-occurring on the same decaying logs at some sites, *B. petasata* is not the closest evolutionary sister of *B. lecontii*. Instead, the closest evolutionary sister of *B. lecontii* is *B. nodulosa*, endemic to Japan, and *B. rosea*, endemic to California. Based on a phylogeny of *Brachycybe* by Brewer*, et al.* (2012), *B. petasata* is closely related to *Brachycybe producta*, a species from California.[24] Similarly, *B. producta* co-occurs with *Brachycybe rosea*, the latter which is more closely related to *B. lecontii* and *B. nodulosa*. The chemistry of their defensive secretions follows this evolutionary relationship, where *B. lecontii*

and *B. rosea* produce the same tricyclic secretion (e.g., **2.1**), while *B. petasata* and *B. producta* both produce the same bicyclic secretions (e.g., **2.3–2.6**). This strong relationship between defensive gland secretion chemistry and phylogeny indicates that the millipedes are themselves producing the secretions *de novo* and suggests that the chemical diversity within the terpenoid alkaloids may arise from the evolution of cyclase genes.

The discovery of these new terpenoid alkaloids adds to the growing knowledge of millipede defensive secretions and is beginning to provide insights into how these compounds might be biosynthesized and their evolution within millipedes. However, additional chemical investigations into unstudied millipedes belonging to the subterclass Colobognatha are necessary to provide insights into key biosynthetic transformations and to fully understand the evolution of this interesting class of compounds. To date, eleven genera of Platydesmida, and 59 species have not yet been chemically investigated, and this cohort undoubtedly includes new terpenoid alkaloids yet to be discovered. This includes many related species, such as *B. nodulosa* from Japan and *B. picta* (sympatric to *B. producta)* from California, with the latter representing the earliest-diverging *Brachycybe* species that is evolutionary sister to others in the genus. Future analyses will undoubtedly provide additional insights into the evolution of these compounds.

2.4. Experimental Methods

2.4.1. General Experimental Procedures

NMR spectra were recorded with deuterated DMSO with the residual solvent peak as an internal standard (δ_C 39.5, δ_H 2.50) on Bruker Avance III 600 MHz instrument equipped with a triple resonance inverse (CP-TCI) Prodigy N_2 cooled CryoProbe (600 and 150 MHz for ^{1}H and ^{13}C NMR, respectively) and a JEOL 400 MHz NMR spectrometer. GCMS was carried out in the electron impact (EI) mode using a Shimadzu QP-2020. LR-LCMS data was obtained using an

Agilent 1200 series HPLC system equipped with a photo-diode array detector and a Thermo LTQ mass spectrometer. HRESIMS was carried out using a Shimadzu LC-q-TOF Mass Spectrometer equipped with a HPLC system. HPLC purifications were carried out using Agilent 1200 series or 1260 Infinity II HPLC systems (Agilent Technologies) equipped with a photodiode array detector. All solvents were of HPLC quality. Optical rotation was measured using a JASCO P-2000 polarimeter.

2.4.2. Millipede Collections

The millipedes were collected at the following locations. (1) *B. petasata*, Haywood Co., North Carolina, Balsam Mountain Campground, nature trail, 35.56764°N, -83.17651°W, Elev. 1622 m, 27 September 2021 (PEM-2021-007, habitat of hemlock, maple, birch/beech); (2) *B. petasata*, Sevier Co., Tennessee, Great Smoky Mountains, Mt. LeConte, Alum Cave Trail, 35.63998°N, -83.44023°W, Elev. 1409 m, 28 September 2021, (PEM-2021-008, habitat *Rhododendron* cove); (3) *B. petasata*, Dade Co., Georgia, Cloudland Canyon State Park, forested area along roadside across from the visitor center, 34.817213°N, -85.487654°W, Elev. 563 m, 15 March, 2021 (MTK-GA-21-BPE13); (4) *B. producta*, Marin Co., California, Lake Lagunitas, Marin Municipal Water District, adjacent to Lake Lagunitas Loop Trail 37.946577°N, -122.597678°W, Elev. 247 m, 5 December 2021 (MTK-CA-21-5); (5) *B. producta*, Marin Co., California, Lake Lagunitas, Marin Municipal Water District, adjacent to Indian Fire Road, Eldridge Grade on Mount Tamalpais 37.934565°N, -122.572577°W, Elev. 418 m, 5 December 2021 (MTK-CA-21-6); (6) *B. rosea*, El Dorado Co., California, El Dorado Irrigation District, Sly Park Recreation Area, forested area adjacent to Miwok trail 38.732112°N, -120.559085°W, Elev. 1083 m, 11 December 2021 (MTK-CA-21-12); (7) *B. rosea*, San Mateo Co., California, Edgewood Park and Nature Preserve, edge of ravine next to restrooms, 37.472201°N, -122.278708°W, Elev. 83 m,

4 December 2021 (MTK-CA-21-3); and (8) *B. rosea*, Tahoe National Forest, Upper Carlton Campground, 39.520737°N, -120.996210°W, Elev. 712 m, 10 December 2021 (MTK-CA-21-13). All collections were placed in small vials with a few mL of methanol for preservation and immediate extraction of the defensive secretions. Voucher specimens have been deposited as natural history specimens in the Virginia Tech Insect Collection (https://collection.ento.vt.edu/).

2.4.3. General GCMS Method Used for All Analyses Described Below

GCMS analyses were carried out in the electron impact (EI) mode using a Shimadzu QP-2020 equipped with an RTX-5 column (30 m x 0.25 mm i.d. column) programmed from 60 °C to 250 °C changing at a rate of 10 °C/min and holding at 250 °C for 12 min.

2.4.4. GCMS Analysis of Collected Millipedes Crude Extracts

An aliquot of each crude extract from distinct millipede collections were analyzed using the general GCMS method (described above). All *B. rosea* collections had a prominent peak matching the retention time (17.7 min) and fragmentation as an authentic sample of deoxybuzonamine (**2.1**). EIMS *m/z* (rel %) 207 (45, M^+), 206 (100), 192 (16), 178 (20), 136 (18), 97 (25), 96 (36), 84 (69), 83 (45). *B. petasata* and *B. producta* collections had variable prominent peaks at 17.6 (**2.4**), 18.0 (**2.3**), 19.0 (**2.6**), and 19.4 (**2.5**) min, which are summarized in **Table 2.1.** The peak at 18.001 matched the retention time and fragmentation as an authentic sample of gosodesmine (**2.3**). EIMS *m/z* (rel %) 205 (17, M^+), 204 (35), 136 (50), 122 (22), 93 (82), 70 (100), 53 (10), 41 (62).

2.4.5. Chemical Derivatization of *Brachycybe petasata* and *B. producta* Crude Extracts

An aliquot of a representative crude extract from both *B. petasata* and *B. producta* millipedes was derivatized using microhydrogenation. A slow stream of hydrogen was bubbled through the original extract, ca 50 µL, containing a few milligrams of PtO_2 until the catalyst turned

black. The supernatant was immediately subjected to GCMS analysis using the general method described above. Hydrogenation of extracts of both species gave two isomers of both 7-(4-methylpentyl)indolizidine (**2.7**) and 2-(4-methylpentylquinolizidine (**2.8**) in a 1:2 ratio (synthesis described below) Hassler*, et al.* (2020). In addition, the alkaloids in one collection of *B. producta* were hydrated by treating a small portion of the extract with 5% HCl in MeOH for 1 h at rt, at which point the mixture was carefully made basic with solid K_2CO_3 and extracted with 200 µL of diethyl ether. Analysis by GCMS showed the original **2.3** and **2.4** along with two new peaks with M^+ water adducts of **2.5** and **2.6**.

2.4.6. Synthesis of 2-(4-Methylpentyl)-quinolizidine (2.8**)**

A 1.6 mol/L solution of *n*-butyllithium in hexane (1.0 mL, 1.6 mmol) was added dropwise to a slurry containing 0.55 g (1.3 mmol) of 4-methylpentyltriphenylphosphonium bromide in 10.0 mL of THF under argon at 0 ºC.[36] The mixture was stirred for 0.5 h followed by the dropwise addition of 0.17 g (1.1 mmol) of 2-quinolizidone in 1 mL of THF and allowed to come to rt overnight.[37] The mixture was filtered through celite and the solvent removed under pressure. The residue was triturated with 15 mL of anhydrous ether and filtered through a silica gel plug to provide 0.15 g of a 1:1 mixture of the starting 2-quinolizidone and a 1:1 mixture of (*E* and *Z*) isomers of 2-(4-methylpentylidine)octahydroquinolizidine with identical mass spectra: MS *m/z* (rel %) 221 (40, M^+), 220 (43), 206 (13), 178 (20), 165 (12), 164 (75), 151 (20), 150 (100), 136 (48), 122 (10), 97 (53), 96 (35), 84 (35). This material was taken up in MeOH and treated with ca. 10 mg (44.0 µmol) of PtO_2 and a slow stream of hydrogen was bubbled through it until the catalyst turned black. After 20 min, the sample was filtered and the mixture analyzed on GCMS, which showed the presence of two isomers of **2.8** in a 12:1 ratio having identical mass spectra. Compound **2.8** was an amorphous colorless solid; EIMS *m/z* (rel %) 223 (43, M^+), 222 (82), 208 (25), 194 (7),

180 (57), 166 (11), 152 (14), 139 (10), 138 (100), 110 (46), 97 (57), 96 (14), 84 (16), 83 (16), 82 (18).

2.4.7. Synthesis of Homogosodesmine (2.5)

A solution containing 0.23 g (1.1 mmol) of piperidine ketone (**2.9**), 0.21 g (1.1 mmol) of diethyl phosphonoacetic acid, and 0.21 g (1.4 mmol) of EDCI in 5 mL of DMF was stirred overnight at rt under an argon atmosphere. The mixture was diluted with 25 mL of water and extracted 3 x 50 mL of diethyl ether. The combined ether extracts were dried over anhydrous $MgSO_4$, filtered and concentrated to provide a crude mixture containing a 1:4 mixture of the diethyl phosphonoacetamide (**2.10**) (M = 387) and lactam **2.11** (M = 233). EIMS *m/z* (rel %) 387 (13, M^+), 262 (51), 208 (35), 140 (20), 123 (10), 98 (52), 84 (100), 69 (7). The residue was taken up in 5 mL of anhydrous acetonitrile (MeCN) and treated with 0.15 g of DBU (0.97 mmol) and 50 mg of LiCl (1.2 mmol) and the solution was stirred overnight at rt. The solvent was removed under reduced pressure, and the residue was taken up in 20 mL of diethyl ether and extracted with 5 mL of water. The ether solution was passed through a short plug of silica gel, and the solvent was removed to provide 0.25 g (1.1 mmol) of nearly pure **2.11**, which was used as is in the next reaction. EIMS *m/z* 233 (19, M^+), 218 (5), 205 (9), 190 (7), 176 (3), 166(12), 165(100), 164 (44), 152 (12), 84 (30), 69 (16), 41, (14).

A solution containing 0.2 g (0.86 mmol) of lactam **2.11** in 2 mL of diethyl ether was added to a mixture containing 0.12 g (3.2 mmol) of $LiAlH_4$ in 40 mL of diethyl ether and stirred for 3 h, rt. The reaction was quenched by sequential addition of 5-6 drops of H_2O, 5-6 drops of 10% NaOH, and 10 drops of H_2O, filtered, and solvent removed by reduced pressure. This yielded 0.18 g (0.72 mmol) of **2.5** whose mass spectrum and retention times matched those of the quinolizidine natural product from *B. producta.* Compound **2.5** was an amorphous colorless solid, ^1H and ^{13}C NMR:

See **Table 2.8.1**; EIMS *m/z* (rel %) 219 (48, M^+), 218 (70), 204 (11), 191 (13), 176 (24), 162 (20), 151 (24), 150 (100), 149 (33), 136 (50), 134 (15), 93 (21), 84 (78), 69 (22), 55 (13), 41 (28); HRESIMS calc for $C_{15}H_{26}N^+$ 220.2060, found $[M+H]^+$ 220.2058, Δ 0.75 ppm.

2.4.8. Synthesis of 7-(4-Hydroxy-4-methylpentyl)-indolizidine (2.18**)**

A 1 mol/L solution of LiHMDS (2.2 mL, 2.2 mmol) in hexanes was added slowly to a solution containing 0.50 g (2.0 mmol) of triethyl-4-phosphonocrotonate in 10 mL of THF at 0 °C under an argon atmosphere. After 0.5 h a solution containing 0.28 g (2.0 mmol) of 7-indolizidone (**2.12**) in 2 mL of THF was added and the mixture was stirred overnight.[37] The mixture was diluted with 70 mL of diethyl ether and stirred with 5 mL of saturated NH_4Cl (aq). The layers were separated, and the organic layer was dried over anhydrous K_2CO_3 and the solvent was removed under reduced pressure to provide 0.22 g (0.93 mmol) of a mixture of geometric isomers of **2.14**. EIMS *m/z* 235 (62, M^+), 206 (22), 190 (18), 162 (29), 176 (28), 162 (34), 160 (11), 83 (100), 81 (53), 70 (24). The crude mixture was taken up in 20 mL of EtOH and treated with 1 mL of 10% HCl, and hydrogenated over 40 mg of 10% Pd/C at 3 atm pressure for 45 min. The mixture was filtered through celite and after removal of the solvent partitioned between diethyl ether and 10% NaOH (aq). The organic layer was dried over anhydrous K_2CO_3, the solvent was removed from the ether solution to provide 0.19 g (0.79 mmol) of the saturated amine ester (**2.16**) as a 2:1 mixture of isomers. EIMS *m/z* 239 (40, M^+), 238 (100), 210 (27), 194 (36), 152 (31), 138 (24), 124 (91), 97 (31), 96 (80), 83 (33). This product was taken up in 10 mL of THF and treated with 2 mL of 3 mol/L MeMgCl in THF and allowed to stir overnight. The mixture was diluted with diethyl ether and treated with 10 mL of saturated NH_4Cl (aq). The organic layer was separated, dried over anhydrous K_2CO_3 and the solvent was removed to provide 0.11 g (0.49 mmol) of **2.18** as a 2:1 mixture of isomers with identical mass spectra. The GC retention time and the mass spectrum of

the first eluting isomer matched that of the hydrated natural product (**2.18**). Compound **2.18** was an amorphous colorless solid, ^{1}H and ^{13}C NMR: See **Table 2.8.2** (major stereoisomer) and **Table 2.8.3** (minor stereoisomer); EIMS *m/z* 225 (44, M^+), 224 (100), 210 (676), 166 (100), 138 (44), 124 (81), 97 (23), 96 (60), 83 (26), 59 (14), 55 (10). HRESIMS calc for $C_{14}H_{28}NO^+$ 226.2165, found $[M+H]^+$ 226.2166, Δ 0.13 ppm.

2.4.9. Synthesis of 2-(4-Hydroxy-4-methylpentyl)-quinolizidine (2.19**)**

This compound was prepared using the same method described for **2.18**, except it started with 2-quinolizidone (**2.13**). A 1 mol/L solution of LiHMDS (2.2 mL, 2.2 mmol) in hexanes was added slowly to a solution containing 0.50 g (2.0 mmol) of triethyl-4-phosphonocrotonate in 10 mL of THF at 0 °C under an argon atmosphere. After 0.5 h a solution containing 0.30 g (2.0 mmol) of 2-quinolizidone in 2.0 mL of THF was added and the mixture was stirred overnight.[37] The mixture was diluted with 70 mL of diethyl ether and stirred with 5 mL of saturated NH_4Cl (aq). The layers were separated, and the organic layer was dried over anhydrous K_2CO_3 and the solvent was removed under reduced pressure to provide a mixture of geometric isomers of **2.15**. EIMS *m/z* 249 (70, M^+), 234 (36), 220 (20), 204 (20), 176 (28), 162 (34), 136 (22), 97 (100), 96 (99), 69 (22). The crude mixture was taken up in 20 mL of EtOH treated with 1.0 mL of 10% HCl, and hydrogenated over 40 mg of 10% Pd/C at 3 atm pressure for 45 min. The mixture was filtered through celite and after removal of the solvent partitioned between diethyl ether and 10% NaOH (aq). After drying over anhydrous K_2CO_3 the solvent was removed from the ether solution to provide the saturated amine ester **2.17**. EIMS *m/z* 253 (35, M^+), 252 (67), 238 (11), 224 (23), 210 (11), 208 (48), 106 (47), 152 (30), 138 (100), 110 (67), 97 (77), 82 (41). This product was taken up in 10 mL of THF and treated with 2.0 mL of 3 mol/L MeMgCl in THF and allowed to stir overnight. The mixture was diluted with diethyl ether and treated with 10 mL of saturated NH_4Cl

(aq). The organic layer was separated, dried over anhydrous K_2CO_3 and the solvent was removed to provide 0.65 g (2.7 mmol) of **2.19** as a 3:1 mixture of isomers with identical mass spectra. The GC retention time and the mass spectrum of the first eluting isomer matched that of the hydrated natural product (**2.19**). Compound **2.19** was an amorphous colorless solid; ^{1}H and ^{13}C NMR: See **Table 2.8.4** (major stereoisomer) and **Table 2.8.5** (minor stereoisomer); EIMS *m/z* 239 (20, M^+), 238 (42), 224 (56), 180 (100), 152 (18), 138 (67), 110 (33), 97 (38), 83 (22), 59 (13), 55 (20); HRMS (ESI) calc for $C_{15}H_{30}NO^+$ 240.2322, found $[M+H]^+$ 240.2319, Δ 1.3 ppm.

2.4.10. Extraction and Isolation of Homogosodesmine (2.5) and Homo-Hydrogosodesmine (2.6) from *B. producta*

The millipedes were extracted using MeOH and dried down. The extract was then resuspended in 1:1 MeCN/H_2O and separated using reverse-phase high performance liquid chromatography (RP-HPLC). The mobile phase was a mixture of MeCN and H_2O with 0.1% formic acid, using a Phenomenex 4 µm Hydro semi-preparative column (250 × 10 mm). The flow was set to 3 mL/min with a 5 min isocratic hold at 20% MeCN/H_2O followed by a linear gradient to 47% MeCN/H_2O over 29 min to yield pure hydrogosodesmine (**2.4**) and homo-hydrogosodesmine (**2.6**).

*Hydrogosodesmine (**2.4**):* amorphous solid; $[\alpha]_D$ 3.75 (MeOH); ^{1}H and ^{13}C NMR: See **Table 2.8.6**; HRMS (ESI) calc for $C_{14}H_{26}N^+$ 208.2060, found $[M+H]^+$ 208.2061, Δ0.55 ppm.

*Homo-hydrogosodesmine (**2.6**):* amorphous solid; $[\alpha]_D$ 7.50 (MeOH); ^{1}H and ^{13}C NMR: See **Table 2.8.7**; HRMS (ESI) calc for $C_{15}H_{28}N^+$ 222.2216, found $[M+H]^+$ 222.2219, Δ1.29 ppm.

2.5. Acknowledgements

This work was supported by the following funding agencies. E.M. and P.B. were supported in part by the National Institutes of Health (R35 GM146740). M.T.K. and A.M.M. were supported

in part by National Geographic (Grant NGS-74229R-20). Awards from The Mycological Society of America provided travel support for B.L. (2021 Forest Fungal Ecology Research Award) and S.M. (2021 Robert W. Lichtwardt Student Research Award). B.L. was also supported by the USDA (USDA-ARS Project 8062-22410-007-000D). All scientific collections were conducted with explicit written permission by various public agencies and included issued permits for Marin Municipal Water District (Marin County, CA) under permit no. R-21-18, Edgewood Park (San Mateo County, CA) under permit no. SP-2021-12-SMP-ECP, and Cloudland Canyon State Park (Dade County, GA) under permit no. 052021. National Forest did not issue permits, but collections were authorized in writing. NIST Disclaimer: Certain equipment, instruments, software, or materials are identified in this paper to specify the experimental procedure adequately. Such identification is not intended to imply recommendation or endorsement of any product or service by NIST, nor is it intended to imply that the materials or equipment identified are necessarily the best available for the purpose.

2.6. References

(1) Shear, W. A. The chemical defenses of millipedes (diplopoda): Biochemistry, physiology and ecology. *Biochemical Systematics and Ecology* **2015**, *61*, 78-117. DOI: 10.1016/j.bse.2015.04.033.

(2) Eisner, T.; Alsop, D.; Hicks, K.; Meinwald, J. Defensive Secretions of Millipeds. In *Arthropod Venoms*, Bettini, S. Ed.; Springer Berlin Heidelberg, 1978; pp 41-72.

(3) Carrel, J. E. Defensive secretion of the pill millipede Glomeris marginata. I. Fluid production and storage. *Journal of Chemical Ecology* **1984**, *10* (4). DOI: 10.1007/BF00994230.

(4) Youngsteadt, N. W. Laboratory observations on the behavior of two troglobitic millipede species in the genus Causeyella (Chordeumatida: Trichopetalidae) from the southern Ozarks.

Transactions of the Kansas Academy of Science **2008**, *111* (1). DOI: 10.1660/0022-8443(2008)111.

(5) Marek, P.; Shear, W.; Bond, J. A redescription of the leggiest animal, the millipede Illacme plenipes, with notes on its natural history and biogeography (Diplopoda, Siphonophorida, Siphonorhinidae). *Zookeys* **2012**, *241*. DOI: 10.3897/zookeys.241.3831.

(6) Ilić, B.; Unković, N.; Ćirić, A.; Glamočlija, J.; Ljaljević Grbić, M.; Raspotnig, G.; Bodner, M.; Vukojević, J.; Makarov, S. Phenol-based millipede defence: antimicrobial activity of secretions from the Balkan endemic millipede Apfelbeckia insculpta (L. Koch, 1867) (Diplopoda: Callipodida). *The Science of Nature* **2019**, *106* (7). DOI: 10.1007/s00114-019-1631-z.

(7) Marek, P. E.; Shear, W. A. The millipede family Striariidae Bollman, 1893. VI. Six new genera and thirteen new species from western North America (Diplopoda, Chordeumatida, Striarioidea). *Zootaxa* **2022**, *5205* (6), 501-531. DOI: 10.11646/zootaxa.5205.6.1.

(8) Shear, W. Spinnerets in the milliped order Polydesmida, and the phylogenetic significance of spinnerets in millipeds (Diplopoda). *International Journal of Myriapodology* **2008**, *1*, 123-146. DOI: 10.1163/187525408X395904.

(9) Wilson, H. M. Juliformian millipedes from the lower devonian of euramerica: implications for the timing of millipede cladogenesis in the paleozoic. *Journal of Paleontology* **2006**, *80* (4). DOI: 10.1666/0022-3360(2006)80.

(10) Rodriguez, J.; Jones, T. H.; Sierwald, P.; Marek, P. E.; Shear, W. A.; Brewer, M. S.; Kocot, K. M.; Bond, J. E. Step-wise evolution of complex chemical defenses in millipedes: a phylogenomic approach. *Scientific Reports* **2018**, *8* (1), 3209. DOI: 10.1038/s41598-018-19996-6.

(11) Minelli, A. *Treatise on Zoology - Anatomy, Taxonomy, Biology. The Myriapoda*; Brill, 2011.

(12) Wood, H. C. Description of New Genera and Species of North American Myriapoda. *Proceedings of the Academy of Natural Sciences of Philadelphia* **1864**, *16* (4), 186-187.

(13) Wong, V. L.; Hennen, D. A.; Macias, A. M.; Brewer, M. S.; Kasson, M. T.; Marek, P. Natural history of the social millipede Brachycybe lecontii Wood, 1864. *Biodiversity Data Journal* **2020**, *8*, e50770. DOI: 10.3897/BDJ.8.e50770.

(14) Smolanoff, J.; Kluge, A. F.; Meinwald, J.; McPhail, A.; Miller, R. W.; Hicks, K.; Eisner, T. Polyzonimine: A Novel Terpenoid Insect Repellent Produced by a Milliped. *Science* **1975**, *188* (4189), 734-736. DOI: doi:10.1126/science.1124395.

(15) Wood, W. F.; Hanke, F. J.; Kubo, I.; Carroll, J. A.; Crews, P. Buzonamine, a new alkaloid from the defensive secretion of the millipede, Buzonium crassipes. *Biochemical Systematics and Ecology* **2000**, *28* (4), 305-312. DOI: 10.1016/S0305-1978(99)00068-X.

(16) Shear, W.; Jones, T.; Wesener, T. Glomerin and homoglomerin from the North American pill millipede Onomeris sinuata (Loomis, 1943) (Diplopoda, Pentazonia, Glomeridae). *International Journal of Myriapodology* **2011**, *4*. DOI: 10.3897/ijm.4.1105.

(17) Dewick, P. *Medicinal Natural Products*; 2009. DOI: 10.1002/9780470742761.

(18) Hassler, M. F.; Harrison, D. P.; Jones, T. H.; Richart, C. H.; Saporito, R. A. Gosodesmine, a 7-Substituted Hexahydroindolizine from the Millipede Gosodesmus claremontus. *Journal of Natural Products* **2020**, *83* (9). DOI: 10.1021/acs.jnatprod.0c00722.

(19) Jones, T. H.; Harrison, D. P.; Menegatti, C.; Mevers, E.; Knott, K.; Marek, P.; Hennen, D. A.; Kasson, M. T.; Macias, A. M.; Lovett, B.; et al. Deoxybuzonamine Isomers from the Millipede Brachycybe lecontii (Platydesmida: Andrognathidae). *Journal of Natural Products* **2022**, *85* (4), 1134-1140. DOI: 10.1021/acs.jnatprod.2c00077.

(20) Meinwald, J.; Smolanoff, J.; McPhail, A. T.; Miller, R. W.; Eisner, T.; Hicks, K. Nitropolyzonamine: A spirocyclic nitro compound from the defensive glands of a milliped (polyzonium rosalbum). *Tetrahedron Letters* **1975**, *16* (28). DOI: 10.1016/0040-4039(75)80013-X.

(21) Kunert, O.; Pferschy-Wenzig, E. M.; Orthaber, A.; Raspotnig, G.; Bodner, M. Alkaloids from millipedes: a re-evaluation of defensive exudates from Polyzonium germanicum. *Frontiers in Ecology and Evolution* **2023**, *11*. DOI: 10.3389/fevo.2023.1212452.

(22) Kuwahara, Y.; Mori, N. M. N.; Tanabe, T. Detection of a neotropical frog alkaloid spiropyrrolizidine 236 from a Japanese polyzoniid millipede Kiusiozonium okai as a major defense component together with polyzonimine and nitropolyzonamine. *Japanese Journal of Environmental Entomology and Zoology* **2007**, *18* (2). DOI: 10.11257/jjeez.18.91.

(23) Macias, A. M.; Marek, P. E.; Morrissey, E. M.; Brewer, M. S.; Short, D. P. G.; Stauder, C. M.; Wickert, K. L.; Berger, M. C.; Metheny, A. M.; Stajich, J. E.; et al. Diversity and function of fungi associated with the fungivorous millipede, Brachycybe lecontii. *Fungal Ecology* **2019**, *41*, 187-197. DOI: 10.1016/j.funeco.2019.06.006.

(24) Brewer, M. S.; Sierwald, P.; Bond, J. E. Millipede Taxonomy after 250 Years: Classification and Taxonomic Practices in a Mega-Diverse yet Understudied Arthropod Group. *Public Library of Science One* **2012**, *7* (5). DOI: 10.1371/journal.pone.0037240.

(25) Monaco, M. R.; Renzi, P.; Schietroma, D. M. S.; Bella, M. Biomimetic Organocatalytic Asymmetric Synthesis of 2-Substituted Piperidine-Type Alkaloids and Their Analogues. *Organic Letters* **2011**, *13* (17). DOI: 10.1021/ol2017406.

(26) Nangia, A.; Prasuna, G. Studies on Horner-Wadsworth-Emmons reaction in base sensitive ketones: Synthesis of (−)-mitsugashiwalactone and formal synthesis of (+)-iridomyrmecin, (−)-

isoiridomyrmecin and (+)-teucriumlactone. *Tetrahedron* **1996**, *52* (10), 3435-3450. DOI: 10.1016/0040-4020(96)00023-3.

(27) Namboothiri, I. N. N.; Hassner, A.; Gottlieb, H. E. A Highly Stereoselective One-Pot Tandem Consecutive 1,4-Addition−Intramolecular 1,3-Dipolar Cycloaddition Strategy for the Construction of Functionalized Five- and Six-Membered Carbocycles. *The Journal of Organic Chemistry* **1997**, *62* (3). DOI: 10.1021/jo961663v.

(28) Daly, J. W.; Garraffo, H. M.; Spande, T. F.; Clark, V. C.; Ma, J.; Ziffer, H.; John F. Cover, J.; Daly, J. W.; Garraffo, H. M.; Spande, T. F.; et al. Evidence for an enantioselective pumiliotoxin 7-hydroxylase in dendrobatid poison frogs of the genus Dendrobates. *Proceedings of the National Academy of Sciences* **2003**, *100* (19). DOI: 10.1073/pnas.1834430100.

(29) Saporito, R. A.; Donnelly, M. A.; Norton, R. A.; Garraffo, H. M.; Spande, T. F.; Daly, J. W. Oribatid mites as a major dietary source for alkaloids in poison frogs. *Proceedings of the National Academy of Sciences* **2007**, *104* (21). DOI: 10.1073/pnas.0702851104.

(30) Saporito, R. A.; Garraffo, H. M.; Donnelly, M. A.; Edwards, A. L.; Longino, J. T.; Daly, J. W. Formicine ants: An arthropod source for the pumiliotoxin alkaloids of dendrobatid poison frogs. *Proceedings of the National Academy of Sciences* **2004**, *101* (21). DOI: 10.1073/pnas.0402365101.

(31) Edwards, M. W.; Daly, J. W.; Myers, C. W. Alkaloids from a Panamanian Poison Frog, Dendrobates speciosus: Identification of Pumiliotoxin-A and Allo-pumiliotoxin Class Alkaloids, 3,5-Disubstituted Indolizidines, 5-Substituted 8-Methylindolizidines, and a 2-Methyl-6-nonyl-4-hydroxypiperidine. *Journal of Natural Products* **1988**, *51* (6), 1188-1197. DOI: 10.1021/np50060a023.

(32) Meinwald, Y. C.; Meinwald, J.; Eisner, T. 1,2-Dialkyl-4(3H)-Quinazolinones in the Defensive Secretion of a Millipede (Glomeris marginata). *Science* **1966**, *154* (3747). DOI: 10.1126/science.154.3747.390.

(33) Schildknecht, H.; Maschwitz, U.; Wenneis, W. F.; Schildknecht, H.; Maschwitz, U.; Wenneis, W. F. Neue Stoffe aus dem Wehrsekret der Diplopodengattung Glomeris. *Naturwissenschaften* **1967**, *54* (8). DOI: 10.1007/BF00594514.

(34) Shorter, P. L.; Hennen, D. A.; Marek, P. E. Cryptic diversity in Andrognathus corticarius Cope, 1869 and description of a new Andrognathus species from New Mexico (Diplopoda, Platydesmida, Andrognathidae). *Zookeys* **2018**, (786), 19-41. DOI: 10.3897/zookeys.786.27631.

(35) Brewer, M. S.; Spruill, C. L.; Rao, N. S.; Bond, J. E. Phylogenetics of the millipede genus Brachycybe Wood, 1864 (Diplopoda: Platydesmida: Andrognathidae): Patterns of deep evolutionary history and recent speciation. *Molecular Phylogenetics and Evolution* **2012**, *64* (1). DOI: 10.1016/j.ympev.2012.04.003.

(36) Dickschat, J. S.; Helmke, E.; Schulz, S. Volatile Organic Compounds from Arctic Bacteria of the Cytophaga-Flavobacterium-Bacteroides Group: A Retrobiosynthetic Approach in Chemotaxonomic Investigations. *Chemistry and Biodiversity* **2005**, *2* (3). DOI: 10.1002/cbdv.200590014.

(37) Hermet, J.-P. R.; Porter, D. W.; Dearden, M. J.; Harrison, J. R.; Koplin, T.; O'Brien, P.; Parmene, J.; Tyurin, V.; Whitwood, A. C.; Gilday, J.; et al. Synthesis of sparteine-like chiral diamines and evaluation in the enantioselective lithiation–substitution of N-(tert-butoxycarbonyl)pyrrolidine. *Organic and Biomolecular Chemistry* **2003**, *1* (22). DOI: 10.1039/B308410H.

2.7. Appendix Figures

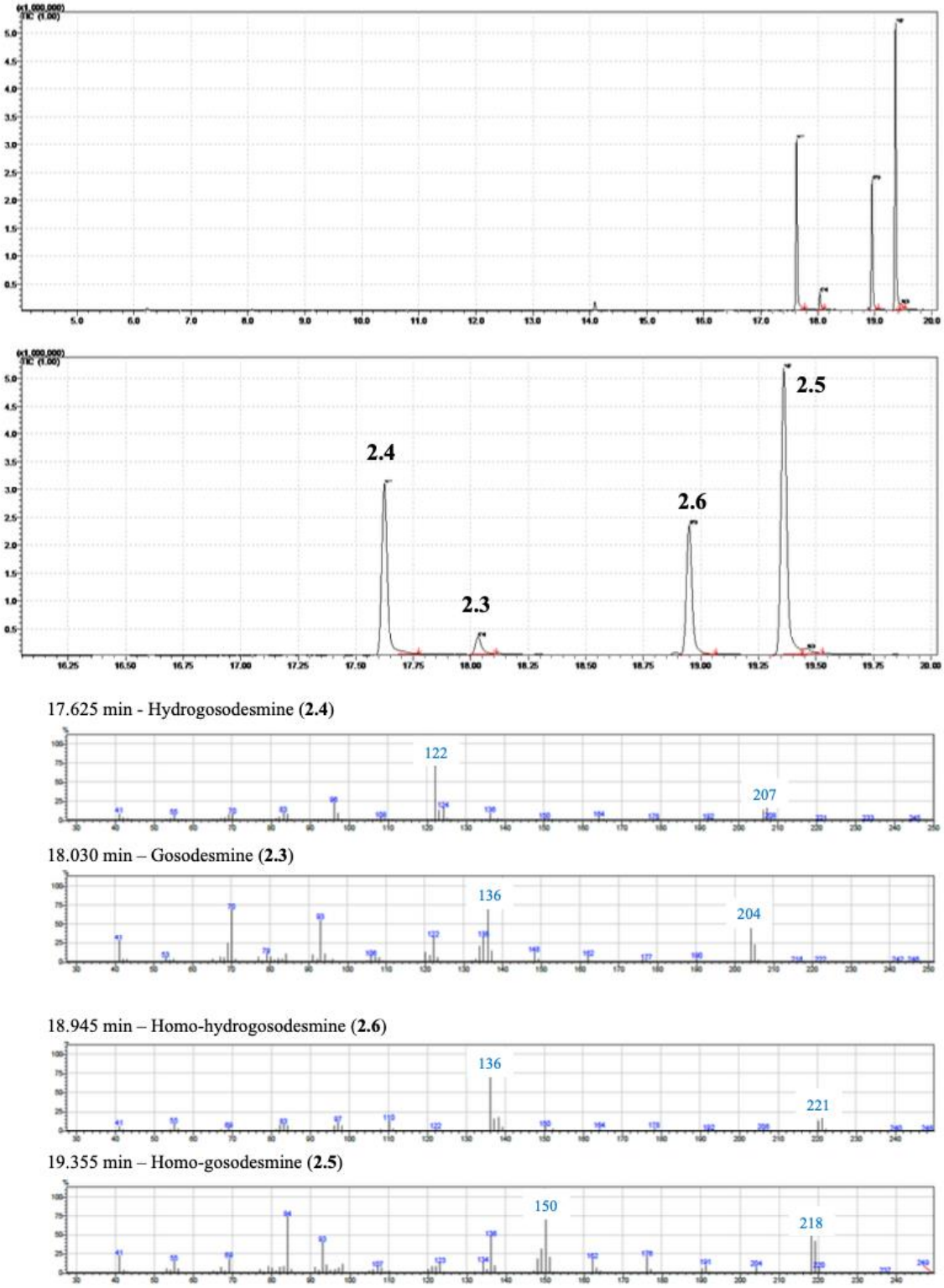

Figure 2.7.1. GCMS chromatogram and spectra of a representative *Brachycybe petaseta* extract (PEM-2021-008). Peaks at 6.3 min is α-pinene and 14 min is borneyl acetate.

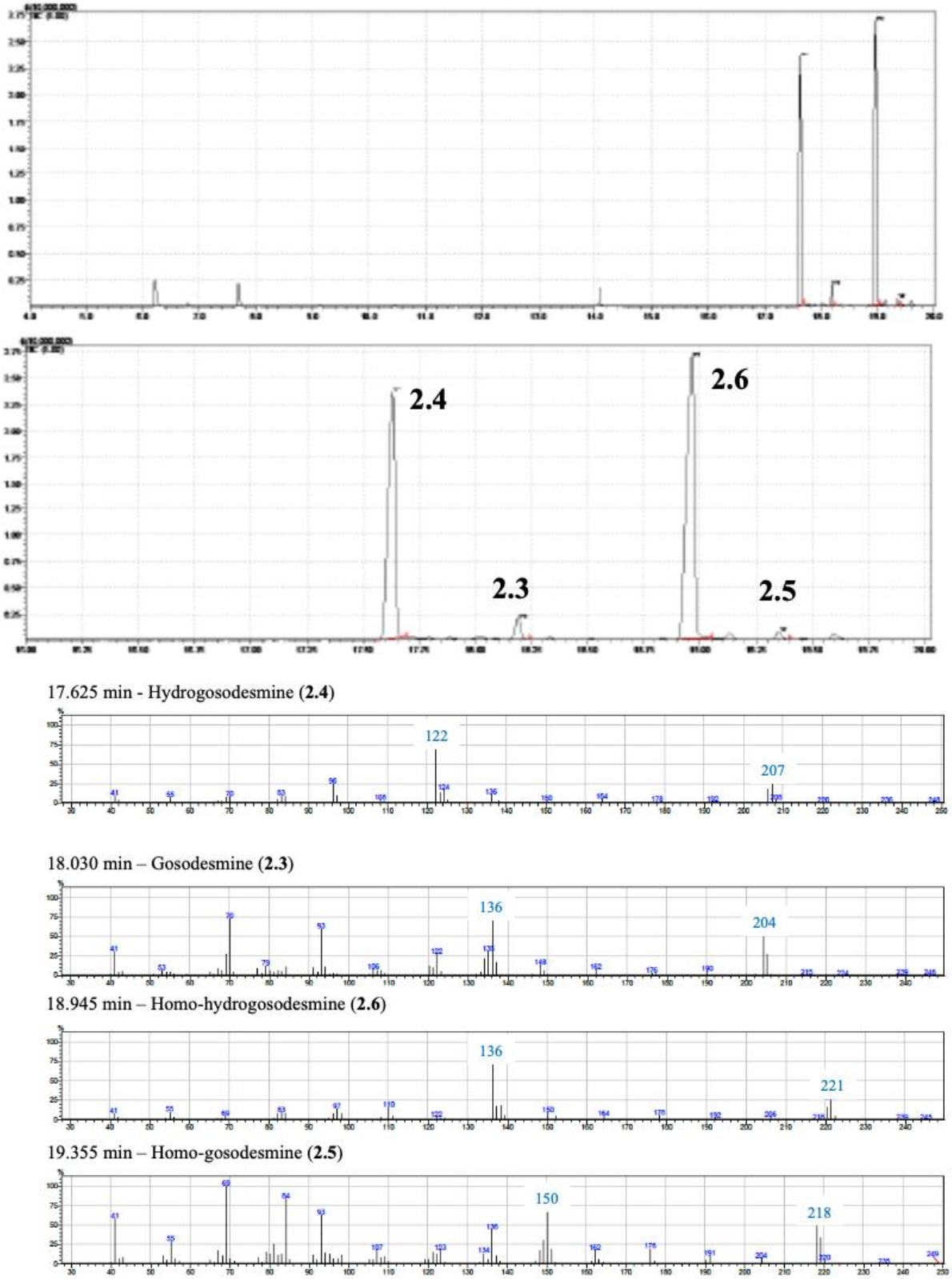

Figure 2.7.2. GCMS chromatogram and spectra of a representative *B. producta* extract.

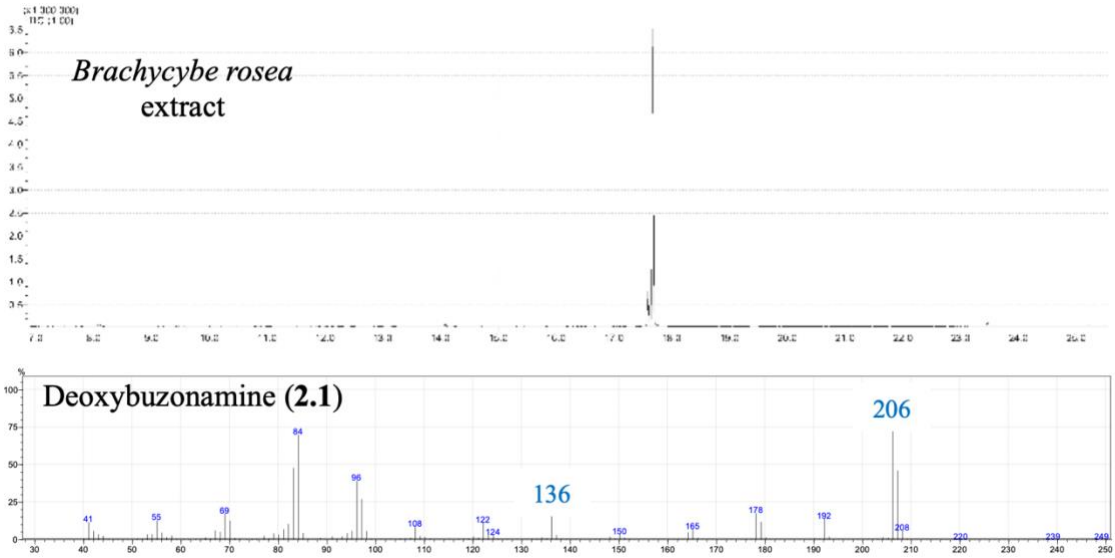

Figure 2.7.3. GCMS chromatogram and spectra of a representative *B. rosea* extract. The smaller peak at 17.595 min appears related to deoxybuzonamine. The fragment at *m/z* = 70 which suggests a of an olefin the middle ring but we did not have enough material for structure elucidation.

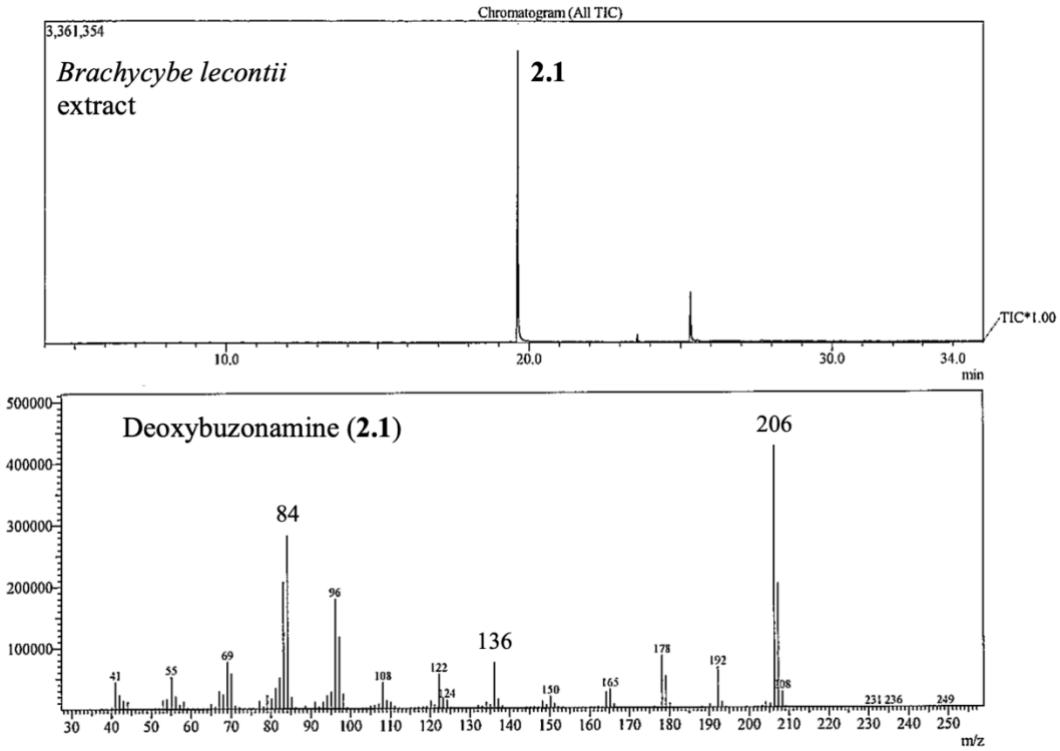

Figure 2.7.4. GCMS chromatogram and spectrum of a representative *B. lecontii* extract.

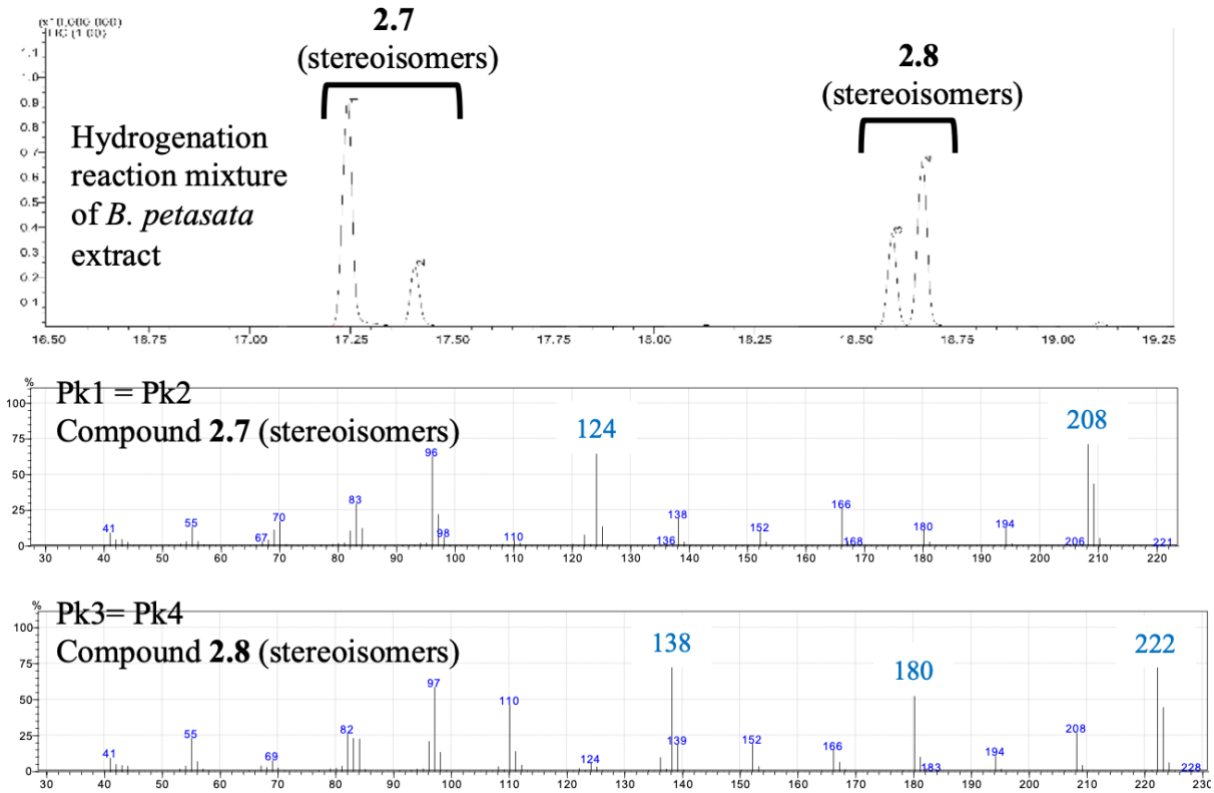

Figure 2.7.5. GCMS chromatogram and spectra of the reaction product of the hydrogenation of *B. petasata* extract. The reduction of gosodesmine (**2.3**) and homogosodesmine (**2.5**) led to stereoisomers. The fragmentation patterns of the stereoisomers were identical.

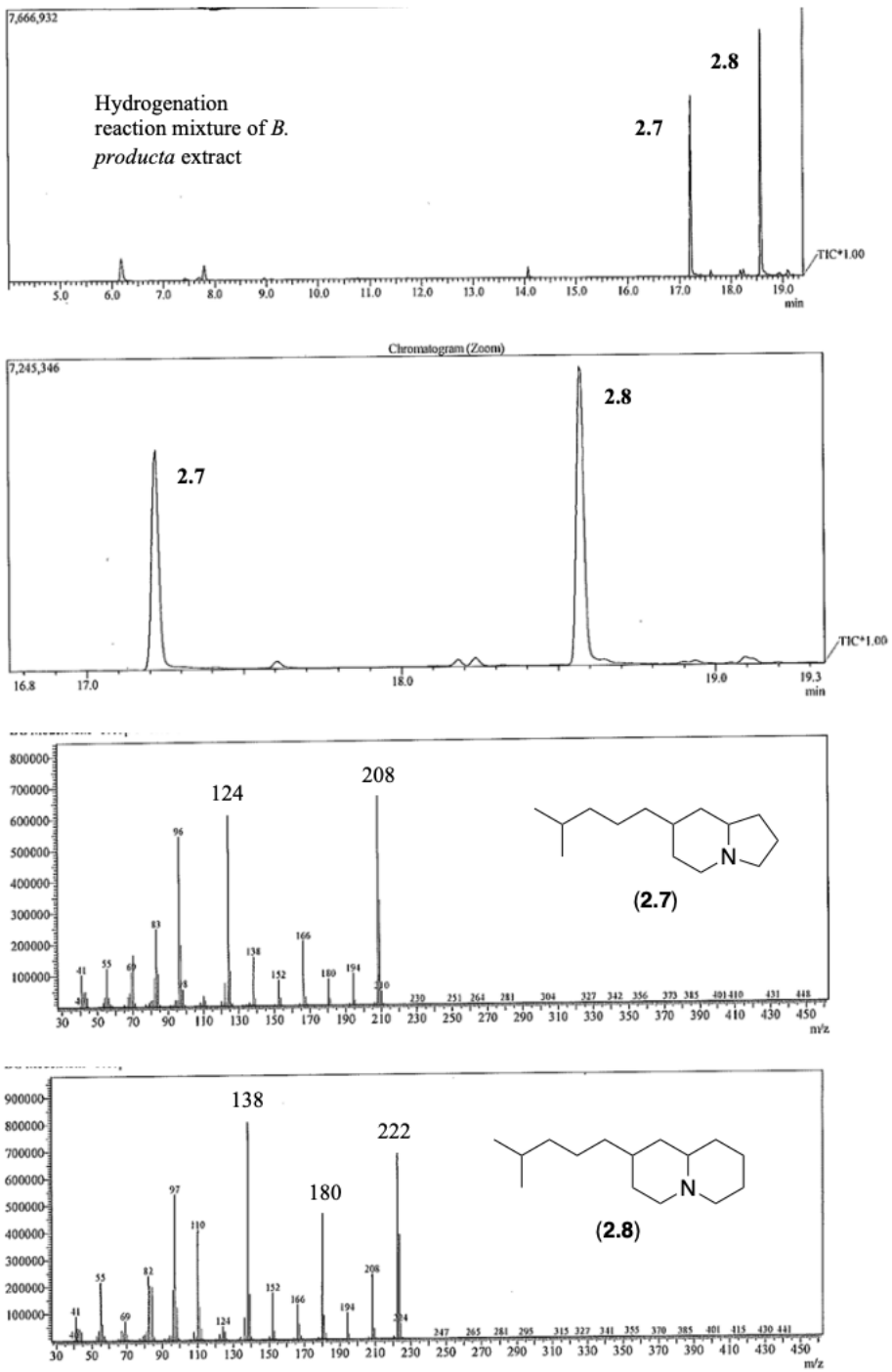

Figure 2.7.6. GCMS chromatogram and spectra of the reaction product of the hydrogenation of *B. producta* extract. The reduction of gosodesmine (**2.3**) and homogosodesmine (**2.5**) led to stereoisomers. The fragmentation patterns of the stereoisomers were identical.

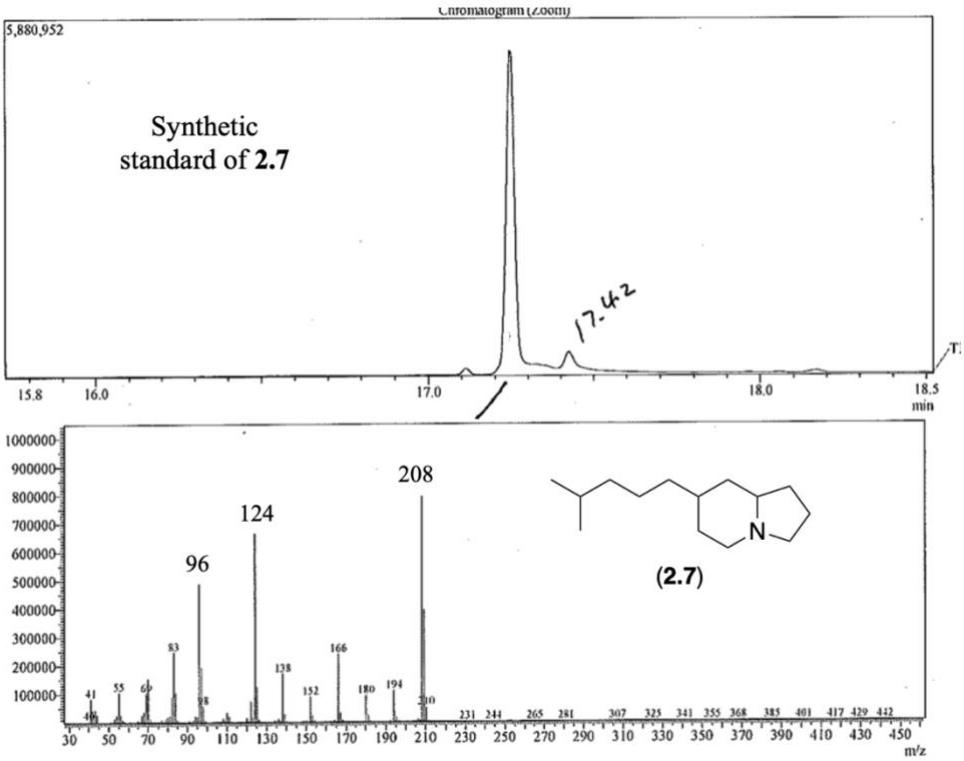

Figure 2.7.7. GCMS chromatogram and spectrum of the synthesized 7-(4-methylpentyl)-indolizidine (**2.7**).

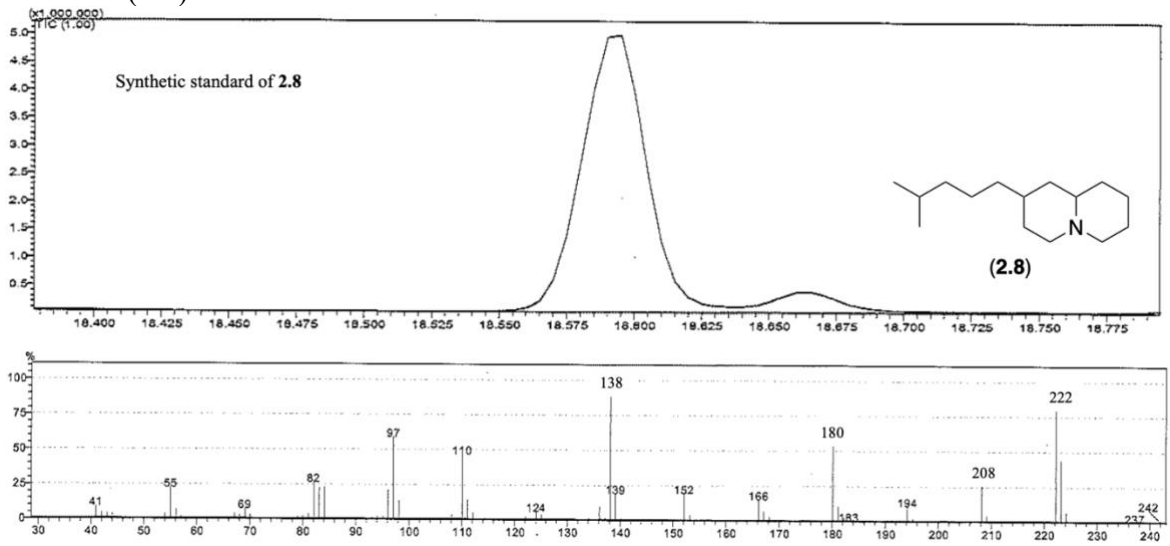

Figure 2.7.8. GCMS chromatogram and spectrum of the synthesized 2-(4-methylpentyl)-quinolizidine (**2.8**).

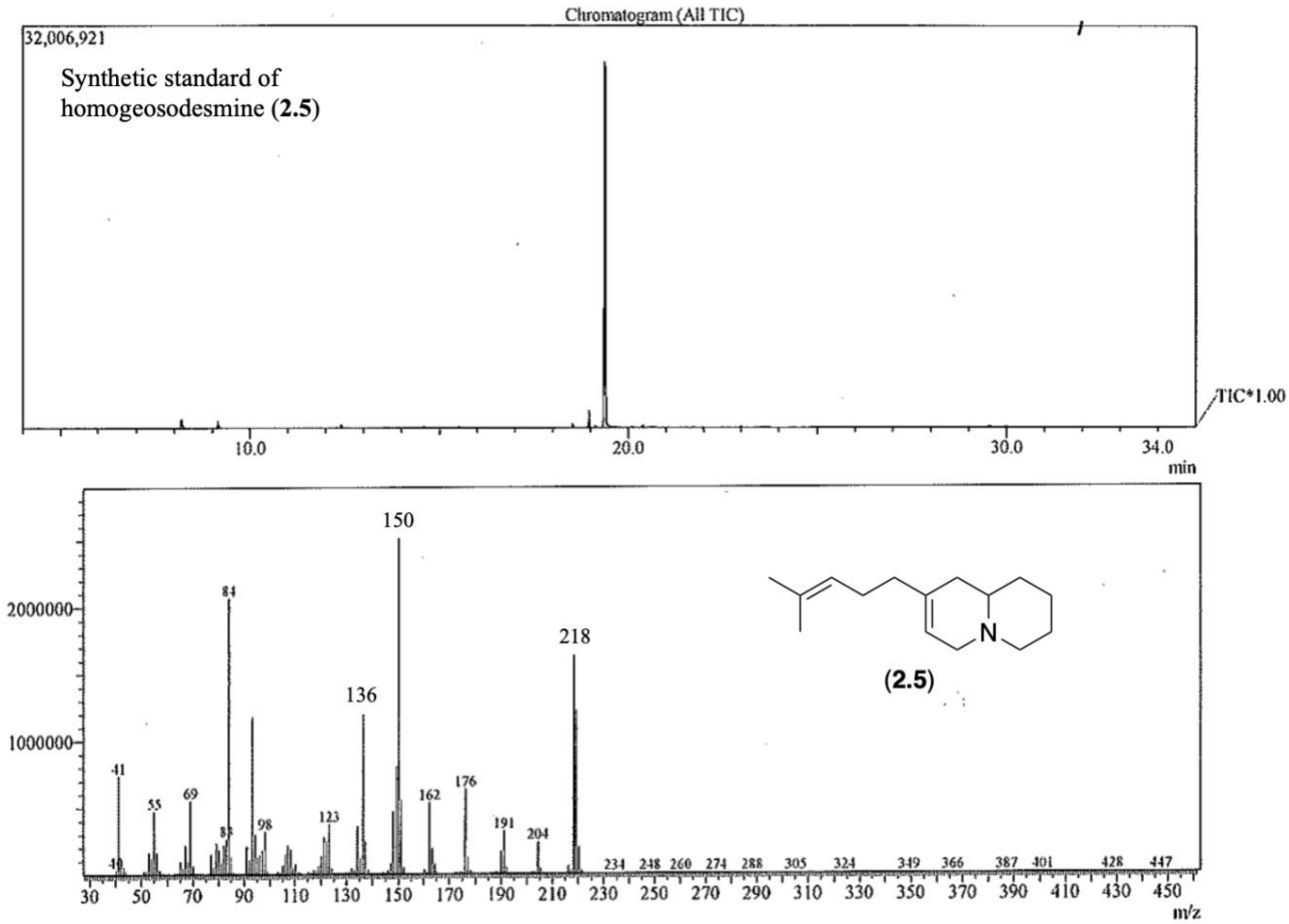

Figure 2.7.9. GCMS chromatogram and spectrum of the synthesized homogosodesmine (**2.5**).

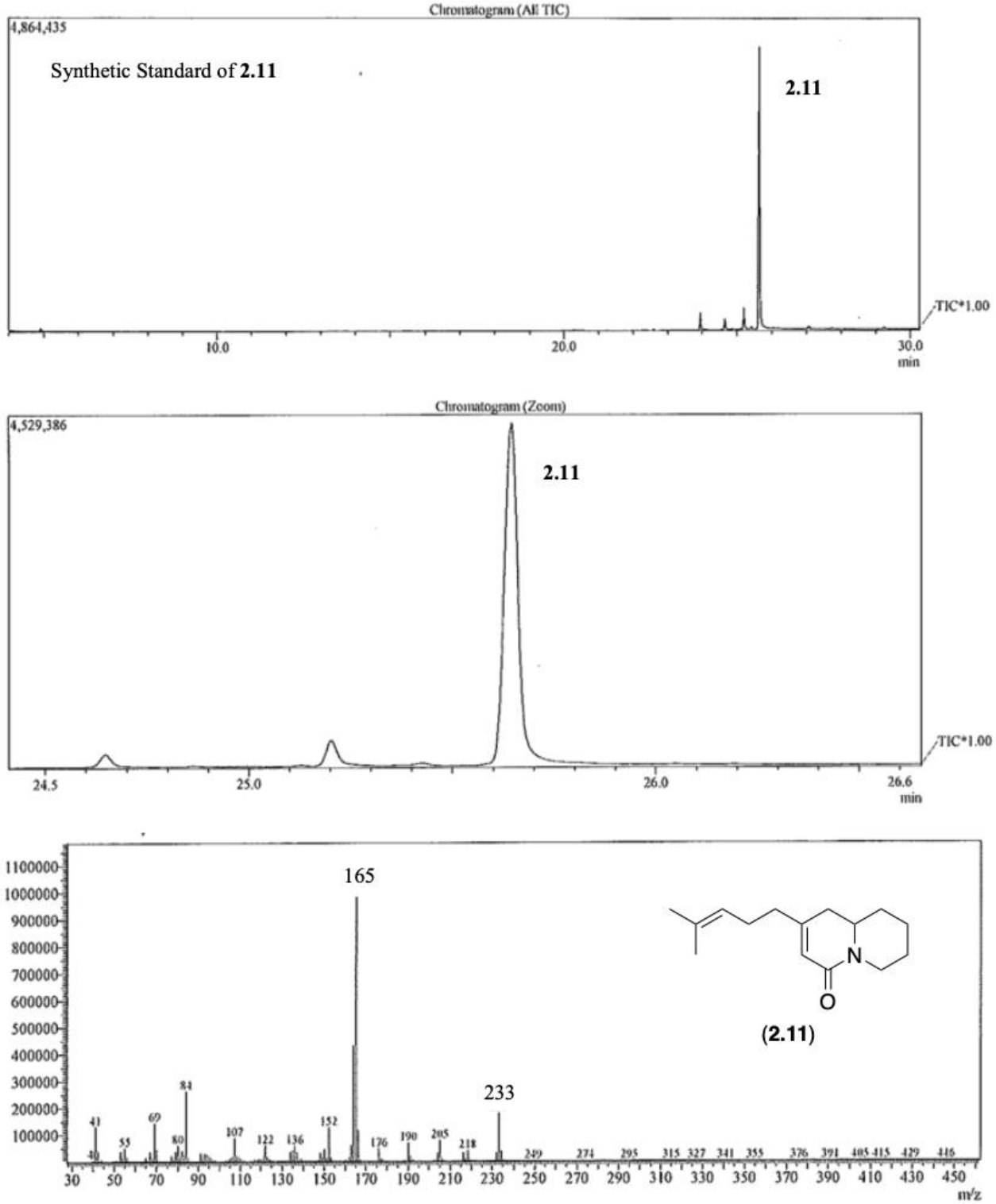

Figure 2.7.10. GCMS chromatogram and spectrum of the synthesized **2.11.**

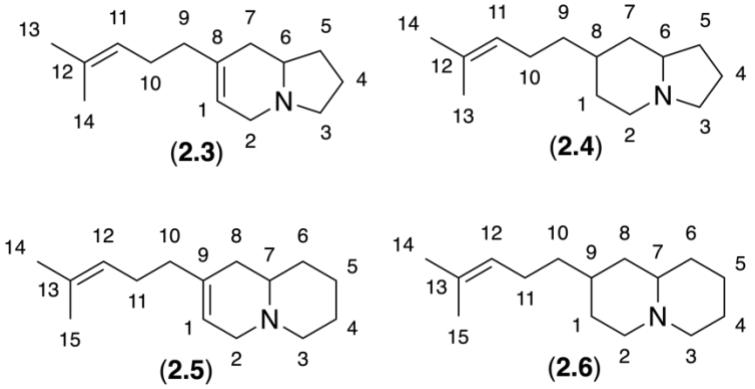

Figure 2.7.11. Numbering of compounds for NMR data tables.

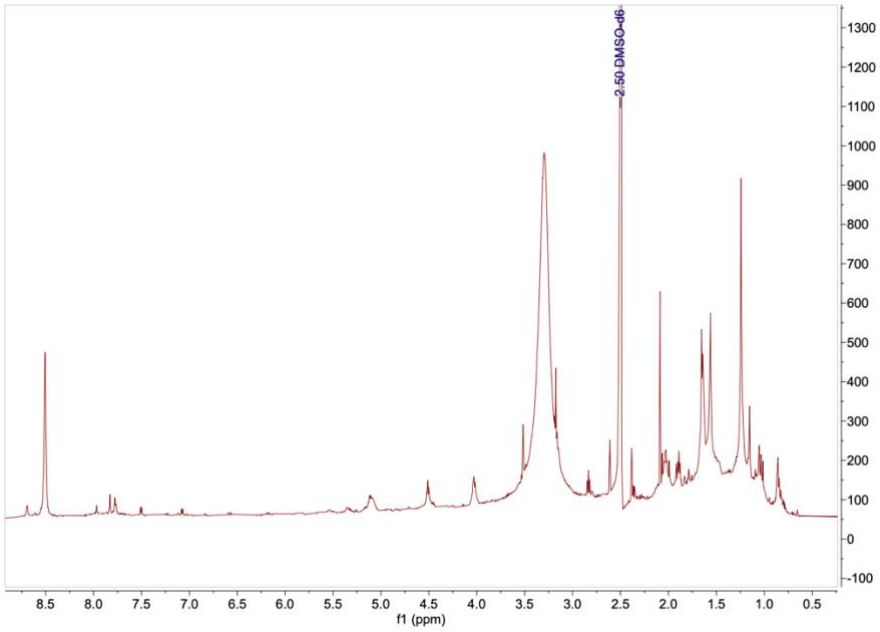

Figure 2.7.12. ^{1}H NMR spectrum for synthetic homogosodesmine (**2.5**) (600 MHz, *d*$_6$-DMSO) 128 scans.

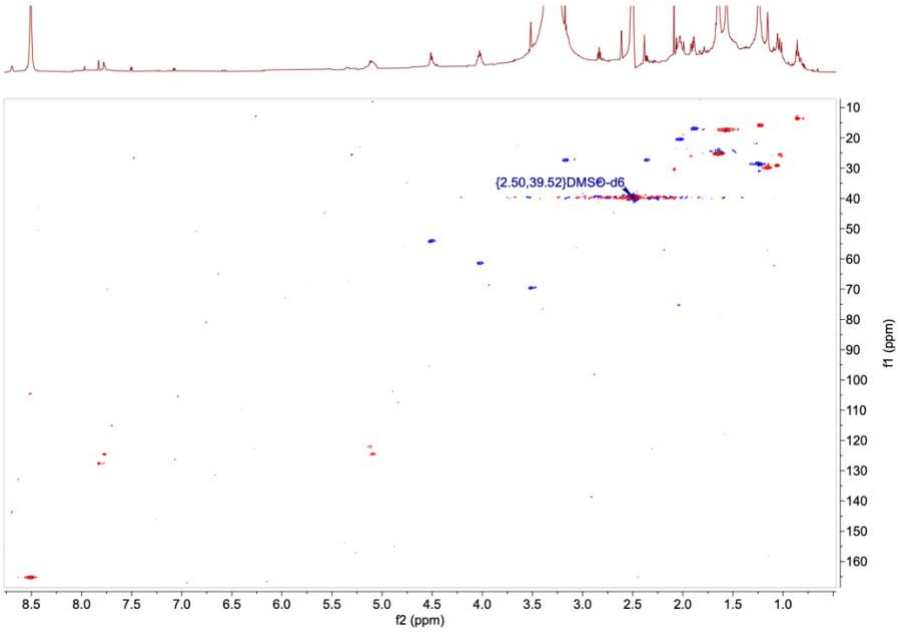

Figure 2.7.13. gHSQC for synthetic homogosodesmine (**2.5**) (600 MHz, d_6-DMSO) 96 scans, NUS25 and 400 increments.

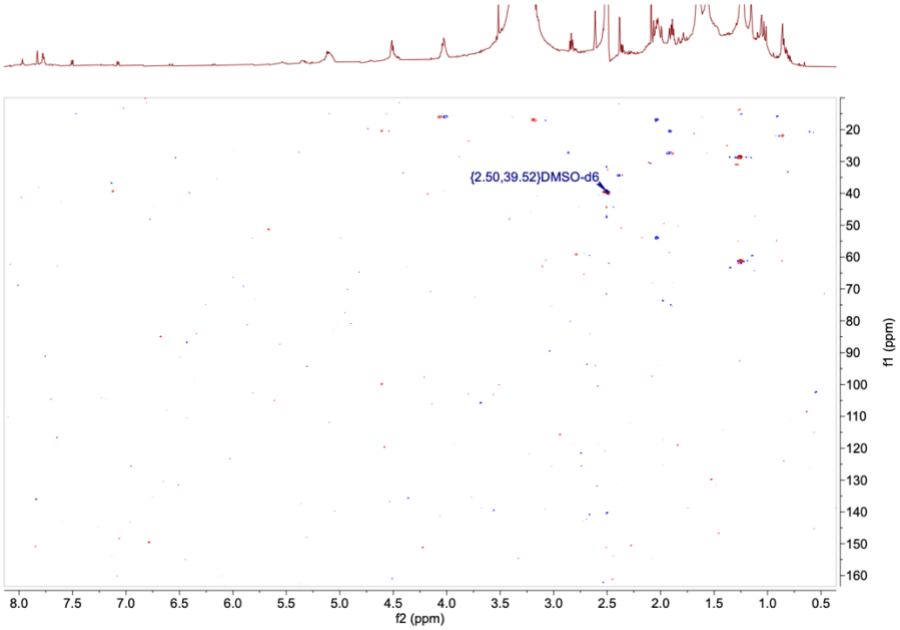

Figure 2.7.14. H2BC for synthetic homogosodesmine (**2.5**) (600 MHz, d_6-DMSO) 160 scans, NUS50 and 400 increments.

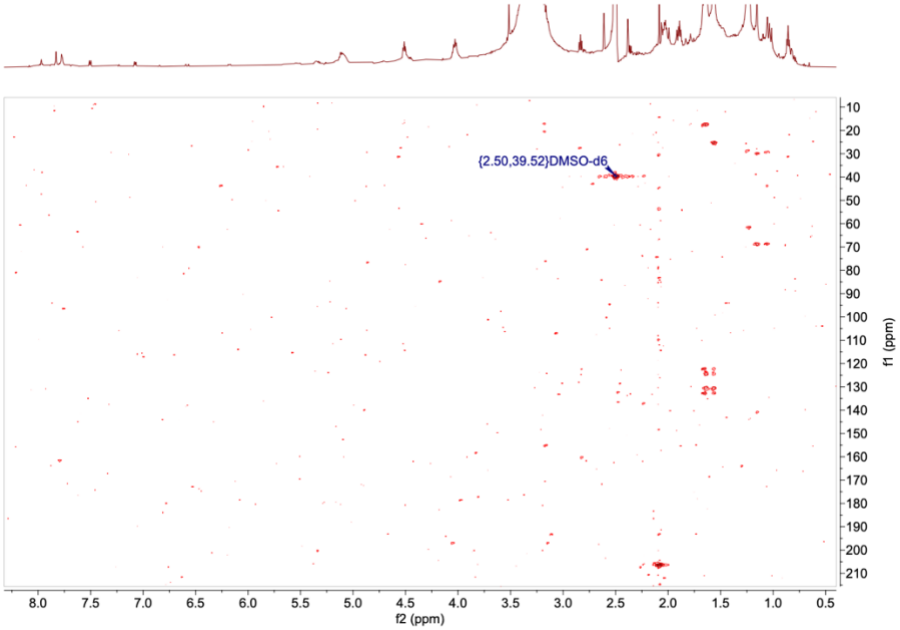

Figure 2.7.15. HMBC for synthetic homogosodesmine (**2.5**) (600 MHz, *d*$_6$-DMSO) 144 scans, NUS50 and 512 increments.

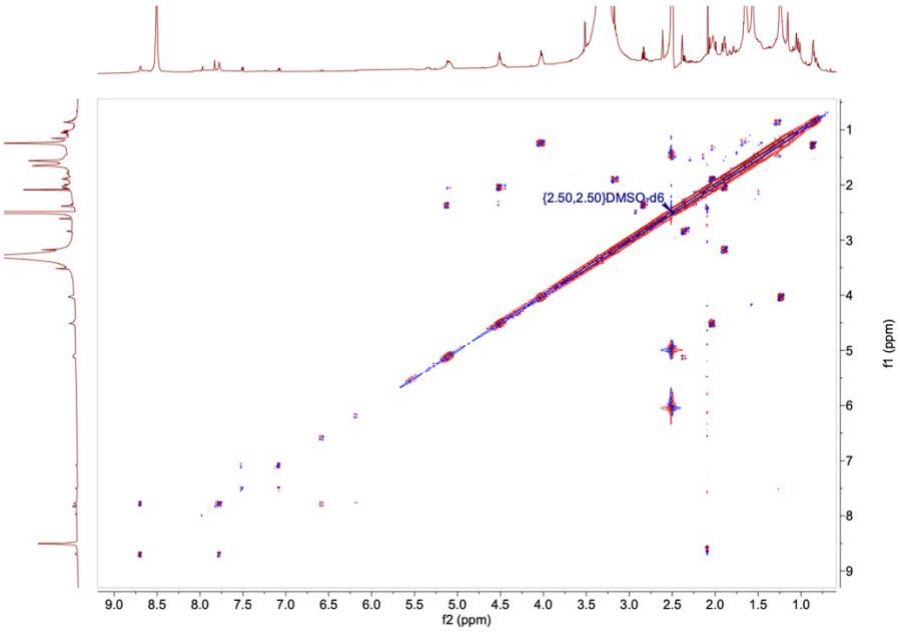

Figure 2.7.16. dqfCOSY for synthetic homogosodesmine (**2.5**) (600 MHz, *d*$_6$-DMSO) 96 scans, NUS50 and 400 increments.

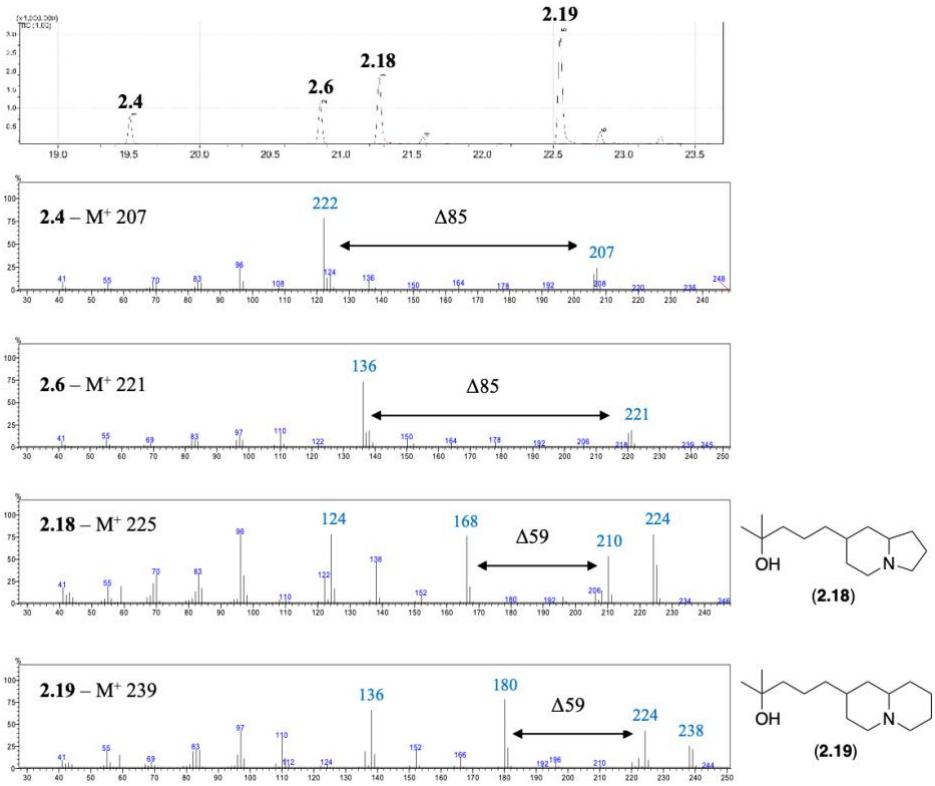

Figure 2.7.17. Hydration product from reaction of *B. petasata* crude extract with dilute HCl (aq).

Compound **2.4** converted to **2.18** and **2.6** converted to **2.19**.

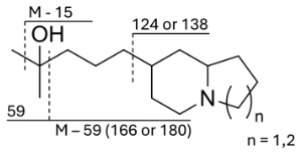

Figure 2.7.18. Fragmentation of **2.18** and **2.19**, the hydrate adducts of **2.4** and **2.6**, respectively.

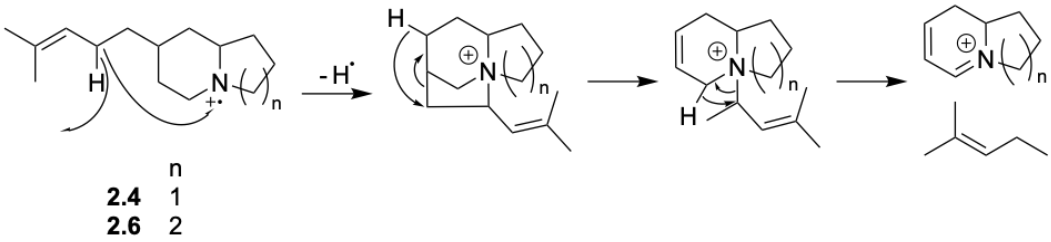

Figure 2.7.19. Plausible fragmentation mechanism that leads to observed loss of 85 Da in both **2.4** and **2.6.**

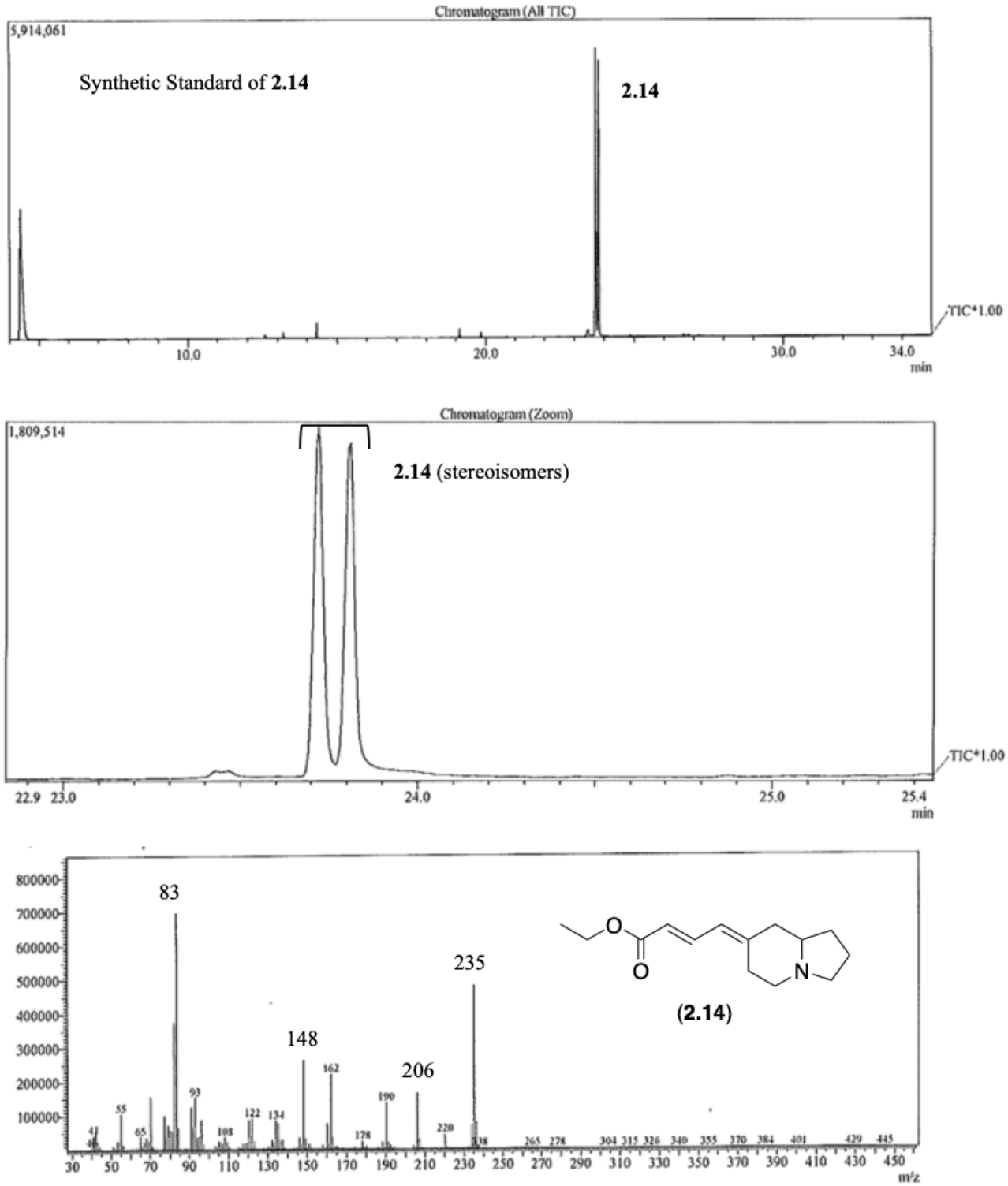

Figure 2.7.20. GCMS chromatogram and spectrum of the synthesized **2.14.**

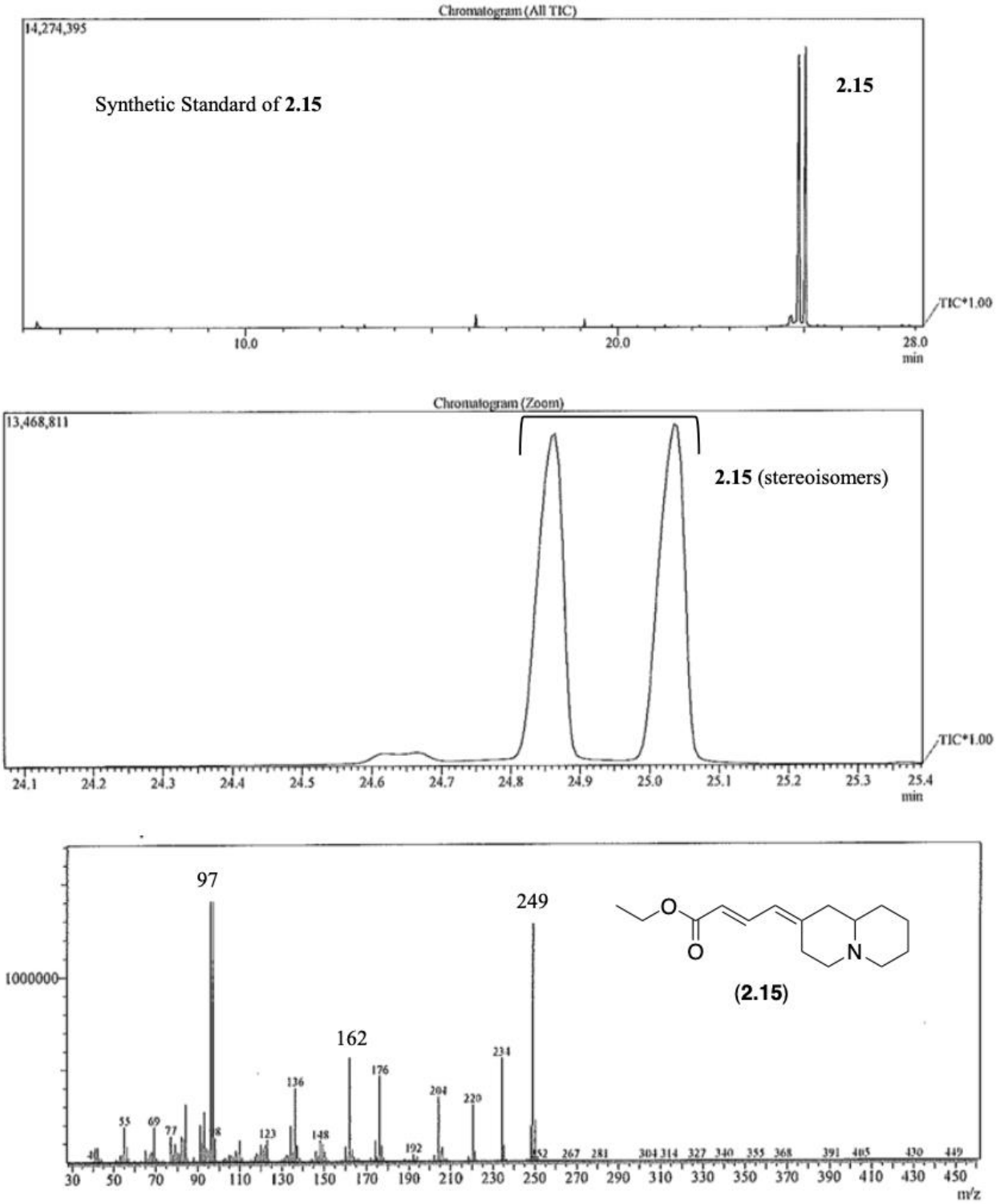

Figure 2.7.21. GCMS chromatogram and spectrum of the synthesized **2.15.**

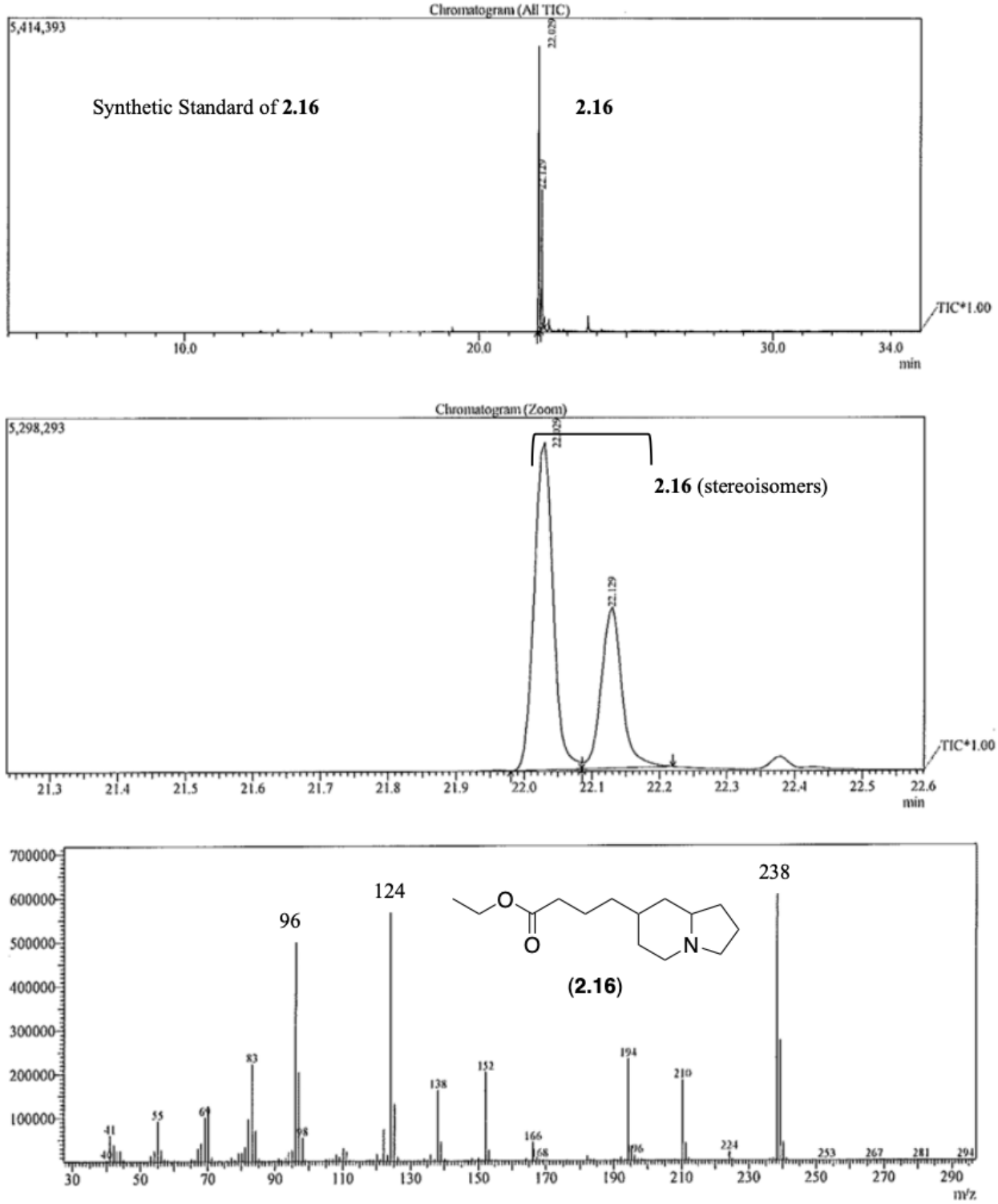

Figure 2.7.22. GCMS chromatogram and spectrum of the synthesized **2.16.**

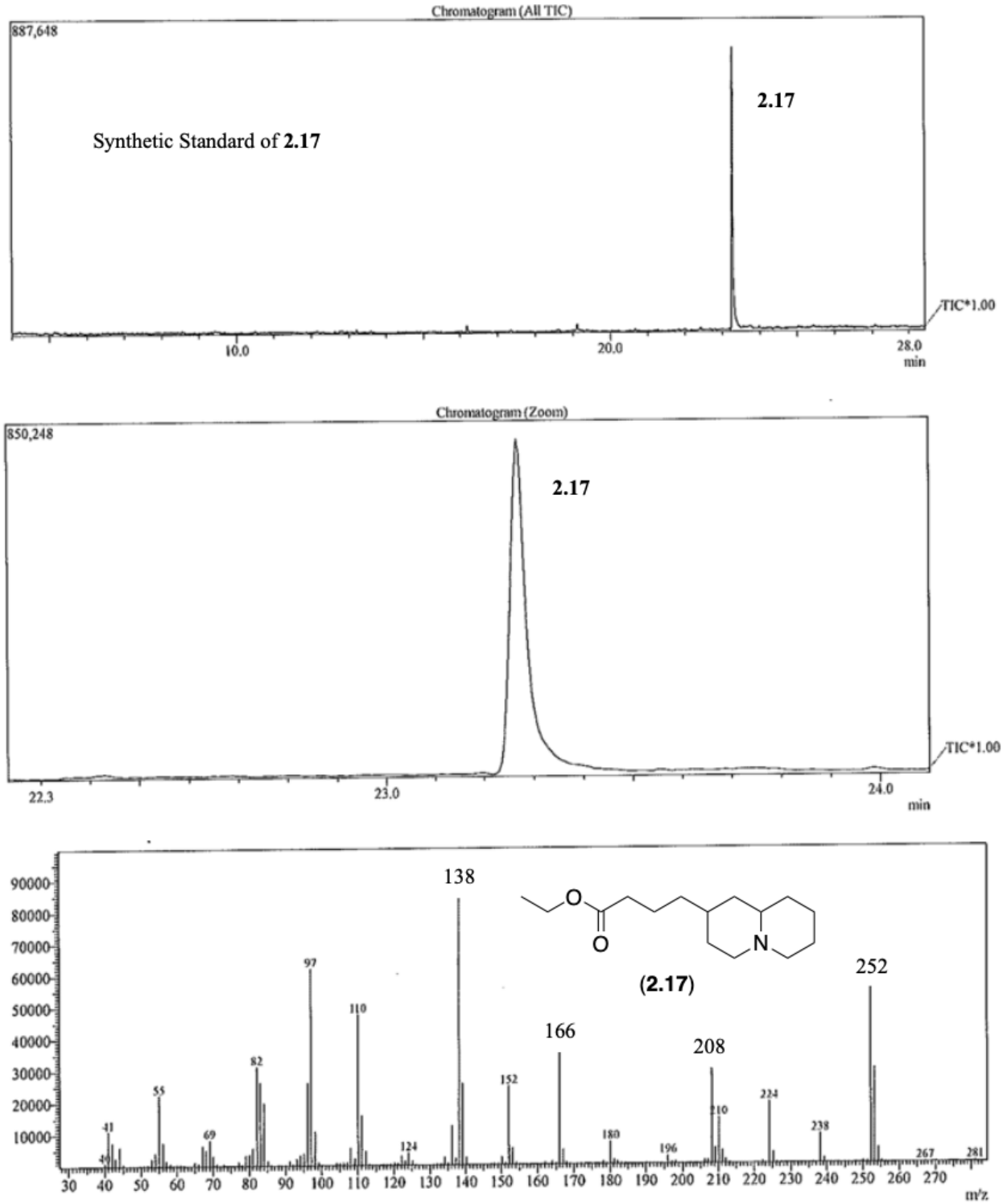

Figure 2.7.23. GCMS chromatogram and spectrum of the synthesized **2.17.**

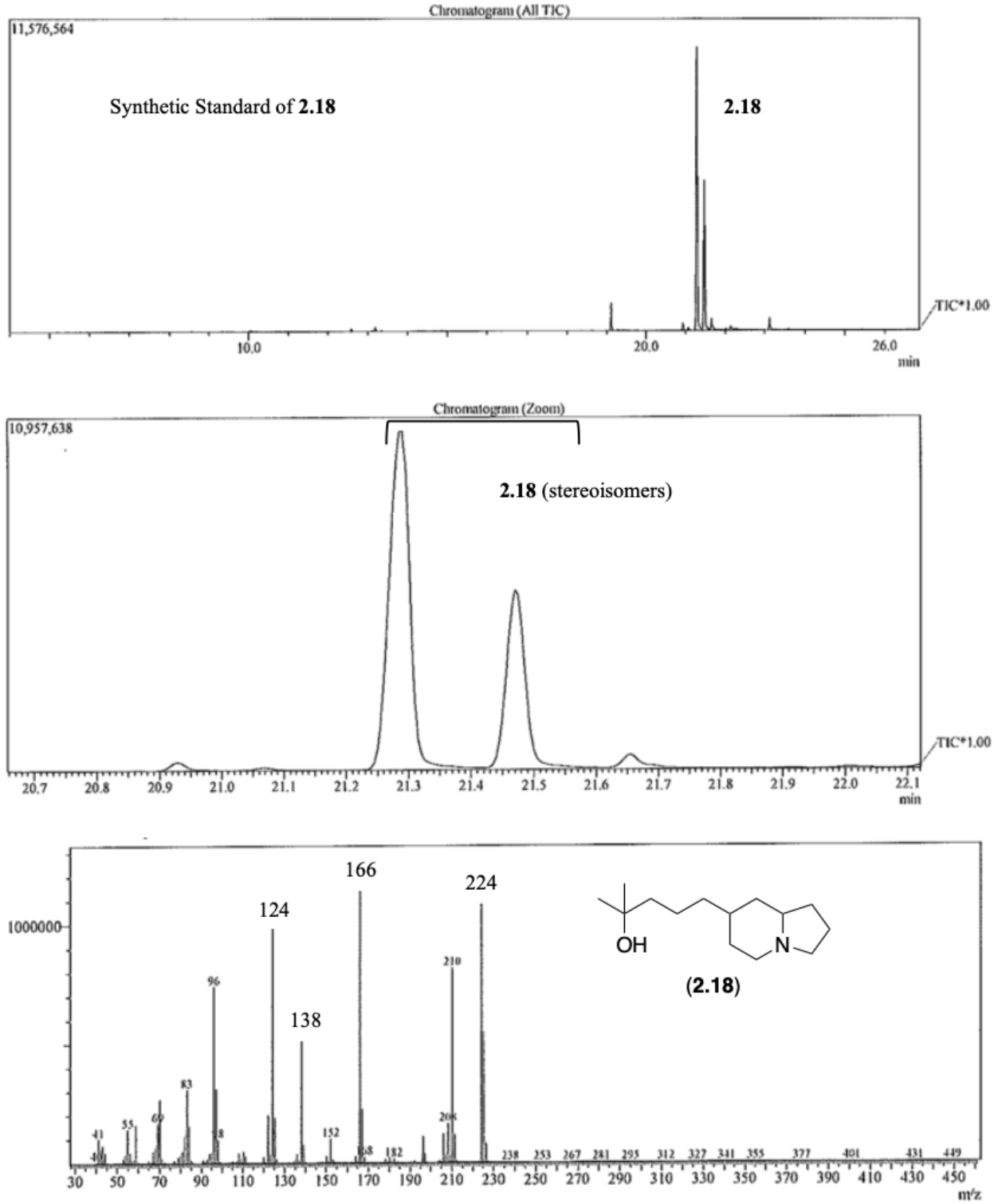

Figure 2.7.24. GCMS chromatogram and spectrum of the synthesized **2.18.**

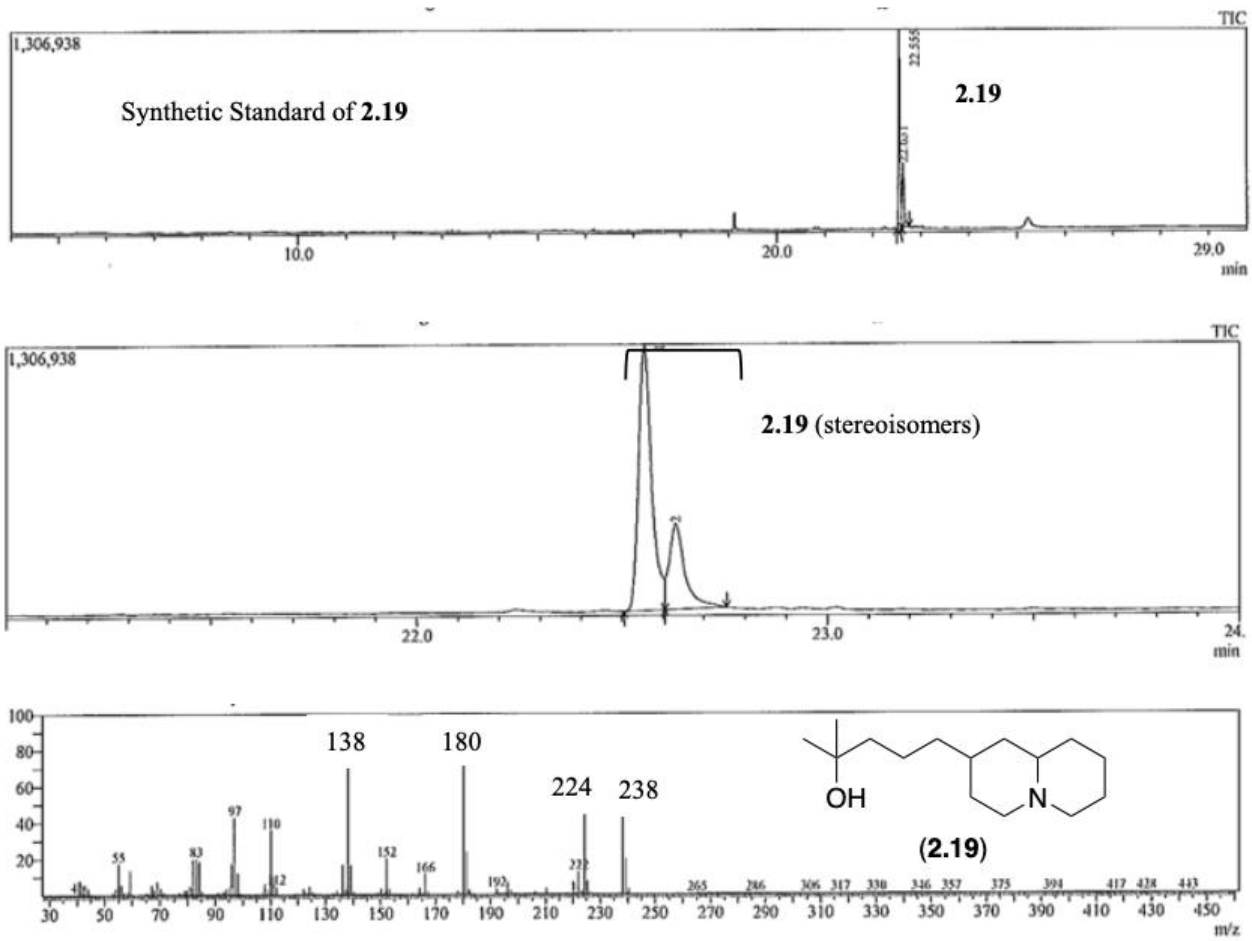

Figure 2.7.25. GCMS chromatogram and spectrum of the synthesized **2.19.**

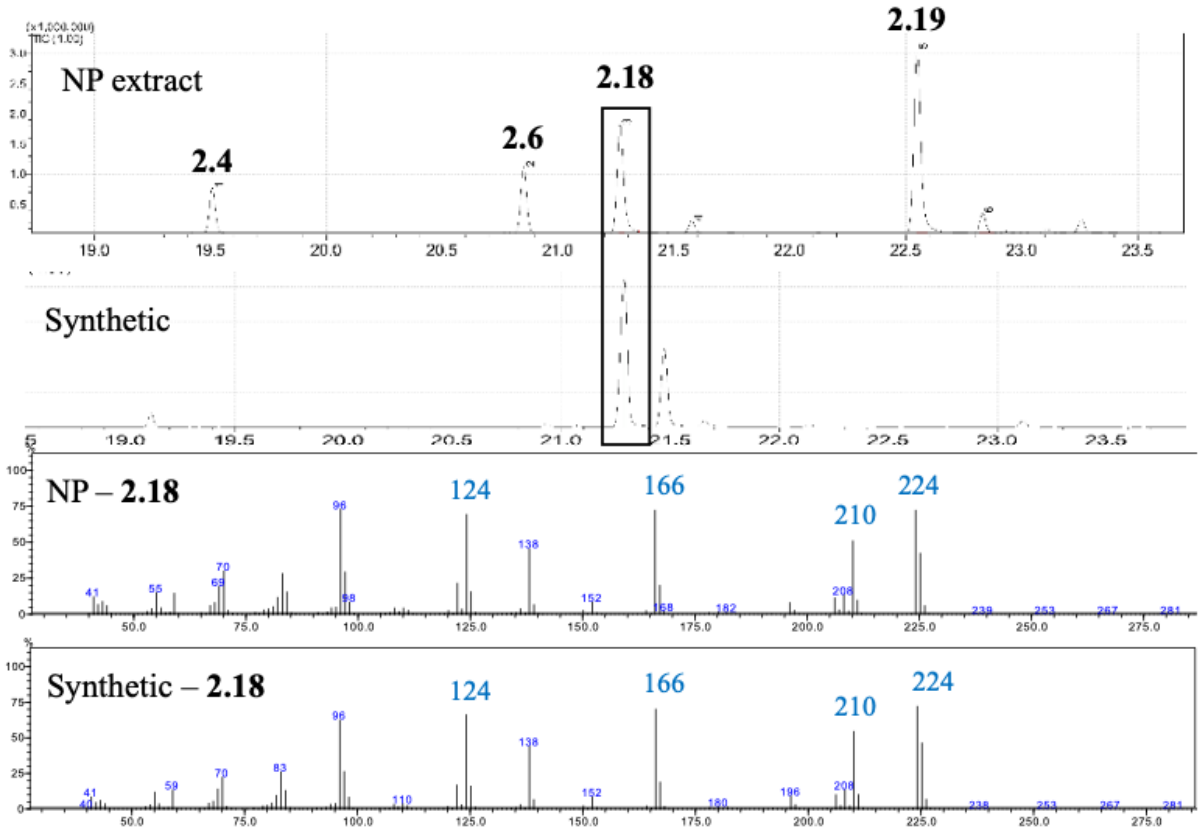

Figure 2.7.26. Comparison of synthetic **2.18** with hydration of *B. petasata* extract. The synthesis is a mixture of isomers with the *syn*-isomer the major product (first eluting peak). The fragmentation patterns for the synthetic and natural material match.

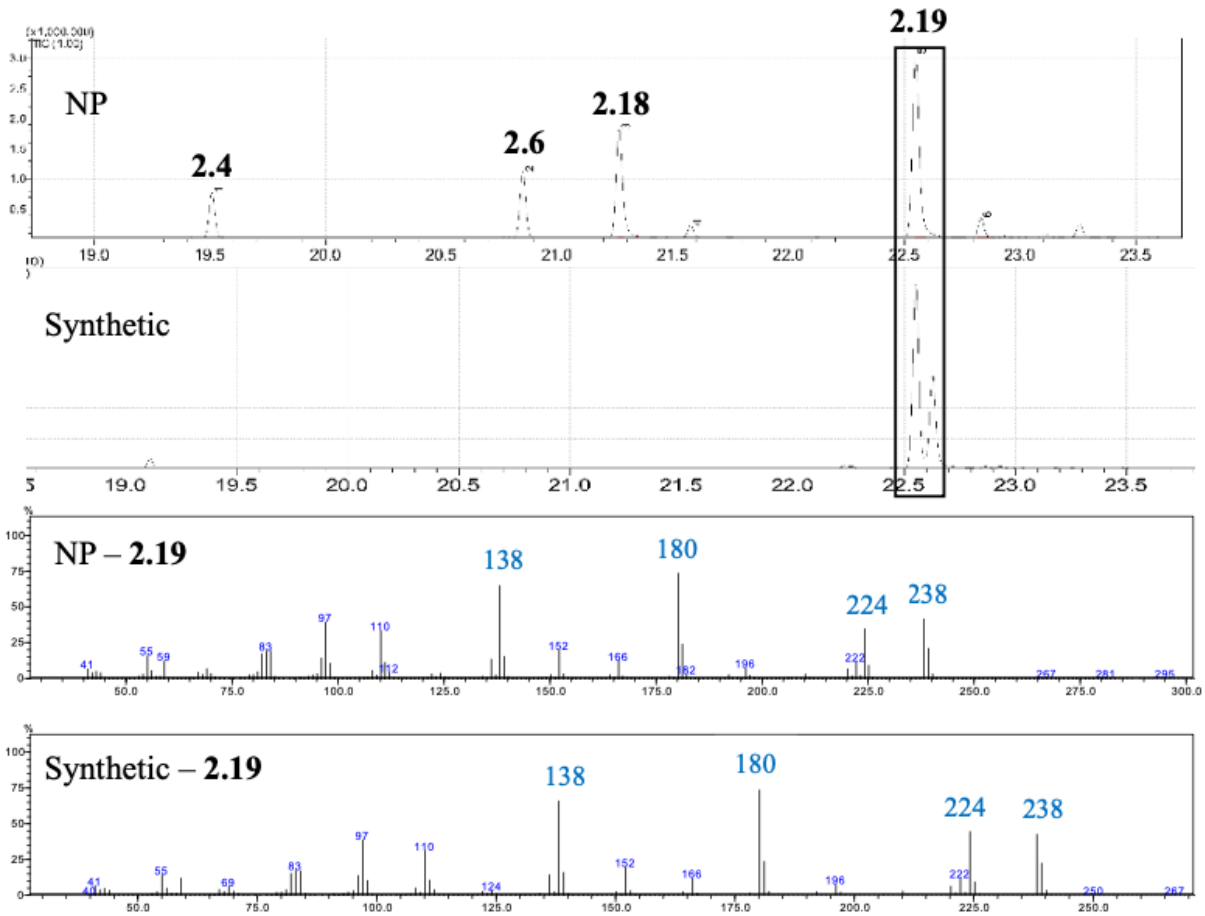

Figure 2.7.27. Comparison of synthetic **2.19** with hydration of *B. petasata* extract. The synthesis is a mixture of isomers with the *syn*-isomer the major product (first eluting peak). The fragmentation patterns for the synthetic and natural material match.

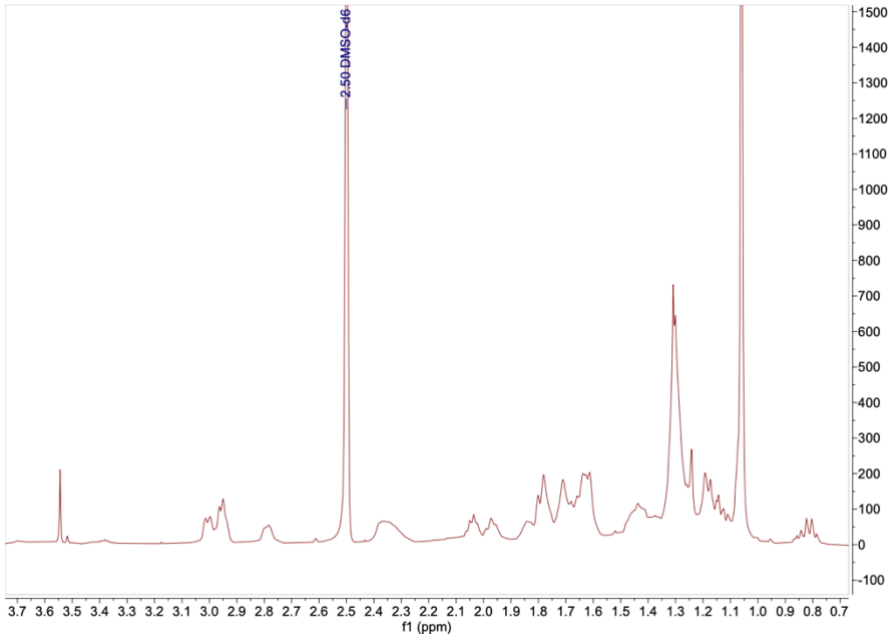

Figure 2.7.28. ^{1}H NMR spectrum for compound **2.18** (600 MHz, *d6*-DMSO) 16 scans, 50° C.

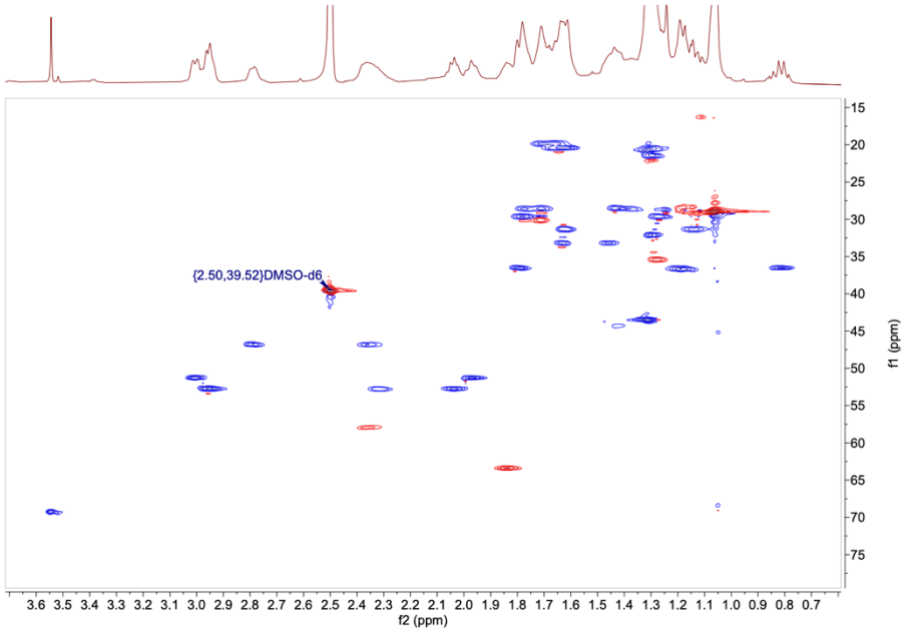

Figure 2.7.29. gHSQC for compound **2.18** (600 MHz, *d6*-DMSO) 16 scans, NUS25, 400 increments, and 50° C.

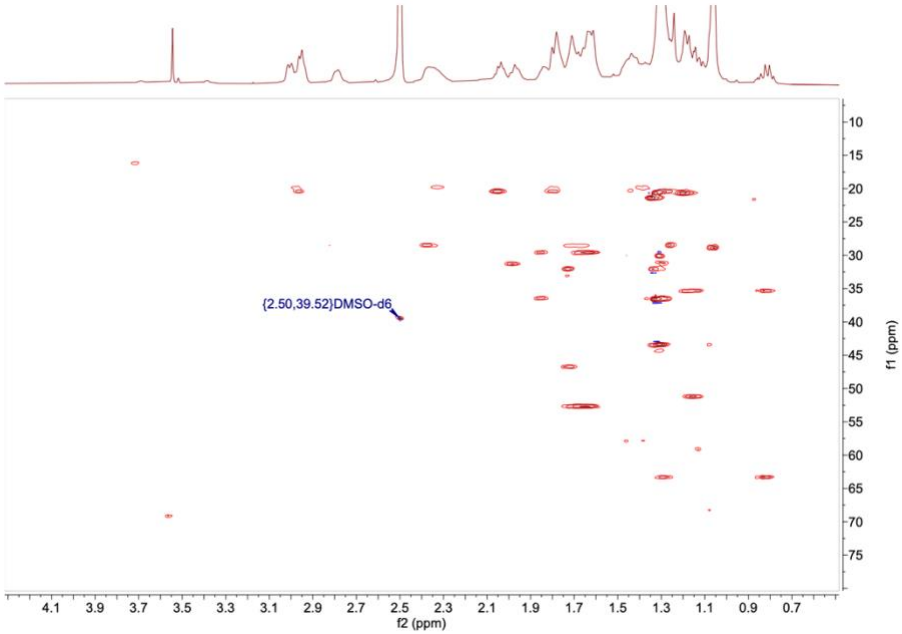

Figure 2.7.30. H2BC for compound **2.18** (600 MHz, *d6*-DMSO) 48 scans, NUS50, 400 increments, and 50° C.

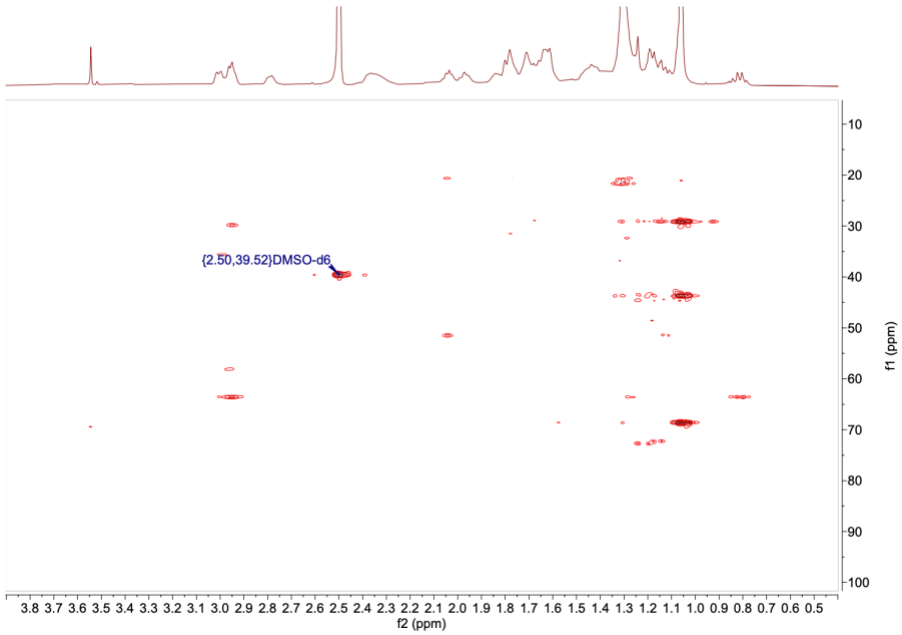

Figure 2.7.31. HMBC for compound **2.18** (600 MHz, *d6*-DMSO) 32 scans, NUS50, 512 increments, and 50° C.

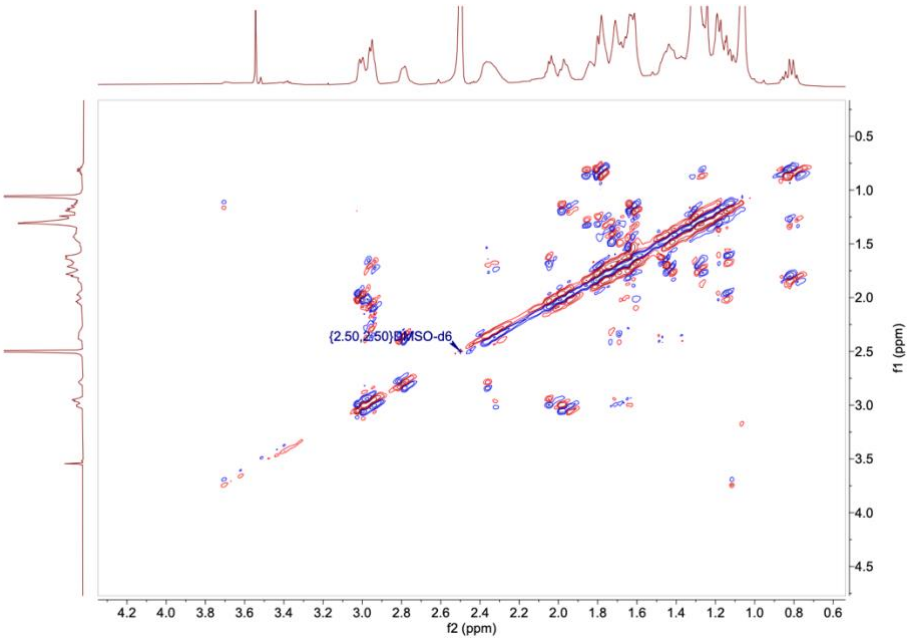

Figure 2.7.32. dqfCOSY for compound **2.18** (600 MHz, *d6*-DMSO) 16 scans, NUS50, and 400 increments, and 50° C.

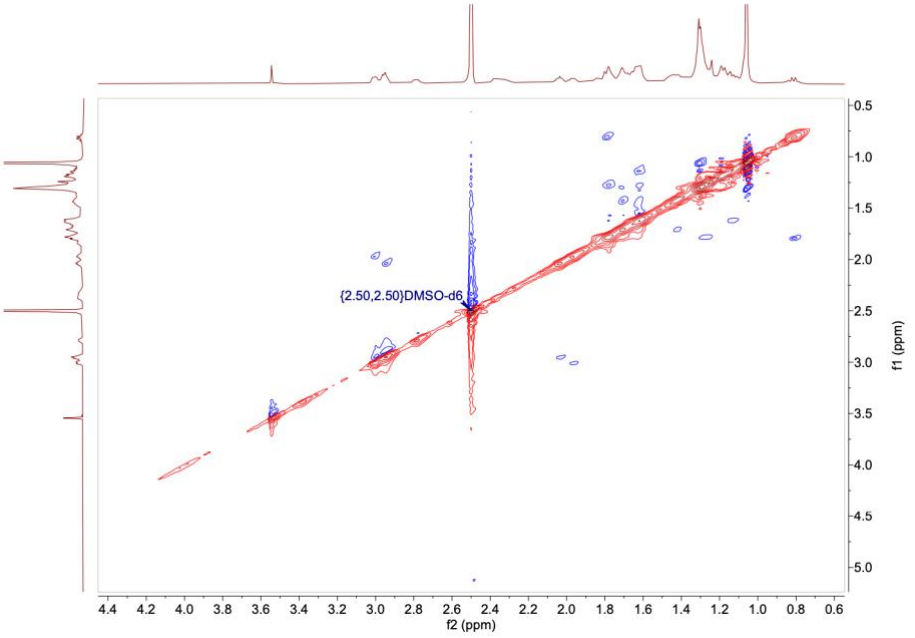

Figure 2.7.33. easyROESY for compound **2.18** (600 MHz, *d6*-DMSO) 40 scans, NUS50, 400 increments, 400 µsec mixing time, and 50° C.

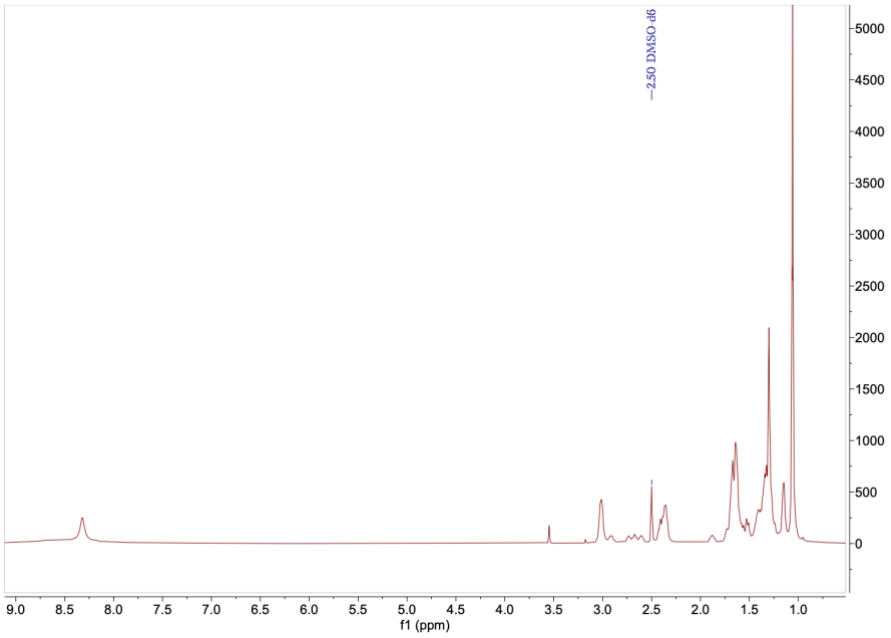

Figure 2.7.34. ^{1}H NMR spectrum for compound **2.19** (600 MHz, *d6*-DMSO) 16 scans, 50° C.

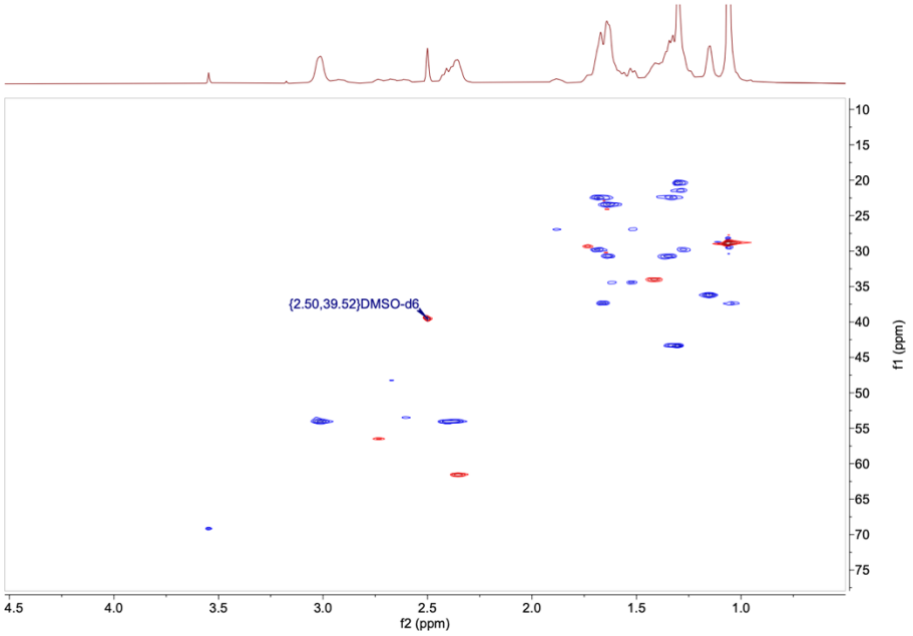

Figure 2.7.35. gHSQC for compound **2.19** (600 MHz, *d6*-DMSO) 16 scans, NUS25, 400 increments, and 50° C.

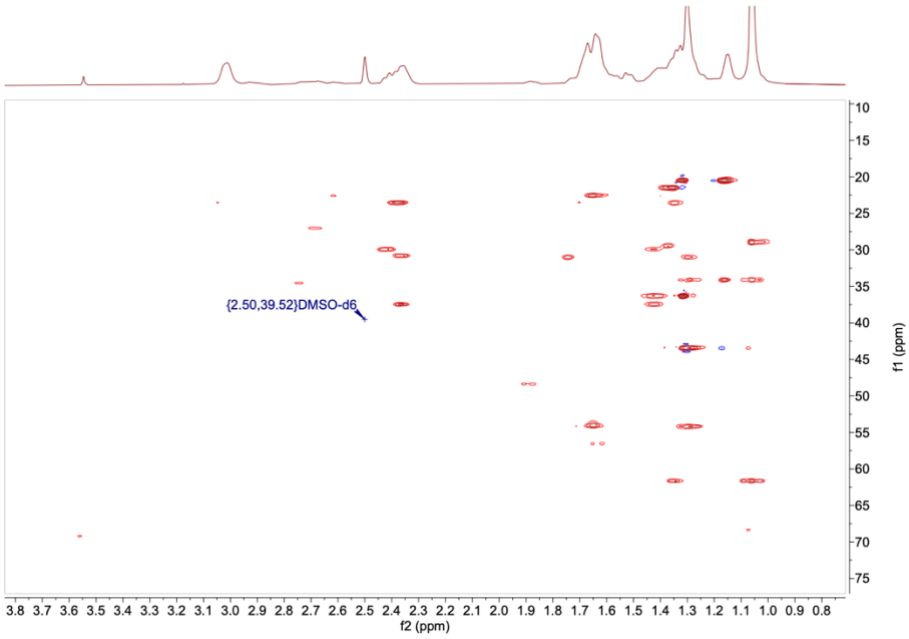

Figure 2.7.36. H2BC for compound **2.19** (600 MHz, *d*$_6$-DMSO) 48 scans, NUS50, 400 increments, and 50° C.

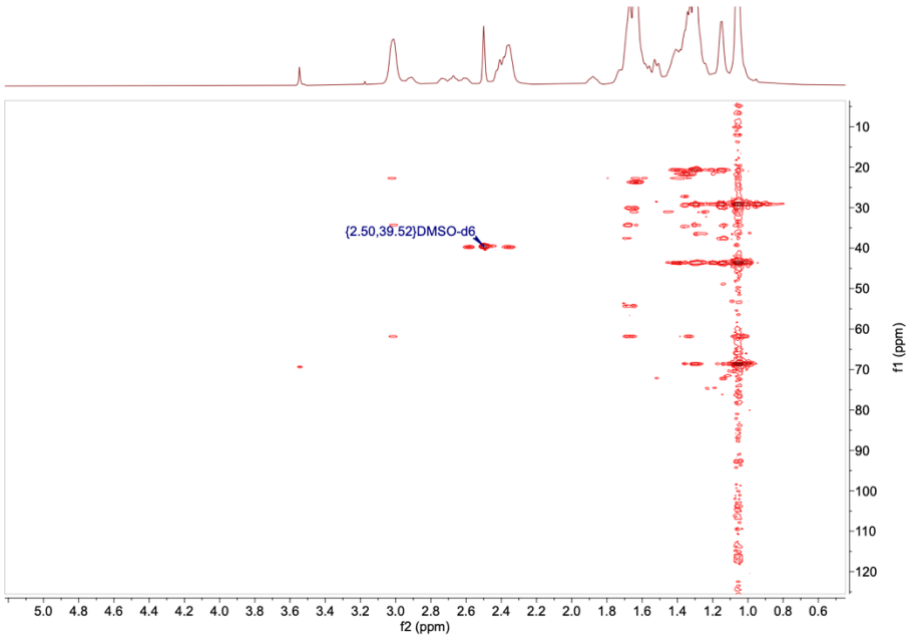

Figure 2.7.37. HMBC for compound **2.19** (600 MHz, *d*$_6$-DMSO) 32 scans, NUS50, 512 increments, and 50° C.

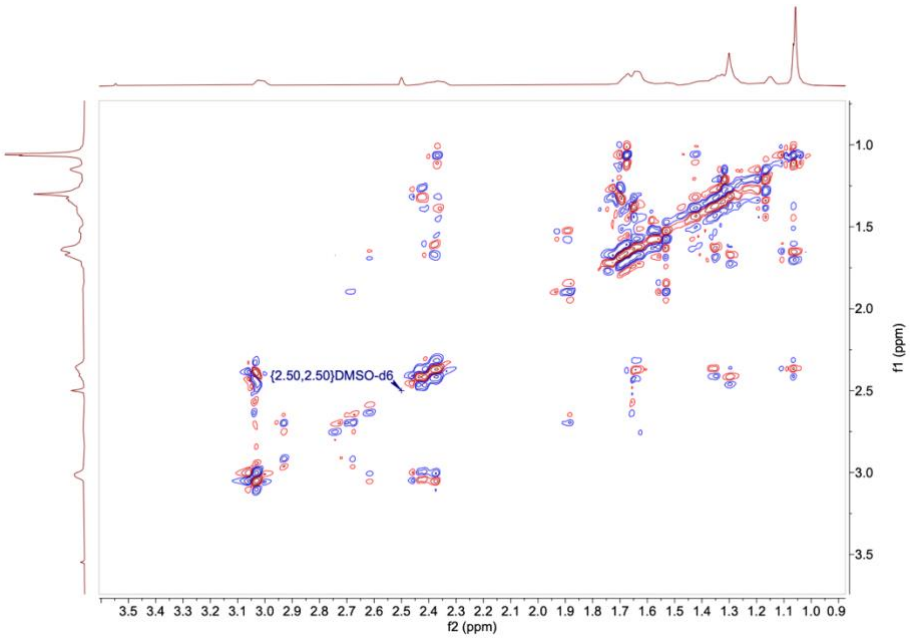

Figure 2.7.38. dqfCOSY for compound **2.19** (600 MHz, *d6*-DMSO) 16 scans, NUS50, and 400 increments, and 50° C.

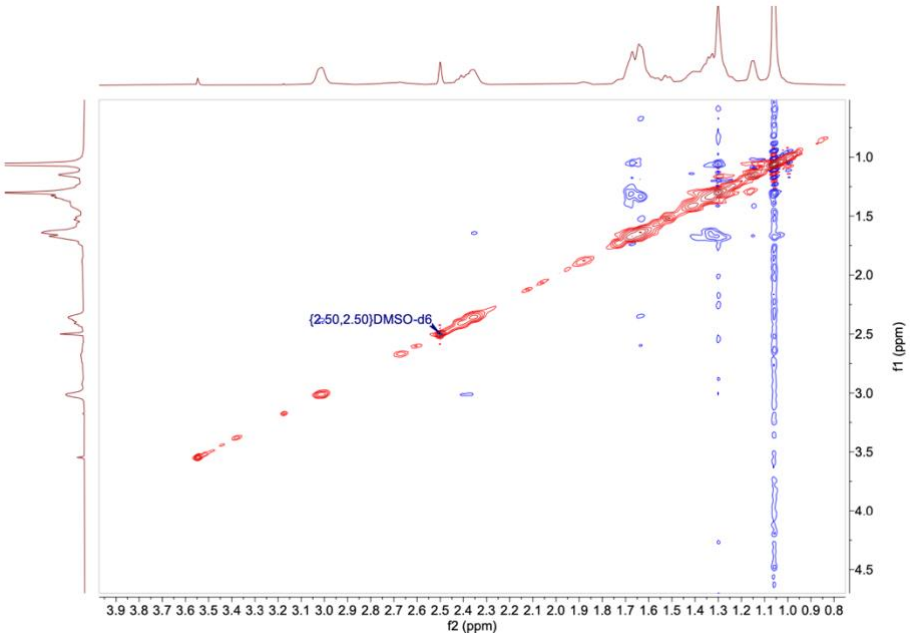

Figure 2.7.39. easyROESY for compound **2.19** (600 MHz, *d6*-DMSO) 40 scans, NUS50, 400 increments, 400 µsec mixing time, and 50° C.

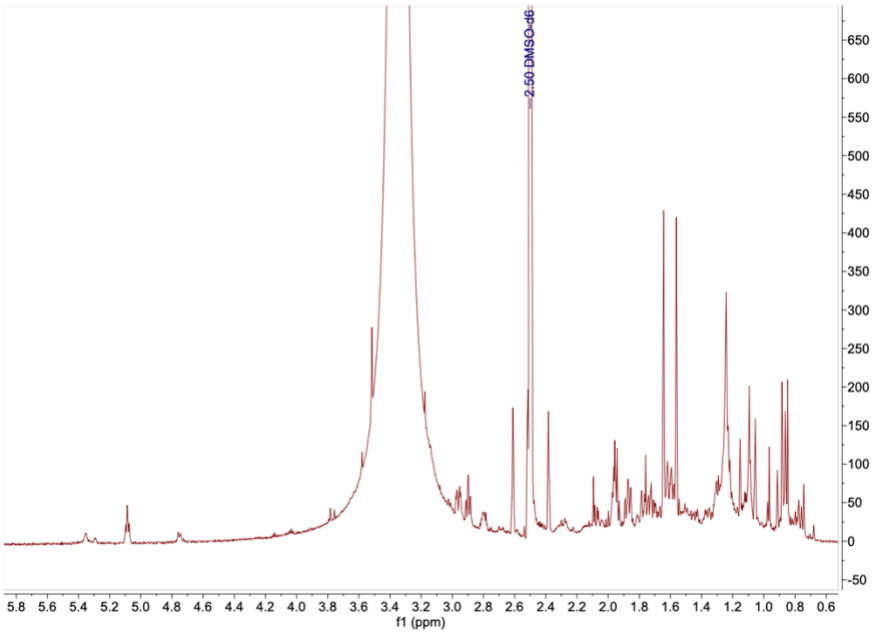

Figure 2.7.40. ^{1}H NMR spectrum for hydrogosodesmine (**2.4**) (600 MHz, *d*$_6$-DMSO) 128 scans, 50° C.

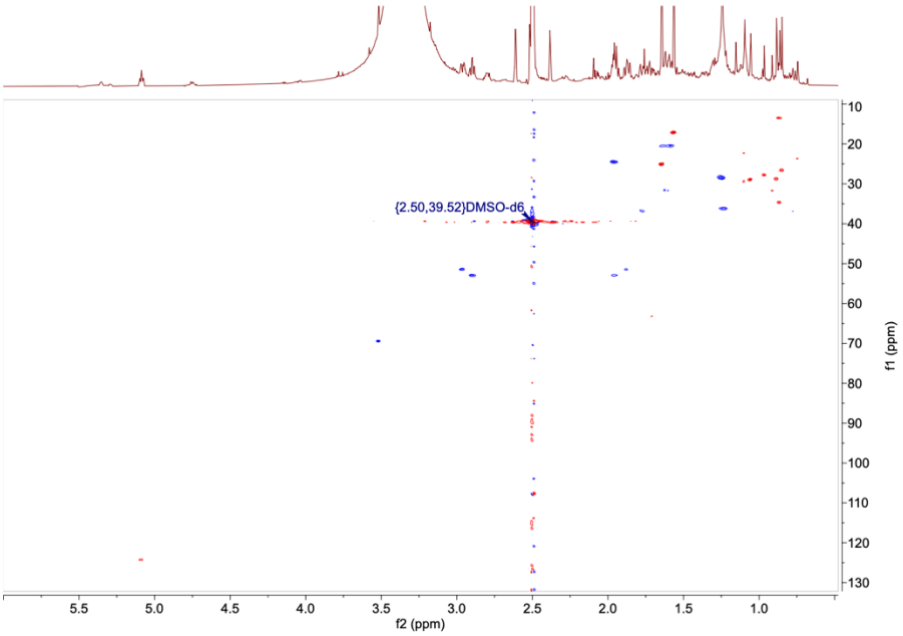

Figure 2.7.41. gHSQC for hydrogosodesmine (**2.4**) (600 MHz, *d*$_6$-DMSO) 96 scans, NUS25, 400 increments.

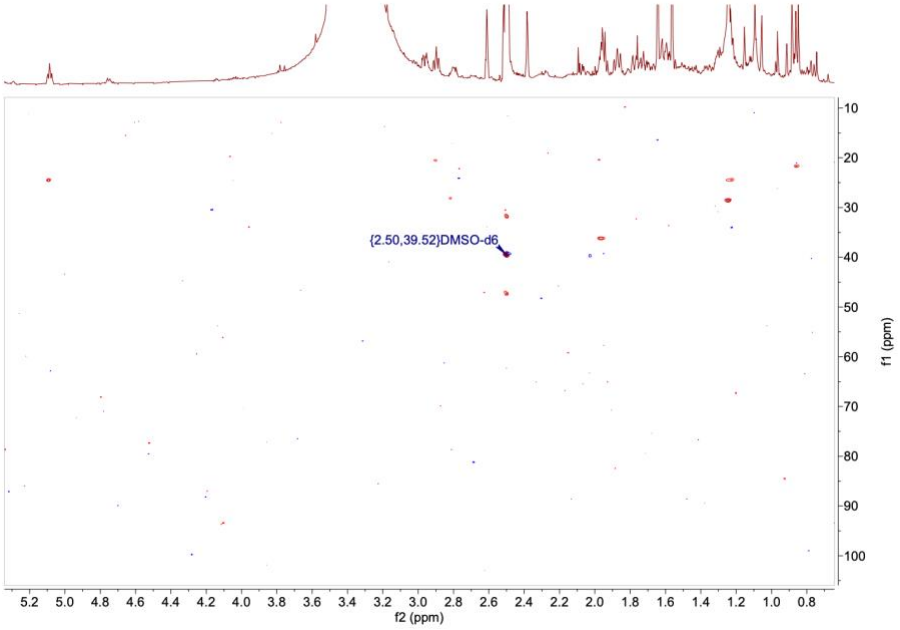

Figure 2.7.42. H2BC for hydrogosodesmine (**2.4**) (600 MHz, *d*$_6$-DMSO) 160 scans, NUS50, 400 increments, and 50° C.

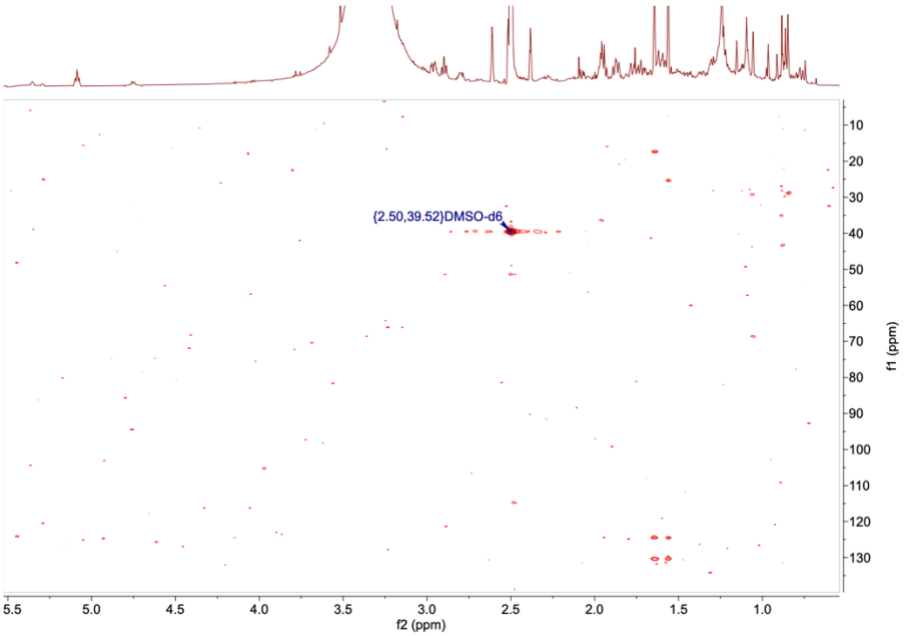

Figure 2.7.43. HMBC for hydrogosodesmine (**2.4**) (600 MHz, *d*$_6$-DMSO) 64 scans, NUS50, and 512 increments.

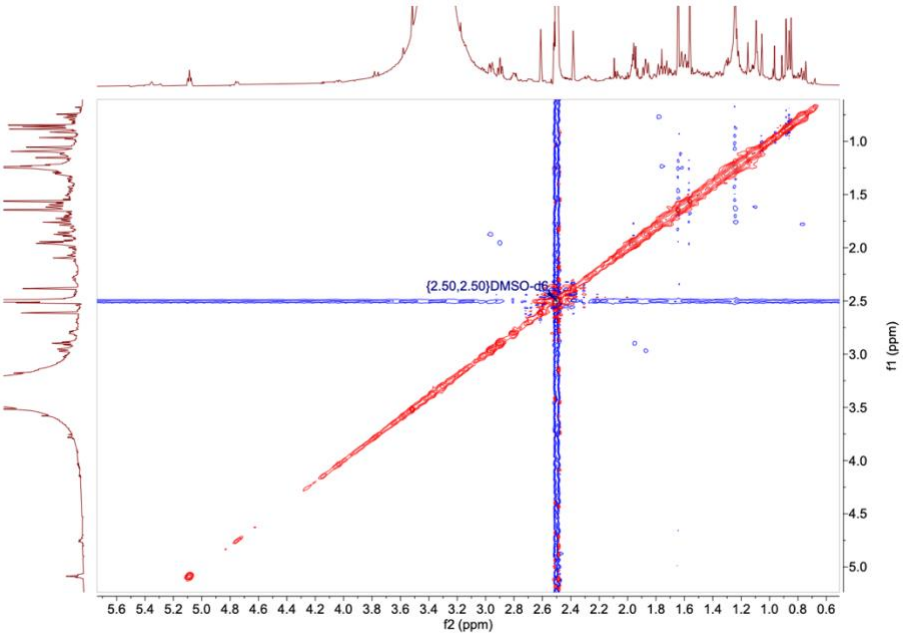

Figure 2.7.44. easyROESY for hydrogosodesmine (**2.4**) (600 MHz, *d6*-DMSO) 128 scans, NUS50, 400 increments, and 400 µsec mixing time.

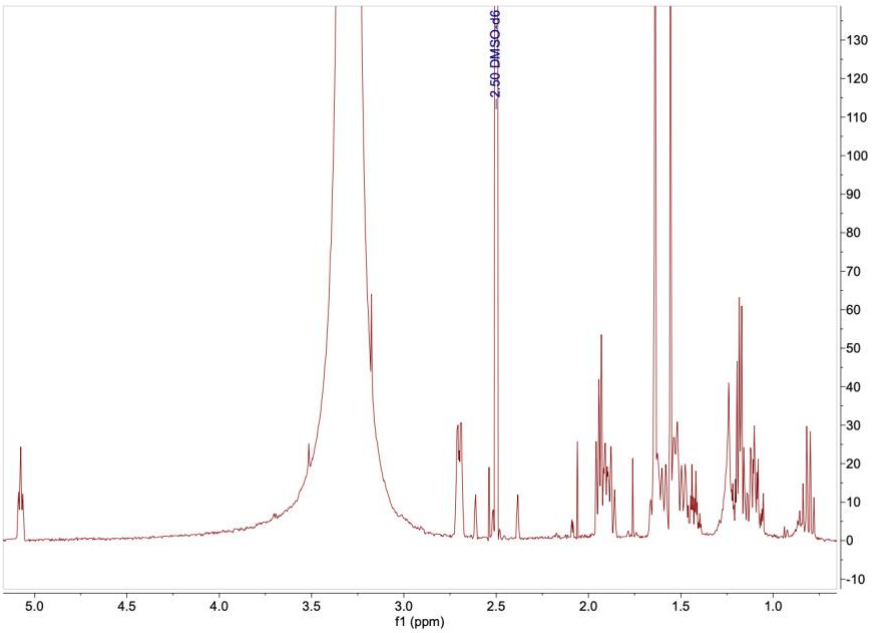

Figure 2.7.45. ^{1}H NMR spectrum for homo-hydrogosodesmine (**2.6**) (600 MHz, *d6*-DMSO) 128 scans, 50° C.

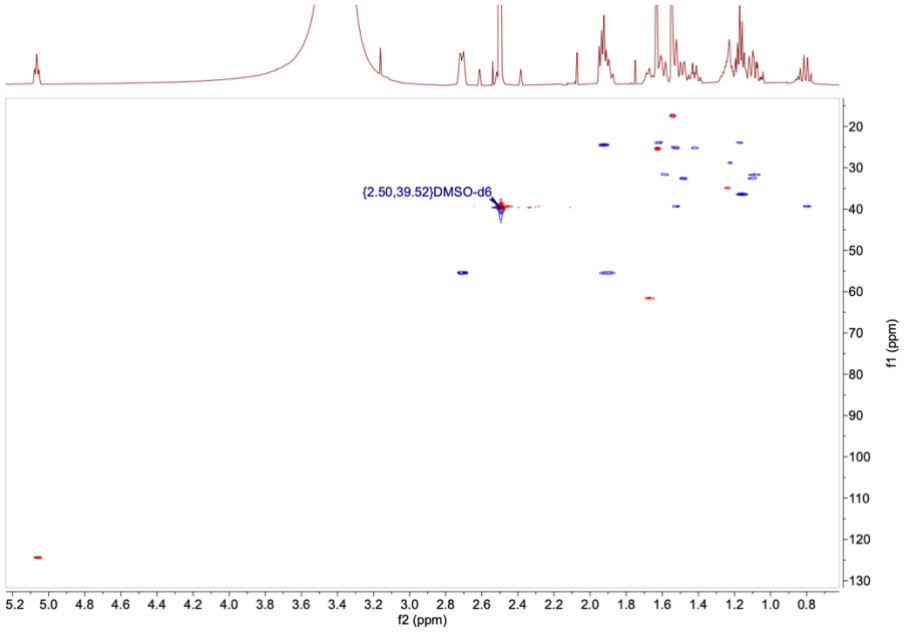

Figure 2.7.46. gHSQC for homo-hydrogosodesmine (**2.6**) (600 MHz, *d6*-DMSO) 32 scans, NUS25, 400 increments.

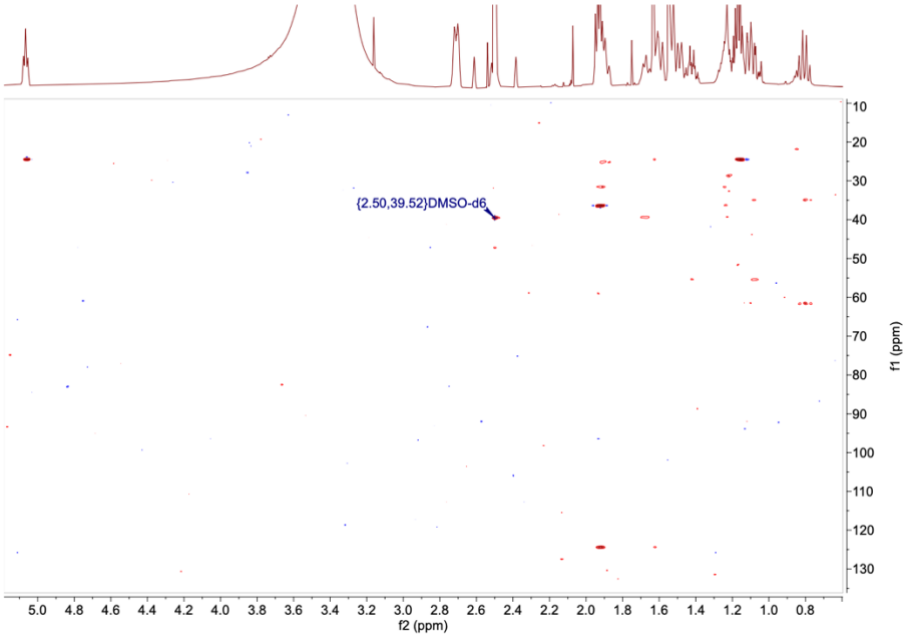

Figure 2.7.47. H2BC for homo-hydrogosodesmine (**2.6**) (600 MHz, *d6*-DMSO) 160 scans, NUS50, 400 increments, and 50° C.

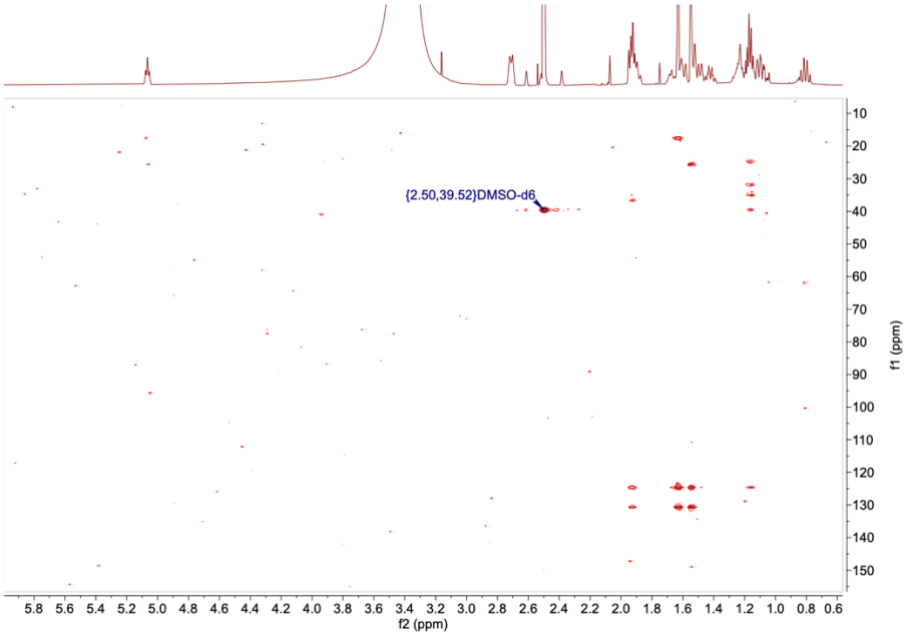

Figure 2.7.48. HMBC for homo-hydrogosodesmine (**2.6**) (600 MHz, *d6*-DMSO) 64 scans, NUS50, and 512 increments.

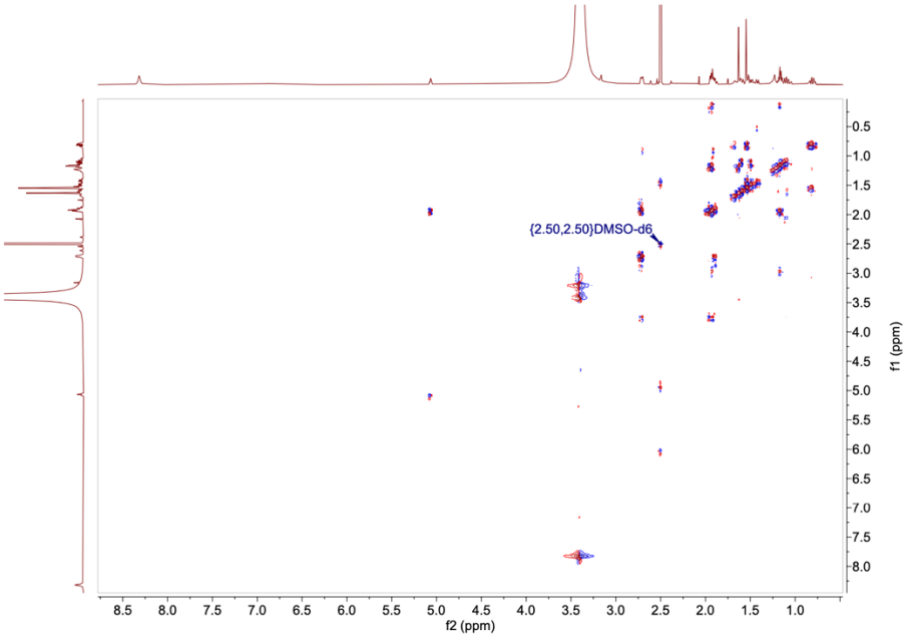

Figure 2.7.49. dqfCOSY for homo-hydrogosodesmine (**2.6**) (600 MHz, *d6*-DMSO) 32 scans, NUS50, and 400 increments.

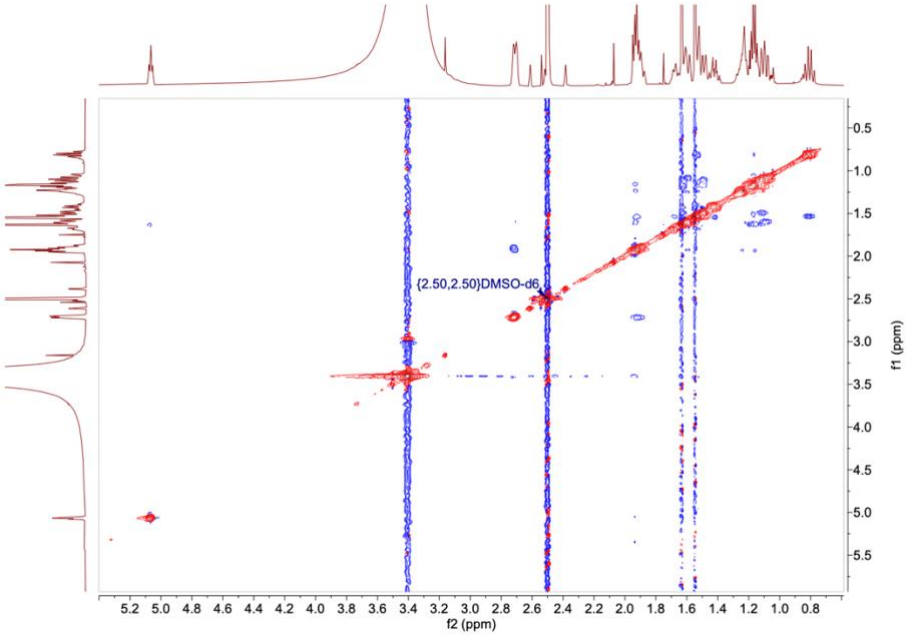

Figure 2.7.50. easyROESY for homo-hydrogosodesmine (**2.6**) (600 MHz, *d*$_6$-DMSO) 128 scans, NUS50, 400 increments, and 400 µsec mixing time.

2.8. Appendix Tables

Table 2.8.1. NMR Spectroscopy Data for Synthetic Homogosodesmine (**2.5**) (600 MHz, *d*$_6$-DMSO, 50° C)

Position	δ_C, type[a]	δ_H (J in Hz)	H2BC	HMBC	COSY
1	124.4, CH	5.09, m			8
2	61.3, CH_2	4.02, m			8
3	54.0, CH_2	4.51, m			4
4	20.4, CH_2	2.02, m	4, 5		3, 5
5	16.8, CH_2	1.88, m			4, 6
6	27.3, CH_2	3.16, m	5	4, 5	5
7	ND[b]				
8	28.6, CH_2	1.24, m			1, 2
9	132.5, C				
10	34.3, CH_2	2.84, t (7.62)		12	11
11	27.1, CH_2	2.36, m	10		10, 12
12	122.0, CH	5.11, m			11
13	130.3, C				
14	17.3, CH_3	1.56, m		12, 13, 15	
15	25.1, CH_3	1.64, m		12, 13, 14	

[a]δ_C obtained indirectly from gHSQC and gHMBC experiments. [b]ND: Not detected. Significant peak broadening occurred in signals near the tertiary amine. This led to weak and/or missing signals.

Table 2.8.2. NMR Spectroscopy Data for Synthetic *Syn*-Isomer of **2.18** (600 MHz, d_6-DMSO, 50° C)

Position	δ_C, type[a]	δ_H (J in Hz)	H2BC	HMBC	COSY
1	31.4, CH_2	1.62, m 1.14, m	2		2
2	51.3, CH_2	3.00, m 1.97, m			1
3	52.7, CH_2	2.95, m 2.04, m	4	2	4
4	20.4, CH_2	1.66, m 1.62, m	3, 5		3
5	29.6, CH_2	1.78, m 1.27, m	4, 6		
6	63.4, CH	1.83, m	5, 7		
7	36.5, CH_2	1.78, m 1.80, m	6, 8	6	8
8	35.4, CH	1.28, m	1		7
9	32.1, CH_2	1.28, m			
10	21.4, CH_2	1.29, m	12		
11	43.7, CH	1.31, m	10	10, 13, 14	
12	68.2, C				
13	29.0, CH_3	1.06, m		11, 12, 14	
14	29.0, CH_3	1.06, m		11, 12, 13	

[a]δ_C obtained indirectly from gHSQC and gHMBC experiments.

Table 2.8.3. NMR Spectroscopy Data for Synthetic *Anti*-Isomer of **2.18** (600 MHz, d_6-DMSO, 50° C)

Position	δ_C, type[a]	δ_H (J in Hz)	H2BC	HMBC	COSY
1	28.6, CH_2	1.71, m			
		1.42, m			
2	46.8, CH_2	2.79, m	1		
		2.36, m			
3	52.8, CH_2	2.95, m	4	3	4
		2.31, m			
4	19.9, CH_2	1.71, m	3, 5	5	3
		1.66, m			
5	28.6, CH_2	1.77, m	4		
		1.36, m			
6	58.0, CH	2.36, m	5		
7	33.2, CH_2	1.62, m			8
		1.46, m			
8	30.1, CH	1.71, m	1		7
9	36.7, CH_2	1.19, m	10		
10	20.7, CH_2	1.31, m	9, 11		
11	43.6, CH	1.32, m	10	10, 13, 14	
12	68.6, C				
13	28.6, CH_3	1.06, m		11, 12, 14	
14	28.6, CH_3	1.06, m		11, 12, 13	

[a] δ_C obtained indirectly from gHSQC and gHMBC experiments.

Table 2.8.4. NMR Spectroscopy Data for Synthetic *Syn*-Isomer of **2.19**

(600 MHz, d_6-DMSO, 50° C)

Position	δ_C, type[a]	δ_H (J in Hz)	H2BC	HMBC	COSY	ROESY
1	31.4, CH_2	1.69, m 1.27, m	2		2	
2	51.3, CH_2	3.01, m 2.40, m	1		1, 6, 14, 15	
3	52.7, CH_2	3.01, m 2.36, m			5	
4	20.4, CH_2	1.69, m 1.30, m				
5	23.5, CH_2	1.64, m			3	
6	30.7, CH_2	1.64, m 1.35, m	5, 7	5	7	
7	61.6, CH	2.35, m	6, 8		6, 14, 15	9
8	37.4, CH_2	1.66, m 1.04, m	7, 9		14, 15	
9	34.1, CH	1.41, m	1, 8	11, 12	14, 15	7
10	36.1, CH_2	1.15, m	9, 11	11. 12		
11	20.4, CH_2	1.30, m	10, 12	12		
12	43.4, CH	1.31, m	11	11, 13, 14, 15		
13	68.6, C					
14	28.9, CH_3	1.06, m		7, 12, 13, 15	7, 8, 9	
15	28.9, CH_3	1.06, m		7, 12, 13, 14	7, 8, 9	

[a]δ_C obtained indirectly from gHSQC and gHMBC experiments.

Table 2.8.5. NMR Spectroscopy Data for Synthetic *Anti*-Isomer of **2.19**

(600 MHz, d_6-DMSO, 50° C)

Position	δ_C, type[a]	δ_H (J in Hz)	H2BC	HMBC	COSY
1	26.9, CH_2	1.88, m 1.52, m	2		2
2	48.3, CH_2	2.91, m 2.67, m	1		1
3	53.5, CH_2	3.03, m 2.61, m			
4	22.4, CH_2	1.64, m 1.39, m			
5	23.4, CH_2	1.60, m			
6	30.8, CH_2	1.64, m 1.32, m	5, 7	5	
7	56.5, CH	2.73, m	8		
8	34.4, CH_2	1.62, m 1.53, m	7, 9		14, 15
9	29.3, CH	1.73, m			
10	36.2, CH_2	1.15, m		12	
11	21.5, CH_2	1.29, m	10, 12	12	
12	43.3, CH	1.34, m	11	11, 13, 14, 15	
13	68.5, C				
14	28.5, CH_3	1.06, m		12, 13, 15	8
15	28.5, CH_3	1.06, m		12, 13, 14	8

[a]δ_C obtained indirectly from gHSQC and gHMBC experiments.

Table 2.8.6. NMR Spectroscopy Data for Natural Hydrogosodesmine (**2.4**)

(600 MHz, d_6-DMSO, 50° C)

Position	δ_C, type[a]	δ_H (J in Hz)	H2BC	HMBC	ROESY
1	29.8, CH_2	1.75, m			
		1.23, m			
2	51.5, CH_2	2.97, m			
		1.88, m			
3	53.0, CH_2	2.90, m	4		
		1.96, m			
4	20.4, CH_2	1.64, m			
		1.59, m			
5	28.5, CH_2	1.25, m			
6	63.3, CH	1.71, m			
7	36.8, CH_2	1.77, m			
		0.78, m			
8	31.4, CH	2.10, m			
9	36.1, CH_2	1.23, m	10		
10	24.4, CH_2	1.96, m		9	
11	124.2, CH	5.09, m	10		14
12	130.3, C				
13	17.1, CH_3	1.57, s		11, 12, 14	
14	25.0, CH_3	1.65, s		11, 12, 13	11

[a]δ_C obtained indirectly from gHSQC and gHMBC experiments.

Table 2.8.7. NMR Spectroscopy Data for Natural Homo-Hydrogosodesmine (**2.6**) (600 MHz, *d*$_6$-DMSO, 50° C)

Position	δ_C, type[a]	δ_H (J in Hz)	H2BC	HMBC	COSY	ROESY
1	31.6, CH_2	1.59, m 1.08, m	2			
2	55.5, CH_2	2.72, m 1.88, m	1		3	1, 3
3	55.4, CH_2	2.70, m 1.92, m	4		2	2
4	25.2, CH_2	1.53, m 1.42, m	3			
5	23.9, CH_2	1.61, m 1.17, m	4			
6	32.6, CH_2	1.48, m 1.10, m	7	5		
7	61.6, CH	1.67, m	6, 8			
8	39.4, CH_2	1.53, m 0.80, m	9, 7			
9	34.9, CH	1.24, m	1, 8		11	
10	36.4, CH_2	1.16, m	11	1, 8, 9, 12, 11	11	11
11	24.5, CH_2	1.92, m	10, 12	10, 12	9, 11, 12	10, 12, 14, 15
12	124.4, CH	5.06, m	11	13, 14	11	11, 15
13	130.6, C					
14	17.5, CH_3	1.54, s		12, 13, 15		11
15	25.4, CH_3	1.62, s		12, 13, 14		11, 12

[a]δ_C obtained indirectly from gHSQC and gHMBC experiment

Chapter 3.

Neuromodulating Alkaloids from Millipede Defensive Secretions

Carla Menegatti,[1+] Jared S. Wood,[2+] Paige Banks,[1+] Kenneth Knott, [1] Jonathan S. Briganti,[3,4] Anthony J. Briganti,[3,4] Samuel V. G. McNally,[5] Paul E. Marek,[6] Anne M. Brown,[3,4] Tappey H. Jones,[7] R. Thomas Williamson,[2] Emily Mevers[1]

1. Department of Chemistry, Virginia Tech, Blacksburg, VA
2. Department of Chemistry & Biochemistry, University of North Carolina Wilmington, Wilmington, NC 28403
3. Department of Biochemistry, Virginia Tech, Blacksburg, VA 24061
4. University Libraries, Virginia Tech, Blacksburg, VA 24061
5. Condor Country Consulting, Inc, Martinez, CA 94553
6. Department of Entomology, Virginia Tech, Blacksburg, VA 24061
7. Department of Chemistry, Virginia Military Institute, Lexington, VA 24450

+. These authors contributed equally

3.0. Abstract

Millipedes have long been known to produce structurally diverse chemical defenses, including hydrogen cyanide, terpenoid alkaloids, and oxidized aromatics. Although the hydrogen cyanide and oxidized aromatic producing millipedes have been well studied, less than 10% of the terpenoid alkaloid producers have been chemically investigated. Several previous studies have shown that alkaloids disorient predators, but their biochemical target is currently unknown. Herein, we investigated the defensive secretions of a colobognath millipede, *Ischnocybe plicata*, and elucidated the constitution, absolute configuration, and conformation of four new highly oxidized terpenoid alkaloids, termed ischnocybines, using a range of analytical techniques. The

ischnocybines are actively secreted from the defensive glands and were shown to disorient ants, a likely common predator. Evaluation of the ischnocybines in a panel of neuroreceptors revealed that ischnocybine A possesses potent (K_i 14 nM) and selective (100-fold) binding affinity for sigma-1, an orphan neuroreceptor, over sigma-2. These molecules represent the most complex alkaloids to be discovered from millipedes and provide the first potential insights into a biochemical target responsible for their defensive properties.

3.1. Introduction

Millipedes are a diverse class (Diplopoda) of arthropods that are known to produce distinct chemical defensive secretions, including alkaloids, oxidized aromatics, and hydrogen cyanide.[1,2] These defensive compounds, or their biosynthetic precursors, are stored in high concentrations within repugnatorial glands and are released upon disturbance.[1] Both hydrogen cyanide and oxidized aromatic containing secretions have reactive functional groups and are believed to deter predation as either a harmful toxin or general irritants, respectively.[3-5] Alkaloid defensive secretions include both quinazolinone and terpenoid alkaloids, with the former hypothesized to represent a hybrid between the oxidized aromatics and cyanide-containing agents.[6] Due to their structural intricacy, the terpenoid alkaloids are distinct from all other classes of millipede defensive compounds and represent the most complex secretions yet to be reported (i.e., larger molecular weight, contain stereocenters, and diverse functionality).[1,6-9] Their defensive mechanism is unknown; however, it is unlikely that the terpenoid alkaloids function as general irritants as they lack the reactive functionalities. Two previous reports indicate that a subset of the terpenoid alkaloids cause disorientation in common predators, thus suggesting a potential neurological mechanism.[8,9]

All known terpenoid alkaloids are produced by millipedes within a single subterclass, Colobognatha (fungus-feeding millipedes), which consists of four orders (Platydesmida, Polyzoniida, Siphonocryptida and Siphonophorida).[1] All four orders have been reported to produce simple monoterpenes, such as α-pinene, however three orders (Platydesmida, Polyzoniida and Siphonocryptida) are known to produce complex terpenoid alkaloids (**Figure 3.3**). Currently, seventeen alkaloids have been described with fourteen being reported recently (since 2020).[6-12] This explosion in defensive secretion chemistry has provided insights into a potential biosynthetic

route. All millipede terpenoid alkaloids are hypothesized to incorporate a nitrogen that is presumably derived from either an amino acid (lysine or ornithine) or cyanide. Structural diversity appears to arise from variations in the terpene cyclization patterns and post-modifications (e.g., oxidation, nitration, and ligation). Nearly all reported alkaloids from Polyzoniida and Siphonocryptida millipedes contain a spirocyclic core (polyzonimine-like), though there is some variation in the number of carbons incorporated into each core structure (10 to 13).[9-11] Conversely, defensive secretions characterized from Platydesmida contain one of two core structures: a bicyclic indolizidine/quinolizidine core (gosodesmine-like) or a 5,6,6-fused tricyclic core (buzonamine-like).[6-8,12] Both the gosodesmine- and buzonamine-like defensive secretions derive from a monoterpene, likely geranyl pyrophosphate, and either ornithine (5-membered rings) or lysine (6-membered rings). Finer structural diversity arises from oxidation events (e.g., formation of olefins and epoxides) that are likely installed after the cyclization.

Although there has been a recent resurgence in chemistry being described from Colobognatha, only about 10% of the described species have been chemically studied. Nearly all of these studies have led to the discovery of new chemical compounds.[1,6,7,11] Herein, we report chemical investigations into the defensive secretions of *Ischnocybe plicata* (Platydesmida, Andrognathidae), a millipede that resides in the U.S. Pacific Northwest (**Figure 3.3**), leading to full structural characterization of four highly functionalized terpenoid alkaloids. The structure elucidation of the ischnocybines (**3.1**–**3.4**; **Figure 3.4**) was accomplished using comprehensive analysis of 2D NMR, computational experimentation, electronic circular dichroism, and chemical derivatization. Notably, three of the ischnocybines potently and selectively bind sigma-1 receptor (σ_1R), an orphan receptor.[13] This receptor is a potential drug target for various disorders, and this is the first report of a molecular target for any of the millipede alkaloid defensive secretions.[14-16]

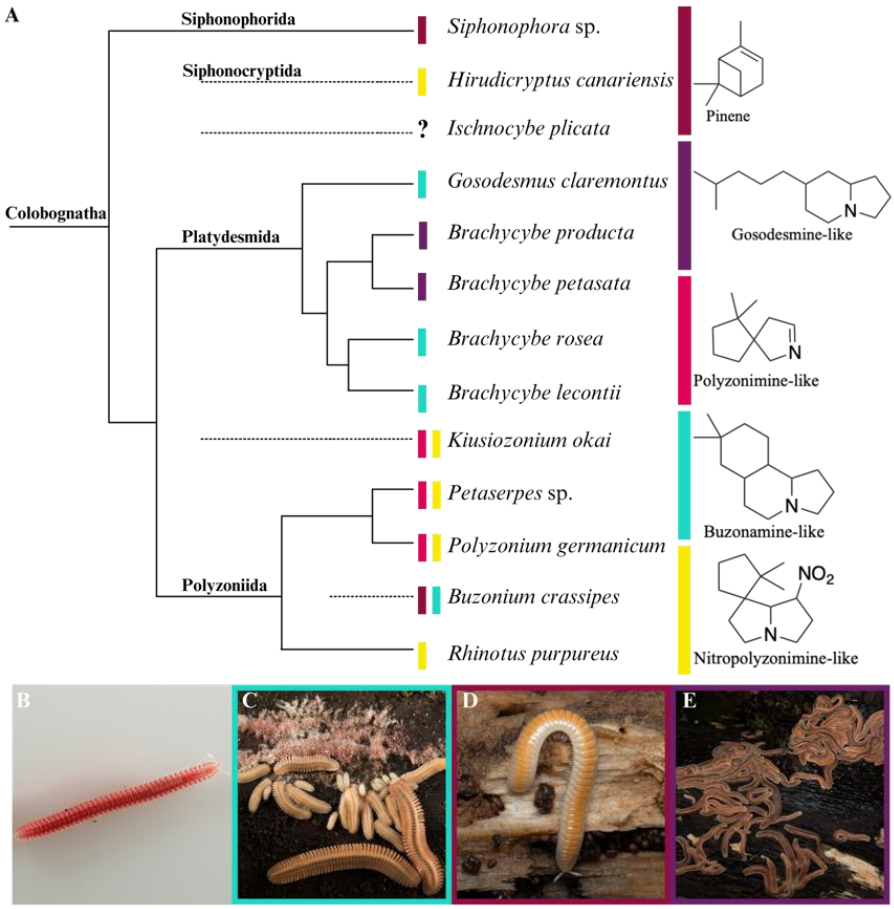

Figure 3.3. Millipede Phylogeny **A**) Millipede phylogenetic tree for subterclass colobognath. The types of compounds produced by each millipede are shown. Supertree from: Brewer*, et al.* (2012), Marek*, et al.* (2021), Benavides*, et al.* (2023). **B–E**) Pictures of diverse Colobognatha millipedes. **B**) *Ischnocybe plicata*; **C**) *Brachycybe lecontii*; **D**) *Buzonium crassipes*; **E**) *Brachycybe producta*.

3.2. Results and Discussion

Field observations suggested that when disturbed (shaken), *I. plicata* exudes a scent reminiscent of pine oil or citrus, indicating terpene production. GCMS analysis of a methanol extract of *I. plicata* collected in downed woody debris in Oregon forests revealed a mixture of monoterpenes and four larger metabolites that possessed fragmentation patterns that were dissimilar to known millipede alkaloids with molecular ions at *m/z* 291 (**3.1**), 305 (**3.2**), 349 (**3.3**)

and 379 (**3.4**) (**Figure 3.7.1–Figure 3.7.5**). Preliminary chemical derivatization of the methanol extract using hydrogenation, basic hydrolysis, and aminolysis revealed that **3.1**–**3.3** each possessed an olefin, **3.1** and **3.2** contained a single butyrate, and **3.3** and **3.4** contained a butyrate and either an acetate or another butyrate, respectively (**Figure 3.7.6–Figure 3.7.13**). Additionally, **3.2** formed a methoxime, suggesting a ketone (**Figure 3.7.14**). Analysis of high resolution MS (HRMS) data indicated molecular formulas of $C_{18}H_{29}NO_2$ (**3.1**, observed $[M+H]^+$ 292.2277, calcd. $C_{18}H_{30}NO_2$, Δ0.0 ppm), $C_{18}H_{27}NO_3$ (**3.2**, observed $[M+H]^+$ 306.2072, calcd. $C_{18}H_{28}NO_3$, Δ0.9 ppm), $C_{20}H_{31}NO_4$ (**3.3**, observed $[M+H]^+$ 350.2335, calcd. $C_{20}H_{32}NO_4$, Δ1.1 ppm), and $C_{22}H_{37}NO_4$ (**3.4**, observed $[M+H]^+$ 380.2794, calcd. $C_{22}H_{38}NO_4$, Δ1.8 ppm) (**Figure 3.7.15–Figure 3.7.18**). These key structural characteristics did not resemble known alkaloids previously isolated from millipedes. Therefore, the four metabolites present in the *I. plicata* extracts were purified via reverse phase high performance liquid chromatography (RP-HPLC) and full 2D NMR datasets (^{1}H, ^{13}C, COSY, easyROESY, HSQC and HMBC) were acquired on each metabolite to elucidate their planar structures (**Figure 3.7.19–Figure 3.7.42** and **Table 3.8.8–Table 3.8.11**).

We began the structure elucidation effort with **3.1,** as it had the simplest NMR data and smallest mass of the isolated metabolites. The molecular formula ($C_{18}H_{29}NO_2$) indicated five degrees of unsaturation and analysis of the ^{13}C NMR spectrum revealed the presence of four deshielded carbons—an ester (δ_C 172.2), two olefinic carbons (δ_C 135.4 and 126.3), and an oxygenated carbon (δ_C 80.1), accounting for two degrees of unsaturation. The ^{1}H NMR spectrum confirmed a tri-substituted olefin with a single proton signal at δ_H 5.65 but also revealed two aliphatic singlet methyl groups (δ_H 23.8 and 27.2). The lack of additional functionality in the 1D NMR spectrum suggested that rings account for the remaining three degrees of unsaturation. Analysis of the 2D NMR spectra, particularly the HMBC and COSY (**Figure 3.5**), revealed that

3.1 is related to the known defensive metabolite buzonamine (**3.5**), isolated from the polyzoniid millipede *Buzonium crassipes*.[8] Compound **3.1** contained a similar 5,6,6-fused tricyclic backbone with modifications in the B and C rings. (**Figure 3.4** and **Figure 3.5**) In the B ring, the signals for an epoxide were clearly absent and replaced by two downfield signals that corresponded to an olefin. The olefinic proton (H-2, δ_H 5.65) exhibited HMBC correlations with C-1 (δ_C 52.1), C-4 (δ_C 80.1) and C-8 (δ_C 39.4). In addition, ring C had an additional oxidized carbon adjacent to the *gem*-dimethyl moiety. Analyzing HMBC correlations led to assignment of a butyrate moiety attached to C-4 (δ_C 80.1) and the planar structure of **3.1** (**Figure 3.4**).

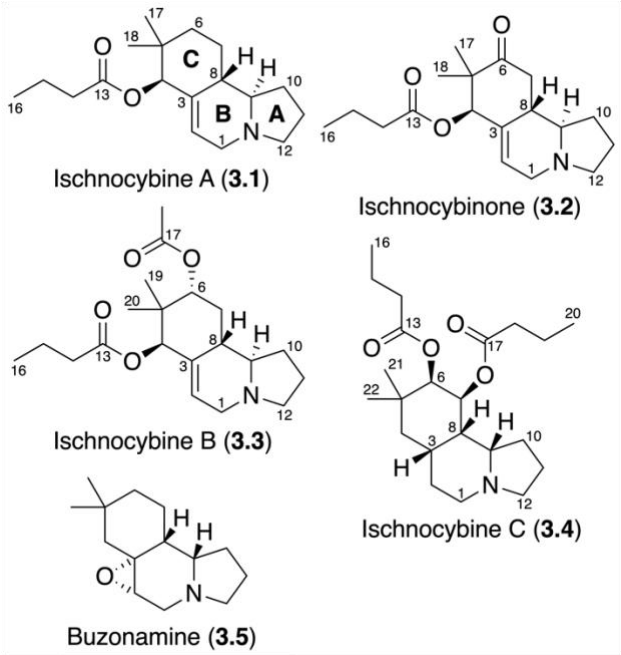

Figure 3.4. Structures of new heterocyclic terpenoid alkaloids, ischnocybine A (**3.1**), Ischnocybinone (**3.2**), Ischnocybine B (**3.3**), and Ischnocybine C (**3.4**), along with the closest analog, buzonamine (**3.5**).

Compounds **3.2**–**3.4** shared a nearly identical carbon backbone with **3.1** but differed in oxidation state at two positions. The molecular formula of **3.2** indicated an additional oxygen atom and an additional degree of unsaturation. The 1D NMR spectra of **3.2** revealed no protons on C-6

and an additional strongly deshielded carbon signal (δ_C 211.7). Analysis of 2D NMR data confirmed C-6 as a ketone as both the *gem*-dimethyls (δ_H 0.92 and 1.08) exhibited HMBC correlations to C-6. Compound **3.3** incorporated an additional $C_2H_2O_2$ compared to **3.1**. The ^{1}H NMR spectra of **3.3** revealed an additional singlet methyl group (δ_H 2.02) and this chemical shift matched the expected shift for an acetate methyl. The presence of an acetate was also supported by an additional deshielded carbon (δ_C 170.6) in the HMBC, and by a prominent loss of 59 (corresponding to the formula CH_3CO_2) in the initial GCMS analysis. A key HMBC correlation between H-6 (δ_H 5.01) and C-17 (δ_C 170.6) further supported assignment of an acetate at C-6.

Though**,** the most dissimilar to **3.1**, **3.4** still contained the same tricyclic moiety. The molecular formula for **3.4** ($C_{22}H_{37}NO_4$) included an additional C_2H_6 while also containing one less degree of unsaturation than **3.3**. Based on the GCMS analysis, **3.4** lacked the olefin between C-2/C-3 and contained two butyrates. Comparison of the ^{13}C spectrum of **3.4** to those of **3.1**–**3.3** confirmed this; the spectrum of **3.4** lacked olefinic signals and had two carbonyl signals consistent with esters (δ_C 172.9 and 172.4). Both sets of *gem*-dimethyl protons shared HMBC correlations to C-6 (δ_C 76.5), from which one butyrate was attached. From C-6, HSQC and COSY data revealed the origin of the second butyrate at C-7 (δ_C 69.3). HMBC correlations from H-6 and H-7 to the ester carbonyls facilitated the placement of the butyrate groups. Thus, we deduced planar structures for ischnocybines A–C and ischnocybinone (**Figure 3.4**)

Relative configurations of **3.1**–**3.3** were established through a combination of ROESY NMR experiments and DELTA50[20] based Density Functional Theory (DFT) calculations. For compound **3.1**, chemical shift predictions were carried out for all four possible stereoisomers. The 4*S*,8*S*,9*R* yielded the best results, with ^{13}C and ^{1}H RMSD values of 2.3 ppm and 0.07 ppm, respectively. Based on a lack of apparent ROESY correlations between H-4, H-8, and H-9,

comparisons to geometry-optimized structures of **3.1**, and chemical shift predictions, it was determined that **3.1** had a relative configuration of 4*S**,8*S**,9*R** (**Table 3.8.12** and **Table 3.8.13**). Compounds **3.2** and **3.3** were similar to **3.1** based on observed ROEs and chemical shift predictions, and were assigned the relative configurations 4*R**,8*S**,9*R** and 4*R**,6*R**,8*S**,9*R**, respectively (**Table 3.8.14**–**Table 3.8.17**).

Analysis of **3.4** was not straightforward, given the significant dissimilarity to **3.1**. Conformational searches yielded far more results for **3.4** relative to **3.1**–**3.3** due to added flexibility at positions 2 and 3. For several possible stereoisomers, chemical shift predictions yielded similar results (**Table 3.8.18**–**Table 3.8.21**); fortunately, ^{1}H signals were relatively clean and fairly well-resolved, allowing for application of *J*-based configuration analysis. Protons H-7 and H-8 shared a large coupling constant of 11.6 Hz, pointing towards a *trans*-diaxial relationship (**Figure 3.5**). The small coupling constant between H-6 and H-7 (2.7 Hz) suggested that H-6 is equatorial; the same holds true for H-3 and H-8 (3.5 Hz), where H-3 is likely equatorial. Additionally, the intensity of the ROESY correlations between H-2, H-7, and H-21, and the correlations between H-3, H-8, and H-9 are highly indicative of the overall conformation of **3.4** (**Figure 3.5**). These correlations were extremely helpful for comparison with 3D models from computationally aided conformational searches. Overall, these data combined with chemical shift predictions facilitated assignment of the relative configuration of **3.4** as 4*R**,6*S**,7*R**,8*R**,9*R**.

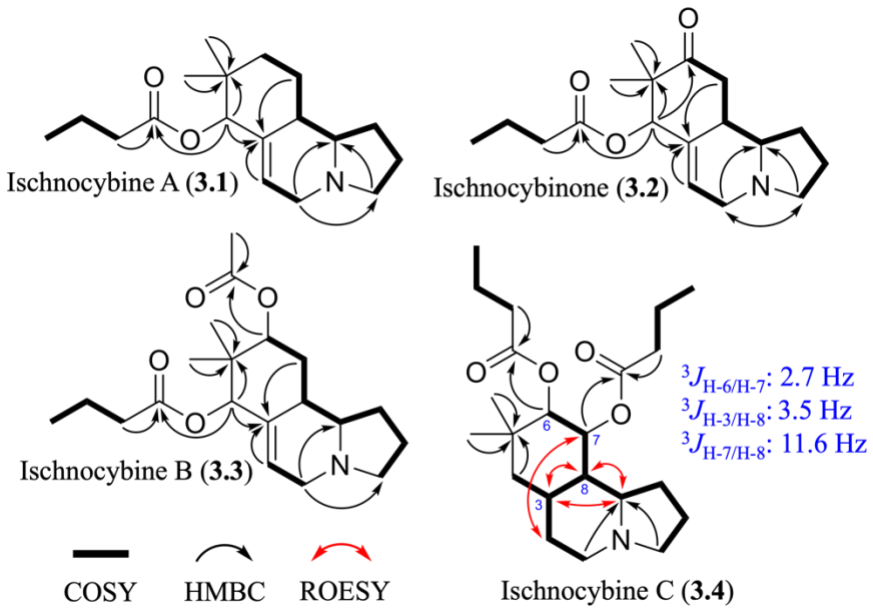

Figure 3.5. Key 2D NMR correlations and coupling constants

Absolute configuration assignments of **3.1**–**3.4** were conducted using a combination of Mosher esterification, electronic circular dichroism (ECD), and time-dependent (TD) DFT calculations. Fortuitously, several milligrams of the free alcohol of **3.1** (**3.6**; **Figure 3.7.43**–**Figure 3.7.48**; **Table 3.8.22)** were obtained during purification of the October 2023 collection material and a portion of this material was derivatized with both (*R*)- and (*S*)-α-methoxy-α-trifluoromethylphenylacetic acid (MTPA).[21] Analysis of the shielded and deshielded patterns in the derivatized products (compound) for protons H-1a, H-1b, H-2, H-17, and H-18 (**Figure 3.6A**) confirmed an absolute configuration of 4*S*, thus indicating an absolute configuration of 4*S*,8*S*,9*R*-**3.1** (**Figure 3.7.49**). Because **3.1–3.3** all possess similar specific rotation values (**3.1**: -2.67; **3.2**: -3.33; **3.3**: -4.67), and contain the same relative configuration, each of the compounds are predicted to have the same absolute configuration. This yields absolute configurations 4*R*,8*S*,9*R* and 4*R*,6*R*,7*S*,8*R* for compounds **3.2** and **3.3**, respectively. Compound **3.4** exhibited a positive specific rotation value, so we used a different approach to assign its absolute configuration. A small aliquot of compound **3.4** was hydrolyzed with sodium hydroxide and the resulting product was

subsequently treated with 4-bromobenzoyl chloride and 4-dimethylaminopyridine to yield the dibromobenzoyl product (**3.9**) (**Figure 3.6B**). The purified derivative exhibited a positive split Cotton effect, indicating an absolute configuration of 4*S*,6*R*,7*S*,8*S*,9*S*-**3.4**. This was further confirmed through TD-DFT predictions of ECD data for **3.4**, which also displayed the positive Cotton effect (**Figure 3.6C**).

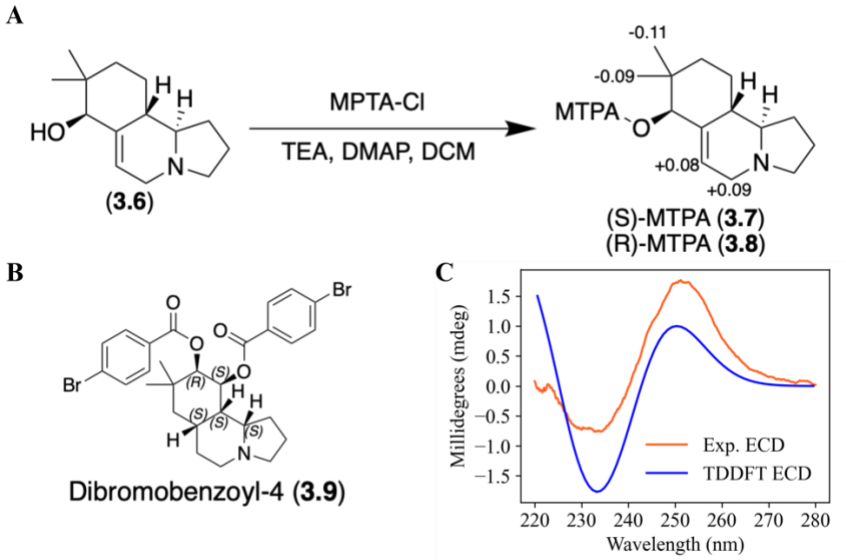

Figure 3.6. Stereochemistry of Ischnocybine A and C. **A)** Free alcohol of **3.1** (**3.6**) forming Mosher esters (**3.7** and **3.8**), $\Delta\delta_{S\text{-}R}$ values **B)** 4*S*,6*R*,7*S*,8*S*,9*S* configuration of the dibromobennzoyl derivative of hydrolyzed **3.4** (**3.9**) **C)** Experimental and TD-DFT-predicted ECD data for **3.9**.

Based on isolated quantities from whole-animal extracts of *I. plicata,* the ischnocybines are produced in significant quantities, with each individual millipede estimated to contain approximately 50 µg (**Table 3.8.23**)**.** This suggests these metabolites play an integral ecological role for the millipedes. Previous work has shown that other millipede derived alkaloids, including polyzonimine and **3.5**, along with the monoterpenes serve to protect the host against predation by ants and spiders, likely natural predators of millipedes.[4,8,9] To ascertain whether defensive secretions of *I. plicata* contained the ischnocybines, the secretions were captured using capillaries

and analyzed via LCMS. High abundances of **3.1**–**3.4** were detected with almost no other metabolites observed (**Figure 3.7A**). In addition, during the Oct. 2023 collection trip, individual millipedes were collected, their body lengths measured, and the secretions extracted and quantified by LCMS. All extracts contained **3.1–3.4**, even the juveniles which were less than 4 mm in length (**Table 3.8.24**). Peak areas of **3.1–3.4** plotted against millipede length, revealed a linear relationship between size and abundance of the alkaloids (**Figure 3.7B**). Finally, **3.1**–**3.4** were evaluated against *Aphaenogaster rudis-picea* complex (winnow ants), an ant local to southwestern Virginia, to determine if these alkaloids affected the ant's behavior (**Figure 3.7C**). Briefly, approximately ten ants were placed in a petri dish and allowed to settle (~5 min). A disc with methanol was subsequently placed in the middle of the dish. The ants had no visible reaction to the methanol. Next, a disc impregnated with the ischnocybines was placed in the petri dish and the ant's behavior was monitored for 20 min. During this time, the ants clearly avoided the impregnated disc, staying on the opposite side of the petri dish. Interestingly, two of the ants that approached the impregnated disc stopped moving for several minutes and then appeared to preen their antennae, suggesting a potential neurological target of the alkaloids.

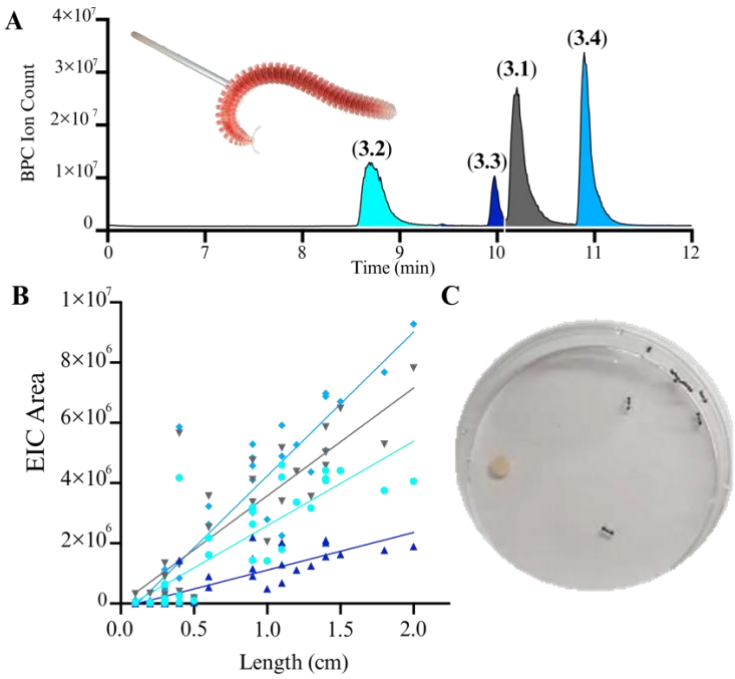

Figure 3.7. *Ischnocybe plicata* Ecology. **(A)** The base peak chromatogram (BPC) of *I. plicata* secretions that were captured by the capillary. All four major peaks corresponded to the alkaloids (**3.1**–**3.4**), **(B)** The relative abundance of each alkaloid correlates with millipede length (**3.1**: R^2 = 0.70***; **3.2**: R^2 = 0.68***; **3.3**: R^2 = 0.67***; **3.4**: R^2 = 0.79***, (*** $p < 0.001$)), and **(C)** Predator assay: a paper disc impregnated with alkaloids (**3.1**–**3.4**) deterred the ants which placed themselves in the opposite direction; Two ants demonstrated motor disorder, leading to paralysis in close contact with the paper disc.

To probe this hypothesis, **3.1**–**3.4,** and **3.6** were screened in a range of neuroreceptor binding assays through the Psychoactive Drug Screening Program (PDSP) at UNC Chapel Hill. The ischnocybines (**3.1**–**3.4**) were first screened broadly at 10 μM against 53 neuroreceptors in a primary assay (**Figure 3.8A** and **Figure 3.7.50**). Secondary radioligand binding assays to measure the inhibitor constant (K_i) were conducted when the primary assay exhibited >50% binding affinity (**Table 3.8.25** and **Table 3.8.26**). Compounds **3.1**, **3.3**, and **3.4** were only found to have potent (K_i < 1 μM) and selective binding affinity for the σ_1R (**Table 3.2**; **Figure 3.8B**). Ischnocybine A

exhibited the highest affinity and selectivity for the σ_1R with a K_i of 14 nM. Interestingly, **3.1** is 10-fold more active than both **3.3** (K_i 380 nM) and **3.4** (K_i 380 nM), and 100-fold more potent than **3.2** (K_i 1500 nM). Compounds **3.1**, **3.3**, and **3.4** all possessed nearly a 10-fold selectivity for σ_1R over σ_2R (**Figure 3.8D** and **E**). Surprisingly, simple addition of the ketone to C-6 in **3.2** leads to a nearly complete loss of activity, but the acetate (**3.3**) and butyrate (**3.4**) functionality are more tolerated. This suggests that steric hindrance only explains part of the reduced binding affinity. Compound **3.6** was screened after **3.1**–**3.4** and was only evaluated against σ_1R over σ_2R. Interestingly, **3.6** was over 150-fold less active than **3.1** (**Figure 3.7.51**).

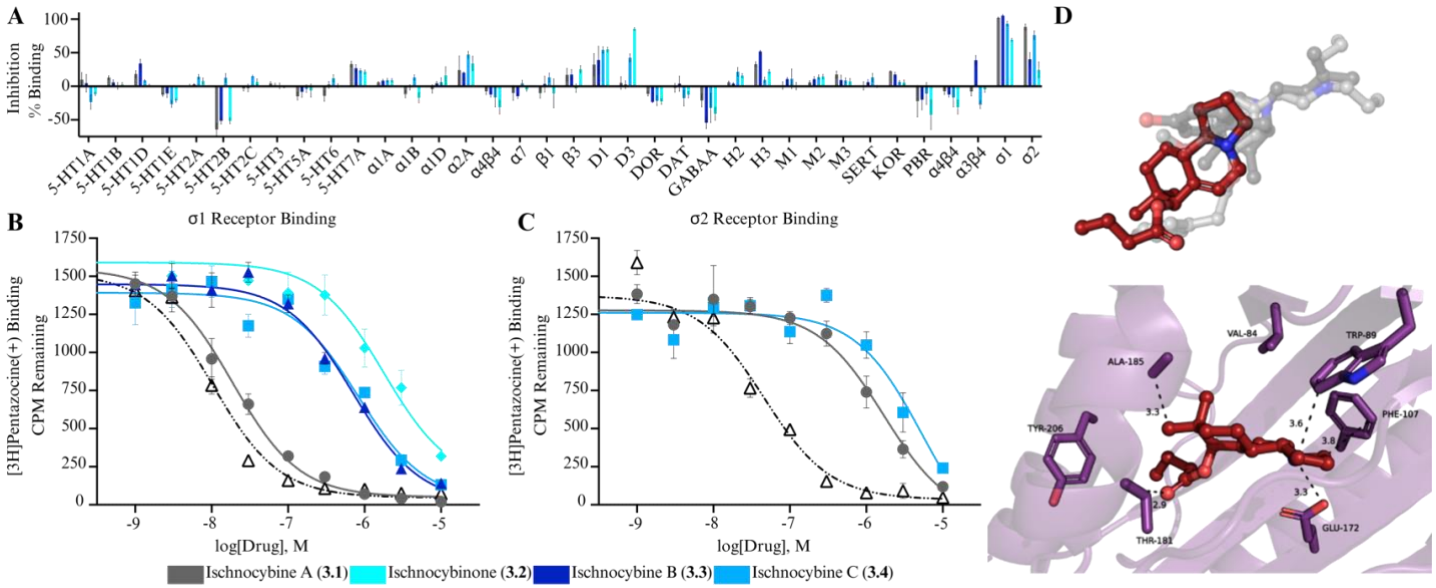

Figure 3.8. PDSP results and σ_1R binding. **(A)** Representative data from the primary binding assay inhibition. A total of 53 neuroreceptors were screened and secondary screens were conducted for any primary inhibition > 50%. **(B)** Competitive binding curves for **3.1**–**3.4**, against the radioactive σ_1R ligand, [3H]-(+)-pentazocine. **(C)** Competitive binding curves for **3.1**–**3.4**, against the radioactive σ_2R ligand, [3H]-(+)pentazocine. Positive control was haloperidol for both σ_1R and σ_2R (open triangles). **(D)** Ischnocybine A (**3.1**) docked into the agonist σ_1R. Compound **3.1**, shown as red sticks (colored by element). (i) Overlay of **3.1** (red) with the agonist (light grey) and antagonist binding positions (dark grey) binding positions from co-crystal structures. (ii) Interactions between residues in the σ_1R (purple, colored by element) binding cavity and **3.1** (red, colored by element).

It is not possible to determine if a ligand is an agonist or antagonist from *in vitro* binding affinity assays, and typically determining this is only possible through phenotypic changes in *in vivo* assays. However, known agonists and antagonists have different binding positions within the σ_1R active site. The antagonist binding position falls almost entirely in the agonist position, with the major difference being a unique region by helix 4 which houses an interaction with Tyr-206 (**Figure 3.7.52**). Agonists are known to perturb helix 4 at Ala-185, causing it to shift further away (**Figure 3.7.53**) from the binding pocket. Using molecular docking, a re-docking experiment was performed on the agonist (PDB ID: 6DK1),[13] antagonist (PDB ID:6DK0),[13] and apo structures (PDB ID: 7W2E)[22] and indicated that molecular docking was able to predict accurate poses of both antagonist and agonist positions in the binding pocket (**Figure 3.7.52**–**Figure 3.7.54**). The agonist structure was also able to re-create antagonistic binding poses of NE-100 accurately (RMSD value of 1.25 Å to co-crystal structure positioning) and with more poses, so the agonist structure was selected for further experiments with the alkaloid compounds (**Figure 3.7.54**).

Table 3.2. Inhibition percent and K_i of σ_1R and σ_2R for **3.1**–**3.4**.

Compound	Receptor	Inhibition %[a]	K_i (nM)
3.1	σ_1	102 ± 2	14
	σ_2	89 ± 9	1300
3.2	σ_1	69 ± 4	1500
	σ_2	25 ± 23	ND[b]
3.3	σ_1	105 ± 4	380
	σ_2	40 ± 19	ND[b]
3.4	σ_1	93 ± 7	380
	σ_2	76 ± 13	2900
3.6	σ_1	62 ± 2	2200
	σ_2	54 ± 13	3800

[a]at 10 μM; [b]not determined (primary screen yielded < 50% binding).

Ischnocybines that docked into the σ_1R agonist structure consistently occupy the unique region in the left quadrant of the binding pocket for the most potent compound and maintain

interactions with Tyr-206 like known antagonists. This suggests that this compound set may be acting as antagonists. Docking studies and predicted free energy of binding MM/GBSA analysis with **3.1** regardless of stereoisomer type had the most favorable predicted free binding energy and ligand efficiency in the agonist σ_1R, as well as participated in the most consistent and close interactions with Tyr-206 (**Figure 3.7.55**; **Table 3.8.27**). Compounds **3.3** and **3.4** participated in more distal interactions with Tyr-206 and had very similar predicted free energy of binding (**Figure 3.7.56** and **Figure 3.7.57**), but to a lesser degree than **3.1**. Compound **3.2** had the least favorable positioning in the binding pocket and was unable to interact with Tyr-206 (**Figure 3.7.58**) to the same degree as **3.1**, **3.3**, and **3.4**, suggesting a lower affinity for the σ_1R that agrees with experimental results. Although σ_1R is an orphan receptor, antagonists of σ_1R have been implicated for the treatment of neuropathic pain, such as MR-309, which is in clinical trials for the treatment of neuropathic pain.[16]

In summary, ischnocybines are new highly modified heterocyclic terpenoid alkaloids produced by *I. plicata* and these compounds are the most complex millipede natural products yet to be discovered. The ischnocybines contain a 5,6,6-fused tricyclic system with five contiguous stereogenic centers, and are the first alkaloids in this class to have absolute configuration determined. Ischnocybines A, B, and C each exhibited potent and specific binding affinity for the σ_1R over all other neuroreceptors and this may provide insights into the biomedical target underpinning the observed defensive properties. This study lays the foundation for other colobognath millipedes to gain a better understanding of the evolution of this intriguing pathway and the true biomedical application of this family of metabolites.

3.3. Experimental Methods

3.3.1. General Experimental Procedures

Optical rotations were measured on a JASCO P-2000 polarimeter, circular dichroism spectrum on a JASCO J-815, and UV spectra on a Hitachi U4100 UV/Visible/Near-infrared spectrophotometer. All NMR data was acquired on a Bruker Neo NMR spectrometer operating at a ^{1}H observation frequency of 499.861999 MHz and equipped with a H/F C/N TCI 5 mm Prodigy CryoProbe using TopSpin (version 4.1.4). Samples were prepared in 3 mm NMR tubes with 150 µL solvent. All data were acquired at 25°C in *d*$_6$-DMSO (99.96%, Cambridge Isotope Laboratories). All NMR data were processed in MestReNova (version 15.0.0). ^{1}H NMR data was referenced to 2.50 ppm for *d*$_6$-DMSO, and absolute referencing was used for all other NMR spectra. HMBC experiments were optimized for $^{n}J_{CH}$ = 8 Hz, and ROESY experiments were performed with a mixing time of 300 ms. GCMS was carried out in the EI mode using a Shimadzu QP-2020 GC-MS equipped with an RTX-5, 30 m x 0.25 mm i.d. column. The instrument was programmed from 60° C to 250° C at 10 ^{o}C/min. LR-LCMS data were obtained using an Agilent 1200 series HPLC system equipped with a photo-diode array detector and a Thermo LTQ mass spectrometer. HRESIMS was carried out using a Shimadzu LC-q-TOF Mass Spectrometer equipped with an UHPLC system. HPLC purifications were carried out using Agilent 1200 series or 1260 Infinity II HPLC systems (Agilent Technologies) equipped with a photodiode array detector. All solvents were of HPLC quality.

3.3.2. Millipede Collections

Millipedes were collected in southwest Oregon by opportunistic searches of down woody debris in coniferous and mixed hardwood forests. Under the assumption that larger individuals produce larger quantities of defensive chemicals, this study focused on adult individuals to

maximize chemical collection: in *B. lecontii*, ozopore secretions are not exuded until stadium III.[23] Thus when aggregations were discovered, typically only the largest individuals were collected, while unpigmented larvae and relatively small individuals (under ~8 – 10 mm in length) were left in situ. Collected millipedes were identified as *I. plicata* by analysis of morphological features and preserved in 100% methanol (MeOH) at -20 ºC. Collections of *I. plicata* took place in (1) Jackson Co., Oregon, Rogue River-Siskiyou NF, 42.131960ºN, -122.814510ºW, Elev. 1153 m, 1 December 2020; (2) Jackson Co., Oregon, Applegate Lake, Collings Mtn. Trail, 42.052980ºN, -123.133900ºW, Elev. 654 m, 6 December 2020; (3) Jackson, Co., Oregon, East Applegate Ridge Trail, 42.245830ºN, -122.982520ºW, Elev. 944 m, 9 December 2020; (4) Jackson, Co., Oregon, East Applegate Ridge Trail, 42.245740ºN, -122.982450ºW, Elev. 944 m, 5 January 2021; (5) Jackson Co., Oregon, East Applegate Ridge Trail, 42.245890ºN, -122.982740ºW, Elev. 938 m, 1 October, 2023; (6) Jackson Co., Oregon, Sterling Mine Ditch Trail, 42.166010 ºN, -122.915980ºW, Elev. 863 m, 3 October, 2023.

3.3.3. Gas Chromatography Mass Spectrometry (GCMS) Analysis of Crude Mixture

Initial GCMS examination of the methanol extracts of *I. plicata* showed the presence of α- and β-pinene and a trace of terpinolene, along with four longer retention time alkaloids: (**3.1**), M = 291, (**3.2**), M = 305, (**3.3**), M = 349, and (**3.4**) M = 379. A slow stream of hydrogen was bubbled through 0.1 mL of the original extract in the presence of a few mg of PtO_2 for 2 min. GCMS analysis of the resulting mixture showed that compounds **3.1**–**3.3** each added one H_2 (M = 293, 307, and 351, respectively). The mass spectra of all four alkaloids showed a distinctive M-87 fragment suggesting a butyl ester. The presence of butyl esters rather than isobutyl esters was confirmed by the formation of *n*-butyl butanamide upon warming 20 μL of the extract with a few drops of *n*-butylamine. Next, a small portion of the original extract was warmed with a few mg of

methoxylamine HCl and 2 drops of pyridine for 18 h. GCMS analysis of the resulting mixture showed that **3.2** formed a methoxime (M = 334) indicating the presence of a ketone in **3.2**. Finally, methanolysis was carried out by treating ca. 200 µL of the methanolic extract with ca 1-2 mg of anhydrous NaOMe at rt overnight. GCMS analysis revealed the presence of a butyrate on **3.1** and **3.2**, a butyrate and acetate on **3.3**, and two butyrates on **3.4**.

3.3.4. Purification of Ischnocybine A-C and Ischnocybinone (3.1–3.4**)**

HPLC purifications were carried out using an Agilent 1200 series HPLC system equipped with a 1260 Infinity II collector (Agilent Technologies) and photodiode array detector. Purification of compounds **3.1–3.4** was performed reversed-phase C_{18} semi-preparative column (Phenomenex Synergi, 10.0 x 250 mm, 4 µm) using the following solvent gradient system: holding 30% acetonitrile (MeCN) + 0.1% formic acid (FA)/70% H_2O + 0.1% FA then gradient to 100% MeCN + 0.1% FA over 30 min with a 3 mL/min flow rate. An aliquot (40 µL) of the crude extract was resuspended at 10 mg/mL in 50% MeCN/H_2O while monitoring at 195 and 210 nm. The compounds eluted at 13.3 (**3.1**), 6.2 (**3.2**), 11.9 (**3.3**), and 17.4 (**3.4**) min, yielding 3.5, 4.6, 2.5 and 4.1 mg, respectively, from 300 individual millipedes. The October 2023 collection followed a similar purification, except the solvent gradient was holding 20% MeCN + 0.1% FA/80% H_2O + 0.1% FA for 5 min then gradient to 55% MeCN + 0.1% FA/45% H_2O + 0.1% FA over 25 min, followed by a hold at 100% MeCN + 0.1% FA for 5 min finally a hold of 20% MeCN + 0.1% FA/80% H_2O + 0.1% FA for 5 min. The compounds eluted at 22.7 (**3.1**) 14.8 (**3.2**), 20.6 (**3.3**), 27.6 (**3.4**) and 8.2 (**3.6**).

*Ischnocybine A (***3.1***):* amorphous solid; $[\alpha]^{23}_{D}$ -2.67 (*c* 0.015, MeOH); UV (MeOH) λ_{max} (log ε) 2.90 (190) nm; NMR (500 MHz, d_6-DMSO) δ 5.65 (dd, *J* =4.4 and 2.3 Hz, 1H, H-2), 4.88 (d, *J* = 1.4, 1H, H-4), 3.30 (ddd, *J* = 16.3, 5.0, 2.3, CH, H-1a), 3.00 (m, CH, H-12a), 2.59 (ddd, *J* = 16.3,

4.4, and 1.7, CH, H-1b), 2.24 (td, J = 7.3 and 1.3, CH_2, H-14), 1.97 (m, 3CH, 2CH_2, H-10a, H-12b) 1.97 (m, CH, H-8), 1.73 (td, J = 9.0 and 6.8 Hz, CH, H-9), 1.65 (m, 4CH, H-6a, H7a, H11), 1.53 (qd, J = 7.3 and 2.8 Hz, CH_2, H-15), 1.32 (m, CH, H-10b), 1.19 (m, CH, H-6b), 1.14 (m, CH, H-7b), 0.87 (t, J = 7.3, CH_3, H-16), 0.84 (s, CH_3, H-18), 0.81 (s, CH_3, H-17); ^{13}C NMR (100 MHz, *d6*-DMSO) δ 172.2 (C, C-13), 135.4 (C, C-3), 126.3 (CH, C-2), 80.1 (CH, C-4), 67.0 (CH, C-9), 54.2 (CH_2, C-12), 52.1 (CH_2, C-1), 39.4 (CH, C-8), 36.3 (CH_2, C-14), 34.5 (C, C-5), 32.4 (CH_2, C-6), 29.4 (CH_2, C-10), 27.2 (CH_3, C-18), 25.8 (CH_2, C-7), 23.8 (CH_3, C-17), 21.6 (CH_2, C-11), 18.6 (CH_2, C-15), 13.9 (CH_3, C-16); EIMS *m/z* 291 [M^+] (31), 204 (41), 203 (28), 188 (63), 148 (6), 135 (5), 134 (100), 119 (81), 71 (16), 70 (63); HRESIMS $[M+H]^+$ *m/z* 292.2277 (calcd. for $C_{18}H_{30}NO_2$ 292.2277, Δ 0.0 ppm).

*Ischnocybinone (**3.2**):* amorphous solid; $[\alpha]^{23}_D$ -3.33 (*c* 0.018, MeOH); UV (MeOH) λ_{max} (log ε) 6.4 (190) nm; NMR (500 MHz, *d6*-DMSO) δ 5.92 (dd, J = 4.9 and 2.1 Hz, CH, H-2), 5.30 (s, CH, H-4), 3.41 (ddd, J = 16.8, 4.9, 2.1 Hz, CH, H-1a), 3.03 (ddd, J = 8.8, 6.7, 3.6, CH, H-12a), 2.74 (ddd, J = 16.8, 4.0, 1.7, CH, H-1b), 2.47 (m, CH, H-8), 2.40 (d, J = 11.4, CH, H-7a), 2.31 (m, CH, H-7b), 2.21 (t, J = 7.4, CH_2, H-14), 2.06 (q, J = 8.8, CH, H-12b), 1.98 (m, CH, H-9), 1.93 (m, CH, H-10a), 1.69 (m, CH_2, H-11), 1.48 (dtd, J = 14.8, 7.4, and 5.9, CH_2, H-15), 1.33 (m, CH, H-10b), 1.08 (s, CH_3, H-17), 0.92 (s, CH_3, H-18), 0.84 (t, J = 7.4, CH_3, H-16) ; ^{13}C NMR (100 MHz, *d6*-DMSO) δ 211.7 (C, C-6), 171.9 (C, C-13), 132.3 (C, C-3), 128.1 (CH, C-2), 83.6 (CH, C-4), 66.9 (CH, C-9), 53.9 (CH_2, C-12), 51.9 (CH_2, C-1), 48.7 (C, C-5), 40.3 (CH, C-8), 40.1 (CH_2, C-7), 36.0 (CH_2, C-14), 29.0 (CH_2, C-10), 24.2 (CH_3, C-17), 21.5 (CH_2, C-11), 20.0 (CH_3, C-18), 18.4 (CH_2, C-15), 13.8 (CH_3, C-16); EIMS *m/z* 305 [M^+] (56), 218 (38), 217 (13), 202 (28), 174 (9), 148 (28), 133 (15), 71 (47), 70 (100), 43 (15); HRESIMS $[M+H]^+$ *m/z* 306.2072 (calcd. for $C_{18}H_{28}NO_3$ 306.2069, Δ 0.9 ppm).

*Ischnocybine B (**3.3**):* amorphous solid; $[\alpha]^{23}_{D}$ -4.67 (*c* 0.015, MeOH); UV (MeOH) λ_{max} (log ε) 1.9 (190) nm; NMR (500 MHz, d_6-DMSO) δ 5.74 (m, CH, H-2), 5.04 (s, CH, H-4), 5.01 (dd, *J* = 12.1 and 4.9, CH, H-6), 3.31 (m, CH, H-1a), 3.00 (m, CH, H-12a), 2.63 (m, CH, H-1b), 2.28 (td, *J* = 7.4, and 2.1, CH_2, H-14), 2.19 (m, CH, H-8), 2.12 (m, CH, H-12b), 2.02 (s, CH_3, H-18), 1.94 (m, CH, H-10a), 1.81 (m, CH, H-7a), 1.81 (m, CH, H-9) 1.67 (m, CH_2, H-11), 1.53 (m, CH_2, H-15), 1.33 (m, CH, H-10b), 1.20 (m, CH, H-7b), 0.87 (t, *J* = 7.4, CH_3, H-16), 0.84 (s, 2CH_3, H-19, H-20); ^{13}C NMR (100 MHz, d_6-DMSO) δ 172.0 (C, C-13), 170.6 (C, C-17), 133.3 (C, C-3), 127.6 (CH, C-2), 81.4 (CH, C-4), 73.6 (CH, C-6), 66.5 (CH, C-9), 54.1 (CH_2, C-12), 52.0 (CH_2, C-1), 38.9 (CH, C-8), 38.5 (C, C-5), 36.2 (CH_2, C-14), 30.7 (CH_2, C-7), 29.2 (CH_2, C-10), 23.0 (CH_3, C-20), 21.6 (CH_2, C-11), 21.3 (CH_3, C-18), 18.6 (CH_3, C-19), 18.6 (CH_2, C-15), 13.9 (CH_3, C-16); EIMS *m/z* 349 [M^+] (23), 262 (47), 261 (30), 248 (40), 202 (7), 186 (23), 150 (43), 135 (13), 133 (16), 132 (100), 71 (20), 70 (63), 43 (16); HRESIMS $[M+H]^+$ *m/z* 350.2335 (calcd. for $C_{20}H_{32}NO_4$ 350.2331, Δ 1.1 ppm).

*Ischnocybine C (**3.4**):* amorphous solid; $[\alpha]^{23}_{D}$ +6.09 (*c* 0.023, MeOH); UV (MeOH) λ_{max} (log ε) 1.6 (190) nm; NMR (500 MHz, d_6-DMSO) δ 5.41 (dd, *J* = 11.6 and 2.7, CH, H-7), 4.87 (d, *J* = 2.7, CH, H-6), 3.00 (m, CH, H-1a), 2.91 (td, *J* = 8.5 and 2.5, CH, H-12a), 2.30 (td, *J* = 7.3 and 1.5, CH_2, H-14), 2.25 (m, CH, H-8), 2.09 (td, *J* = 7.4 and 2.9, CH_2, H-18), 2.04 (m, CH, H-9), 1.90 (d, *J* = 8.5, CH, H-12b), 1.86 (m, CH, H-3), 1.86 (m, CH, H-2a), 1.81 (m, CH, H-1b), 1.77 (m, CH, H-10a), 1.70 (dd, *J* = 14.2 and 4.9, CH, H-4a), 1.63 (ddd, *J* = 13.7, 9.2, and 5.3, CH, H-10b), 1.57 (qd, *J* = 7.3 and 3.6, CH_2, H-15), 1.52 (m, CH, H-11a), 1.48 (q, *J* = 7.4, CH_2, H-19), 1.44 (m, CH, H-11b), 1.35 (m, CH, H-2b), 1.26 (d, *J* = 14.2, CH, H-4b), 1.10 (s, CH_3, H-22), 0.91 (t, *J* = 7.3, CH_3, H-16), 0.84 (t, *J* = 7.4, CH_3, H-20), 0.77 (s, CH_3, H-21); ^{13}C NMR (100 MHz, d_6-DMSO) δ 172.9 (C, C-13), 172.4 (C, C-17), 76.5 (CH, C-6), 69.3 (CH, C-7), 66.9 (CH, C-9), 54.3 (CH_2, C-

12), 54.1 (CH_2, C-1), 39.0 (CH_2, C-4), 36.7 (CH, C-3), 36.2 (CH_2, C-18), 36.1 (CH_2, C-14), 35.8 (CH, C-8), 35.0 (C, C-5), 29.3 (CH_2, C-2), 29.3 (CH_3, C-2), 27.9 (CH_3, C-22), 27.7 (CH_2, C-10), 21.7 (CH_2, C-11), 18.6 (CH_2, C-15), 17.9 (CH_2, C-19), 13.9 (CH_3, C-20), 13.8 (CH_3, C-16); EIMS *m/z* 379 [M^+] (20), 378 (13), 293 (17), 292 (100), 222 (7), 204 (53), 97 (7), 96 (23), 84 (90), 83 (22), 43 (12); HRESIMS $[M+H]^+$ *m/z* 380.2794 (calcd. for $C_{22}H_{37}NO_4$ 380.2801, Δ 1.8 ppm).

*Ischnocybine A alcohol (***3.6***):* amorphous solid; $[\alpha]^{23}_D$ +2.98 (*c* 0.019, MeOH); NMR (600 MHz, d_6-DMSO) δ 5.46 (m, CH, H-2), 3.41 (m, CH, H-4), 3.39 (m, CH, H-1a), 3.13 (m, CH, H-12b), 2.82 (m, CH, H-1b), 2.22 (m, CH, H-8), 2.21 (m, CH, H-12a), 2.01 (m, CH, H-9), 2.01 (m, CH, H-10b), 1.73 (m, CH_2, H-11), 1.71 (m, CH, H-6b), 1.56 (m, CH, H-7b), 1.37 (m, CH, H-10a), 1.07 (m, CH, H-7a), 1.03 (m, CH, H-6a), 0.89 (s, CH_3, H-13), 0.70 (s, CH_3, H-14); ^{13}C NMR (125 MHz, d_6-DMSO) δ 140.5 (C, C-3), 119.8 (CH, C-2), 77.8 (CH, C-4), 66.4 (CH, C-9), 53.1 (CH_2, C-12), 50.8 (CH_2, C-1), 37.2 (CH, C-8), 34.7 (C, C-5), 30.9 (CH_2, C-6), 28.4 (CH_2, C-10), 27.2 (CH_3, C-13), 25.7 (CH_2, C-7), 23.8 (CH_3, C-14), 20.8 (CH_2, C-11); HRESIMS $[M+H]^+$ *m/z* 222.1856 (calcd. for $C_{14}H_{23}NO$ 222.1852, Δ 1.25 ppm).

3.3.5. DFT & TD-DFT Results for All Configurations of Ischnocybine Compounds (3.1–3.4)

For NMR δ prediction analysis of **3.1–3.4**, to reduce computational overhead, alkyl chains from butyrate groups were truncated to yield acetate groups for quantum mechanical calculations. Structures were MMFF94 energy-minimized in Chem3D and extended mixed torsional/low-mode (MTLMOD) conformational searches were performed using the OPLS4[24] force field in the Schrödinger MacroModel software package. NMR predictions were based on the DELTA50[20] methodology; ^{13}C δ predictions were performed at the PCM-ωB97X-D/def2-SVP//PCM-B3LYP-D3/6-311G(d,p) level of theory, and ^{1}H δ predictions were performed at the PCM-WP04/6-311++G(2d,p)//PCM-B3LYP-D3/6-311G(d,p) level of theory, both of which utilized an integral

equation formalism (IEF) polarizable continuum model (PCM) for DMSO. Linear scaling factors include a slope of -1.0099 and intercept of 196.0386 for ^{13}C, and a slope of -1.0080 and intercept of 32.0998 for ^{1}H. Predicted chemical shifts were Boltzmann-weighted based on the total Gibbs free energy of each conformer. No imaginary frequencies were present within the frequency calculation results. Relative mean standard deviation (RMSD) and mean absolute error (MAE) of chemical shifts were compared between all possible configurations for **3.1–3.4**.

For ECD analysis of **3.4**, time-dependent (TD) DFT calculations were carried out for the prediction of frequency data at the PCM-ωB97X-D/6-311++G(2d,p)//B3LYP-D3/6-311G level of theory for n = 100 excited states, with an IEFPCM for MeOH. Transition energies, oscillator strengths, and rotatory strengths were extracted from the resulting Gaussian output files. Then, UV-vis and ECD spectra were generated with the following equation:

$$y(x) = \sum_i y_i(x) = \sum_i S_i \times \exp\left(-\frac{(x - E_i)^2}{2\sigma^2}\right)$$

Above, "$y_i(x)$" is the contribution to the spectrum from the i-th transition, "S_i" is the strength of the i-th transition (oscillator strength for UV-vis, rotatory strength for ECD), "E_i" is the energy of the i-th transition, "σ" is the broadening factor (optimized based on experimental data band widths), and "x" is the energy variable over which the spectrum is calculated. Respective energies (derived in units of eV) were converted to wavelengths (nm) through the relationship: wavelength (nm) × energy (eV) = 1240. Data for all conformers were Boltzmann-weighted based on the total Gibbs free energies, and relative intensities were scaled to match the experimental data for superimposition. Wavelength corrections were applied based on experimental UV-vis data.

3.3.6. Prey Deterrent Assays

To test the repellent effect of **3.1–3.4** on a likely predator, approximately 10 *Aphaenogaster* sp. ants were placed on petri plates (100 x 15 mm) with a paper disc containing 100 µg of **3.1–3.4** dissolved in methanol. First, each compound was tested separately and then combined on a single paper disc. A paper disc impregnated with only methanol was used as a negative control. The ants' behaviors were monitored for 5 to 15 min.[25]

3.3.7. Relative Quantification of Ischnocybines (3.1–3.4) on Individual Millipedes

To determine whether the size of the millipede impacts how much of the alkaloids are produced, we collected 29 individual *I. plicata* in 1.5 mL Eppendorf tubes. Each of the millipedes were measured with a ruler and then preserved in 0.5 mL of MeOH. A small aliquot was taken from each millipede and run on LR-LCMS (LTQ) using a Kinetex 5 µm EVO C18 100 x 3.0 mm column and the following solvent gradient system: holding 10% MeCN + 0.1% FA/90% H_2O + 0.1% FA for 3 min followed by a gradient to 100% MeCN + 0.1% FA over 11 min, holding for 3 min. The .raw files were converted to mzML using MSConvert (Version 3.0.20337). The data was processed in MzMine3 (Version 3.2.8). Mass detections were conducted with a noise threshold of 2.0E4. The ADAP chromatogram builder used a minimum group size of 5, a group intensity threshold of 2.0E4, minimum height intensity of 2.0E4 and *m/z* tolerance was 0.5. The local minimum resolver utilized the following settings: Chromatographic threshold: 95%, Search minimum in RT range (min)=0.2, minimum relative height=1%, minimum absolute height = 1.0E2 minimum ratio or peak top/edge=1.4, Minimum number of data points=3 and peak duration range (min) = 0.00–1. The 13C isotope filler had an *m/z* tolerance of 0.5 *m/z*, retention time tolerance of 0.3, maximum charge of 3 and representative isotope of most intense. Finally, the join aligner had an *m/z* tolerance of 0.5 *m/z*, a weight for *m/z* of 75, retention time tolerance of 0.3 min, and weight

for RT of 25. The .csv file was then exported, the peak areas for extracted ion chromatograms corresponding to the $[M+H]^+$ for each ischnocybine [292 (**3.1**), 206 (**3.2**), 350 (**3.3**), and 380 (**3.4**)], were plotted against the length of each millipede using Prism (Version 10.2.0).

3.3.8. Mosher Esterification of Ischnocybine A Alcohol (3.6)

Mosher esterification reactions were performed following literature precedent.[21] Briefly, two solutions of ischnocybine A alcohol (**3.6**) (1.25 mg, 5.66 µmol), two chunks (dimethylamino)pyridine (DMAP), and two drops triethylamine (TEA) in 150 µL of DCM. One was treated with (*R*)-(−)-α-Methoxy-α-(trifluoromethyl)phenylacetyl chloride (MTPA) chloride (7.5 µL, 40 µmol), while the other was treated with (*S*)-MTPA chloride (7.5 µL, 40 µmol). Both mixtures were left at rt overnight. Each reaction was extracted with 1-butanol (1 mL) and the organic layer was washed with brine (1 mL). The organic layer was dried and suspended in 50% MeCN/50% H and purified on HPLC using a C_{18} semi-preparative column (Phenomenex Synergi, 10.0 x 250 mm, 4 µm) using the following solvent gradient system: holding 45% acetonitrile (MeCN) + 0.1% FA/55% H_2O + 0.1% FA for 5 min then gradient to 90% MeCN + 0.1% FA/10% H_2O + 0.1% FA over 10 min with a 3 mL/min flow rate, the product eluted at 8.2 min (**3.7** and **3.8**).

3.3.9. Chemical Derivatization of Ischnocybine C (3.4) and Electronic Circular Dichroism Analysis

Ischnocybine C (1 mg, 2.63 µmol) was treated with 1.5 mL 0.5N NaOH, heated to 40 ºC and let stir for 2 d. The solution was quenched with 1.5 mL 0.5 N HCl and dried down, the product was carried through. The hydrolysis product was treated with bromobenzoyl chloride (6 mg, 27.3 µmol), DMAP (2 chunks) and tetrahydrofuran (2.0 mL, 25 mmol). The reaction was heated to 50 ºC for two days. The reaction was extracted with EtOAc and the organic layer was washed with

brine. The product was dried and resuspended in 50% MeCN/50% H_2O then purified with HPLC using a C_{18} semi-preparative column (Phenomenex Synergi, 10.0 x 250 mm, 4 μm) using the following solvent gradient system: holding 50% MeCN + 0.1% FA/50% H_2O + 0.1% FA for 5 min then gradient to 100% MeCN + 0.1% FA over 15 min with a 3 mL/min flow rate, the product eluted at 16.6 min.

3.3.10. Binding Assay for the Sigma-1 and -2 Receptors

HEKT cell lines were used to make membrane pallets for binding assays. In the primary binding assays, compounds were tested at a single concentration (10 μM) and in quadruplicate in 96-well plates. Compounds showing a minimum of 50% inhibition at 10 μM were tagged for secondary radioligand binding assays to determine equilibrium binding affinity at specific targets. In secondary binding assays, compounds were tested at 11 concentrations (0.1, 0.3, 1, 3, 10, 30, 100, 300, 1,000, 3,000, and 10,000 nM) and in triplicate (3 sets of 96-well plates). Both primary and secondary radioligand binding assays were carried out in a final volume of 125 μL per well in appropriate binding buffers (50 mM Tris HCl, pH 8.0, rt). Pentazocine was used as a radioligand and the hot ligand concentration was determined close to its K_i. Total binding and nonspecific binding were determined in the absence and presence of 10 μM of haloperidol, the reference compound. Plates were incubated at room temperature and in the dark for 90 min. Reactions were stopped by vacuum filtration onto 0.3% polyethyleneimine (PEI) soaked 96-well filter mats using a 96-well Filtermate harvester, followed by three washes with cold wash buffers (50 mM Tris HCl, pH 7.4). Scintillation cocktail was then melted onto the microwave-dried filters on a hot plate and radioactivity was counted in a Microbeta counter. K_i values for [3H]-(+)-pentazocine (σ_1R: 6.70 nM), (σ_2R: 14.50) were determined via separate homologous competitive binding experiments. K_i

values were determined from at least three independent experiments and are reported as mean ± SEM.

3.3.11. Molecular Docking

To investigate the binding mechanism of action for alkaloid compounds to the σ_1R binding pocket, molecular docking was performed. Several σ_1R crystal structures were redocked with their original co-crystalized ligand and docked with our novel alkaloid compounds. The alkaloid compounds, ischnocybine A, B, C and ischnocybinone were prepared as pdb files by the Mevers lab. Each compound was prepared with *R* and *S* configuration, for a total of eight ligand files. Crystal structures representing agonistic (PDB ID: 6DK1),[26] antagonistic (PDB ID: 6DK0),[13] and apo (PDB ID: 7W2E)[22] conformations of the σ_1R were used to avoid potential bias in docking studies. The receptor files were prepared for docking in PyMOL 2.5.0[26] where glycolipids, sulfates, glycerols, and waters were removed from the environment. Oligomeric structures were reduced to a single monomeric unit. The agonist receptor contained pentazocine and the antagonist receptor contained NE-100 as co-crystallized ligands.

The pentazocine, NE-100, and alkaloid compounds were redocked and docked using GNINA 1.0.3,[26] a successor to AutoDock Vina[27] that uses deep-learning scoring functions. AutoDock Tools 1.5.6[28] was used to center the grid box onto the co-crystalized ligands in their respective structures, establishing x, y, z coordinates of 10.343, 38.597, and -34.851 (agonist, PDB ID: 6DK1), 16.549, 37.608, and -35.618 (antagonist, PDB ID: 6KD0), and -65.0, 3.0, and 80 (apo, PDB ID: 7W2E). A box size of 40 Å x 40 Å x 40 Å was utilized. Redocked root mean square deviation (RMSD) values for pentazocine in the agonist and NE-100 in the antagonist were as low as 0.74 Å and 1.25 Å respectively (**Figure 3.7.54**). Additionally, both co-crystallized ligands were docked into their counterpart structure and successfully mimicked their original binding position

(**Figure 3.7.52** and **Figure 3.7.53**), further validating the protocol and the ability to predict if compounds sampled antagonistic or agonistic positioning in the binding pocket. The 8 alkaloid compounds ligands were docked into each of the 3 structures individually, generating 9 poses each. Poses found within the binding cavity were analyzed further. Analysis of the predicted binding poses was performed in PyMOL 2.5.0. Schrödinger Maestro 2021-2 was used to perform molecular mechanics with generalized Born and surface area solvation (MM/GBSA) energy calculations for each binding pose located in the binding pocket.[29]

3.4. Data Availability Statement

The original NMR data (FIDs) of compound **3.1–3.4** and **3.6** is available via NP-MRD (accession #: NP0333129, NP0333130, NP0333131, NP0350550 and NP0350551) at https://np-mrd.org/.

3.5. Acknowledgements

This work was funded by NIH [R35 GM146740 (EM)] and Virginia Tech Startup funds (EM). We thank the Virginia Tech NMR facility and Virginia Tech Mass Spectrometry Incubator for analytical services. Primary binding assays and K_i determinations were generously provided by the National Institute of Mental Health's Psychoactive Drug Screening Program, Contract # HHSN-271-2018-00023-C (NIMH PDSP). The NIMH PDSP is Directed by Bryan L. Roth at the University of North Carolina at Chapel Hill and Project Officer Jamie Driscoll at NIMH, Bethesda MD, USA. National Science Foundation grant numbers CHE0821552 and CHE2116395 for NMR spectrometers utilized in this work are acknowledged.

3.6. References

(1) Shear, W. A. The chemical defenses of millipedes (diplopoda): Biochemistry, physiology and ecology. *Biochemical Systematics and Ecology* **2015**, *61*, 78-117. DOI: 10.1016/j.bse.2015.04.033.

(2) Shorter, P. L.; Hennen, D. A.; Marek, P. E. Cryptic diversity in Andrognathus corticarius Cope, 1869 and description of a new Andrognathus species from New Mexico (Diplopoda, Platydesmida, Andrognathidae). *Zookeys* **2018**, (786), 19-41. DOI: 10.3897/zookeys.786.27631.

(3) Eisner, H. E.; Alsop, D. W.; Eisner, T. Defense mechanisms of arthropods. XX. Quantitative assessment of hydrogen cyanide production in two species of millipedes. *Psyche* **1967**, *74*, 107-117. DOI: 10.1155/1967/861501.

(4) Whitfield, J. The Insects: An Outline of Entomology. *American Entomologist* **1995**, *41*. DOI: 10.1093/ae/41.3.188.

(5) Stebbins, R. C. Lizards Killed by a Millipede. *The American Midland Naturalist* **1944**, *32* (3), 777-778. DOI: 10.2307/2421250.

(6) Banks, P.; Funkhouser, E. M.; Macias, A. M.; Lovett, B.; Meador, S.; Hatch, A.; Garraffo, H. M.; Cartwright, K. C.; Kasson, M. T.; Marek, P. E.; et al. The Chemistry of the Defensive Secretions of Three Species of Millipedes in the Genus Brachycybe. *Journal of Chemical Ecology* **2024**, *50* (9), 478-488. DOI: 10.1007/s10886-024-01518-6.

(7) Jones, T. H.; Harrison, D. P.; Menegatti, C.; Mevers, E.; Knott, K.; Marek, P.; Hennen, D. A.; Kasson, M. T.; Macias, A. M.; Lovett, B.; et al. Deoxybuzonamine Isomers from the Millipede Brachycybe lecontii (Platydesmida: Andrognathidae). *Journal of Natural Products* **2022**, *85* (4), 1134-1140. DOI: 10.1021/acs.jnatprod.2c00077.

(8) Wood, W. F.; Hanke, F. J.; Kubo, I.; Carroll, J. A.; Crews, P. Buzonamine, a new alkaloid from the defensive secretion of the millipede, Buzonium crassipes. *Biochemical Systematics and Ecology* **2000**, *28* (4), 305-312. DOI: 10.1016/S0305-1978(99)00068-X.

(9) Smolanoff, J.; Kluge, A. F.; Meinwald, J.; McPhail, A.; Miller, R. W.; Hicks, K.; Eisner, T. Polyzonimine: A Novel Terpenoid Insect Repellent Produced by a Milliped. *Science* **1975**, *188* (4189), 734-736. DOI: doi:10.1126/science.1124395.

(10) Meinwald, J.; Smolanoff, J.; McPhail, A. T.; Miller, R. W.; Eisner, T.; Hicks, K. Nitropolyzonamine: A spirocyclic nitro compound from the defensive glands of a milliped (polyzonium rosalbum). *Tetrahedron Letters* **1975**, *16* (28). DOI: 10.1016/0040-4039(75)80013-X.

(11) Kunert, O.; Pferschy-Wenzig, E. M.; Orthaber, A.; Raspotnig, G.; Bodner, M. Alkaloids from millipedes: a re-evaluation of defensive exudates from Polyzonium germanicum. *Frontiers in Ecology and Evolution* **2023**, *11*. DOI: 10.3389/fevo.2023.1212452.

(12) Hassler, M. F.; Harrison, D. P.; Jones, T. H.; Richart, C. H.; Saporito, R. A. Gosodesmine, a 7-Substituted Hexahydroindolizine from the Millipede Gosodesmus claremontus. *Journal of Natural Products* **2020**, *83* (9). DOI: 10.1021/acs.jnatprod.0c00722.

(13) Schmidt, H. R.; Betz, R. M.; Dror, R. O.; Kruse, A. C. Structural basis for σ(1) receptor ligand recognition. *Nature Structural and Molecular Biology* **2018**, *25* (10), 981-987. DOI: 10.1038/s41594-018-0137-2.

(14) Maurice, T.; Su, T. P. The pharmacology of sigma-1 receptors. *Pharmacology and Therapeutics* **2009**, *124* (2), 195-206. DOI: 10.1016/j.pharmthera.2009.07.001.

(15) Ryskamp, D. A.; Korban, S.; Zhemkov, V.; Kraskovskaya, N.; Bezprozvanny, I. Neuronal Sigma-1 Receptors: Signaling Functions and Protective Roles in Neurodegenerative Diseases. *Frontiers in Neuroscience* **2019**, *13*, 862. DOI: 10.3389/fnins.2019.00862.

(16) Bruna, J.; Videla, S.; Argyriou, A. A.; Velasco, R.; Villoria, J.; Santos, C.; Nadal, C.; Cavaletti, G.; Alberti, P.; Briani, C.; et al. Efficacy of a Novel Sigma-1 Receptor Antagonist for

Oxaliplatin-Induced Neuropathy: A Randomized, Double-Blind, Placebo-Controlled Phase IIa Clinical Trial. *Neurotherapeutics* **2018**, *15* (1), 178-189. DOI: 10.1007/s13311-017-0572-5.

(17) Brewer, M. S.; Spruill, C. L.; Rao, N. S.; Bond, J. E. Phylogenetics of the millipede genus Brachycybe Wood, 1864 (Diplopoda: Platydesmida: Andrognathidae): Patterns of deep evolutionary history and recent speciation. *Molecular Phylogenetics and Evolution* **2012**, *64* (1). DOI: 10.1016/j.ympev.2012.04.003.

(18) Marek, P. E.; Buzatto, B. A.; Shear, W. A.; Means, J. C.; Black, D. G.; Harvey, M. S.; Rodriguez, J. The first true millipede—1306 legs long. *Scientific Reports* **2021**, *11* (1), 23126. DOI: 10.1038/s41598-021-02447-0.

(19) Benavides, L. R.; Edgecombe, G. D.; Giribet, G. Re-evaluating and dating myriapod diversification with phylotranscriptomics under a regime of dense taxon sampling. *Molecular Phylogenetics and Evolution* **2023**, *178*, 107621. DOI: 10.1016/j.ympev.2022.107621.

(20) Cohen, R. D.; Wood, J. S.; Lam, Y. H.; Buevich, A. V.; Sherer, E. C.; Reibarkh, M.; Williamson, R. T.; Martin, G. E. DELTA50: A Highly Accurate Database of Experimental (1)H and (13)C NMR Chemical Shifts Applied to DFT Benchmarking. *Molecules* **2023**, *28* (6). DOI: 10.3390/molecules28062449.

(21) Ohtani, I.; Kusumi, T.; Kashman, Y.; Kakisawa, H. High-field FT NMR application of Mosher's method. The absolute configurations of marine terpenoids. *Journal of the American Chemical Society* **1991**, *113* (11), 4092-4096. DOI: 10.1021/ja00011a006.

(22) Meng, F.; Xiao, Y.; Ji, Y.; Sun, Z.; Zhou, X. An open-like conformation of the sigma-1 receptor reveals its ligand entry pathway. *Nature Communications* **2022**, *13* (1), 1267. DOI: 10.1038/s41467-022-28946-w.

(23) Wong, V. L.; Hennen, D. A.; Macias, A. M.; Brewer, M. S.; Kasson, M. T.; Marek, P. Natural history of the social millipede Brachycybe lecontii Wood, 1864. *Biodiversity Data Journal* **2020**, *8*, e50770. DOI: 10.3897/BDJ.8.e50770.

(24) Lu, C.; Wu, C.; Ghoreishi, D.; Chen, W.; Wang, L.; Damm, W.; Ross, G. A.; Dahlgren, M. K.; Russell, E.; Von Bargen, C. D.; et al. OPLS4: Improving Force Field Accuracy on Challenging Regimes of Chemical Space. *Journal of Chemical Theory and Computation* **2021**, *17* (7), 4291-4300. DOI: 10.1021/acs.jctc.1c00302.

(25) Estrada, C.; Wcislo, W. T.; Van Bael, S. A. Symbiotic fungi alter plant chemistry that discourages leaf-cutting ants. *New Phytologist* **2013**, *198* (1), 241-251. DOI: 10.1111/nph.12140.

(26) McNutt, A. T.; Francoeur, P.; Aggarwal, R.; Masuda, T.; Meli, R.; Ragoza, M.; Sunseri, J.; Koes, D. R. GNINA 1.0: molecular docking with deep learning. *Journal of Cheminformatics* **2021**, *13* (1), 43. DOI: 10.1186/s13321-021-00522-2.

(27) Trott, O.; Olson, A. J. AutoDock Vina: improving the speed and accuracy of docking with a new scoring function, efficient optimization, and multithreading. *Journal of Computational Chemistry* **2010**, *31* (2), 455-461. DOI: 10.1002/jcc.21334.

(28) Morris, G. M.; Huey, R.; Lindstrom, W.; Sanner, M. F.; Belew, R. K.; Goodsell, D. S.; Olson, A. J. AutoDock4 and AutoDockTools4: Automated docking with selective receptor flexibility. *Journal of Computational Chemistry* **2009**, *30* (16), 2785-2791. DOI: 10.1002/jcc.21256.

(29) Maestro, version 9.4. New York, NY: Schrödinger, LLC; 2013.

3.7. Appendix Figures

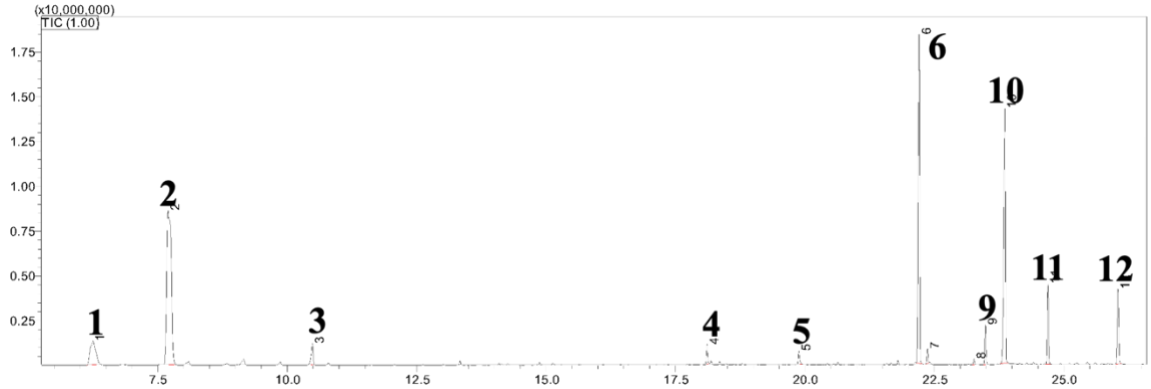

Peak	Compound ID	Rel amounts
1	α-pinene	6.1
2	β-pinene	32.6
3	α-terpenolene	1.9
4	germacrene-4-ol	1.1
5	Ischnocybine A free alcohol (**3.6**)	0.9
6	Ischnocybine A (**3.1**)	24.5
9	FAME Me 9-octadecenoate	2.2
10	Ischnocybinone (**3.2**)	19.8
11	Ischnocybine B (**3.3**)	4.5
12	Ischnocybine C (**3.4**)	5.3

Figure 3.7.1. GCMS total ion chromatogram of the crude MeOH extract of the *Ischnocybe plicata* collections.

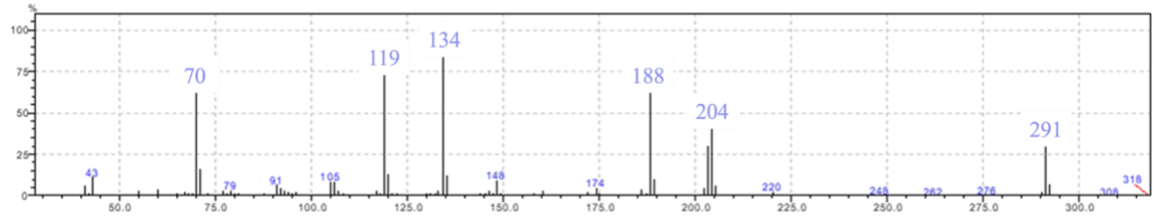

Figure 3.7.2. EIMS spectrum for ischnocybine A (**3.1**) *m/z* 291

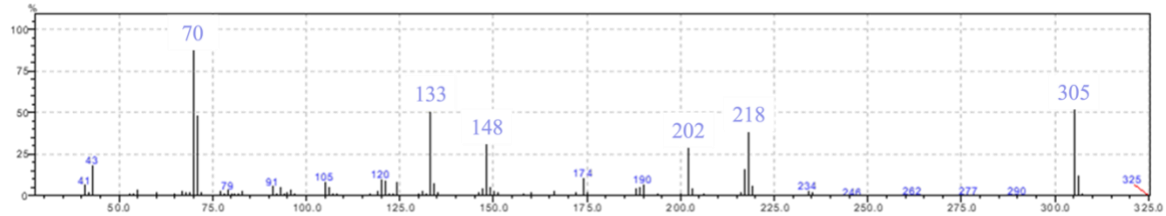

Figure 3.7.3. EIMS spectrum for ischnocybinone (**3.2**) *m/z* 305

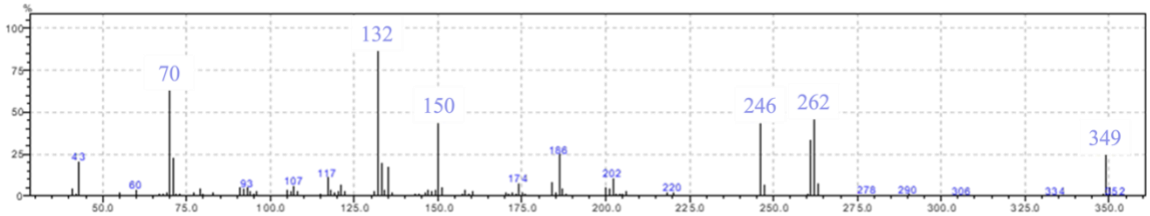

Figure 3.7.4. EIMS spectrum for ischnocybine B (**3.3**) *m/z* 349

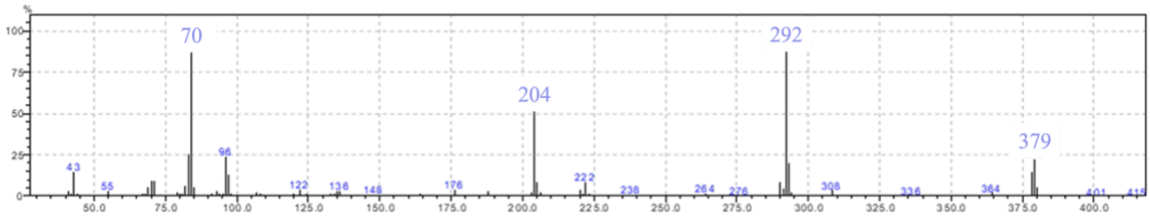

Figure 3.7.5. EIMS spectrum for ischnocybine C (**3.4**) *m/z* 379

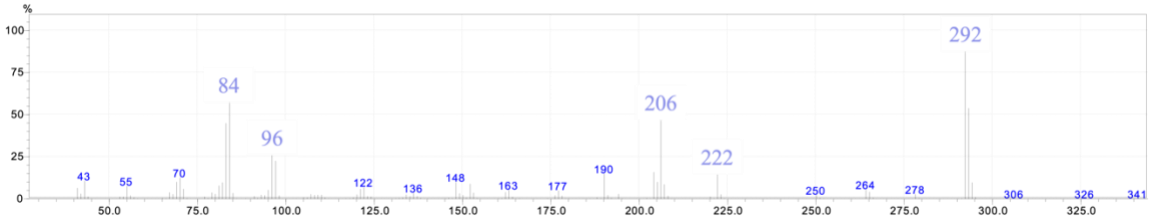

Figure 3.7.6. EIMS spectrum for hydrogenated ischnocybine A (**3.1**) (two isomers with *m/z* 293)

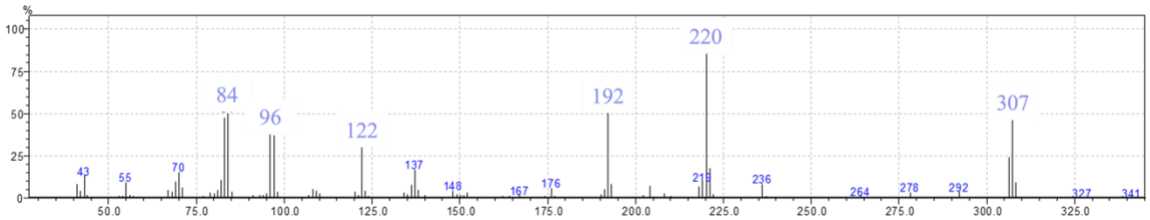

Figure 3.7.7. EIMS spectrum for hydrogenated ischnocybinone (**3.2**) (one isomer with *m/z* 307)

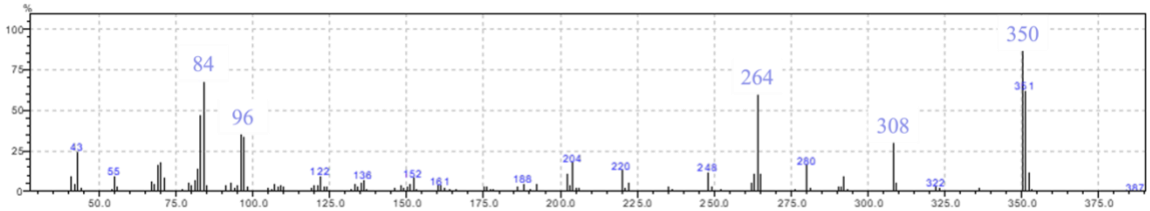

Figure 3.7.8. EIMS spectrum for hydrogenated ischnocybine B (**3.3**) (one isomer with *m/z* 351)

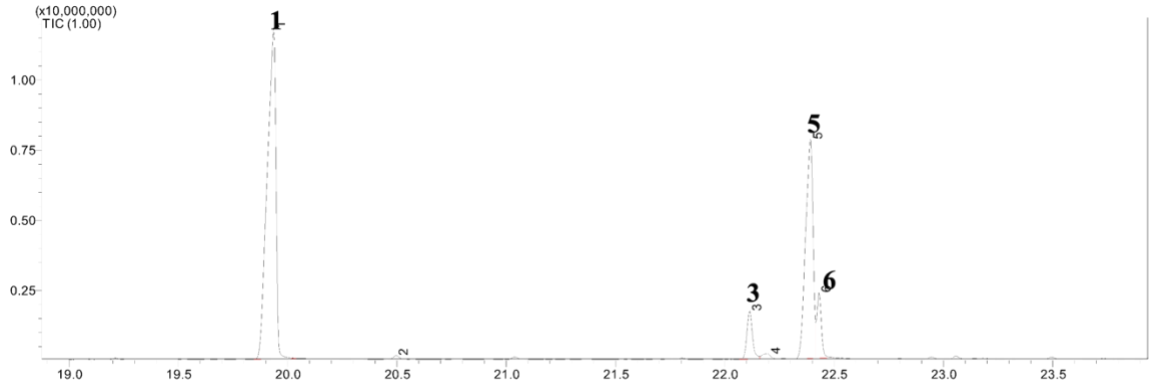

Figure 3.7.9. Chromatogram of base hydrolysis of *I. plicata* extract

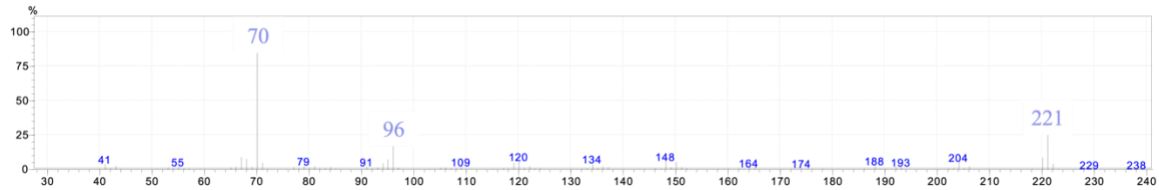

Figure 3.7.10. EIMS spectrum for methanolysis adduct (peak 1) of ischnocybine A (**3.1**) *m/z* 221.

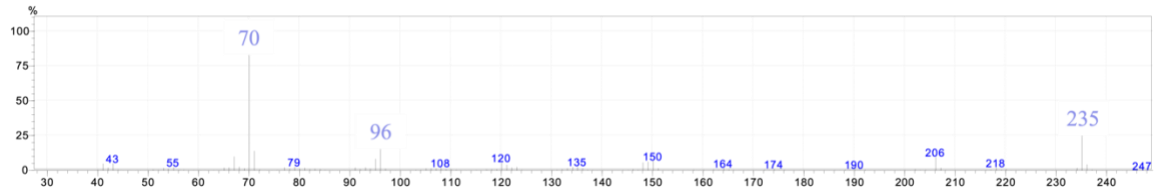

Figure 3.7.11. EIMS spectrum for methanolysis adduct (peak 5) of ischnocybinone (**3.2**) *m/z* 235.

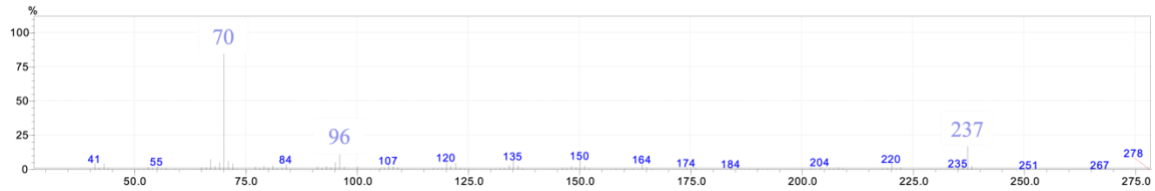

Figure 3.7.12. EIMS spectrum for methanolysis adduct (peak 6) of ischnocybine B (**3.3**) *m/z* 237.

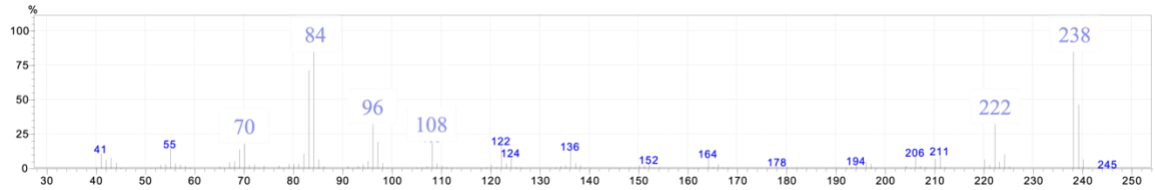

Figure 3.7.13. EIMS spectrum for methanolysis adduct (peak 3) of ischnocybine C (**3.4**) *m/z* 238.

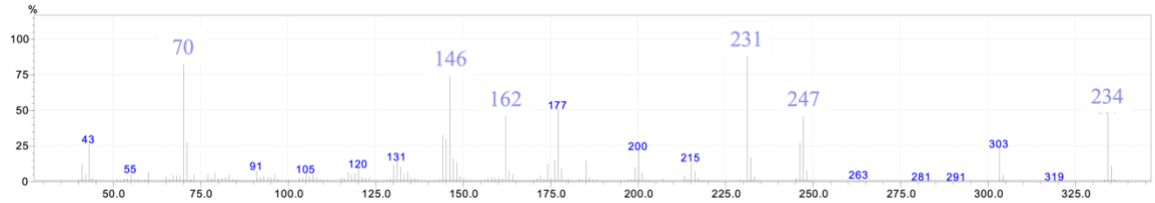

Figure 3.7.14. EIMS spectrum for methoxylamine adduct of ischnocybinone (**3.2**)

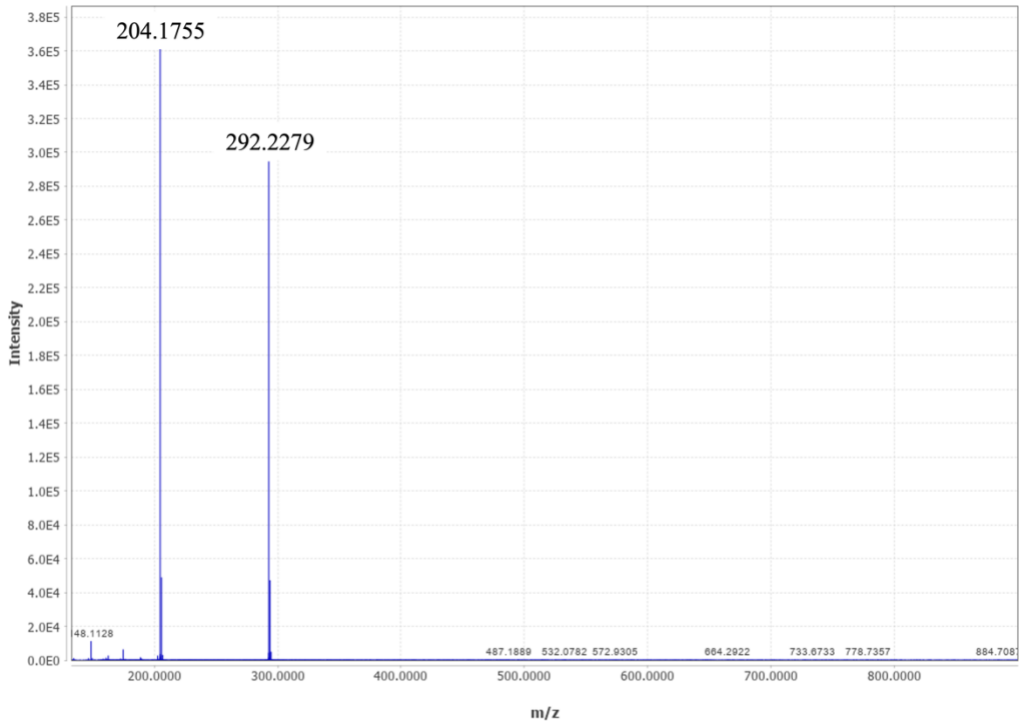

Figure 3.7.15. HRESIMS spectrum of ischnocybine A (**3.1**)

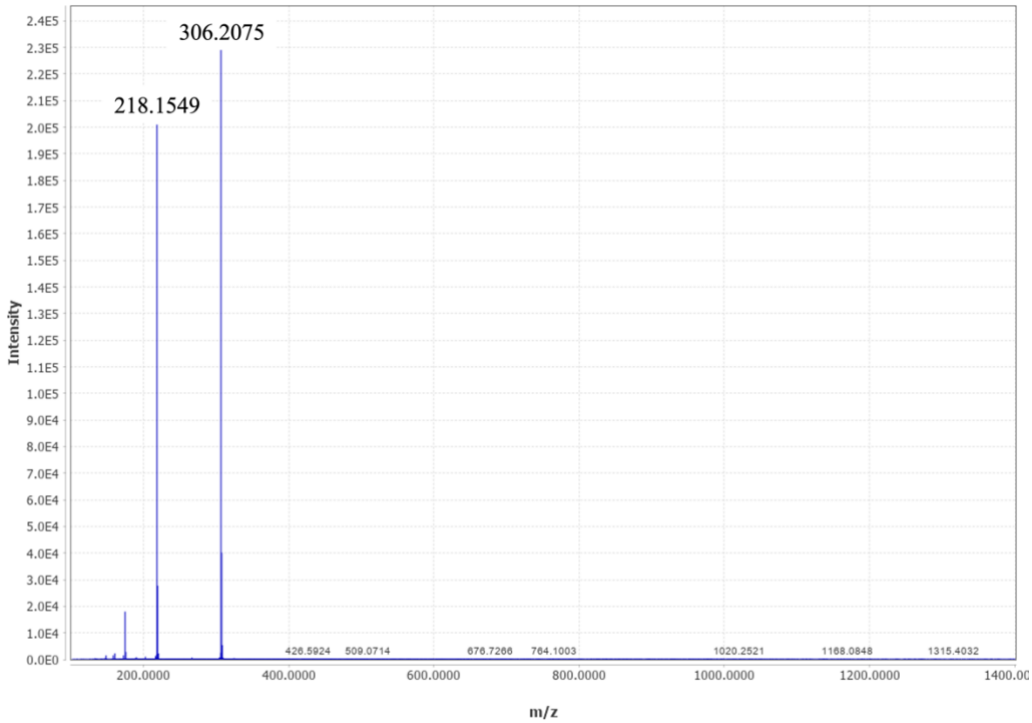

Figure 3.7.16. HRESIMS spectrum of ischnocybinone (**3.2**)

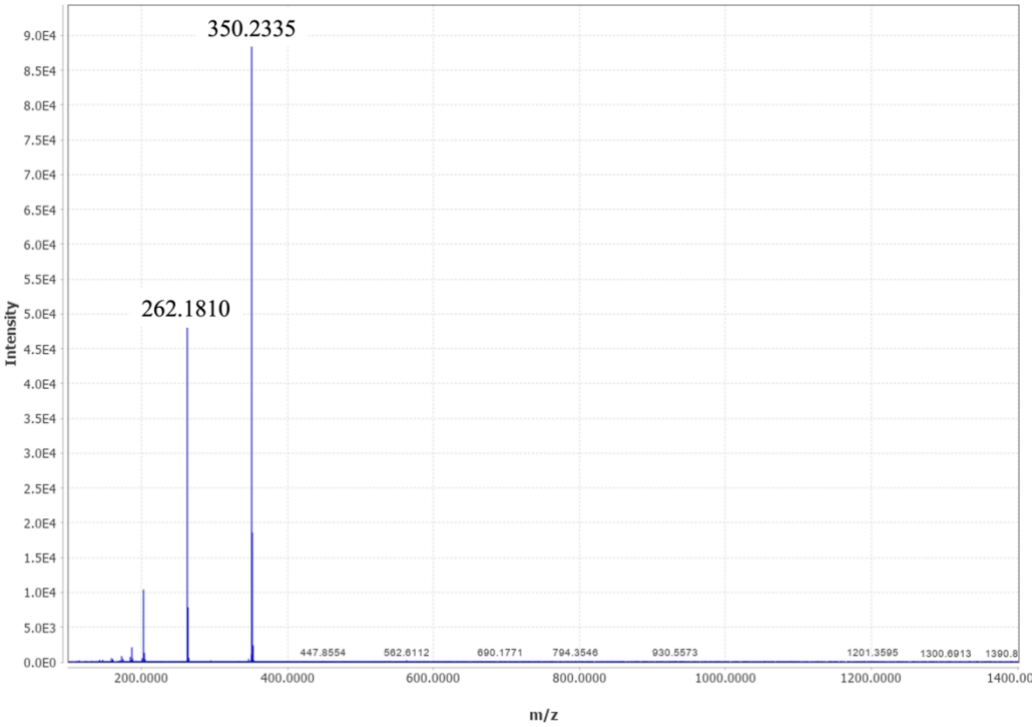

Figure 3.7.17. HRESIMS spectrum of ischnocybine B (**3.3**)

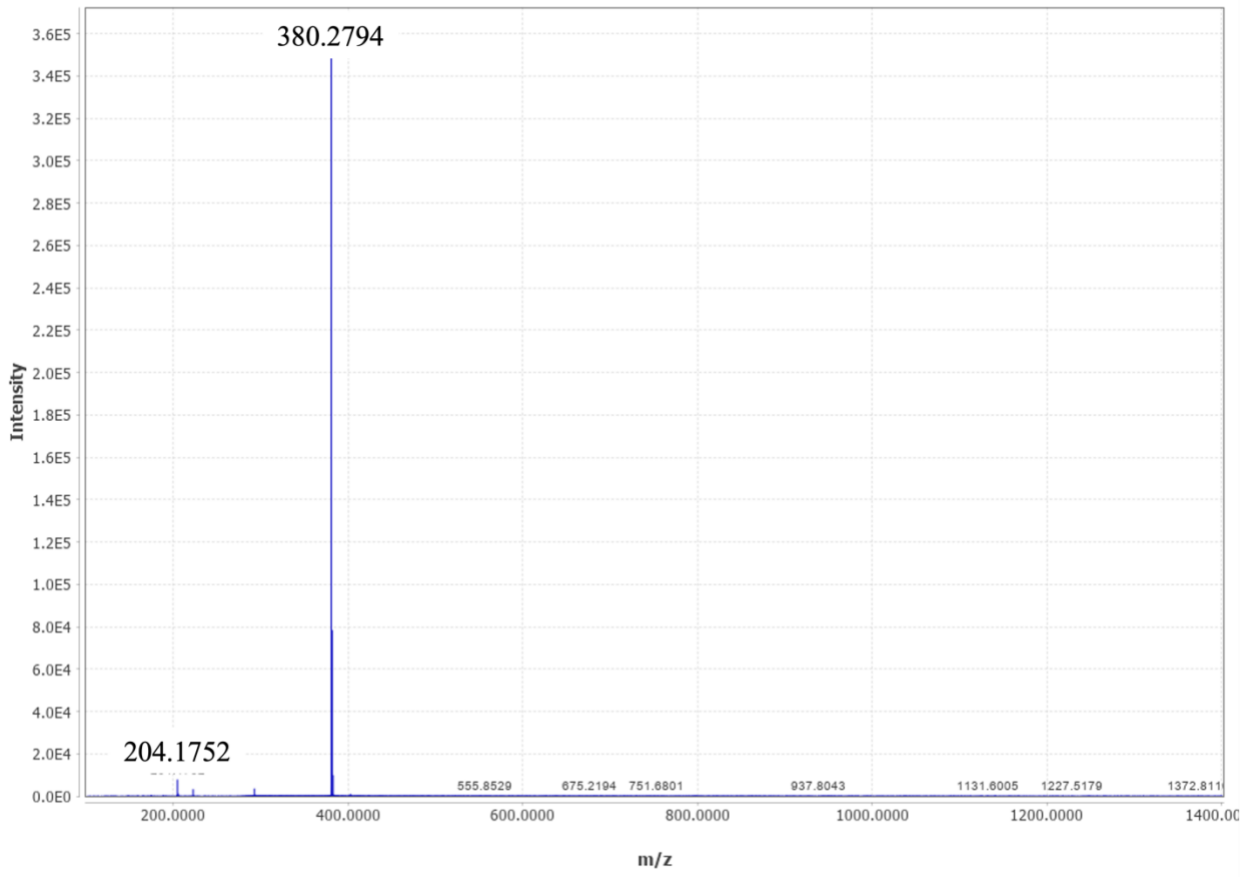

Figure 3.7.18. HRESIMS $[M+H]^+$ spectrum of ischnocybine C (**3.4**)

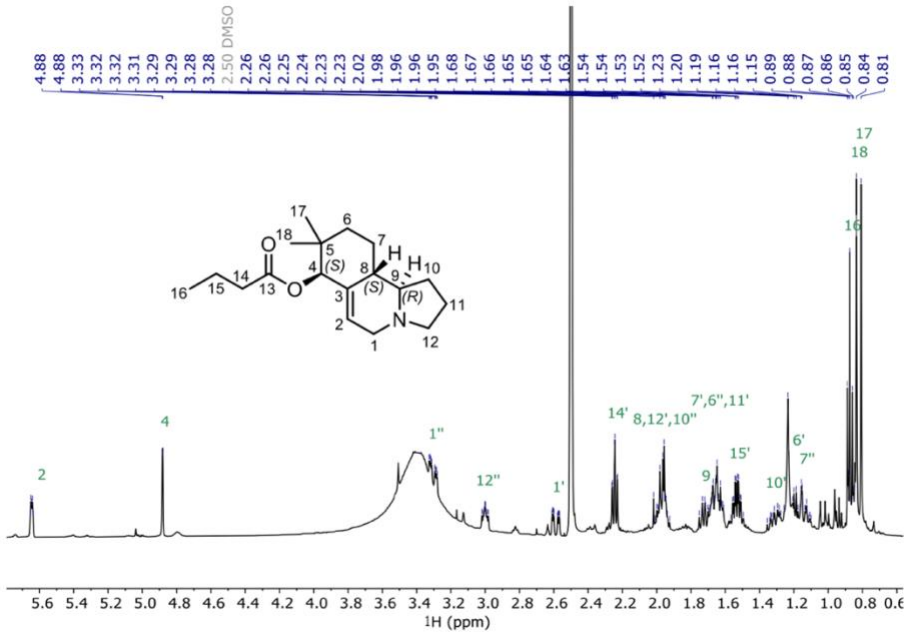

Figure 3.7.19. ^{1}H NMR spectrum of ischnocybine A (**3.1**) (500 MHz, d_6-DMSO).

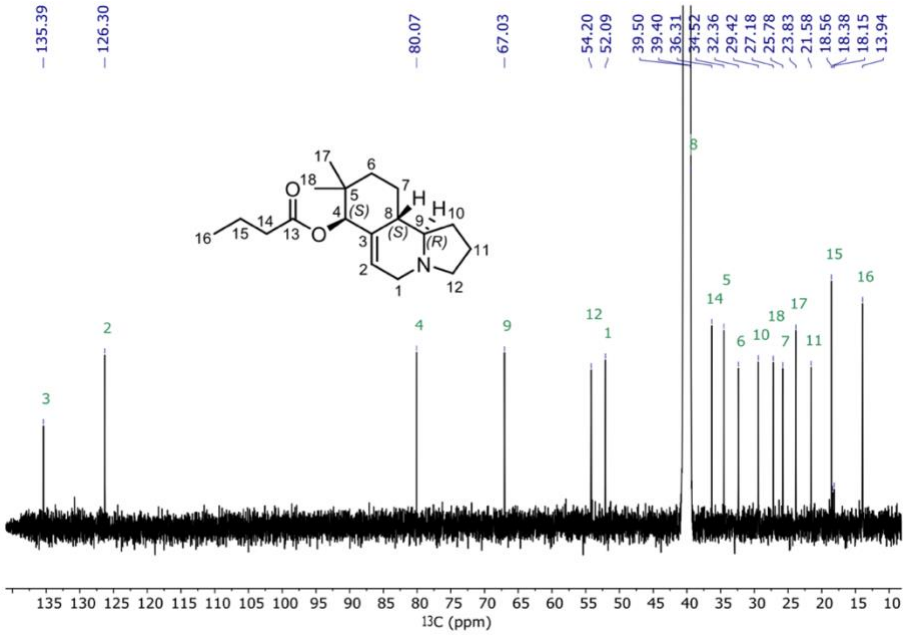

Figure 3.7.20. ^{13}C NMR spectrum of ischnocybine A (**3.1**) (500 MHz, d_6-DMSO).

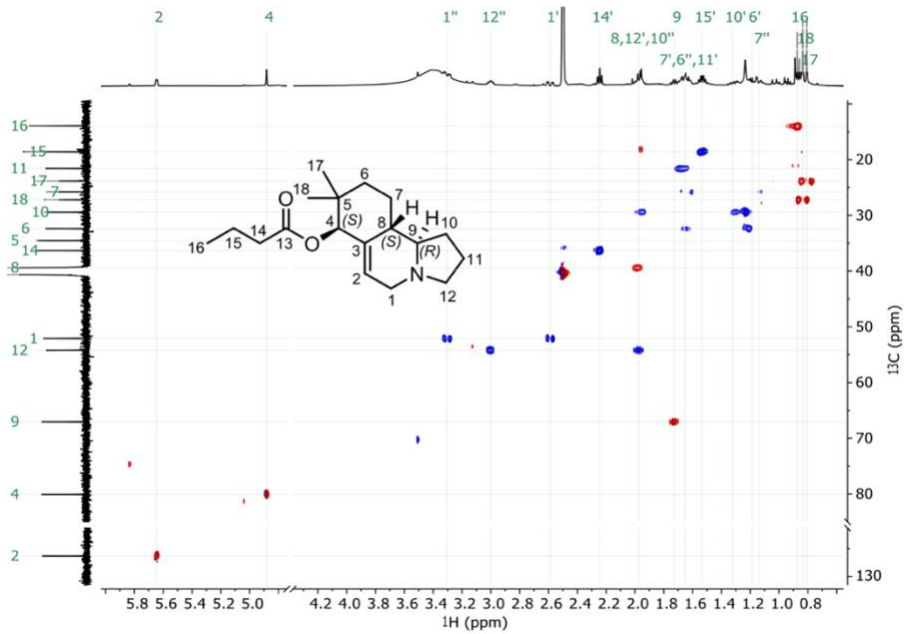

Figure 3.7.21. Multiplicity-edited ^{1}H-^{13}C HSQC NMR spectrum of ischnocybine A (**3.1**) (500 MHz, d_6-DMSO).

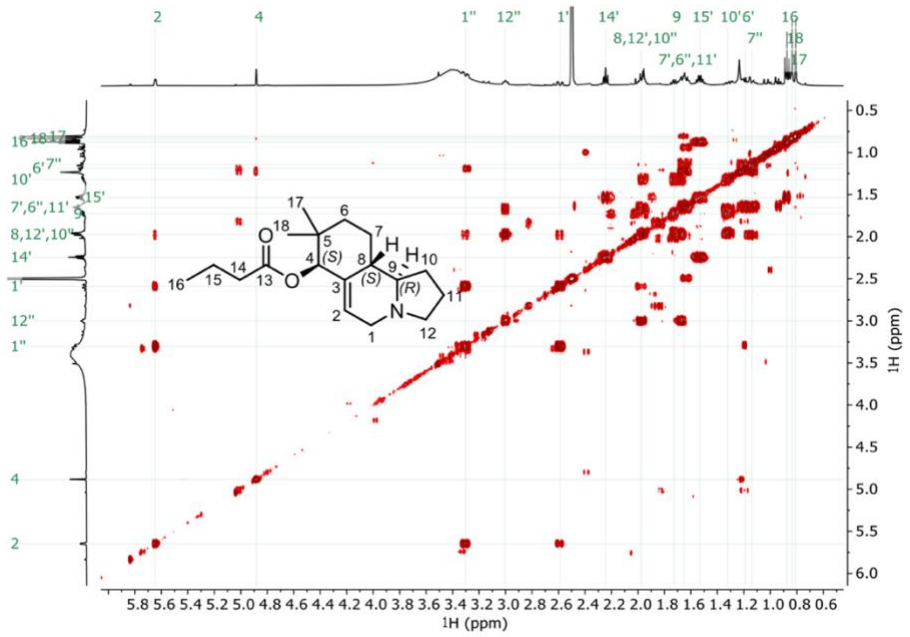

Figure 3.7.22. COSY NMR spectrum of ischnocybine A (**3.1**) (500 MHz, *d6*-DMSO).

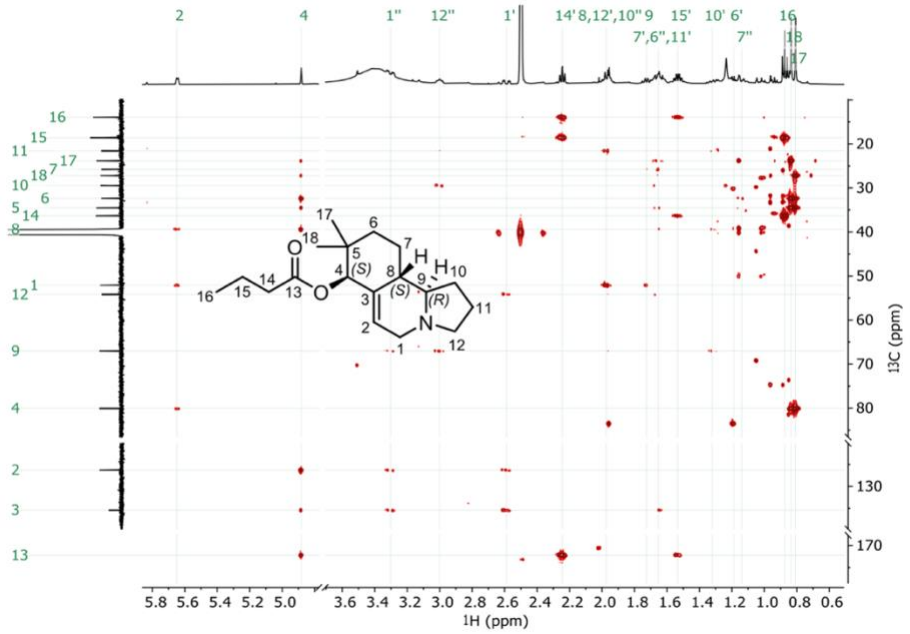

Figure 3.7.23. ^{1}H-^{13}C HMBC NMR spectrum of ischnocybine A (**3.1**) (500 MHz, *d6*-DMSO).

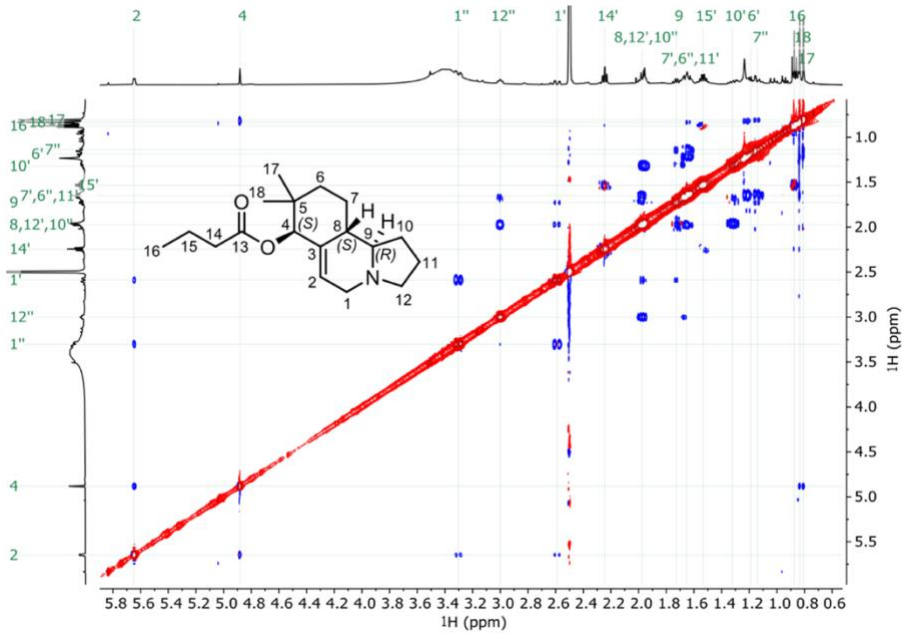

Figure 3.7.24. easyROESY NMR spectrum of ischnocybine A (**3.1**) (500 MHz, d_6-DMSO).

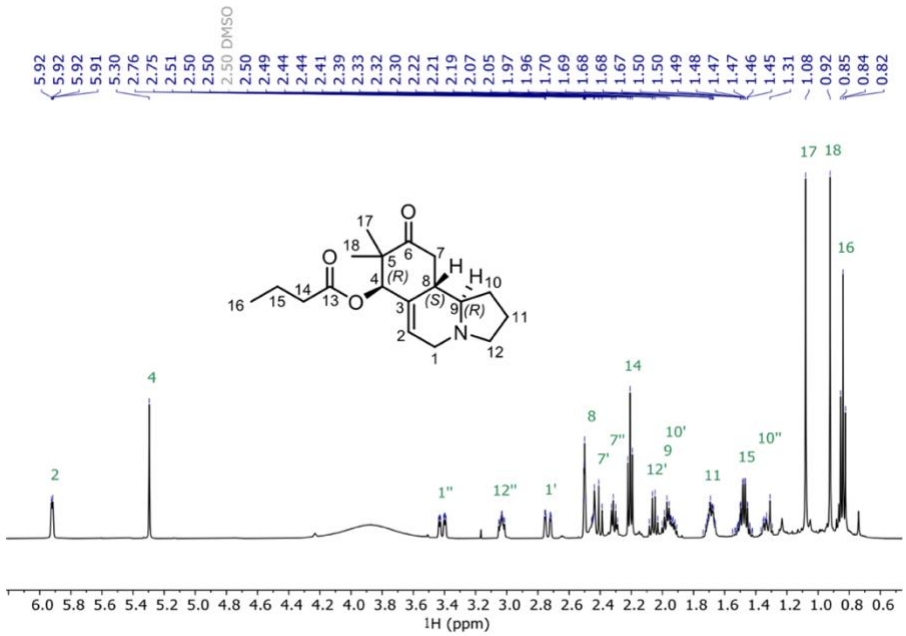

Figure 3.7.25. ^{1}H NMR spectrum of ischnocybinone (**3.2**) (500 MHz, d_6-DMSO).

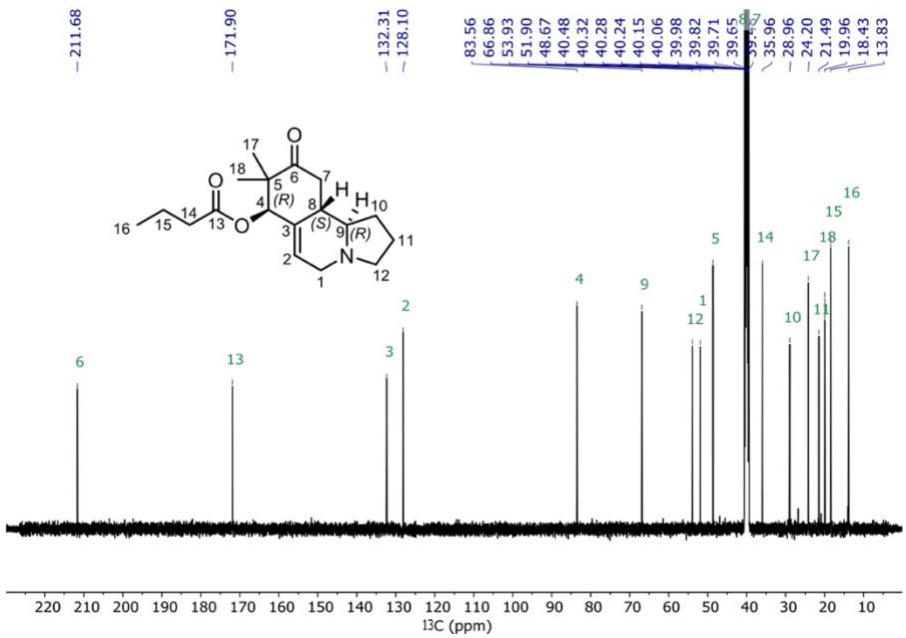

Figure 3.7.26. ^{13}C NMR spectrum of ischnocybinone (**3.2**) (500 MHz, *d*$_6$-DMSO).

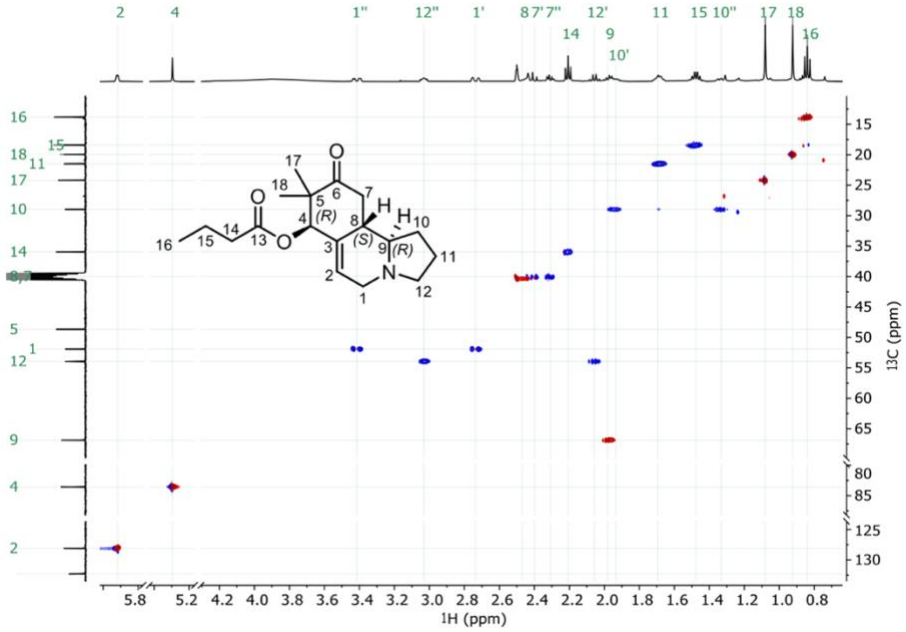

Figure 3.7.27. Multiplicity-edited ^{1}H-^{13}C HSQC NMR spectrum of ischnocybinone (**3.2**) (500 MHz, *d*$_6$-DMSO).

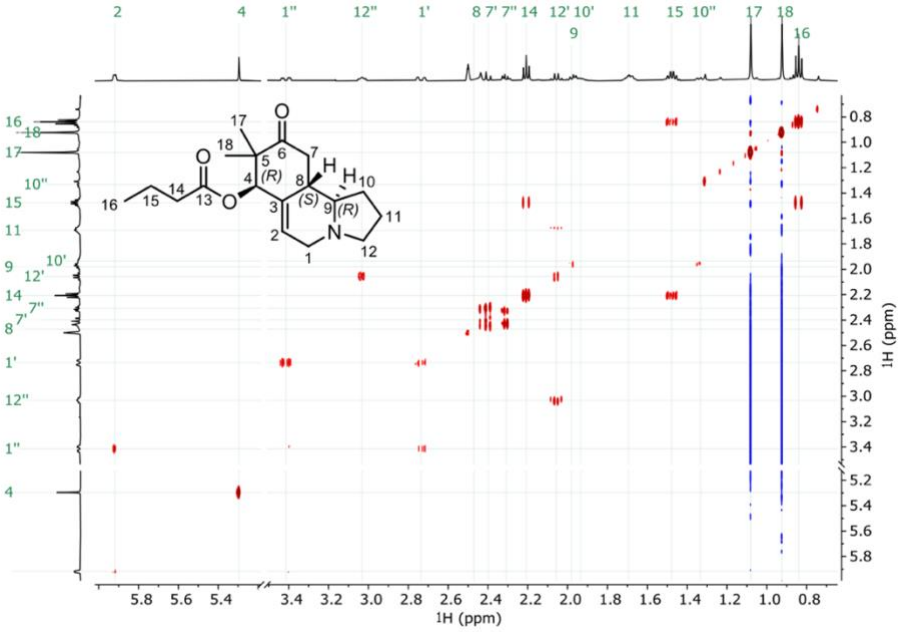

Figure 3.7.28. COSY NMR spectrum of ischnocybinone (**3.2**) (500 MHz, *d6*-DMSO).

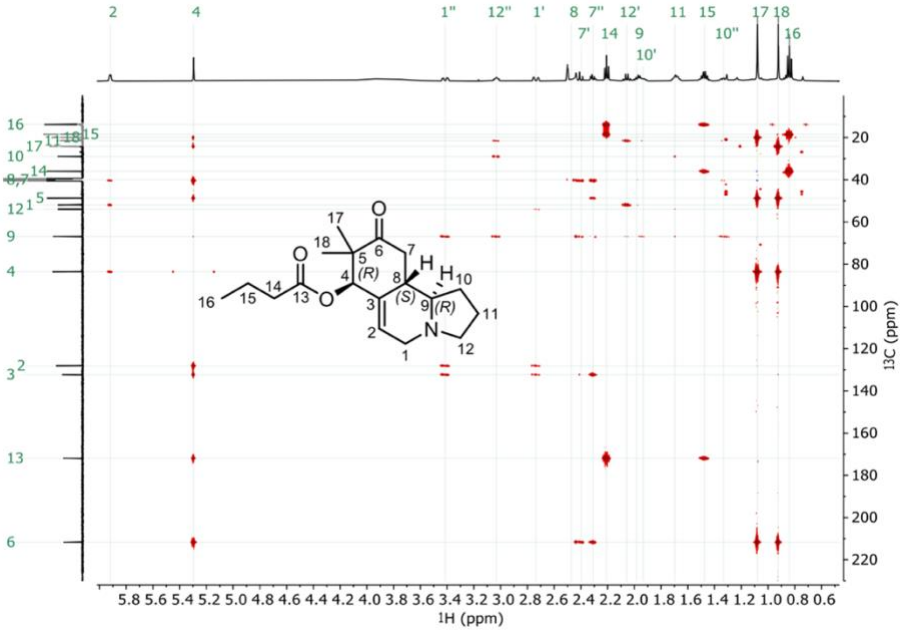

Figure 3.7.29. ^{1}H-^{13}C HMBC NMR spectrum of ischnocybinone (**3.2**) (500 MHz, *d6*-DMSO).

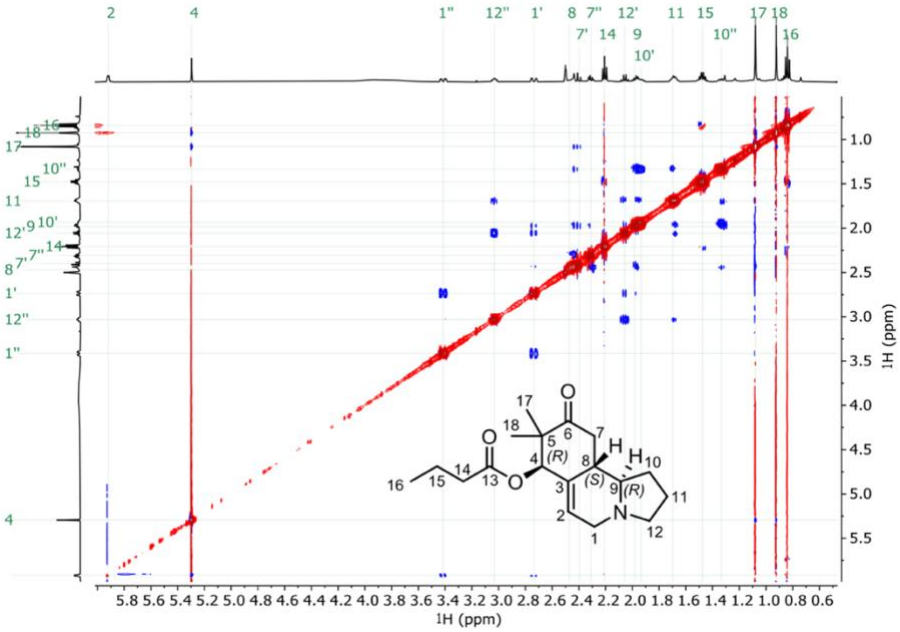

Figure 3.7.30. easyROESY NMR spectrum of ischnocybinone (**3.2**) (500 MHz, *d6*-DMSO).

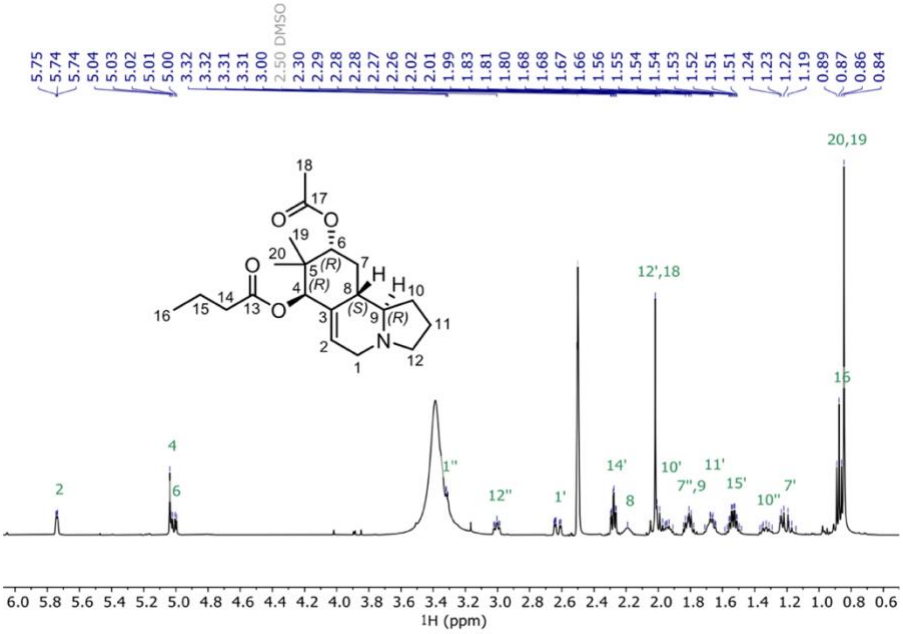

Figure 3.7.31. ^{1}H NMR spectrum of ischnocybine B (**3.3**) (500 MHz, *d6*-DMSO).

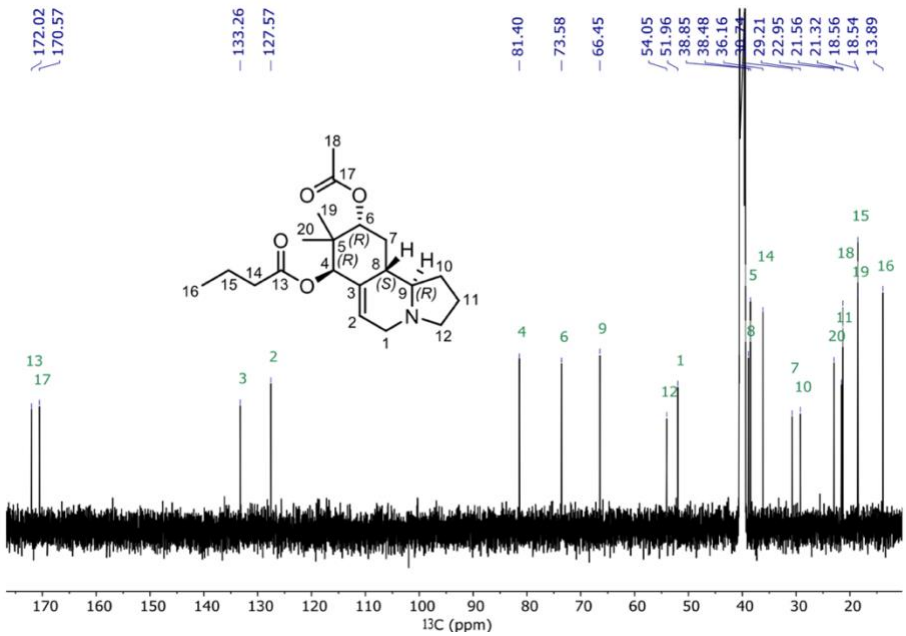

Figure 3.7.32. ^{13}C NMR spectrum of ischnocybine B (**3.3**) (500 MHz, *d6*-DMSO).

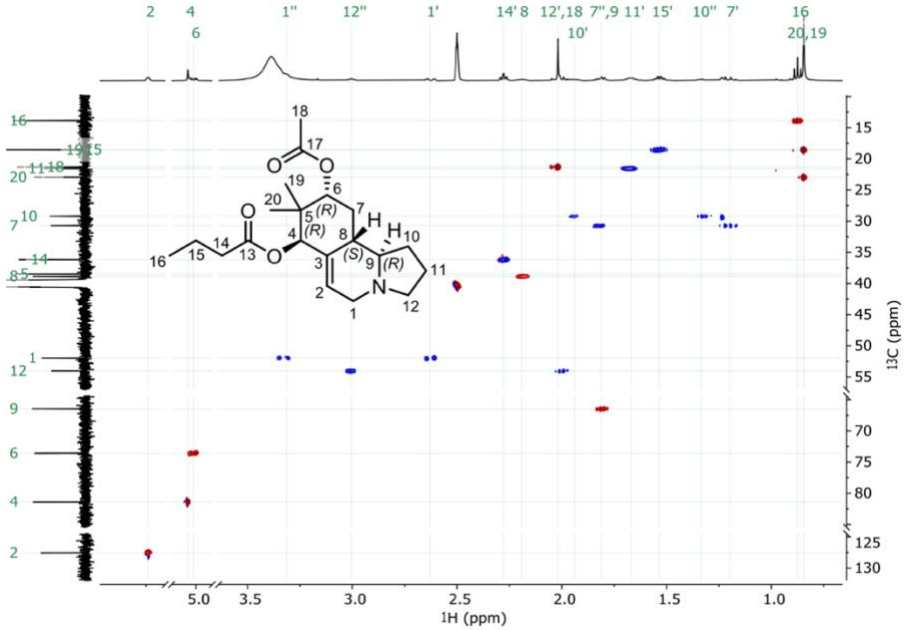

Figure 3.7.33. Multiplicity-edited ^{1}H-^{13}C HSQC NMR spectrum of ischnocybine B (**3.3**) (500 MHz, *d6*-DMSO).

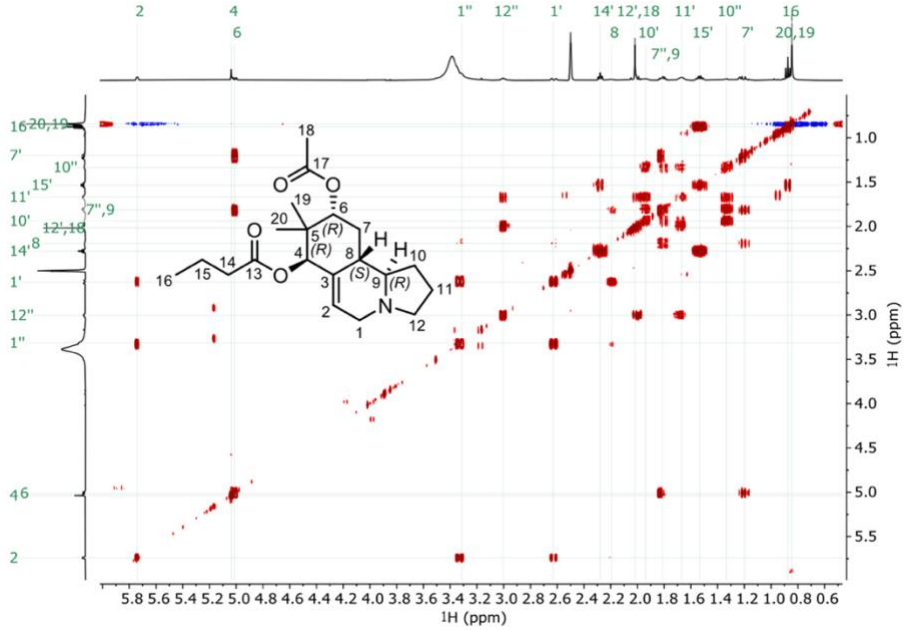

Figure 3.7.34. COSY NMR spectrum of ischnocybine B (**3.3**) (500 MHz, *d6*-DMSO).

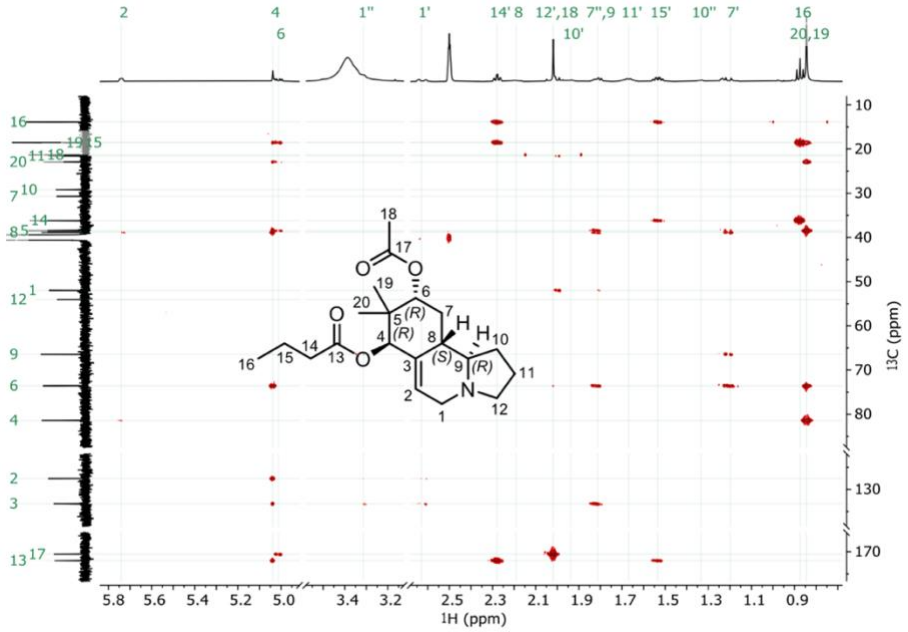

Figure 3.7.35. ^{1}H-^{13}C HMBC NMR spectrum of ischnocybine B (**3.3**) (500 MHz, *d6*-DMSO).

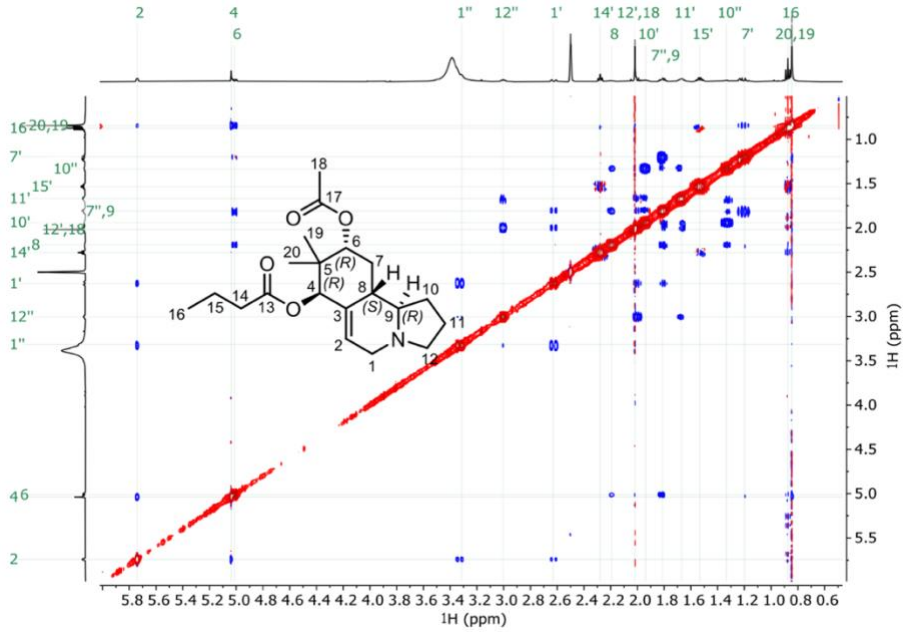

Figure 3.7.36. easyROESY NMR spectrum of ischnocybine B (**3.3**) (500 MHz, *d6*-DMSO).

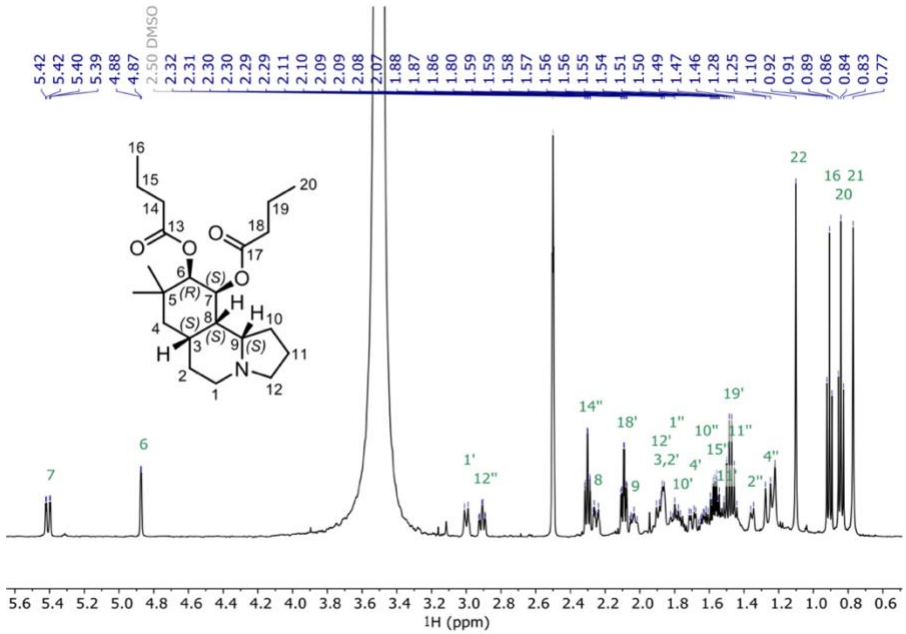

Figure 3.7.37. ^{1}H NMR spectrum of ischnocybine C (**3.4**) (500 MHz, *d6*-DMSO).

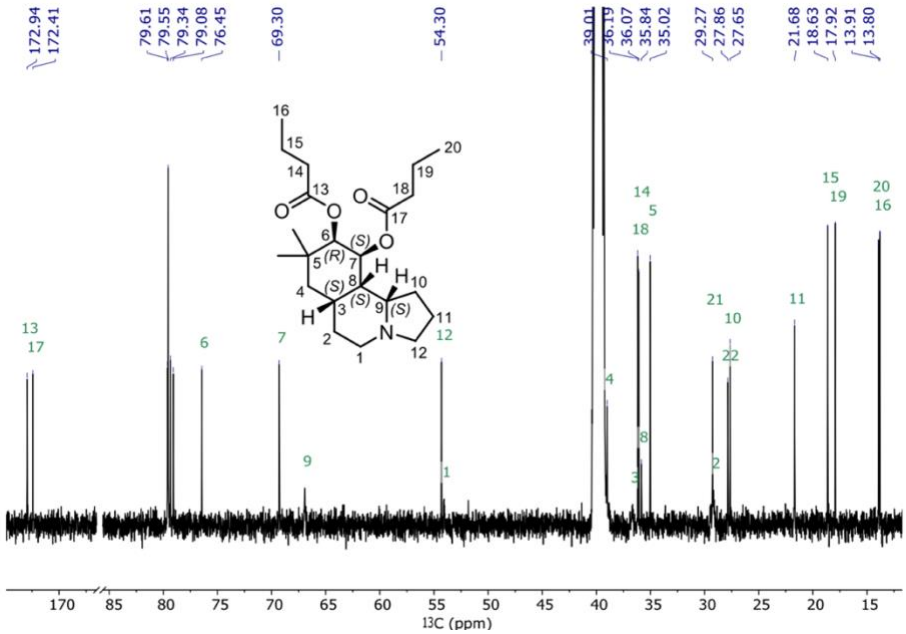

Figure 3.7.38. ^{13}C NMR spectrum of ischnocybine C (**3.4**) (500 MHz, *d6*-DMSO).

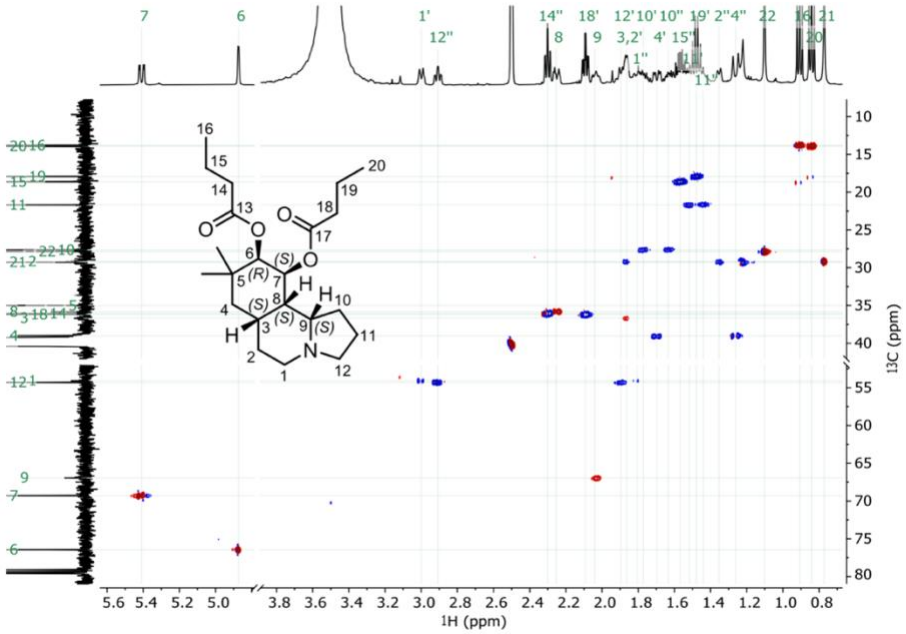

Figure 3.7.39. Multiplicity-edited ^{1}H-^{13}C HSQC NMR spectrum of ischnocybine C (**3.4**) (500 MHz, *d6*-DMSO).

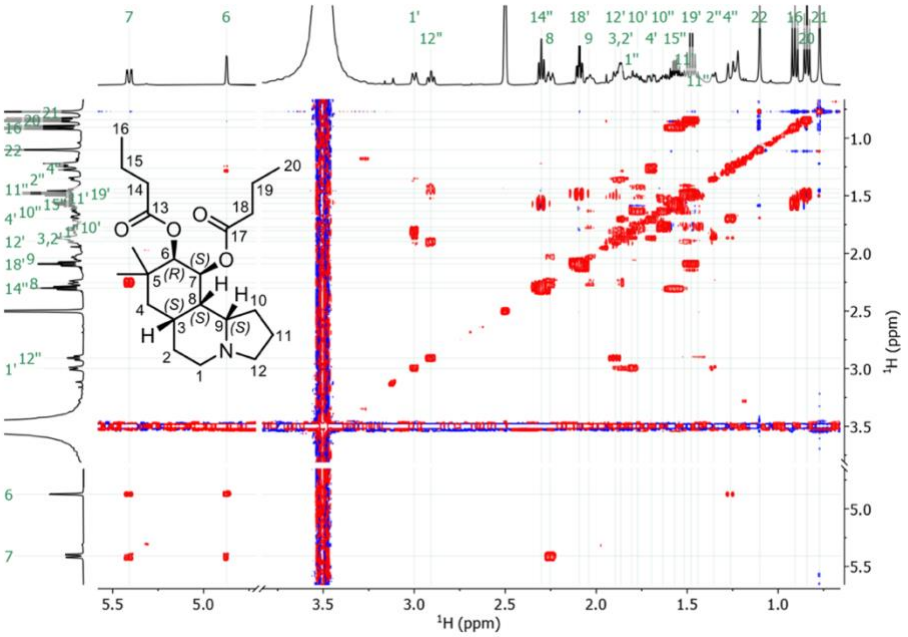

Figure 3.7.40. COSY NMR spectrum of ischnocybine C (**3.4**) (500 MHz, d_6-DMSO).

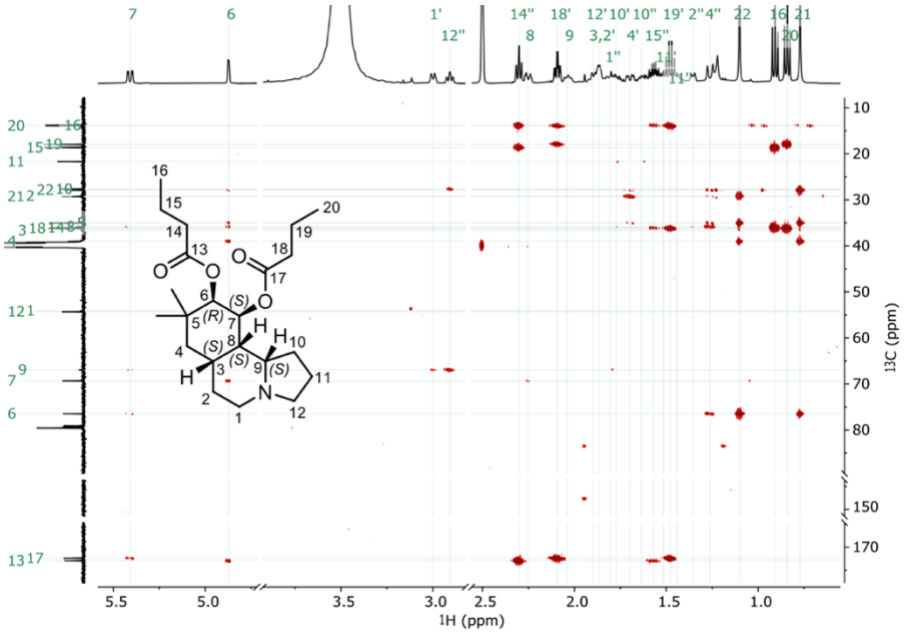

Figure 3.7.41. ^{1}H-^{13}C HMBC NMR spectrum of ischnocybine C (**3.4**) (500 MHz, d_6-DMSO).

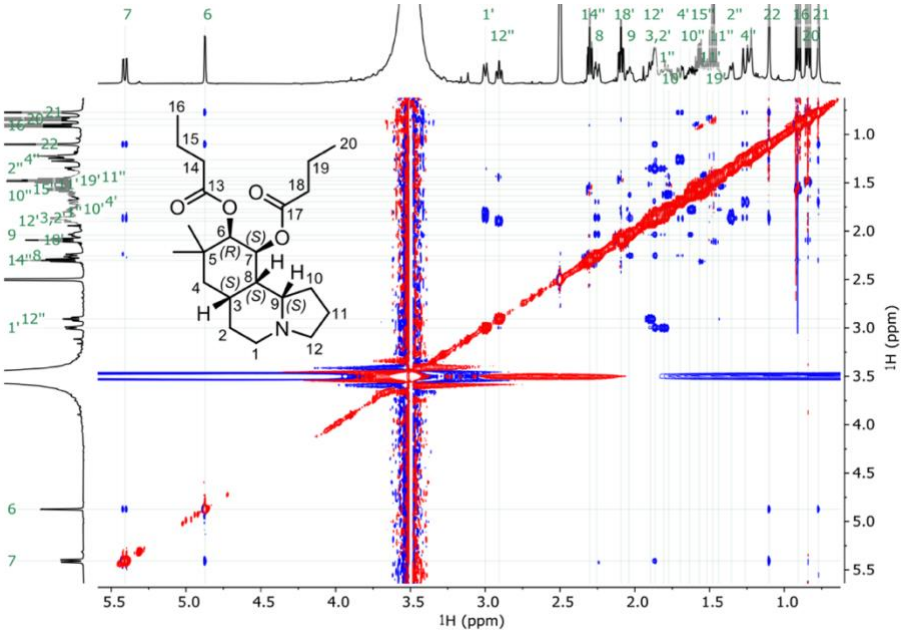

Figure 3.7.42. easyROESY NMR spectrum of ischnocybine C (**3.4**) (500 MHz, *d*$_6$-DMSO).

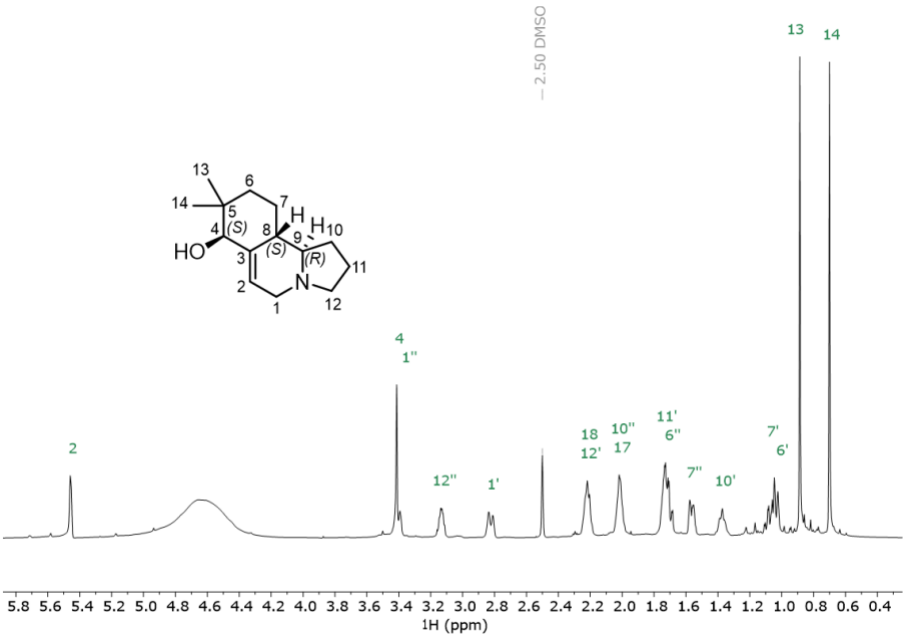

Figure 3.7.43. ^{1}H NMR spectrum of ischnocybine A alcohol (**3.6**) (600 MHz, *d*$_6$-DMSO).

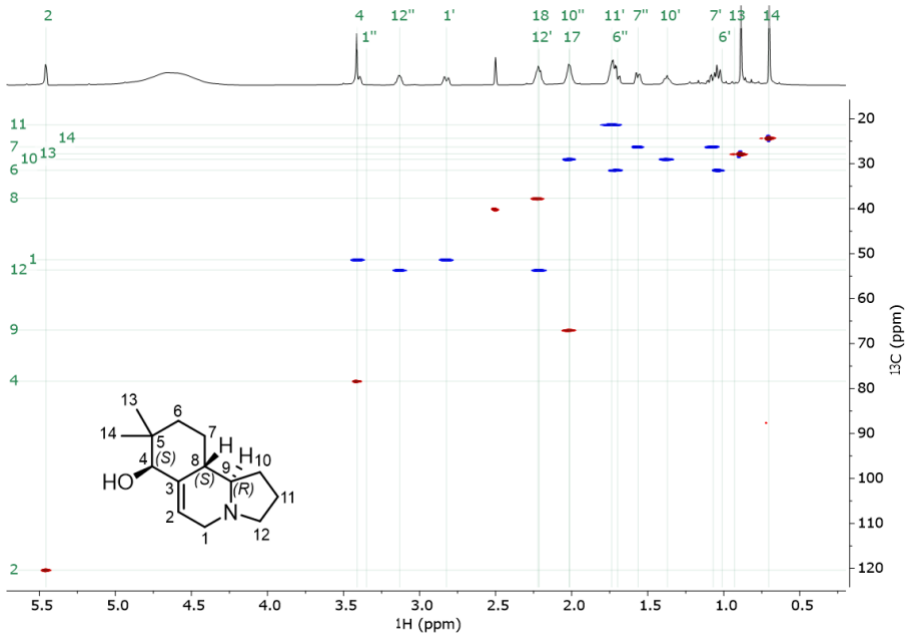

Figure 3.7.44. Multiplicity-edited ^{1}H-^{13}C HSQC NMR spectrum of ischnocybine A alcohol (**3.6**) (600 MHz, *d*$_6$-DMSO).

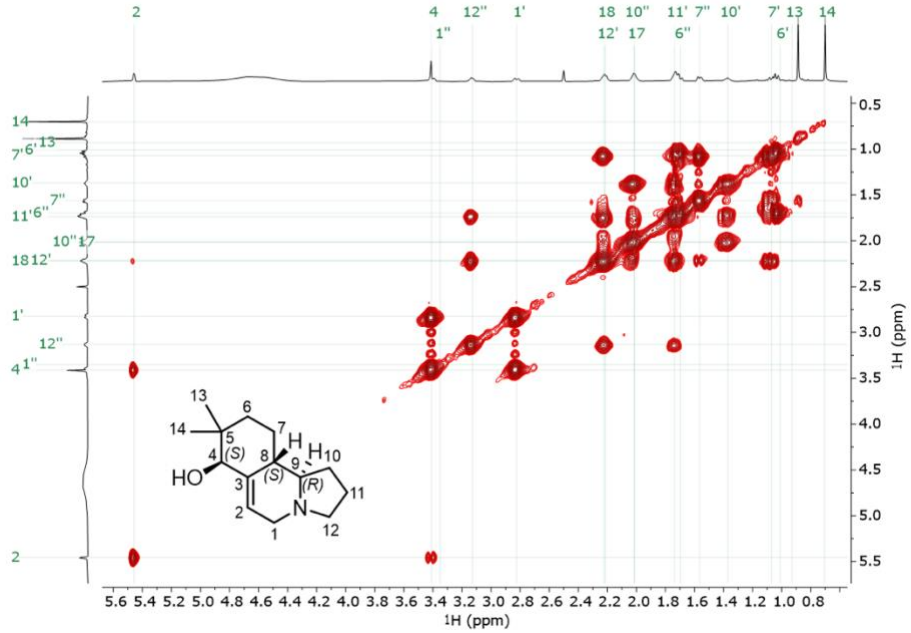

Figure 3.7.45. dqfCOSY NMR spectrum of ischnocybine A alcohol (**3.6**) (600 MHz, *d*$_6$-DMSO).

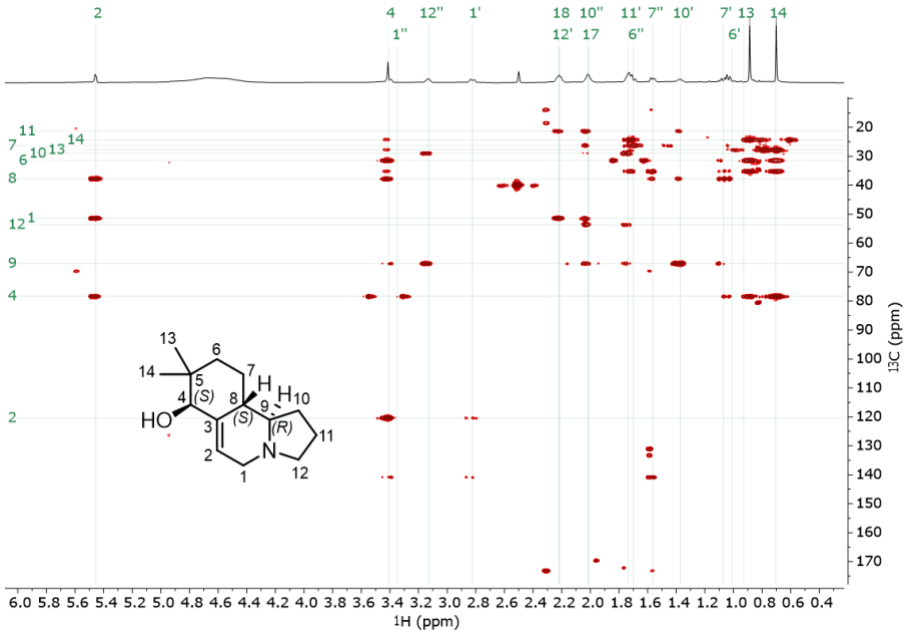

Figure 3.7.46. ^{1}H-^{13}C HMBC NMR spectrum of ischnocybine A alcohol (**3.6**) (600 MHz, *d*$_6$-DMSO).

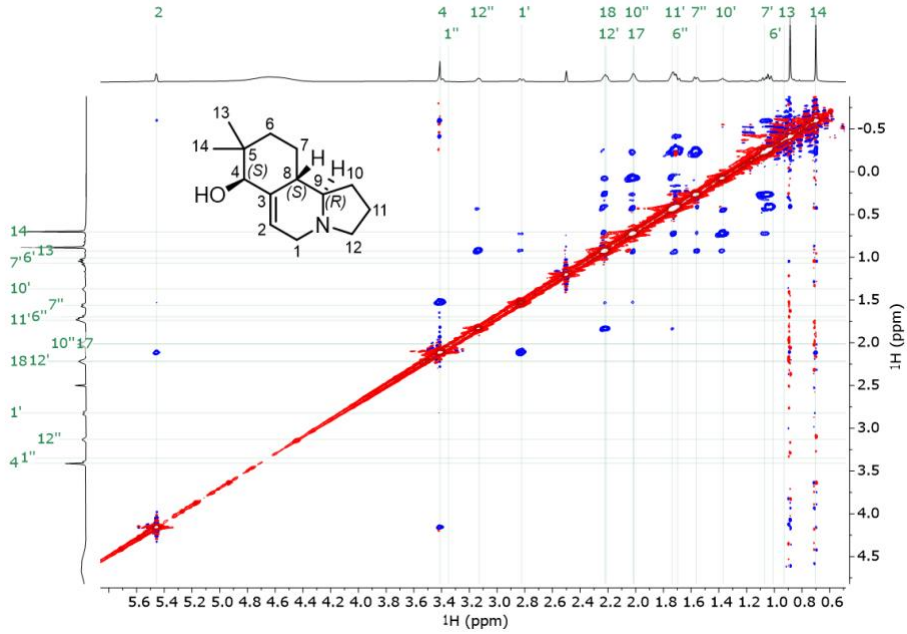

Figure 3.7.47. easyROESY NMR spectrum of ischnocybine A alcohol (**3.6**) (600 MHz, *d*$_6$-DMSO).

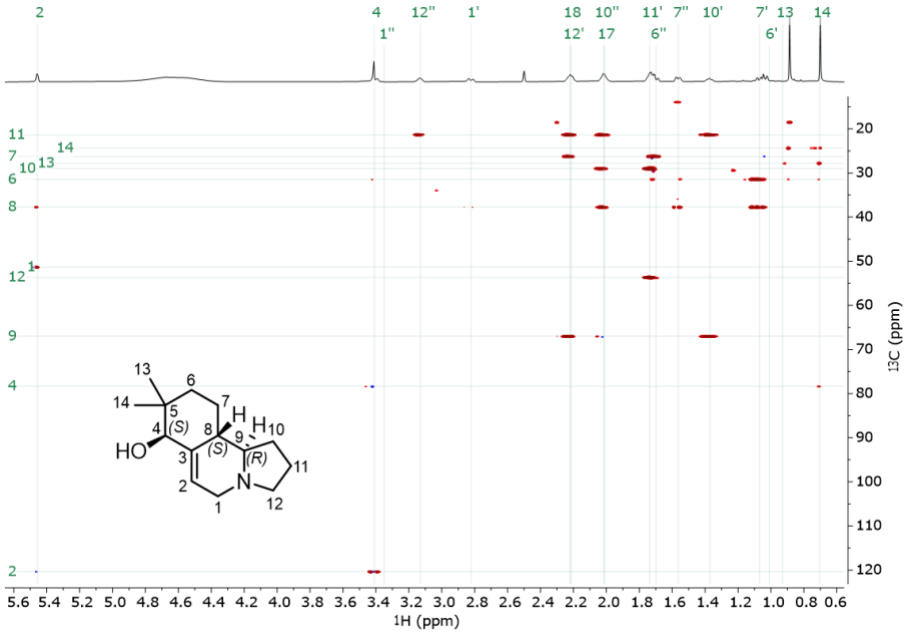

Figure 3.7.48. H2BC NMR spectrum of ischnocybine A alcohol (**3.6**) (600 MHz, *d*6-DMSO).

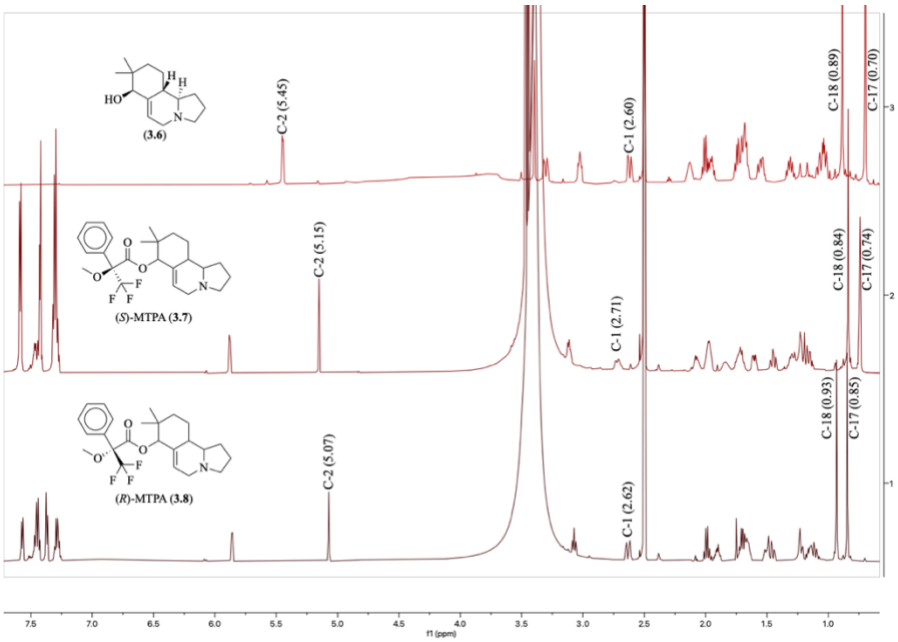

Figure 3.7.49. Mosher's analysis of ischnocybine A (**3.1**)

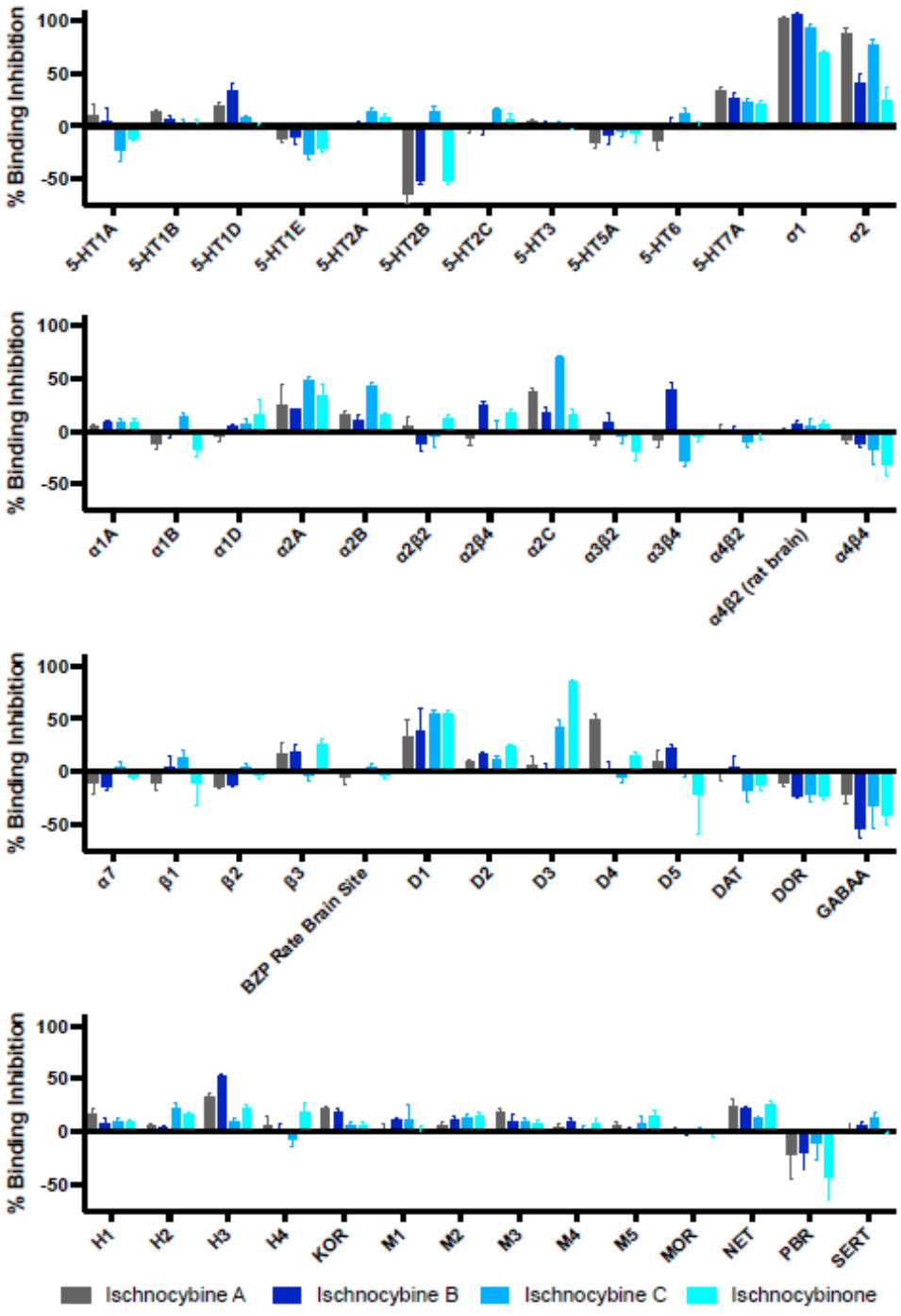

Figure 3.7.50. All preliminary PDSP data graphed. Bars represent the mean and error bars represent standard error.

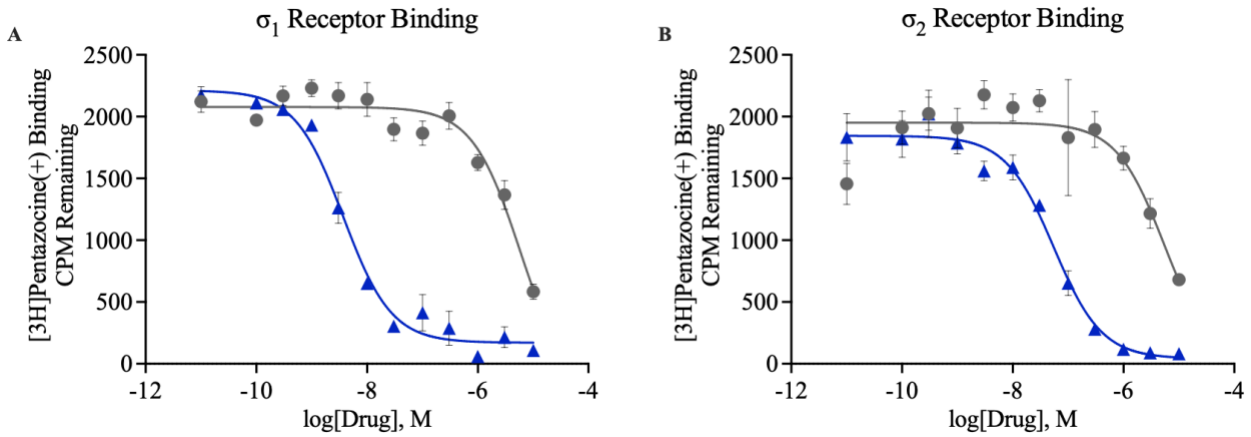

Figure 3.7.51. Sigma-1 and Sigma-2 binding curves for Compound **3.6.** Competitive binding curves for **3.6**, against the radioactive σ_1R ligand, [3H]-(+)-pentazocine. Competitive binding curves for **3.6**, against the radioactive σ_2R ligand, [3H]-(+)pentazocine. Positive control was haloperidol for both σ_1R and σ_2R (triangles).

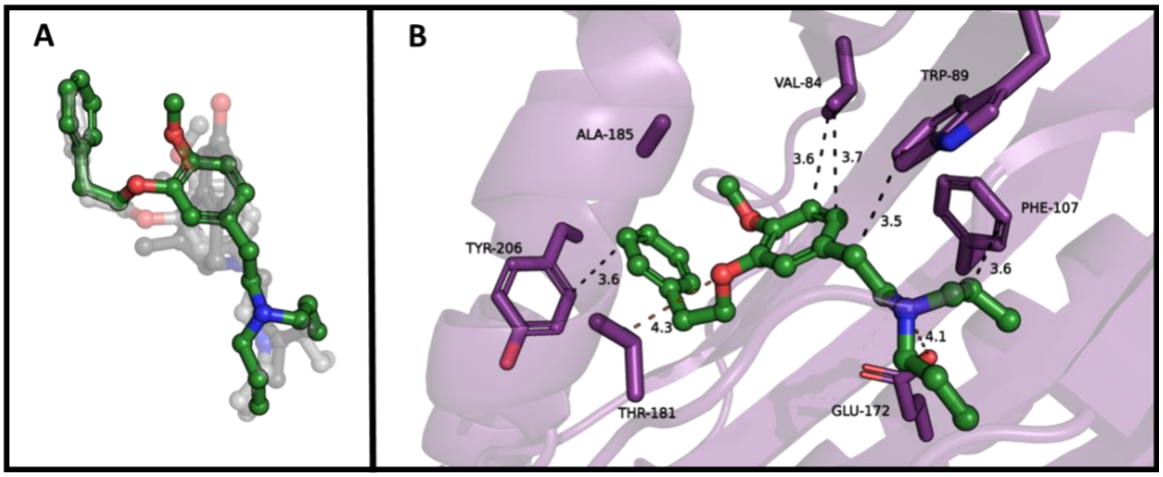

Figure 3.7.52. NE-100 docked into the agonist σ_1R. NE-100 docked into the agonist σ_1R (PDB ID: 6DK1). NE-100 binding, shown as green sticks (colored by element), is coordinated by Tyr-206 in the left quadrant of the binding pocket. (A) Overlay of the NE-100 docked pose (green) with the agonist (light grey) and antagonist (dark grey) binding positions from co-crystal structures. (B) Interactions between residues in the σ_1R (purple, colored by element) binding cavity and NE-100 (green, colored by element).

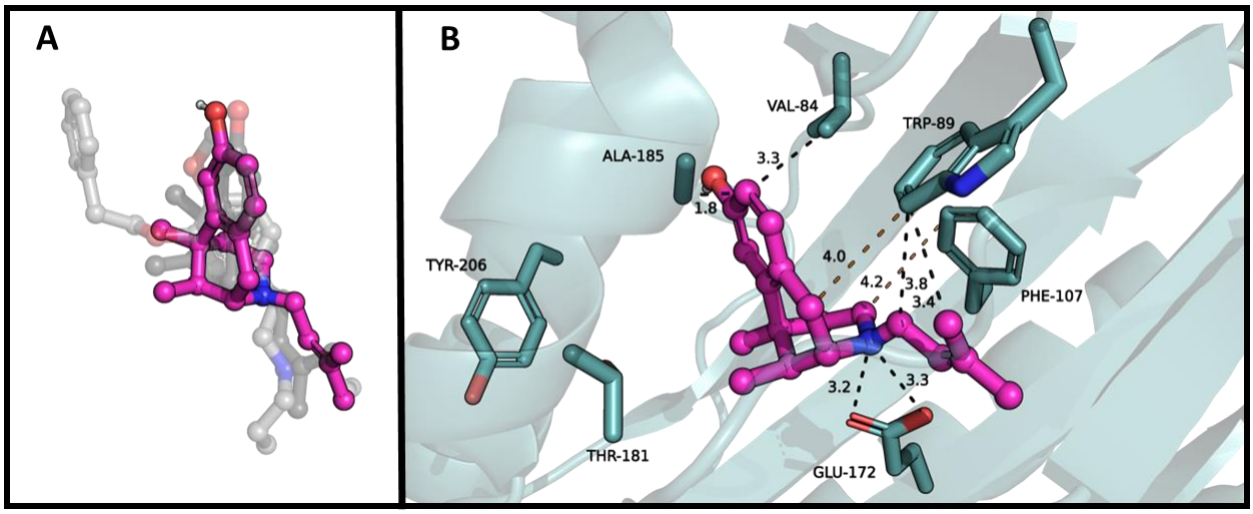

Figure 3.7.53. Pentazocine docked into the antagonist σ_1R. Pentazocine docked into the antagonist σ_1R (PDB ID: 6DK0). Pentazocine binding, shown as pink sticks (colored by element), is coordinated through hydrophobic interactions with Ala-185 and Val-84 in the top of the binding pocket. (A) Overlay of pentacozine (pink) with the agonist (light grey) and antagonist (dark grey) binding positions from co-crystal structures. (B) Interactions between residues in the σ_1R (teal, colored by element) binding cavity and pentazocine (pink, colored by element).

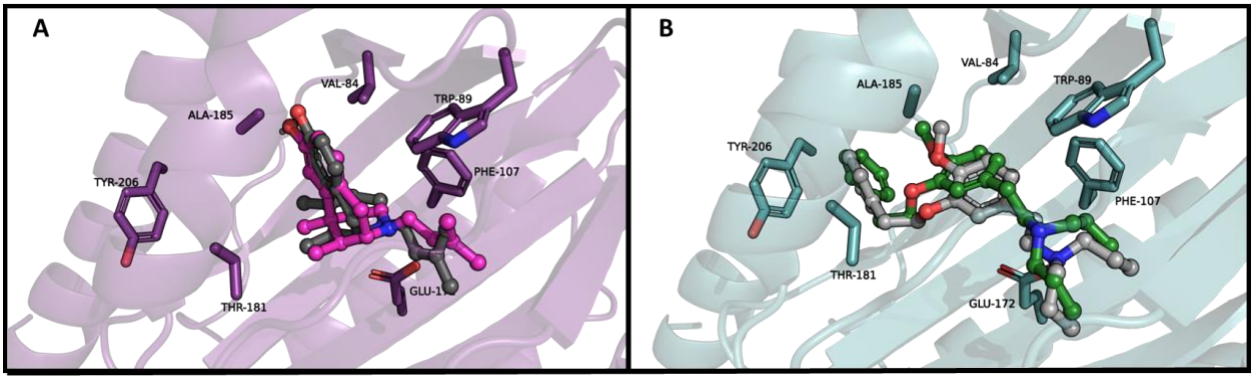

Figure 3.7.54. Redocking of pentazocine and NE-100 into agonist and antagonist σ_1R structures. Redocking of pentazocine and NE-100 into agonist (PDB ID: 6DK1) and antagonist (PDB ID: 6DK0) σ_1R structures. (A) Pentazocine, shown as pink sticks and colored by element, re-docked into agonist structure, shown in purple cartoon, (PDB ID: 6DK1) with an RMSD value of 0.74 Å. (B) NE-100, shown as green sticks and colored by element, re-docked into antagonist structure, shown in teal cartoon, (PDB ID: 6DK0) with an RMSD value of 1.25 Å. Crystal structure ligand positioning is shown as grey sticks in both.

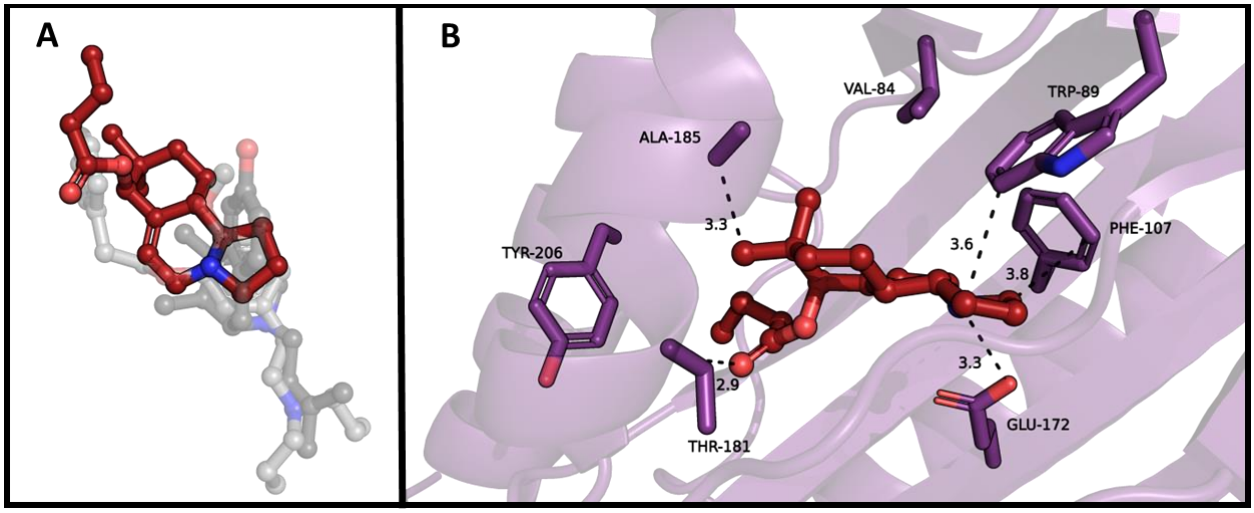

Figure 3.7.55. Ischnocybine A-SSR (**3.1**) docked into the agonist σ_1R. Ischnocybine A-SSR (**3.1**) docked into the agonist σ_1R (PDB ID: 6DK1). Ischnocybine A-SSR, shown as red sticks (colored by element), mimics binding coordination of A-RRS with Glu-172, Phe-107, Trp-89, and Ala-185 interactions. (A) Overlay of ischnocybine A-SSR (red) with the agonist (light grey) and antagonist binding positions (dark grey) binding positions from co-crystal structures. (B) Interactions between residues in the σ_1R (purple, colored by element) binding cavity and ischnocybine A-SSR (red, colored by element).

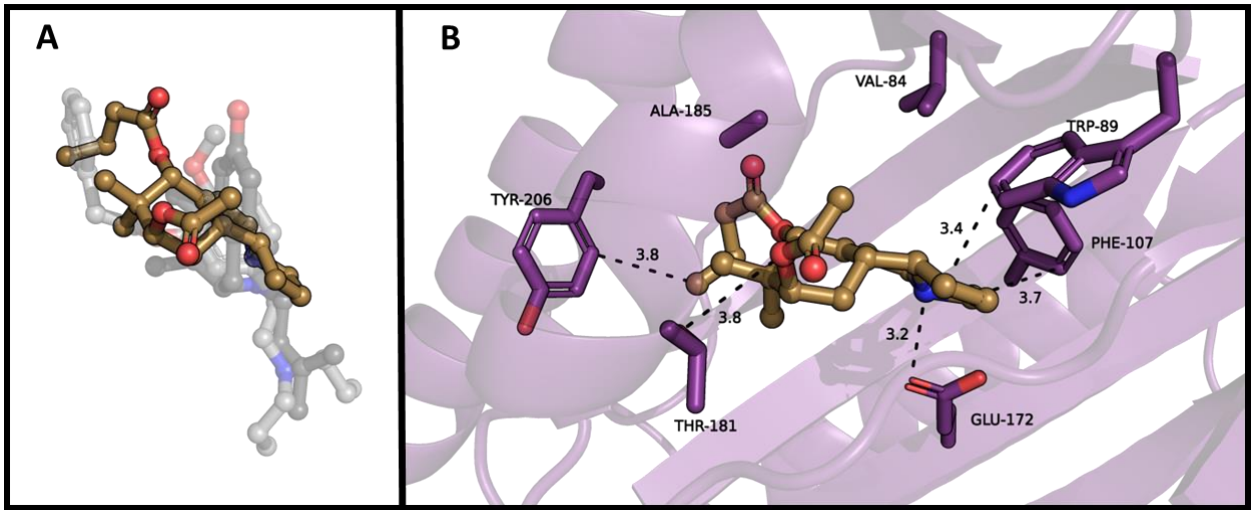

Figure 3.7.56. Ischnocybine B-RRSR (**3.3**) docked into the agonist σ_1R. Ischnocybine B-RRSR (**3.3**) docked into the agonist σ_1R (PDB ID: 6DK1). Ischnocybine B-RRSR, shown as tan sticks (colored by element), is coordinated by Tyr-206 in the left quadrant of the binding pocket. (A) Overlay of ischnocybine B-RRSR (tan) with the agonist (light grey) and antagonist (dark grey) binding positions from co-crystal structures. (B) Interactions between residues in the σ_1R (purple, colored by element) binding cavity and ischnocybine B-RRSR (tan, colored by element).

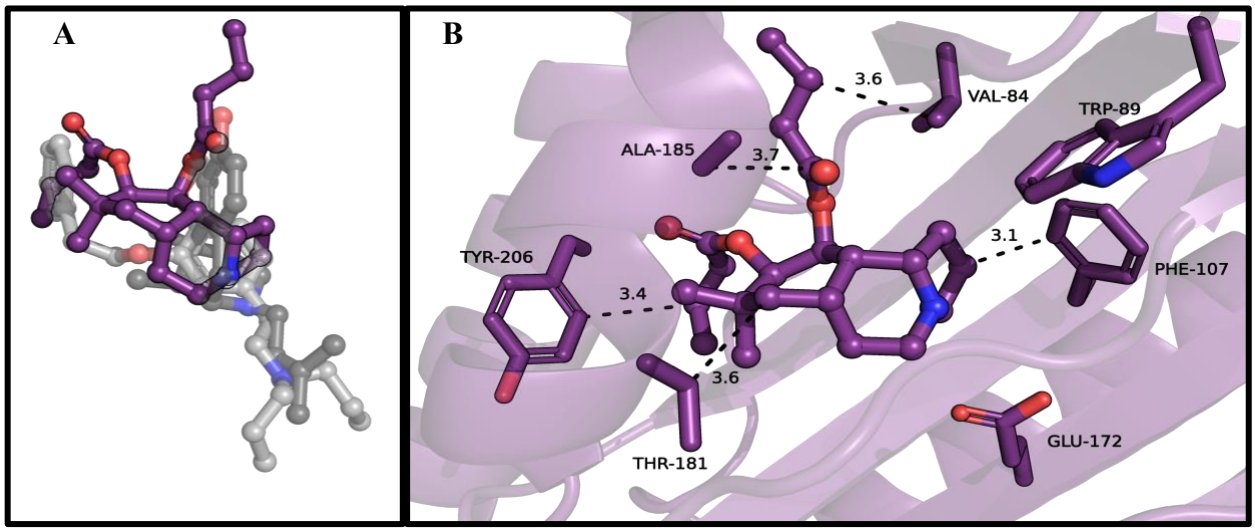

Figure 3.7.57. Ischnocybine C-SRSSS (**3.4**) docked into the agonist σ_1R. Ischnocybine C-SRSSS (**3.4**) docked into the agonist σ_1R (PDB ID: 6DK1). Ischnocybine C-SRRSS, shown as purple sticks (colored by elements), is coordinated distally by Tyr-206 in the left quadrant of the binding pocket. (A) Overlay of ischnocybine C-SRSSS (purple) with the agonist (light grey) and antagonist (dark grey) binding positions from co-crystal structures. (B) Interactions between residues in the σ_1R (purple, colored by element) binding cavity and ischnocybine C-SRSSS (purple, colored by element).

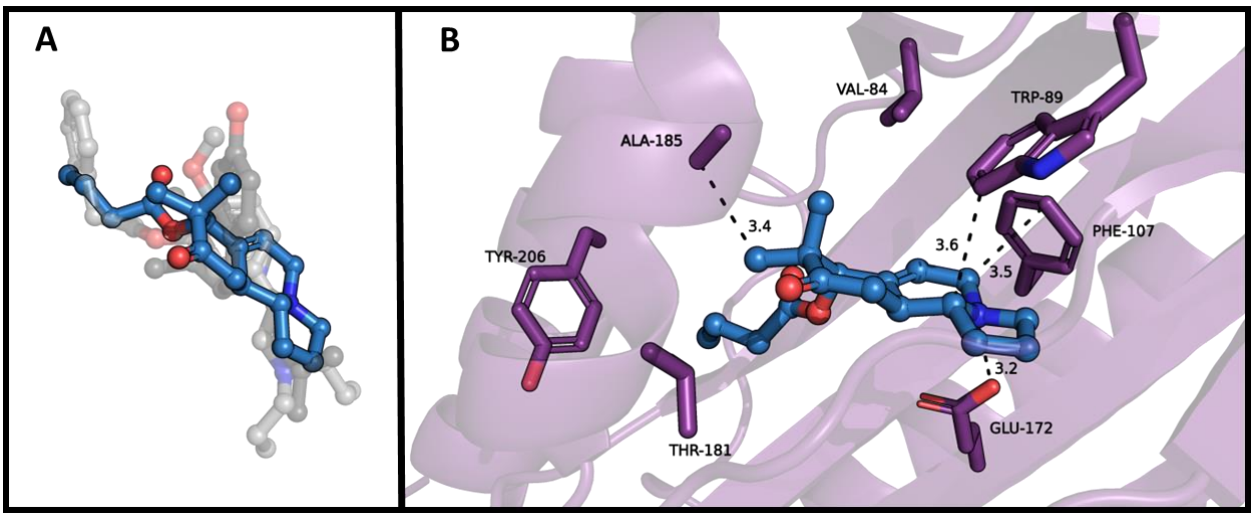

Figure 3.7.58. Ischnocybinone-RSR (**3.2**) docked into the agonist σ_1R. Ischnocybinone-RSR (**3.2**) docked into the agonist σ_1R (PDB ID: 6DK1). Ischnocybinone-RSR, shown as blue sticks (colored by element), does not interact with Tyr-206 A) Overlay of isc ischnocybinone-RSR (blue) with the agonist (light grey) and antagonist (dark grey) binding positions from co-crystal structures. (B) Interactions between residues in the σ_1R (purple, colored by element) binding cavity and ischnocybinone-RSR (blue, colored by element

3.8. Appendix Tables

Table 3.8.8. NMR Spectroscopy Data for Ischnocybine A (**3.1**) (500 MHz, d_6-DMSO)

Atom Number	δ_C, type	δ_H, (*J* in Hz)	HMBC Correlations
1a	52.1, CH_2	3.30, ddd (16.3, 5.0, 2.3)	C2, C3, C9, C12
1b		2.59, ddd (16.3, 4.4, 1.7)	
2	126.3, CH	5.65, dd (4.4, 2.3)	C1, C4, C8
3	135.4, C		
4	80.1, CH	4.88, d (1.4)	C2, C3, C5, C6, C8, C13, C17, C18
5	34.5, C		
6a	32.4, CH_2	1.65, m	C5, C7, C8, C17, C18
6b		1.19, m	
7a	25.8, CH_2	1.65, m	C3, C5, C6, C8
7b		1.14, m	
8	39.4, CH	1.97, m	
9	67.0, CH	1.73, td (9.0, 6.8)	C1
10a	29.4, CH_2	1.97, m	C8, C9, C11, C12
10b		1.32, m	
11	21.6, CH_2	1.65, m	C10
12a	54.2, CH_2	3.00, m	C1, C9, C10, C11
12b		1.97, m	
13	172.2, C		
14	36.3, CH_2	2.24, td (7.3, 1.3)	C13, C15, C16
15	18.6, CH_2	1.53, qd (7.3, 2.8)	
16	13.9, CH_3	0.87, t (7.3)	C14, C15
17 (ax)	23.8, CH_3	0.81, s	C4, C5, C6, C18
18 (eq)	27.2, CH_3	0.84, s	C4, C5, C6, C17

Table 3.8.9. NMR Spectroscopy Data for Ischnocybinone (**3.2**) (500 MHz, d_6-DMSO)

Atom Number	δ_C, type	δ_H, (*J* in Hz)	HMBC Correlations
1a	51.9, CH_2	3.41, ddd (16.8, 4.9, 2.1)	C2, C3, C9, C12
1b		2.74, ddd (16.8, 4.0, 1.7)	
2	128.1, CH	5.92, dd (4.9, 2.1)	C1, C4, C8
3	132.3, C		
4	83.6, CH	5.30, s	C2, C3, C5, C6, C8, C17, C18
5	48.7, C		
6	211.7, C		
7a	40.1, CH_2	2.40, d (11.4)	C3, C5, C6, C8, C9
7b		2.31, m	
8	40.3, CH	2.47, m	
9	66.9, CH	1.98, m	C1
10a	29.0, CH_2	1.93, m	C9, C11, C12
10b		1.33, m	
11	21.5, CH_2	1.69, m	C9, C10, C12
12a	53.9, CH_2	3.03, ddd (8.8, 6.7, 3.6)	C1, C9, C10, C11
12b		2.06, q (8.8)	
13	171.9, C		
14	36.0, CH_2	2.21, t (7.4)	C13, C15, C16
15	18.4, CH_2	1.48, dtd (14.8, 7.4, 5.9)	C13, C14, C16
16	13.8, CH_3	0.84, t (7.4)	C14, C15
17 (ax)	24.2, CH_3	1.08, s	C4, C5, C6, C18
18 (eq)	20.0, CH_3	0.92, s	C4, C5, C6, C17

Table 3.8.10. NMR Spectroscopy Data for Ischnocybine B (**3.3**) (500 MHz, *d*$_6$-DMSO)

Atom Number	δ_C, type	δ_H, (*J* in Hz)	HMBC Correlations
1a	52.0, CH_2	3.31, m	C2, C3, C9
1b		2.63, m	
2	127.6, CH	5.74, m	C4, C8
3	133.3, C		
4	81.4, CH	5.04, s	C2, C3, C5, C6, C8, C13, C20
5	38.5, C		
6	73.6, CH	5.01, dd (12.1, 4.9)	C5, C17, C20
7a	30.7, CH_2	1.81, m	C3, C5, C6, C8, C9
7b		1.20, m	
8	38.9, CH	2.19, m	
9	66.5, CH	1.81, m	C1
10a	29.2, CH_2	1.94, m	
10b		1.33, m	
11	21.6, CH_2	1.67, m	
12a	54.1, CH_2	3.00, m	C1, C11
12b		2.12, m	
13	172.0, C		
14	36.2, CH_2	2.28, td (7.4, 2.1)	C13, C15, C16
15	18.6, CH_2	1.53, m	C13, C14, C16
16	13.9, CH_3	0.87, t (7.4)	C14, C15
17	170.6, C		
18	21.3, CH_3	2.02, s	C17
19 (ax)	18.6, CH_3	0.84, s	C4, C5, C6, C20
20 (eq)	23.0, CH_3	0.84, s	C4, C5, C6, C19

Table 3.8.11. NMR Spectroscopy Data for Ischnocybine C (**3.4**) (500 MHz, d_6-DMSO)

Atom Number	δ_C, type	δ_H, (*J* in Hz)	HMBC Correlations
1a	54.1, CH_2	3.00, m	C9
1b		1.81, m	
2a	29.3, CH_2	1.86, m	C8
2b		1.35, m	
3	36.7, CH	1.86, m	
4a	39.0, CH_2	1.70, dd (14.2, 4.9)	C5, C6, C8, C21, C22
4b		1.26, d (14.2)	
5	35.0, C		
6	76.5, CH	4.87, d (2.7)	C4, C5, C7, C8, C13, C21
7	69.3, CH	5.41, dd (11.6, 2.7)	C6, C8, C9, C17
8	35.8, CH	2.25, m	C7
9	66.9, CH	2.04, m	
10a	27.7, CH_2	1.77, m	C9, C11
10b		1.63, ddd (13.7, 9.2, 5.3)	
11a	21.7, CH_2	1.52, m	
11b		1.44, m	
12a	54.3, CH_2	2.91, td (8.5, 2.5)	C9, C10
12b		1.90, d (8.5)	
13	172.9, C		
14	36.1, CH_2	2.30, td (7.3, 1.5)	C13, C15, C16
15	18.6, CH_2	1.57, qd (7.3, 3.6)	C13, C14, C16
16	13.8, CH_3	0.91, t (7.3)	C14, C15
17	172.4, C		
18	36.2, CH_2	2.09, td (7.4, 2.6)	C17, C19, C20
19	17.9, CH_2	1.48, q (7.4)	C17, C18, C20
20	13.9, CH_3	0.84, t (7.4)	C18, C19
21 (ax)	29.3, CH_3	0.77, s	C4, C5, C6, C22
22 (eq)	27.9, CH_3	1.10, s	C4, C5, C6, C21

Table 3.8.12. ^{13}C NMR Chemical Shifts Predictions for Ischnocybine A (**3.1**)

Gaussian Numbering[a]	Experimental	srr	srs	ssr	sss
1	34.0	38.0	36.6	35.1	36.8
2	80.1	81.8	79.9	81.7	83.2
3	135.4	139.5	137.7	137.1	139.1
4	39.4	41.4	43.8	40.4	37.0
5	25.8	24.0	26.2	25.8	23.8
6	32.4	38.1	37.0	32.8	34.4
7	27.2	29.1	28.9	28.0	27.9
8	23.8	20.3	20.2	24.4	25.1
9	126.3	117.4	118.5	128.4	125.1
10	52.1	51.2	51.0	50.9	51.3
12	67.0	62.4	66.3	66.1	62.5
13	54.2	54.5	54.3	54.4	54.4
14	21.6	23.6	22.9	22.8	23.7
15	29.4	24.7	29.7	29.6	24.5
17	172.2	169.4	169.5	169.1	169.3
RMSD		3.9	3.1	1.3	2.7
MAE		3.3	2.3	1.1	2.3

[a]*Note the Gaussian atom numberings do not match the experimental literature numberings. Experimental chemical shifts have been reordered accordingly. Configurations are presented in the form "rrs" corresponding to numerical order of the literature numbering for stereopositions. Example, ischnocybine A's "ssr" corresponds to the literature assignment "4S,8S,9R."*

Table 3.8.13. ^{1}H NMR Chemical Shifts Predictions for Ischnocybine A (**3.1**)

Gaussian Numbering[a]	**Experimental**	**srr**	**srs**	**ssr**	**sss**
20	1.97	1.99	1.96	2.04	2.21
21	1.73	2.45	2.02	1.99	2.40
22	4.88	4.96	5.18	4.94	4.82
23 (24)	1.65	1.52	1.47	1.52	1.56
24 (23)	1.14	1.36	1.12	1.15	1.40
25 (26)	1.65	1.46	1.43	1.69	1.68
26 (25)	1.19	1.37	1.40	1.21	1.28
27,28,29	0.84	0.89	0.86	0.86	0.90
30,31,32	0.81	0.79	0.80	0.76	0.78
33	5.65	5.33	5.37	5.73	5.63
34 (35)	3.30	3.19	3.15	3.18	3.18
35 (34)	2.59	2.76	2.79	2.80	2.79
36 (37)	3.00	2.80	2.81	2.82	2.79
37 (36)	1.97	2.14	2.14	2.14	2.13
38 (39)	1.65	1.60	1.66	1.65	1.59
39 (38)	1.65	1.57	1.60	1.60	1.57
40 (41)	1.97	1.65	1.83	1.83	1.66
41 (40)	1.32	1.58	1.35	1.34	1.56
RMSD		0.24	0.17	0.12	0.22
MAE		0.18	0.14	0.09	0.16

[a]*Note the Gaussian atom numberings do not match the experimental literature numberings. Experimental chemical shifts have been reordered accordingly. Configurations are presented in the form "rrs" corresponding to numerical order of the literature numbering for stereopositions. Example, ischnocybine A's "ssr" corresponds to the literature assignment "4S,8S,9R."*

Table 3.8.14. ^{13}C NMR Chemical Shifts Predictions for Ischnocybinone (**3.2**)

Gaussian Numbering[a]	Experimental	rrr	rrs	rsr	srr
1	48.7	53.0	51.3	49.6	51.2
2	83.6	78.8	77.3	84.9	84.0
3	132.3	136.7	134.5	133.5	136.1
4	40.3	36.9	40.6	41.5	36.9
5	40.1	39.9	40.7	40.1	39.5
6	211.7	215.3	214.7	216.0	217.0
7	24.2	22.3	22.3	24.7	25.5
8	20.0	21.2	21.5	21.8	21.8
9	128.1	121.1	123.0	130.8	128.6
10	51.9	50.8	50.8	50.6	51.0
12	66.9	61.6	66.2	66.0	62.0
13	53.9	53.9	54.2	54.1	53.9
14	21.5	23.9	22.8	22.7	23.9
15	29.0	24.7	29.3	29.2	24.5
17	171.9	169.2	169.1	168.6	168.8
RMSD		3.7	2.6	1.8	2.9
MAE		3.1	2.0	1.4	2.4

[a]*Note the Gaussian atom numberings do not match the experimental literature numberings. Experimental chemical shifts have been reordered accordingly. Configurations are presented in the form "rrs" corresponding to numerical order of the literature numbering for stereopositions. Example, ischnocybine A's "ssr" corresponds to the literature assignment "4S,8S,9R."*

Table 3.8.15. ^{1}H NMR Chemical Shift Predictions for Ischnocybinone (**3.2**)

Gaussian Numbering[a]	Experimental	rrr	rrs	rsr	srr
20	2.47	2.21	2.24	2.50	2.62
21	1.98	2.65	2.19	2.23	2.56
23	5.30	5.11	5.35	5.31	5.15
24 (25)	2.40	2.72	2.36	2.34	2.69
25 (24)	2.31	2.33	2.26	2.26	2.34
26,27,28	1.08	1.05	1.09	1.08	1.04
29,30,31	0.92	1.04	1.00	1.00	1.03
32	5.92	5.68	5.75	5.97	5.95
33 (34)	3.41	3.32	3.28	3.29	3.34
34 (33)	2.74	2.93	2.93	2.96	2.94
35 (36)	3.03	2.84	2.85	2.85	2.85
36 (35)	2.06	2.25	2.22	2.24	2.23
37 (38)	1.69	1.61	1.69	1.67	1.62
38 (37)	1.69	1.58	1.63	1.62	1.60
39 (40)	1.93	1.64	1.84	1.84	1.61
40 (39)	1.33	1.55	1.36	1.34	1.55
RMSD		0.25	0.13	0.12	0.22
MAE		0.20	0.11	0.09	0.17

[a]*Note the Gaussian atom numberings do not match the experimental literature numberings. Experimental chemical shifts have been reordered accordingly. Configurations are presented in the form "rrs" corresponding to numerical order of the literature numbering for stereopositions. Example, ischnocybine A's "ssr" corresponds to the literature assignment "4S,8S,9R."*

Table 3.8.16. ^{13}C NMR Chemical Shifts Predictions for Ischnocybine B (**3.3**)

Gaussian Numbering[a]	**Experimental**	**rrrr**	**rrrs**	**rrsr**	**rsrr**	**rsrs**	**rssr**	**srrr**	**ssrr**
1	38.5	41.8	40.3	39.4	42.4	41.1	38.2	40.3	40.7
2	81.4	78.2	76.1	82.6	79.4	78.3	79.8	81.8	83.0
3	133.3	138.6	136.6	134.8	137.5	134.1	135.9	138.1	137.0
4	38.9	36.4	39.6	39.6	37.0	30.2	36.7	32.9	35.5
5	30.7	28.2	29.7	30.4	28.1	31.3	30.6	29.2	27.9
6	73.6	79.5	78.8	74.4	78.2	77.4	76.1	76.9	77.1
7	18.6	24.3	24.2	19.6	25.6	25.2	25.3	23.4	24.5
8	23.0	20.2	20.6	24.2	15.9	16.1	23.7	25.6	20.4
9	127.6	118.6	119.4	129.9	119.2	118.1	130.1	126.6	127.0
10	52.0	51.1	50.8	50.7	51.0	45.0	50.8	51.1	51.1
12	66.5	61.9	65.7	65.6	61.8	62.0	65.5	61.9	62.0
13	54.1	54.3	54.2	54.2	54.3	48.7	54.3	54.2	54.2
14	21.6	23.7	22.9	22.7	23.6	22.5	22.8	23.9	23.7
15	29.2	24.6	29.5	29.4	24.7	30.5	29.5	24.4	24.5
17	172.0	169.4	169.5	168.9	169.3	169.3	169.2	169.4	169.1
23	170.6	169.2	169.4	169.8	169.7	169.7	169.6	169.5	169.8
24	21.3	21.0	21.0	21.0	20.9	20.9	21.3	21.3	21.0
RMSD		4.0	3.3	1.3	4.2	4.8	2.2	3.1	3.0
MAE		3.4	2.4	1.0	3.4	3.9	1.6	2.5	2.5

[a]*Note the Gaussian atom numberings do not match the experimental literature numberings. Experimental chemical shifts have been reordered accordingly. Configurations are presented in the form "rrs" corresponding to numerical order of the literature numbering for stereopositions. Example, ischnocybine A's "ssr" corresponds to the literature assignment "4S,8S,9R."*

Table 3.8.17. ^{1}H NMR Chemical Shift Predictions for Ischnocybine B (**3.3**)

Gaussian Numbering[a]	Experimental	rrrr	rrrs	rrsr	rsrr	rsrs	rssr	srrr	ssrr
20	2.19	2.31	2.19	2.25	2.05	1.91	2.29	2.52	2.36
21	1.81	2.50	2.04	2.07	2.51	2.72	2.00	2.48	2.46
26	5.04	5.40	5.67	5.06	4.96	5.03	5.09	4.93	4.91
27 (28)	1.81	1.91	1.89	1.79	1.99	1.90	1.81	1.83	2.01
28 (27)	1.20	1.61	1.33	1.24	1.38	1.06	1.35	1.69	1.40
29	5.01	4.77	4.70	5.26	4.63	4.62	4.79	4.95	5.00
30,31,32	0.84	0.99	0.94	0.85	0.97	0.96	0.85	0.94	0.98
33,34,35	0.84	0.87	0.86	0.91	0.91	0.93	0.94	0.87	0.88
36	5.74	5.41	5.44	5.81	5.46	5.42	5.83	5.74	5.76
37 (38)	3.31	3.19	3.17	3.21	3.21	3.40	3.21	3.21	3.20
38 (37)	2.63	2.77	2.81	2.86	2.80	3.00	2.85	2.84	2.81
39 (40)	3.00	2.79	2.82	2.81	2.80	2.64	2.83	2.80	2.82
40 (39)	2.12	2.14	2.16	2.18	2.16	2.62	2.17	2.16	2.14
41 (42)	1.67	1.58	1.66	1.66	1.60	1.77	1.65	1.59	1.59
42 (41)	1.67	1.55	1.60	1.60	1.56	1.72	1.59	1.57	1.55
43 (44)	1.94	1.55	1.79	1.81	1.61	1.75	1.81	1.58	1.61
44 (43)	1.33	1.53	1.28	1.35	1.59	1.58	1.30	1.57	1.60
48,49,50	2.02	2.06	2.07	2.03	2.03	2.04	2.09	2.09	2.03
RMSD		0.27	0.21	0.12	0.25	0.32	0.12	0.25	0.22
MAE		0.21	0.15	0.09	0.19	0.24	0.10	0.18	0.16

[a]*Note the Gaussian atom numberings do not match the experimental literature numberings. Experimental chemical shifts have been reordered accordingly. Configurations are presented in the form "rrs" corresponding to numerical order of the literature numbering for stereopositions. Example, ischnocybine A's "ssr" corresponds to the literature assignment "4S,8S,9R."*

Table 3.8.18. ^{13}C NMR Chemical Shifts Predictions for Ischnocybine C (**3.4**)

Gaussian Numbering[a]	Experimental	rrrrr	rrrrs	rrrss	rrsss	rsrss	rssrs	rsssr	rssss
1	76.5	80.7	74.6	79.7	83.7	78.8	74.5	80.7	81.0
2	69.3	75.8	72.0	74.7	78.2	71.1	74.6	78.7	77.4
3	35.8	43.2	44.9	39.4	40.4	43.2	43.5	49.7	45.5
4	36.7	37.1	27.0	26.3	29.1	26.4	29.5	34.7	28.8
5	39.0	41.6	34.8	41.2	39.4	45.4	37.7	43.7	43.8
6	35.0	36.7	34.3	34.9	36.8	35.3	36.0	36.5	36.7
7	66.9	66.2	59.2	62.7	59.4	62.7	58.0	66.4	59.8
9	54.1	51.7	47.4	46.6	46.9	46.6	46.5	50.6	46.7
10	29.3	27.9	30.9	33.5	32.6	33.0	30.3	32.3	32.5
11	27.7	26.5	29.4	24.9	22.4	24.4	32.2	31.1	22.7
12	21.7	24.8	21.9	22.6	22.3	22.5	21.8	22.3	22.3
13	54.3	54.1	54.6	54.1	54.7	53.9	53.2	53.5	54.7
14	27.9	31.9	25.5	25.7	24.6	22.8	21.2	21.2	21.1
15	29.3	25.7	28.8	29.1	28.2	30.8	29.7	29.6	29.5
18	172.9	170.6	169.2	170.4	169.9	170.3	169.4	169.9	170.1
20	172.4	169.6	169.0	169.6	168.8	170.2	170.1	169.2	169.2
RMSD		3.4	4.7	4.2	5.0	4.7	4.8	5.2	5.4
MAE		2.8	3.5	3.3	4.1	3.7	3.8	3.8	4.6

[a]*Note the Gaussian atom numberings do not match the experimental literature numberings. Experimental chemical shifts have been reordered accordingly. Configurations are presented in the form "rrs" corresponding to numerical order of the literature numbering for stereopositions. Example, ischnocybine A's "ssr" corresponds to the literature assignment "4S,8S,9R."*

Table 3.8.19. ^{13}C NMR Chemical Shifts Predictions for Ischnocybine C (**3.4**) (cont.)

Gaussian Numbering[a]	Experimental	srrss	srsrs	srssr	srsss	ssrrs	ssrsr	ssrss	sssrs
1	76.5	78.3	84.0	80.3	76.9	81.6	76.3	79.3	81.4
2	69.3	74.0	77.2	71.7	71.3	75.4	76.7	68.0	76.7
3	35.8	34.7	49.2	46.9	37.0	44.6	45.3	38.2	44.9
4	36.7	34.8	31.1	26.6	36.9	34.9	30.2	34.7	31.0
5	39.0	38.9	44.6	38.2	39.1	39.6	34.5	42.3	40.7
6	35.0	33.6	36.7	36.4	35.3	36.4	35.3	34.5	35.8
7	66.9	65.0	63.2	58.7	65.9	66.4	59.6	64.9	62.9
9	54.1	52.4	50.7	46.7	51.7	50.8	47.3	52.2	50.7
10	29.3	29.7	32.4	30.1	28.7	32.7	31.0	29.8	32.9
11	27.7	26.4	28.8	29.8	26.8	31.6	32.4	26.1	28.8
12	21.7	21.7	22.2	21.9	24.6	22.2	21.9	21.8	22.2
13	54.3	54.3	54.0	54.3	53.9	53.5	53.6	54.4	54.0
14	27.9	28.2	30.3	30.7	28.7	28.1	28.2	24.6	28.5
15	29.3	30.7	22.5	22.0	29.9	24.7	25.3	32.3	25.4
18	172.9	169.0	169.1	169.9	169.9	170.1	168.5	170.5	168.0
20	172.4	170.5	169.8	169.0	170.6	169.1	169.4	170.2	168.3
RMSD		2.0	5.4	5.3	1.5	3.7	4.9	2.1	4.3
MAE		1.5	4.3	4.0	1.2	2.9	3.8	1.8	3.5

[a]*Note the Gaussian atom numberings do not match the experimental literature numberings. Experimental chemical shifts have been reordered accordingly. Configurations are presented in the form "rrs" corresponding to numerical order of the literature numbering for stereopositions. Example, ischnocybine A's "ssr" corresponds to the literature assignment "4S,8S,9R."*

Table 3.8.20. ^{1}H NMR Chemical Shift Predictions for Ischnocybine C (**3.4**)

Gaussian Numbering[a]	**Experimental**	**rrrrr**	**rrrrs**	**rrrss**	**rrsss**	**rsrss**	**rssrs**	**rsssr**	**rsssss**
24	2.25	1.91	1.64	2.07	2.26	1.83	2.05	1.31	1.88
25	2.04	2.30	2.46	2.78	2.91	2.76	2.30	2.00	2.97
26	1.86	1.73	2.03	1.76	1.53	1.76	1.97	1.36	1.55
27	4.87	5.01	4.81	4.20	4.28	4.56	5.17	4.86	4.89
28	5.41	5.08	4.76	4.73	4.47	5.34	4.91	4.41	4.38
29 (30)	1.70	1.53	1.76	1.25	1.36	1.47	1.69	1.36	1.37
30 (29)	1.26	1.39	0.91	1.25	1.16	1.06	1.04	1.17	1.16
31 (32)	3.00	2.84	2.57	2.42	2.40	2.38	2.52	2.77	2.39
32 (31)	1.81	2.06	2.23	2.30	2.37	2.30	2.22	2.09	2.37
33 (34)	1.86	1.89	1.68	1.47	1.39	1.44	1.65	1.44	1.38
34 (33)	1.35	1.26	1.35	1.18	1.22	1.15	1.33	1.24	1.17
35 (36)	1.77	2.01	1.61	1.83	1.69	1.80	1.87	1.48	1.71
36 (35)	1.63	1.58	1.33	1.32	1.32	1.16	1.04	1.44	1.36
37 (38)	1.52	1.46	1.61	1.87	1.93	1.84	1.56	1.59	1.93
38 (37)	1.44	1.35	1.53	1.49	1.53	1.46	1.50	1.47	1.54
39 (40)	2.91	2.73	2.75	2.60	2.66	2.58	2.73	2.73	2.67
40 (39)	1.90	2.16	2.20	2.60	2.66	2.58	2.17	2.12	2.66
41,42,43	1.10	1.06	1.03	1.00	0.99	1.07	0.96	0.94	0.93
44,45,46	0.77	0.85	0.81	0.85	0.93	0.86	0.86	0.81	0.82
RMSD		0.18	0.31	0.42	0.46	0.37	0.28	0.39	0.47
MAE		0.16	0.24	0.34	0.37	0.30	0.22	0.27	0.37

Table 3.8.21. ^{1}H NMR Chemical Shift Predictions for Ischnocybine C (**3.4**) (cont.)

Gaussian Numbering[a]	Experimental	srrss	srsrs	srssr	srsss	ssrrs	ssrsr	ssrss	sssrs
24	2.25	1.88	1.18	1.76	2.18	1.61	1.89	1.78	1.43
25	2.04	2.23	2.04	2.13	2.26	1.88	2.69	2.17	1.99
26	1.86	1.66	1.66	2.08	1.76	1.35	1.91	1.62	1.61
27	4.87	4.54	4.16	4.18	5.10	4.47	5.07	4.58	4.21
28	5.41	4.64	4.60	5.19	5.54	4.83	4.62	5.59	4.43
29 (30)	1.70	1.73	1.48	1.66	1.66	1.34	1.77	1.57	1.27
30 (29)	1.26	1.36	1.12	1.14	1.20	1.12	0.88	1.54	1.19
31 (32)	3.00	2.79	2.74	2.55	2.80	2.76	2.56	2.78	2.75
32 (31)	1.81	1.90	2.07	2.24	2.06	2.09	2.24	1.93	2.08
33 (34)	1.86	2.18	1.46	1.66	1.77	1.40	1.71	2.18	1.45
34 (33)	1.35	1.22	1.18	1.35	1.21	1.28	1.38	1.25	1.21
35 (36)	1.77	1.55	1.69	1.80	2.12	1.61	1.83	1.44	1.61
36 (35)	1.63	1.43	1.37	1.43	1.55	1.48	1.08	1.42	1.32
37 (38)	1.52	1.57	1.66	1.65	1.45	1.62	1.56	1.48	1.66
38 (37)	1.44	1.53	1.54	1.56	1.40	1.49	1.50	1.48	1.54
39 (40)	2.91	2.68	2.75	2.76	2.66	2.72	2.73	2.69	2.75
40 (39)	1.90	1.99	2.17	2.22	2.14	2.12	2.17	1.96	2.16
41,42,43	1.10	1.13	1.04	1.09	1.04	0.99	0.98	1.16	1.05
44,45,46	0.77	0.87	0.91	0.91	0.83	0.89	0.86	0.86	0.84
RMSD		0.26	0.39	0.28	0.17	0.31	0.34	0.22	0.39
MAE		0.20	0.29	0.21	0.14	0.26	0.26	0.18	0.29

Table 3.8.22. NMR Spectroscopy Data for Ischnocybine A Alcohol (**3.6**) (600 MHz, d_6-DMSO)

Atom Number	δ_C, type	δ_H, (*J* in Hz)	HMBC Correlations	H2BC
1a	50.8, CH_2	3.39, m		
1b		2.82, m		
2	119.8, CH	5.46, m	C1, C4, C8	
3	140.5, C			
4	77.8, CH	3.41, m	C2, C3, C5, C6, C8, C9, C13, C14	
5	34.7, C			
6a	30.9, CH_2	1.03, m	C4, C5, C8, C14	C7
6b		1.71, m		
7a	25.7, CH_2	1.07, m	C3, C5, C8. C9	C6, C8
7b		1.56, m		
8	37.2, CH	2.22, m		C7, C9
9	66.4, CH	2.01, m		C8
10a	28.4, CH_2	1.37, m	C9	C9, C11
10b		2.01, m		
11	20.8, CH_2	1.73, m	C10	C10, C12
12a	53.1, CH_2	2.21, m	C1, C9, C11	C11
12b		3.13, m		
13 (ax)	27.2, CH_3	0.89, s	C5, C6, C14	
14 (eq)	23.8, CH_3	0.70, s	C5, C6, C13	

Table 3.8.23. Isolated quantity of ischnocybines from 300 individual *Ischnocybe plicata*

Compound	Isolated yields (mg)
Ischnocybine A (**3.1**)	3.5
Ischnocybinone (**3.2**)	4.6
Ischnocybine B (**3.3**)	2.5
Ischnocybine C (**3.4**)	4.1

Table 3.8.24. *I. plicata* Length Versus Alkaloid Study

Length (cm)	Ischnocybinone (3.2) Peak Area	Ischnocybine A (3.1) Peak Area	Ischnocybine B (3.3) Peak Area	Ischnocybine C (3.4) Peak Area	Average Peak Area
0.3	1.76E+04	6.57E+04	1.85E+03	1.85E+04	2.59E+04
0.2	2.56E+04	3.35E+05	3.67E+03	9.18E+04	1.14E+05
0.1	3.53E+04	3.17E+05	6.05E+03	1.08E+05	1.17E+05
0.5	9.70E+04	1.83E+05	2.90E+04	2.11E+05	1.30E+05
0.3	4.84E+04	2.93E+05	1.42E+04	1.67E+05	1.31E+05
0.4	4.29E+04	3.97E+05	1.39E+04	2.10E+05	1.66E+05
0.3	6.48E+04	5.55E+05	1.72E+04	2.78E+05	2.29E+05
0.3	1.07E+05	8.94E+05	2.76E+04	4.77E+05	3.76E+05
0.3	1.51E+05	9.22E+05	5.28E+04	5.64E+05	4.22E+05
0.4	2.63E+05	1.29E+06	8.16E+04	8.42E+05	6.19E+05
0.3	6.41E+05	1.34E+06	1.73E+05	1.13E+06	8.21E+05
1.1	1.79E+06	1.84E+06	6.81E+05	2.25E+06	1.64E+06
1.0	1.42E+06	2.05E+06	4.88E+05	2.79E+06	1.69E+06
0.6	2.18E+06	2.52E+06	8.97E+05	2.63E+06	2.06E+06
0.6	1.62E+06	3.56E+06	5.38E+05	3.23E+06	2.24E+06
0.9	2.64E+06	4.11E+06	9.17E+05	4.11E+06	2.94E+06
0.9	3.05E+06	3.01E+06	1.49E+06	4.57E+06	3.03E+06
0.9	1.44E+06	3.36E+06	2.20E+06	5.29E+06	3.07E+06
1.3	3.17E+06	3.55E+06	1.25E+06	4.37E+06	3.09E+06
0.9	3.18E+06	4.76E+06	1.16E+06	4.83E+06	3.48E+06
1.2	3.37E+06	4.38E+06	1.11E+06	5.27E+06	3.53E+06
1.1	4.61E+06	3.39E+06	2.02E+06	4.89E+06	3.73E+06
1.4	4.08E+06	4.57E+06	1.56E+06	5.08E+06	3.82E+06
1.1	4.20E+06	5.17E+06	1.30E+06	5.92E+06	4.14E+06
0.4	4.18E+06	5.65E+06	1.44E+06	5.87E+06	4.29E+06
1.4	4.15E+06	5.02E+06	2.11E+06	6.88E+06	4.54E+06
1.8	3.75E+06	5.29E+06	1.78E+06	7.68E+06	4.63E+06
1.5	4.41E+06	6.48E+06	1.63E+06	6.71E+06	4.81E+06
1.4	4.42E+06	5.86E+06	2.02E+06	6.98E+06	4.82E+06
2.0	4.06E+06	7.82E+06	1.89E+06	9.28E+06	5.76E+06

Table 3.8.25. Primary Binding Assay (Inhibition %). The Psychoactive Drug Screening Program performed each assay in quadruplet

Compound	Receptor	Inhibition 1	Inhibition 2	Inhibition 3	Inhibition 4	Mean %
3.1	5-HT1A	-0.8	21	33	-14	10
3.1	5-HT1B	14	20	8	10	13
3.1	5-HT1D	4	19	28	21	18
3.1	5-HT1E	-14	-6	-17	-13	-13
3.1	5-HT2A	-5	5	2	0.9	0.9
3.1	5-HT2B	-57	-91	-59	-51	-64
3.1	5-HT2C	0	6	-8	-11	-3
3.1	5-HT3	-3	8	9	2	4
3.1	5-HT5A	-22	-26	-9	-2	-15
3.1	5-HT6	-6	-0.8	-38	-12	-14
3.1	5-HT7A	42	37	32	21	33
3.1	α1A	4	3	8	7	6
3.1	α1B	-7	-24	-16	3	-12
3.1	α1D	3	2	0.8	-22	-4
3.1	α2A	46	-37	55	34	24
3.1	α2B	11	20	24	5	15
3.1	α2C	33	46	37	34	38
3.1	β1	-30	-11	-5	5	-10
3.1	β2	-10	-16	-11	-17	-13
3.1	β3	42	22	7	-2	17
3.1	BZP Rat Brain Site	12	-4	-14	-16	-6
3.1	D1	8	55	66	1	32
3.1	D2	13	6	11	7	9
3.1	D3	32	-10	-0.6	-2	5
3.1	D4	52	56	54	34	49
3.1	D5	26	10	21	-23	9
3.1	DAT	-15	-9	3	13	-2
3.1	DOR	-4	-9	-18	-14	-11
3.1	GABAA	-24	-46	-13	-2	-21
3.1	H1	32	11	10	14	17
3.1	H2	0.7	6	10	7	6
3.1	H3	40	35	23	33	33
3.1	H4	-12	19	25	-10	6
3.1	KOR	24	20	21	23	22
3.1	M1	-4	5	15	-11	1
3.1	M2	0.7	12	9	2	6
3.1	M3	27	25	12	6	18
3.1	M4	-6	2	13	4	3
3.1	M5	11	11	-6	4	5

3.1	MOR	9	-3	-3	3	1
3.1	NET	39	37	10	7	23
3.1	PBR	17	16	-80	-40	-22
3.1	SERT	14	-2	5	-15	0.7
3.1	Sigma 1	100	100	100	100	100
3.1	Sigma 2	100	84	83	85	89
3.1	α2β2	23	11	-0.8	-12	5
3.1	α2β4	1	-20	-14	7	-6
3.1	α3β2	-13	-6	-17	3	-8
3.1	α3β4	9	-14	-22	-3	-8
3.1	α4β2	-12	-6	3	16	0.4
3.1	α4β2 (Rat Brain)	-5	2	7	-0.5	0.8
3.1	α4β4	6	-8	-10	-17	-7
3.1	α7	-41	10	1	-10	-10
3.2	5-HT1A	-13	-9	-18	-7	-12
3.2	5-HT1B	3	6	-8	7	2
3.2	5-HT1D	4	-3	2	3	2
3.2	5-HT1E	-22	-16	-20	-27	-21
3.2	5-HT2A	21	5	-0.5	6	8
3.2	5-HT2B	-41	-51	-52	-62	-52
3.2	5-HT2C	6	-0.3	0.8	19	6
3.2	5-HT3	-2	-3	-0.6	-2	-2
3.2	5-HT5A	-25	-21	13	8	-6
3.2	5-HT6	-2	8	3	-5	1
3.2	5-HT7A	24	25	24	13	21
3.2	α1A	3	8	13	12	9
3.2	α1B	-25	1	-33	-11	-17
3.2	α1D	-4	8	54	6	16
3.2	α2A	33	7	59	38	34
3.2	α2B	14	15	9	23	15
3.2	α2C	6	26	20	11	16
3.2	β1	-73	22	-4	14	-10
3.2	β2	0.3	-8	-10	3	-4
3.2	β3	36	18	16	32	25
3.2	BZP Rat Brain Site	6	-5	0.4	-14	-3
3.2	D1	58	46	60	55	55
3.2	D2	23	28	24	17	23
3.2	D3	87	89	79	86	86
3.2	D4	20	19	10	12	15
3.2	D5	17	10	-140	20	-22
3.2	DAT	-8	-13	-26	-4	-13
3.2	DOR	-27	-12	-21	-30	-23
3.2	GABAA	-26	-32	-69	-37	-41
3.2	H1	11	16	4	4	9
3.2	H2	11	22	21	10	16

3.2	H3	23	21	15	29	22
3.2	H4	26	27	-6	29	19
3.2	KOR	6	12	-5	10	6
3.2	M1	-13	0.1	13	2	0.5
3.2	M2	9	24	12	12	14
3.2	M3	16	5	12	-3	7
3.2	M4	13	0.6	19	-3	8
3.2	M5	27	3	20	6	14
3.2	MOR	2	3	-6	-9	-3
3.2	NET	30	18	36	19	26
3.2	PBR	-15	-29	-19	-110	-43
3.2	SERT	-0.8	3	0.6	-4	-0.2
3.2	Sigma 1	75	65	70	67	69
3.2	Sigma 2	51	32	-5	21	25
3.2	α2β2	20	7	5	16	12
3.2	α2β4	28	18	12	12	18
3.2	α3β2	-9	-34	-33	0.6	-19
3.2	α3β4	-0.5	-4	-17	3	-4
3.2	α4β2	-4	-13	-5	10	-3
3.2	α4β2 (Rat Brain)	15	0.8	12	0.3	7
3.2	α4β4	-8	-43	-53	-21	-31
3.2	α7	-10	-3	2	-8	-5
3.3	5-HT1A	37	13	-18	-14	5
3.3	5-HT1B	6	-5	10	12	6
3.3	5-HT1D	51	36	21	28	34
3.3	5-HT1E	-10	-28	-2	-2	-10
3.3	5-HT2A	1	5	-0.6	5	3
3.3	5-HT2B	-41	-47	-62	-56	-51
3.3	5-HT2C	6	-2	4	-18	-2
3.3	5-HT3	2	9	0.6	-5	2
3.3	5-HT5A	-20	-15	17	-14	-8
3.3	5-HT6	11	8	3	-12	2
3.3	5-HT7A	23	39	32	14	27
3.3	α1A	6	4	11	12	8
3.3	α1B	-12	-4	5	3	-2
3.3	α1D	1	-1	6	11	4
3.3	α2A	18	19	24	20	20
3.3	α2B	0.6	16	9	18	11
3.3	α2C	14	26	24	6	18
3.3	β1	-7	-26	22	24	3
3.3	β2	-10	-14	-10	-15	-12
3.3	β3	29	30	-0.8	12	18
3.3	BZP Rat Brain Site	5	3	-2	-2	1
3.3	D1	-22	64	55	59	39
3.3	D2	16	19	11	17	16

3.3	D3	-0.2	3	17	-11	2
3.3	D4	5	-20	18	6	2
3.3	D5	9	29	23	25	21
3.3	DAT	-16	-16	24	23	4
3.3	DOR	-25	-23	-21	-25	-23
3.3	GABAA	-31	-70	-64	-52	-54
3.3	H1	22	5	-3	4	7
3.3	H2	2	3	9	2	4
3.3	H3	56	53	50	49	52
3.3	H4	17	5	-7	-6	2
3.3	KOR	27	15	17	11	17
3.3	M1	10	4	12	17	11
3.3	M2	3	13	20	7	11
3.3	M3	5	24	17	-9	9
3.3	M4	0.5	16	18	3	9
3.3	M5	9	-6	0.4	0.5	0.9
3.3	MOR	-0.5	-6	-4	3	-2
3.3	NET	26	23	16	21	21
3.3	PBR	0	3	-20	-62	-20
3.3	SERT	11	10	9	-5	6
3.3	Sigma 1	110	110	110	100	110
3.3	Sigma 2	68	33	23	38	40
3.3	α2β2	-30	-6	-9	0	-11
3.3	α2β4	35	26	21	14	24
3.3	α3β2	9	-1	-5	32	9
3.3	α3β4	34	48	52	22	39
3.3	α4β2	6	-6	-4	8	1
3.3	α4β2 (Rat Brain)	5	13	-2	13	7
3.3	α4β4	-12	-6	-23	-8	-12
3.3	α7	-12	-16	-23	-8	-15
3.4	5-HT1A	-39	-12	-43	0.5	-24
3.4	5-HT1B	-7	-7	13	4	0.7
3.4	5-HT1D	9	7	6	12	9
3.4	5-HT1E	-21	-16	-36	-34	-27
3.4	5-HT2A	22	12	6	17	14
3.4	5-HT2B	26	20	8	-3	13
3.4	5-HT2C	13	20	13	13	15
3.4	5-HT3	8	-6	7	-7	0.7
3.4	5-HT5A	0	-19	-3	7	-4
3.4	5-HT6	4	25	4	16	12
3.4	5-HT7A	22	27	16	28	23
3.4	α1A	12	15	4	6	9
3.4	α1B	11	23	14	4	13
3.4	α1D	-12	8	10	19	6
3.4	α2A	41	60	48	39	47

3.4	α2B	49	40	37	47	43
3.4	α2C	75	70	71	66	71
3.4	β1	23	25	-3	7	13
3.4	β2	0.3	-8	4	16	3
3.4	β3	15	-6	-7	-13	-3
3.4	BZP Rat Brain Site	5	11	-5	8	5
3.4	D1	52	49	47	68	54
3.4	D2	19	15	6	3	11
3.4	D3	27	50	53	40	42
3.4	D4	3	-12	-15	2	-6
3.4	D5	-3	6	-2	-10	-2
3.4	DAT	-23	-48	4	-3	-18
3.4	DOR	-13	-23	-9	-41	-22
3.4	GABAA	-32	-56	-69	29	-32
3.4	H1	3	5	19	8	9
3.4	H2	33	32	10	11	22
3.4	H3	20	11	5	2	10
3.4	H4	3	-6	-28	2	-7
3.4	KOR	12	2	3	8	6
3.4	M1	-19	-5	21	47	11
3.4	M2	11	22	6	15	14
3.4	M3	18	0.1	11	6	9
3.4	M4	0.5	7	-5	9	3
3.4	M5	12	-6	-2	27	8
3.4	MOR	11	-4	-5	1	0.9
3.4	NET	18	6	17	9	13
3.4	PBR	22	-3	-6	-56	-11
3.4	SERT	21	2	26	4	13
3.4	Sigma 1	100	96	95	83	93
3.4	Sigma 2	95	70	71	69	76
3.4	α2β2	19	2	-17	-24	-5
3.4	α2β4	-12	7	-16	24	0.9
3.4	α3β2	-15	-0.8	17	-17	-4
3.4	α3β4	-18	-18	-38	-36	-27
3.4	α4β2	-24	-7	-11	3	-10
3.4	α4β2 (Rat Brain)	-13	5	8	18	5
3.4	α4β4	-38	-14	23	-37	-16
3.4	α7	15	8	0.8	-7	4
3.6	Sigma 1	63	59	63	62	62
3.6	Sigma 2	73	42	49	52	54

Table 3.8.26. Inhibitor Constant (K_i) for Compounds **3.1–3.4**

Compound	Receptor	K_i (nM)
3.1	5-HT2B	9300
3.1	σ_2	1300
3.1	σ_1	14
3.2	5-HT2B	> 10,000
3.2	D3	5400
3.2	D1	> 10,000
3.2	σ_1	1500
3.3	5-HT2B	5400
3.3	H3	1100
3.3	σ_1	380
3.3	GABAA	1700
3.3	α3β4	> 10,000
3.4	5-HT1E	> 10,000
3.4	α2C	2900
3.4	σ_2	2900
3.4	D1	> 10,000
3.4	σ_1	380
3.6	σ_1	2200
3.6	σ_2	2100

Table 3.8.27. MM/GBSA Calculated Predicted Free Energy of Binding for poses bound into the agonist receptor binding pocket. Ischnocybine A (**3.1**) consistently had more poses dock into the binding pocket, better predicted free binding energies, and ligand efficiencies than ischnocybine B (**3.3**).

Structure	Ligand	Pose	Predicted Free Energy of Binding (kcal/mol)	Ligand Efficiency (kcal/mol/heavy atom)
Agonist (PDB ID: 6DK1)	**1**	1	-52.2	-2.48
	1	2	-34.2	-1.63
	1	3	-29.6	-1.41
	1	4	-30.1	-1.43
	1	5	-24.6	-1.17
	1	9	-13.6	-0.65
	2	1	-43.9	-1.99
	3	5	-11.8	-0.47
	4	5	-31.4	-1.16

Chapter 4.

The Discovery of Complex Heterocycles from Millipede Secretions Provides Insights into Biosynthesis and Evolution

Paige Banks,[1] Carla Menegatti,[1] Lin Du, [2] Kenneth Knott, [1] Paul E. Marek,[3] Emily Mevers[1]

1. Department of Chemistry, Virginia Tech, Blacksburg, Virginia, USA
2. Molecular Targets Program, Center for Cancer Research, National Cancer Institute, Frederick, MD, USA
3. Department of Entomology, Virginia Tech, Blacksburg, Virginia, USA

4.0. Abstract

The recent explosion in the described chemistry from Colobognatha, a millipede subterclass, has rekindled interest in the defensive secretions from these ancient animals. Prior to 2020, studies into defensive secretions by Colobognatha—the only subterclass that produce terpenoid alkaloids—explored a single order, Polyzoniida. However, recently, numerous species of the order Platydesmida have been shown to produce structurally diverse terpenoid alkaloids with potent biological activities. Platydesmida defensive secretions encompass multiple natural product scaffolds with greater chemical complexity compared to previously reported millipede-derived alkaloids. Here we report an analysis of defensive secretions of *Andrognathus corticarius*, a millipede that is sister to all other Platydesmida, and is currently considered one of the oldest genera within the order. Analyzing defensive secretions revealed that *A. corticarius* produces an arsenal of alkaloids that are dissimilar to all previously reported metabolites. Using a variety of analytical techniques, we accomplished complete structural assignment of two distinct scaffolds: a 5,6-fused heterocycle named the andrognathines and a 6,6,6,5-bridged heterocycle containing seven continuous stereogenic centers named the andrognathanols. Each scaffold contains diverse

fatty acids; this leads an extraordinary number of unique metabolites in secretions. Alkaloids, actively secreted upon physical disturbance, likely serve to defend millipedes from predation. This discovery provides support for a plausible biosynthetic pathway that appears to be evolving simplicity within Platydesmida.

4.1. Introduction

A single subterclass, the Colobognatha produce all millipede-derived terpenoid alkaloids. This monophyletic group consists of four species-rich orders. Unlike other millipedes, colobognath possess unique characteristics—feeding primarily on fungus, forming large aggregations, and exhibiting other social behaviors such as parental egg care.[1,2] The size of these aggregations varies greatly, and their function remains unclear, but some contain over 100 millipedes.[3] Despite the fascinating biology observed in Colobognatha, few studies have focused on the chemical composition of their defensive secretions. Only three terpenoid alkaloids—buzonamine (*Buzonium crassipes*), polyzonimine (*Petaserpes rosalbus*) and spiropyrrolizidine *O*-methyloxime 236 (*Rhinotus purpureus*)—appear prior to 2020, all from defensive secretions of species within a single order, Polyzoniida.[4-7] Very few studies examine millipedes from the other three orders of Colobognatha; in those limited studies, only simple monoterpenes appear.[8] However, recent findings indicate an increase in new chemistry from species of Platydesmida (**Figure 4.9**).[9-11] First, *Brachycybe producta* and *B. petasata* defensive secretions contain indolizidine and quinolizidines.[10] Next, *B. lecontii* and *B. rosea* secretions contain deoxybuzonamine isomers.[11,12] Finally, *Ischnocybe plicata* secretions contain the oxidized ischnocybines.[13] The ecological role of terpenoid alkaloids remains unclear; however, most likely, they serve a defensive role, act as pheromones, or function in both capacities.[14,15] Like all millipedes, Colobognatha have evolved specialized repugnatorial glands, that store and secrete defensive compounds. These glands open through ozopores and are located bilaterally, with two glands per segment.[8] Some species of Colobognatha possess up to 330 segments.[16] Several alkaloids (e.g, glomerin, polyzonimine, buzonamine, and the ischnocybines) deter commonly encountered predators (e.g., spiders, cockroaches, flies and ants, respectively).[8,17-20] However, only the ischnocybines and

spiropyrrolizidines have been evaluated in a range of receptor assays. Ischnocybine A potently and selectively binds the sigma-1 receptor (σ_1R), an orphan neuroreceptor, over the sigma-2 receptor (σ_2R). Molecular docking experiments suggest the ischnocybines act as σ_1R antagonists.[9] Conversely, the spiropyrrolizidine oximes appear to block nicotinic receptors with selectivity for ganglionic-type receptors.[21] Additionally, both spiropyrrolizidine oximes and polyzonimine have been isolated from the skin of poison dart frogs—researchers hypothesized that the frog acquired these alkaloids through their diet for defensive purposes.[22] Given the social characteristics displayed by Colobognatha, terpenoid alkaloids might function as pheromones, aiding in forming large aggregations and brood care.[8]

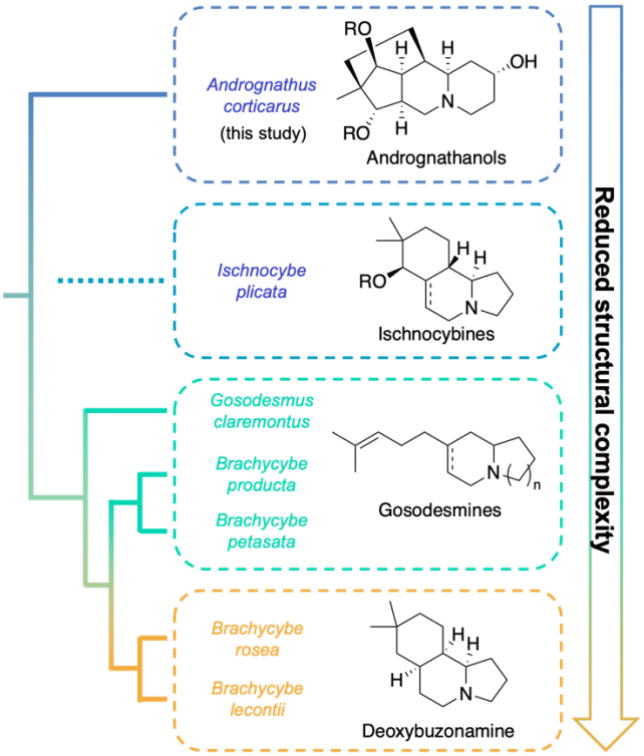

Figure 4.9. Platydesmida phylogeny with chemistry described. Uncertain placement of *I. plicata* denoted by dotted line. This study is focused on the defensive secretions of *Andrognathus corticarius*.[14,16,23]

To date, the defense secretion composition from Platydesmida species show the greatest structural diversity with the production of two distinct core structures: a 5,6,6-fused heterocycle and an indolizidine/quinolizidine core.[10] In addition, Platydesmida secretions contain significantly more predicted post-modification events (e.g., multiple oxidations, ligation events, and incorporation of different precursors).[9-11,21] Yet, chemists have studied less than 10% of Colobognatha species, with an entire genera unstudied. This includes *Andrognathus corticarius*, ostensibly one of the oldest genera of the Platydesmida with a fossil record dated to the Late Cretaceous period (99 mya).[14,24] Gaining an understanding of the structural diversity of these unstudied genera will provide key insights into a potential biosynthetic pathway and how this family of compounds have diversified.

4.2. Results and Discussion

4.2.1. Chemical Investigations into Defensive Secretions of *Andrognathus corticarius*

A. corticarius specimens were primarily collected in downed woody debris in southwestern Virginia (**Table 4.7.28**) between May and September, with large aggregations commonly found from May through July. Field observations across multiple years suggested that these large aggregations were more active toward the beginning of August, as pairs of adult millipedes along with juveniles were more frequently encountered. By October, it became increasingly difficult to locate any millipedes on the same woody debris, leading to the hypothesis that *A. corticarius* spends the winter months underground, potentially protecting themselves from cold temperatures and low humidity.

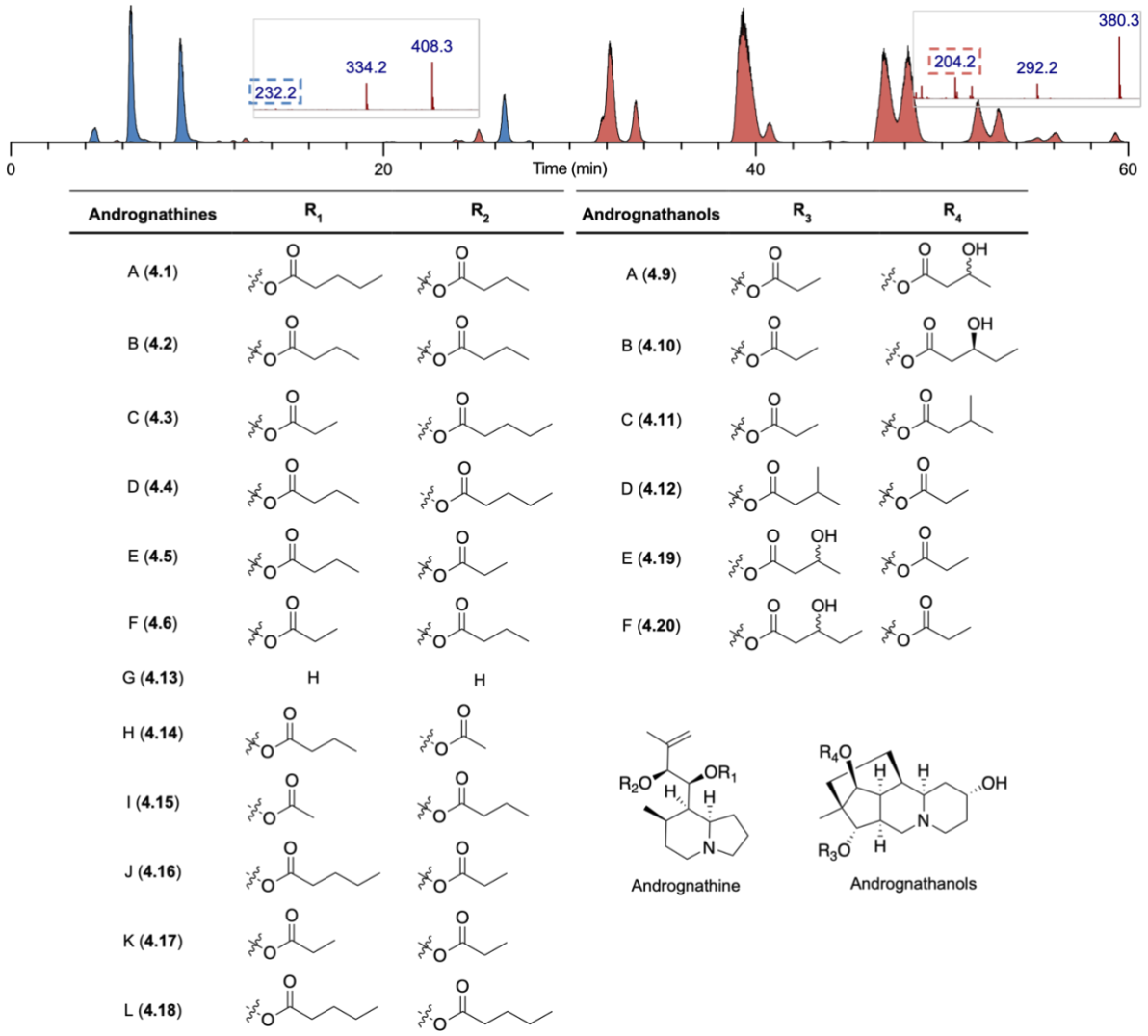

Figure 4.10. Andrognathine and andrognathanol structures. HPLC-MS chromatogram of a representative *A. corticarius* crude extract. The andrognathanols are highlighted blue and the andrognathines are highlighted red with key tandem MS fragments shown in the respective boxes. Structures of the andrognathines (**4.1**–**4.6**, **4.13**–**4.18**) and andrognathanols (**4.9**–**4.12**, **4.19** and **4.20**) from *A. corticarius*.

Analysis of the defensive secretions from collected millipedes by high resolution liquid chromatography mass spectrometry (HR-LCMS) revealed that *A. corticarius* produces a significant array of diverse alkaloids (>18 compounds), with molecular ions ranging from

240.1965 to 424.3053 Da (**Figure 4.10**). Tandem MS analysis revealed two different structural classes, as indicated by key fragment ions (232.1695 and 204.1753 Da), which are structurally distinct from all previously reported colobognath alkaloids. The alkaloids were purified using reverse-phase HPLC-MS, yielding andrognathines A–F (**4.1–4.6**) and andrognathanols A–D (**4.9–12**).

4.2.2. Complete Structural Assignment of the Andrognathines (4.1–4.6**)**

Full 2D NMR datasets (^{1}H, dqfCOSY, gHSQC, H2BC, HMBC and easyROESY) on **4.1–4.6** (**Figure 4.9.1**–**Figure 4.9.31**; **Table 4.10.29**–**Table 4.10.34**) were acquired. Compound **4.1** had a $[M+H]^+$ of 394.2954 *m/z*, suggesting a molecular formula (MF) of $C_{23}H_{39}NO_4$ and indicating five degrees of unsaturation (DoU). Tandem MS analysis of **4.1** revealed two neutral losses of 88.0523 and 102.0683 Da, suggesting the presence of butyrate and pentanoate esters. ^{1}H and ^{13}C NMR chemical shifts established two ester carbonyls (δ_C 172.3 and 171.8), verifying the acyl moieties. Additionally, an exomethylene (δ_C 118.1; δ_H 5.10/5.04) was identified, thereby accounting for three of the five DoUs. The ^{1}H NMR spectrum clearly represented four methyl groups, each integrating to three protons: three aliphatic methyl groups (δ_H 1.00, 0.87, and 0.86) and one vinyl methyl (δ_H 1.70). Comparison of the spectroscopic data to previously reported millipede alkaloids suggested **4.1** contained an indolizidine core similar to hydrogosodesmine.[10] The HSQC spectrum revealed a diagnostic bridgehead methine (δ_C 64.3) and diastereomeric methylenes (δ_C 53.1 and 51.8) that are alpha to the tertiary nitrogen, thereby accounting for the remaining two DoUs. However, detailed analysis of H2BC and COSY correlations (**Figure 4.11A**) revealed a different substitution pattern on the indolizidine ring compared to hydrogosodesmine.

Continuous H2BC correlations from the bridgehead methine (H-8: δ_H 1.76) through three diastereomeric methylenes (H-7: δ_H 1.53/2.03; H-6: δ_H 1.65; H-5: δ_H 1.96/2.94) confirmed an

unsubstituted pyrrolidine ring. Further analysis of H2BC correlations for H-8 revealed another correlation to a methine, C-9 (δ_C 47.1). H-9 (δ_H 1.16) exhibited two additional H2BC correlations to another methine (C-2: δ_C 32.5), within the indolizidine ring, and an oxygenated methylene (C-10: δ_C 70.1), which was positioned on a side chain. To continue establishing the indolizidine system, H-2 (δ_H 1.21) had a strong H2BC correlation to a doublet methyl (C-1: δ_C 19.8) and two COSY correlations to diastereomeric methylenes (H-3: δ_H 1.21/1.58; H-4: δ_H 1.85/2.91). The chemical shifts of C-4, consistent with a carbon alpha to the tertiary amine, thereby establishing a 7,8-disubstituted indolizidine.

Additional 2D NMR analysis provided further structural insights. The oxygenated methine, H-10 (δ_H 5.38), previously assigned to C-9, exhibited an H2BC correlation to the other oxygenated carbon, C-11 (δ_C 76.1). HMBC correlations from H-11 (δ_H 5.45) to the quaternary carbon C-12 (δ_C 139.9), the exomethylene C-14 (δ_C 118.1), and the singlet vinyl methyl C-13 (δ_C 17.5), allowed for assigning the carbon backbone of **4.1**. The two aliphatic esters detected by tandem MS remained unassigned until key HMBC correlations clarified their positions: H-10 (δ_H 5.38) correlated with C-15 (δ_C 172.3), confirming the pentanoate, while H-11 (δ_H 5.45) correlated with C-19 (δ_C 171.8), confirming the butyrate. This completed the planar structural assignment of **4.1**, named andrognathine A (**Figure 4.10**).

Compounds **4.2**–**4.6** had nearly identical NMR data to **4.1**, but HRMS indicated each had slightly different MF (**4.2**: $C_{22}H_{37}NO_4$, **4.3**: $C_{22}H_{37}NO_4$, **4.4**: $C_{23}H_{39}NO_4$, **4.5**: $C_{21}H_{35}NO_4$, and **4.6**: $C_{21}H_{35}NO_4$). Tandem MS analysis confirmed the presence of a conserved indolizidine core as evidenced by the key 204 Da fragment, while distinct neutral losses distinguished each compound. Structural isomers **4.2** and **4.3** differed in their fatty acid composition. Tandem MS data for **4.2** contained two distinct neutral losses of 88.0515 Da, which indicated two butyrate side chains. In

contrast, **4.3** revealed neutral losses of 74.0370 and 102.0670 Da, which indicating the presence of propionate and pentanoate, respectively. Compound **4.4**, a structural isomer of **4.1**, showed identical neutral losses (88.0526 and 102.0670 Da), indicating incorporation of butyrate and pentanoate, respectively, but were in opposite positions. Isomers **4.5** and **4.6** both displayed neutral losses of 88.0515 and 74.0360 Da, indicating butyrate and propionate, respectively. Analysis of 2D NMR spectra confirmed the planar structures and positions of the side chains for **4.2**–**4.6**, andrognathines B–F.

The relative and absolute configurations of andrognathines were determined through key ROESY correlations, chemical derivation, and ECD analysis. First, we assigned the relative configuration among the three adjacent stereocenters within the indolizine portion of **4.1** through key ROESY correlations (**Figure 4.11A**). Correlations between H-1 (δ_H 1.00) and H-10 (δ_H 5.38), as well as H-8 (δ_H 1.76) and H-9 (δ_H 1.16), confirmed a *syn* stereochemistry among H-2, H-8, and H-9 in the bicyclic system. However, the flexibility of the side chain attached at C-9 challenged attempts to link the relative configuration of the indolizidine to the side chain. To address this, hydrogenating an aliquot of the crude extract mixture reduced the olefin, hydrolysis removed ester side chains, and subsequent acetonide protection gave **4.7**. We purified **4.7** by HPLC and analyzed it by 2D NMR (**Figure 4.9.32**–**Figure 4.9.37**; **Table 4.10.35**). First, closeness of the ^{13}C NMR chemical shifts of the acetonide *gem*-dimethyls (δ_C 26.3 and 27.1) indicated an *anti*-configuration as both experienced similar shielding (**Figure 4.11B**).[25] Further support arose in key ROESY correlations between H-17 (δ_H 1.28) and both H-10 (δ_H 4.10) and H-12 (δ_H 1.73). We assigned absolute configuration of H-10 and H-11 by esterifying a portion of the hydrolyzed diol product with *para*-bromobenzoate to generate **4.8**. Subsequent analysis of **4.8** by ECD yielded a positive split Cotton effect (**Figure 4.11C**), confirming the absolute configuration of the diol as 10*S*,11*S*.[26]

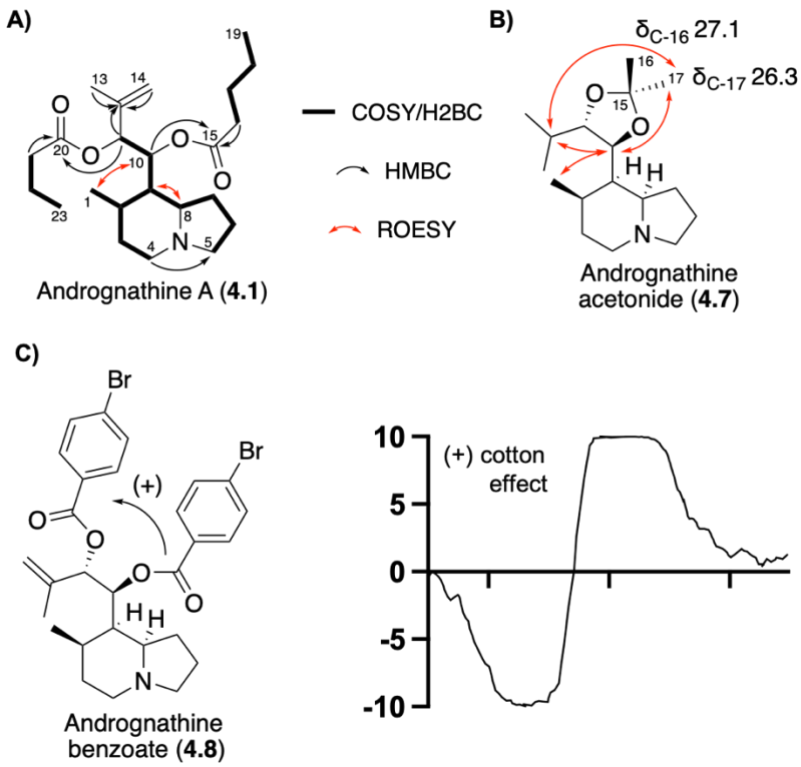

Figure 4.11. Andrognathine stereochemistry. **A)** Key 2D NMR correlations for andrognathine A (**4.1**), **B)** Key ROESY correlations and ^{13}C NMR chemical shifts of the andrognathine acetonide (**4.7**). These correlations support a *syn*-relationship between the 10,11-diol. **C**) Positive split Cotton effect was observed in the ECD spectra of the andrognathine benzoate (**4.8**) confirmed the absolute configuration as 10*S*,11*S*-**4.8**.

Finally, density functional theory (DFT) calculations refined the side chain conformations. Conformer libraries for two possible diastereomers (2*R**,8*R**,9*R**,10*S**,11*S**-**4.7A** and 2*S**,8*S**,9*S**, 10*S**,11*S**-**4.7B**) were generated in Spartan, and chemical shifts were calculated using Gaussian09. Experimental ^{1}H and ^{13}C NMR shifts (**Table 4.10.36**) were compared, though peak broadening of the nuclei near the tertiary amine complicated assignments of some shifts. This approach enabled the assignment of all stereogenic centers and the entire side chain. Despite similar root mean square deviation (RMSD) of ^{13}C NMR chemical shifts (**4.7A**: 2.38 vs **4.7B**: 2.30 ppm), significant differences in ^{1}H NMR accuracy (**4.7A**: 0.10 vs **4.7B**: 0.20 ppm) occurred. This

difference resided primarily with two protons, H-9 (δ_H expt: 1.65; **4.7A:** 1.55; **4.7B**: 1.86) and H-12 (δ_H expt: 1.73; **4.7A**: 1.59; **4.7B**: 2.53), indicating 2*R*,8*R*,9*R*,10*S*,11*S*-**4.7A** represented the correct configuration for the andrognathines.

4.2.3. Structural Assignment of the Andrognathanols (4.9–4.12**)**

Analyzing HR-LCMS data for **4.9** indicated a molecular ion of $[M+H]^+$ 410.25427 *m/z*, providing a MF of $C_{22}H_{35}NO_6$, requiring six DoUs. Comparing the 2D NMR dataset for **4.9** (**Figure 4.9.38**–**Figure 4.9.43**; **Table 4.10.37**) with **4.1**–**4.6** revealed significant structural differences, notably the absence of a vinyl methyl and exomethylene. The ^{13}C NMR spectrum revealed two esters (δ_C 172.9 and 171.1) and four oxygenated carbons (δ_C 78.0, 75.4, 67.7 and 63.2). Tandem MS data showed two neutral losses, 104.0488 and 74.0367 Da, suggesting a hydroxybutanoate and propionate, respectively. Analyzing the ^1H NMR spectrum confirmed the four oxygenated carbons as sp^3-hybridized with protons at δ_H 4.92, 4.60, 4.02 and 3.60, and revealed three aliphatic methyl groups (δ_H 0.78, 1.01 and 1.10). However, with no obvious functionality accounting for the additional DoUs, we predicted that **4.9** contained four rings.

Detailed analysis of the 2D NMR dataset for **4.9** led to the elucidation the planar structure (**Figure 4.12A**). The diagnostic bridgehead methine (H-8: δ_H 1.89) alpha to the tertiary amine exhibited H2BC correlations to both methylene C-7 (δ_C 32.0) and methine C-9 (δ_C 30.3), and HMBC correlations to an oxygenated carbon C-6 (δ_C 67.7). Additional HMBC correlations from H-6 (δ_H 4.92) to methylenes C-5 (δ_C 28.8) and C-4 (δ_C 49.5), with C-4 being alpha to the tertiary amine, indicated that, unlike in **4.1**–**4.6**, an oxygenated pyrrole replaced the pyrrolidine ring in andrognathanols. The final methylene alpha to the amine, H-3 (δ_H 2.16/2.93), had an H2BC correlation to methine C-2 (δ_C 43.4), further distinguishing **4.9** from **4.1**–**4.6**. The H-2 (δ_H 1.70) showed two additional H2BC correlations to two methines, including C-10 (δ_C 40.8) and C-1 (δ_C

75.4), with C-1 being oxygenated. A singlet methyl at δ_H 0.78 exhibited several HMBC correlations, including to C-12 (δ_C 42.6), a sp^3 hybridized quaternary carbon, to C-1 (δ_C 75.4), to C-11 (δ_C 78.0), and to C-13 (δ_C 30.6). This established a 6,6,5-fused tricyclic system seen in **Figure 4.10**. Diastereomeric methylenes, H-13 (δ_H 1.14/1.73) and H-14 (δ_H 1.30/1.90), exhibited mutual H2BC correlations, while H-14 also correlated with C-9 (δ_C 30.3) confirming the connectivity of the final ring. Finally, H2BC correlations between methylene H-20 (δ_H 2.37) and oxygenated carbon C-21 (δ_C 63.2), as well as C-21 and a doublet methyl, H-22 (δ_H 1.10) confirmed a 3-hydroxybutanoate. An HMBC correlation between H-11 (δ_H 4.60) and C-19 (δ_C 171.1) established the 3-hydroxybutanoate attachment to C-11, while another HMBC correlation between H-1 (δ_H 3.60) and C-16 (δ_C 172.9) established the propionate attachment to C-16. Thus, we established the planar structure of **4.9** as a 6,6,6,5-bridged heterocycle.

Comparing NMR and tandem MS spectra for **4.10**–**4.12** (**Figure 4.9.44**–**Figure 4.9.59**; **Table 4.10.37**–**Table 4.10.40**) with **4.9** confirmed structural similarity, with all containing the key fragment at 232.1695 Da, indicative of the 6,6,6,5-bridged heterocyclic system. However, like andrognathines, HR-LCMS confirmed that **4.10**–**4.12** had different retention times and distinct chemical compositions, $C_{23}H_{37}NO_6$ (**4.10**), $C_{23}H_{37}NO_5$ (**4.11**), and $C_{23}H_{37}NO_5$ (**4.12**), as well as different neutral losses. For **4.10** tandem MS spectra showed neutral losses of 74.0361 and 118.0645 Da, indicating propionate and hydroxypentanoate, respectively. Analyzing 2D NMR spectra revealed the latter as a 3-hydroxypentanoate attached to C-11. A key HMBC correlation between H-1 (δ_H 3.60) and C-16 (δ_C 172.9) within propionate moiety establishing the final connection. Compounds **4.11** and **4.12**, structural isomers with identical neutral losses (102.0686 and 74.0362 Da), contained either an isobutyrate or pentanoate and propanoate, respectively. Analyzing 1D NMR confirmed isobutyrate as evidenced by two doublet methyl groups that

exhibited strong HMBC correlation to one another. Key HMBC correlations confirmed the propionate attached to C-11 in **4.11**, and on C-1 in **4.12**.

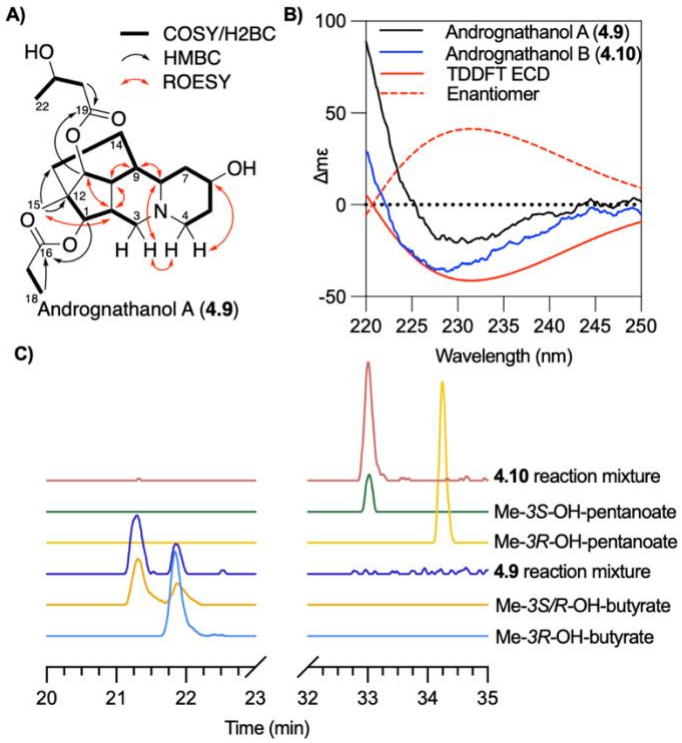

Figure 4.12. Androgrnathanol Stereochemistry. **A)** Key 2D NMR correlations for androgrnathanol A (**4.9**). **B)** Experimental and TD-DFT data for both **4.9** and **4.10** along with predicted data and the enantiomer. **C)** Stacked chromatograms of the methylated hydrolysate of **4.9** and **4.10** along with Me-OH-pentanoate and Me-OH-butyrate standards, confirming the absolute configuration as Me-3*S*-OH-pentanoate for **4.10** and a mixture of Me-OH-butyrate isomers in **4.9**.

We established relative configurations of **4.9**–**4.12** by observing key ROESY correlations. Bridgehead methine, H-2 (δ_H 1.70), correlated with H-10 (δ_H 2.01), H-11 (δ_H 4.61), and H-15 (δ_H 0.78), indicating these groups are *syn* to one another (**Figure 4.12A**). Strong ROESY correlations were observed between H-9 (δ_H 1.51) and both H-6 (δ_H 4.92) and H-8 (δ_H 1.90), while H-1 (δ_H 3.61) exhibited no ROESY correlations with any stereogenic centers. However, H-1 showed a strong ROESY correlation to H-13a (δ_H 1.13), confirming an *anti*-relationship to H-2, H-9, H-10,

and H-11. Unfortunately, H-6 (δ_H 4.92), the proton attached to the secondary alcohol did not exhibit ROESY correlations to any stereogenic centers. Nevertheless, H-6 showed a strong ROESY correlation to nearby downfield diastereotopic protons, H-5b (δ_H 1.67) and H-7b (δ_H 1.53). Similarly, the bridgehead methine, H-8, exhibited strong ROESY correlations to the upfield diastereotopic proton, H-7a (δ_H 1.43). Taken together, we assigned the relative configuration of the andrognathanol core as 1*S**,2*S**,6*R**,8*R**,9*R**,10*S**,11*S**,12*S**. Absolute configuration was established by comparing the experimental ECD spectra to TD-DFT calculated spectra of both enantiomers (**Figure 4.12B**). Both **4.9** and **4.10** exhibited a negative split Cotton effect, matching the1*S*,2*S*,6*R*,8*R*,9*R*,10*S*,11*S*,12*S* enantiomer.

The final structural assignment involved determining the absolute configuration of both 3-hydroxybutanoate in **4.9** and 3-hydroxypentanote **4.10**. First, we treated a crude millipede extract with 6N HCl to hydrolyze the esters, followed by treatment with (trimethylsilyl)diazomethane to form the methyl esters. Chiral GCMS comparison of the derivatized natural product with authentic standards revealed both enantiomers for both 3-hydroxybutanoate and 3-hydroxypentanoate present in equal quantities (**Figure 4.9.60**). Next, we treated aliquots of purified **4.9** and **4.10** with the same conditions and analyzed each. The reaction mixture for **4.10** contained only methyl-3*S*-hydroxypentanoate (**Figure 4.12C**). However, the reaction mixture for **4.9** still contained a mixture of both enantiomers of methyl-3-hydroxybutanoate (**Figure 4.12C**), indicating **4.9** as a mixture of diastereomers.

4.2.4. Mass Spectrometry-Based Structure Elucidation of Low Abundant Andrognathines and Andrognathanols

Compounds **4.1**–**4.6** and **4.9**–**4.12** represent a subset of all the alkaloids detected in defensive secretions by LCMS. Notably, all detected metabolites contained either the

andrognathine or andrognathanol core structures, as evidenced by two characteristic fragment ions: 204.1753 Da for the andrognathines and 232.1695 Da for the andrognathanols. Further analyses of neutral losses in tandem MS spectra for each metabolite revealed the only structural differences among metabolites were in the composition of the alkyl side chains. In total, we identified six additional andrognathines (**4.13**–**4.18**), which exhibited various masses: 240.1965, 352.2491, 366.2636, 394.2954, 408.3107, and two andrognathanols (**4.19**–**4.20**) with masses: 410.3903 and 424.3054 Da, respectively. Compound **4.13** had a MF of $C_{14}H_{25}NO_2$, eluted very early in the chromatogram and underwent two obvious in-source fragmentations corresponding to losses of water. Its retention time matched of one hydrolysis products in the crude extract, confirming it shared the same backbone as **4.1** but lacks the ester functionality.

Analyzing HRMS data for **4.14**–**4.18** revealed three pairs of isobaric masses with identical neutral losses, but distinct retention times. This suggested that each pair shared the same acyl side chains, with inverted attachment positions. For example, **4.14** and **4.15**, both contain neutral losses representing an acetate and a butyrate, indicating that **4.14** has the acetate attached to C-10 while in **4.15** has attached to C-11, with butyrate occupying the opposite position. Similarly, **4.16** incorporates the same esters as **4.3,** a pentanoate and propanoate with their positions inverted. Likewise, **4.17** and **4.18** incorporate two propanoates and two pentanoates, respectively. The two additional analogs of andrognathanols, **4.19** and **4.20**, incorporate the same esters as **4.9** and **4.10**, respectively, but with inverted positions.

4.2.5. Ecological Role of the *A. corticarius* Chemical Secretions

Previous studies on Colobognatha alkaloid secretions have hypothesized that they serve a defensive and/or pheromone role. Experimental trials with predators support the former; social behaviors of colobognath millipedes, which include forming large aggregations and brood care,

support the latter.[1,8] Many terpenoid alkaloids are actively secreted through ozopores when disturbed and a subset (e.g, polyzonimine, buzonamine, and the ischnocybines) appear to deter common predators (e.g., cockroaches, tethered flies, and ants, respectively).[8,17-19] The gosodesmines might also act as pheromones, antiparasitic, or other roles.[10]

During field collections, it was noticed that *A. corticarius* produces significant liquid when placed in a scintillation vial (**Figure 4.13A**).[3] Examining individual millipedes under the microscope confirmed secretions exuding from the ozopores upon disturbance. Analyses of captured secretions by LR-LCMS confirmed both andrognathines and andrognathanols (**Figure 4.13B**; **Table 4.10.41**).[3] Although development of *A. corticarius* remains unstudied, ozopores are visible in hatchling *B. lecontii* millipedes; secretions did appear until stadium III.[1,3] Aggregations of *A. corticarius* consisted of millipedes of different developmental stages as indicated by size (0.2–3 cm), number of rings and pigmentation. We hypothesized that adult *A. corticarius* produces terpenoid alkaloids to protect juveniles and/or eggs. To test this hypothesis, based on the presumption that adults with greater rings protect the young, we collected individual millipedes of different sizes and quantified their defensive secretions by LR-LCMS (**Figure 4.13C**). Millipede length corresponded to the number of segments, and thus the number of individual ozopores. Plotting average peak area for all alkaloids against overall millipede length revealed a positive, statistically significant linear correlation ($R^2 = 0.82$***, *** $p < 0.001$). This correlation persisted across distinct collection sites in SW Virginia. Finally, we collected millipedes across a larger geographical range: SW North Carolina, SW Virginia, and Central Alabama. All collections contained both the andrognathines and andrognathanols, albeit with some variation in relative abundance (**Figure 4.13D**). Thus, we concluded that geographical regions have no significant impact on the composition of *A. corticarius* defensive secretions.

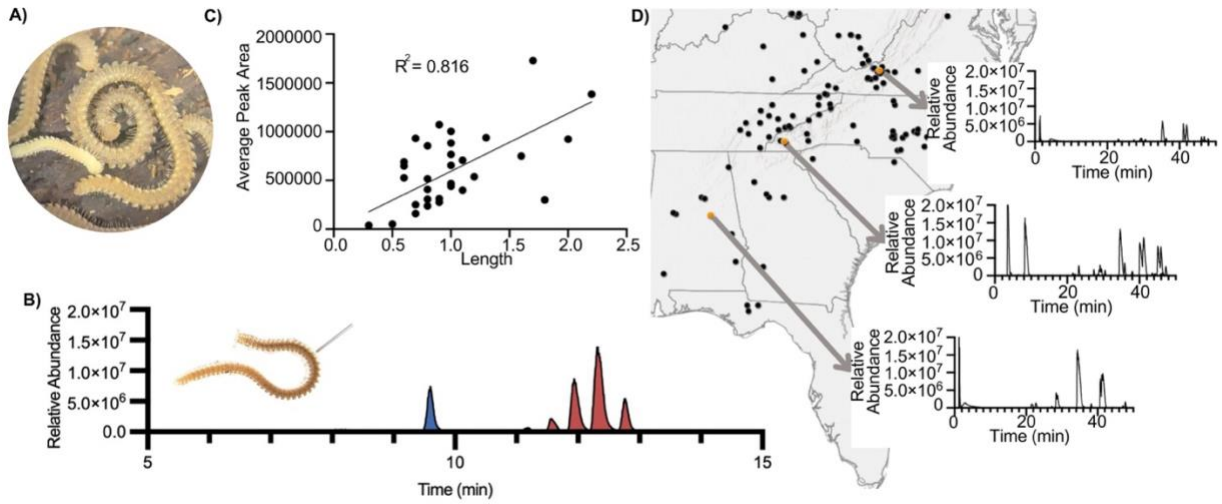

Figure 4.13. Ecological roles of andrognathines and andrognathanols. **A)** *A. corticarius* aggregation. **B)** Chromatogram of a single droplet collected from an ozopore of *A. corticarius* by capillary. The droplet contains the andrognathanols (blue) and andrognathines (red). **C)** Average peak area versus length of individual millipedes confirms a positive linear relationship (R^2 = 0.81***, *** $p < 0.001$). **D)** LCMS analysis of *A. corticarius* samples collected in distinct locations (Alabama, North Carolina and Virginia) all contain both classes of compounds and do not show major differences in the composition.

4.2.6. Biological Activity of the Andrognathines and Andrognathanols

Recent studies have shown that ischnocybines potently inhibit the σ_1R neuroreceptor (K_i 14 nM) and exhibit 100-fold selectivity over the σ_2R.[13] Due to similar structural features, we evaluated two andrognathines (**4.1** and **4.5**) and three andrognathanols (**4.9**, **4.10**, and **4.11**) against σ_1R and σ_2R in collaboration with the PDSP at UNC Chapel Hill (**Figure 4.9.61** and **Figure 4.9.62**; **Table 4.10.42** and **Table 4.10.43**). The andrognathines showed mixed results, where **4.1** exhibited marked decrease in potency against σ_1R (K_i 840 nM) but maintained a 3-fold selectivity for σ_1R over σ_2R (K_i 2100 nM), while **4.5** showed no activity against both receptors. We note that the andrognathines may have limited stability, and, possibly, both **4.1** and **4.5** have partially degraded

prior to the assay. Surprisingly, the more complex andrognathanols show no activity against both receptors (K_i > 5 μM). Structurally, the millipede alkaloids resemble the pumilotoxins, potent inhibitors of voltage-gated sodium channels (VGSCs).[27] However, **4.1** and **4.9** show no activity against two Nav receptors, Nav1.5 and 1.8, at concentrations up to 10 μM (**Table 4.10.44** and **Table 4.10.45**).

4.3. Conclusion

Millipede defensive secretions reveal a remarkable evolutionary story, with repugnatorial glands evolving over 385 million years ago, and defensive secretions having significantly diversified across the more than 12,000 known species.[28] Only Colobognatha produce terpenoid alkaloids, a structurally intriguing subset of these defensive secretions. These alkaloids remain poorly studied compared to hydrogen cyanide and oxidized aromatics. However, a recent surge in the characterizing chemistry from Colobognatha, from the order Platydesmida, reveals significant, unexplored novel chemistry. This study shows the defensive secretions of *Andrognathus*, the evolutionary sister to all other Platydesmida, and the presumed oldest genus within the order. To gain insights into the evolutionary history of terpenoid alkaloids within this order, our analytical investigations of *A. corticarius* have discovered andrognathines and andrognathanols, monoterpene alkaloids which are structurally distinct from all previously described chemistry. Andrognathanols show unique chemistry with an unprecedented 6,6,6,5-bridged heterocyclic core with seven continuous stereogenic centers. These alkaloids clearly serve an essential role for the millipedes as they are actively secreted from ozopores in the repugnatorial glands when physically agitated. The growing body of reported chemistry strongly supports a plausible common biosynthetic route that leads to all reported Platydesmida alkaloids. The discovery of the andrognathanols also contributes to revealing the terpenoid alkaloid pathway within

Platydesmida—ostensibly evolving toward simplicity, with significant loss of structural complexity later in evolutionary history of the order.

4.4. Author Information

The manuscript was written through contributions of all authors. All authors have given approval to the final version of the manuscript.

4.5. Funding Sources

This work was funded by NIH [R35 GM146740 (EM)] and Virginia Tech Startup funds (EM).

4.5.1. Notes

The authors declare no competing financial interests.

4.6. Acknowledgments

We thank the Virginia Tech NMR facility and Virginia Tech Mass Spectrometry Incubator for analytical services. Primary binding assays and K_i determinations were generously provided by the National Institute of Mental Health's Psychoactive Drug Screening Program, Contract # HHSN-271-2018-00023-C (NIMH PDSP). The NIMH PDSP is Directed by Bryan L. Roth at the University of North Carolina at Chapel Hill and Project Officer Jamie Driscoll at NIMH, Bethesda MD, USA. This research was funded in part by the Intramural Research Program of the NIH, National Cancer Institute, Center for Cancer Research and with federal funds from the National Cancer Institute, National Institutes of Health under contract HHSN261200800001E. We thank Prof. Tappey Jones for helping us uncover the mystery of millipedes. We also thank Benjamin Blackburn, Lois Kyei, Karla Piedl, Rose Campbell, Arden Hatch and Joe Barton, Lillian Banks, Alan Banks, Lynn Banks, Abigail Stanley, Tierney Liriano, Kim Mevers, and Anne Jones who assisted with millipede collection.

4.7. Experimental Methods

4.7.1. General Experimental Procedures

NMR spectra were recorded with *d_6*-DMSO with the residual solvent peak as an internal standard (δ_C 39.5, δ_H 2.50) on Bruker Advance III 600 MHz instrument equipped with a triple resonance inverse (CP-TCI) Prodigy N2 cooled CryoProbe (600 and 150 MHz for ^{1}H and ^{13}C NMR, respectively). LR-LCMS data was obtained using an Agilent 1200 series HPLC system equipped with a photo-diode array detector and a Thermo LTQ mass spectrometer. HR-ESI-MS was carried out using a Shimadzu LC-q-TOF Mass Spectrometer equipped with a HPLC system. HPLC purifications were carried out using Agilent 1200 series or 1260 Infinity II HPLC systems (Agilent Technologies) equipped with a photodiode array detector. All solvents were of HPLC quality.

4.7.2. Millipede Collections

The millipedes were collected from the underside of decaying logs underneath trees, often feeding on fungus, and preserved in methanol, which was then removed, replaced and dried down for a crude extract. The locations collected are shown in **Table 4.7.28**.

Table 4.7.28. *Andrognathus corticarius* Collections

Millipede	Location	Coordinates	Elevation	Date
A. corticarius	Virginia, Montgomery Co., Blacksburg, Virginia Tech, Stadium Woods	37.22124, -80.41586	Elev. 647 m	29 June 2022
A. corticarius	Virginia, Montgomery Co., Caldwell Fields Campground	37.33553, -80.32430	Elev. 521 m	25 April 2023
A. corticarius	Virginia, Montgomery Co., Blacksburg, Virginia Tech, Stadium Woods	37.22124, -80.41586	Elev. 647 m	18 May 2023
A. corticarius	Virginia, Montgomery Co., Blacksburg, Virginia Tech, Stadium Woods	37.22124, -80.41586	Elev. 647 m	18 May 2023
A. corticarius	Virginia, Montgomery Co., Pandapas Pond	37.28257, -80.46991	Elev. 672 m	19 July 2023
A. corticarius (single millipedes)	Virginia, Montgomery Co., Blacksburg, Virginia Tech, Stadium Woods	37.22124, -80.41586	Elev. 647 m	09 August 2023
A. corticarius (single millipedes)	Virginia, Montgomery Co., Pandapas Pond	37.28257, -80.46991	Elev. 672 m	09 August 2023
A. corticarius	Talladega County, Alabama, Sylaward Trail at Lake Howard	33.19511, -86.19370	Elev. 187 m	24 September 2023
A. corticarius	Swain County, North Carolina, Findley Falls Trailhead	35.28291, -83.67422	Elev. 621 m	06 July 2023

4.7.3. Extraction and Purifcation of the Andrognathines and Andrognathanols from *A. corticarius*

The millipedes were extracted using MeOH and the combined organic material was dried down under vacuum. The extract was then resuspended in 1:1 MeCN/H_2O and separated using reverse-phase high performance liquid chromatography (RP-HPLC) equipped with a Phenomenex 4 µm Hydro semi-preparative column (250 × 10 mm) under the following conditions. Holding 20% MeCN + 0.1% formic acid (FA)/80% H_2O + 0.1% FA for 5 min then a linear gradient to 60% MeCN + 0.1% FA/40% H_2O + 0.1% FA over 45 min at a flow rate of 3 mL/min to yield pure andrognathines and andrognathanols.

*Andrognathine A (**4.1**):* amorphous solid; $[\alpha]^{23}_{D}$ +23.6 (*c* 0.015, MeOH); ^{1}H NMR (600 MHz, d_6-DMSO) δ 5.45 (m, *J* = 9.3, CH_2, H-11), 5.38 (m, *J* = 9.3, CH, H-10), 5.10 (s, CH_2, H-14b), 5.04 (s, CH_2, H-14a), 2.94 (m, CH_2, H-5b), 2.91 (m, CH_2, H-4b), 2.27 (m, CH_2, H-21b), 2.25 (m, CH_2, H-16b), 2.22 (m, CH_2, H-21a), 2.21 (m, CH_2, H-16a), 2.03 (m, CH_2, H-7b), 1.96 (m, CH_2, H-5a), 1.85 (m, CH_2, H-4a), 1.76 (m, *J* = 10.2, CH, H-8), 1.70 (s, CH_3, H-13), 1.65 (m, CH_2, H-6), 1.58 (m, CH_2, H-3b), 1.53 (m, CH_2, H-7a), 1.53 (m, CH_2, H-22), 1.45 (m, CH_2, H-17), 1.24 (m, CH_2, H-18), 1.21 (m, CH, H-2), 1.21 (m, CH_2, H-3a), 1.16 (m, CH, H-9), 1.00 (d, *J* =5.2, CH_3, H-1), 0.87 (m, CH_3, H-19), 0.86 (m, CH_3, H-23); ^{13}C NMR (125 MHz, d_6-DMSO) δ 172.3 (C, C-15), 171.8 (C, C-20), 139.9 (C, C-12), 118.1 (CH_2, C-14b), 118.1 (CH_2, C-14a), 76.1 (CH_2, C-11), 70.1 (CH, C-10), 64.3 (CH, C-8), 53.1 (CH_2, C-5b), 53.1 (CH_2, C-5a), 51.8 (CH_2, C-4b), 51.8 (CH_2, C-4a), 47.1 (CH, C-9), 35.3 (CH_2, C-21b), 35.3 (CH_2, C-21a), 34.1 (CH_2, C-3b), 34.1 (CH_2, C-3a), 33.2 (CH_2, C-16b), 33.2 (CH_2, C-16a), 32.5 (CH, C-2), 29.7 (CH_2, C-7b), 29.7 (CH_2, C-7a), 26.5 (CH_2, C-17), 21.9 (CH_3, C-23), 21.6 (CH_2, C-18), 20.5 (CH_2, C-6), 19.8 (CH_3, C-1), 17.9 (CH_2, C-22), 17.5 (CH_3, C-13), 13.3 (CH_3, C-19); ESI MS/MS (q-TOF) *m/z* 394.29538 ($C_{23}H_{39}NO_4$), 306.24292 ($C_{19}H_{31}NO_2$), 292.22729 ($C_{18}H_{29}NO_2$), 222.18568 ($C_{14}H_{23}NO$), 204.17494 ($C_{14}H_{21}N$), 138.12798 ($C_9H_{15}N$); HRESIMS $[M+H]^+$ *m/z* 394.29538 (calcd. $C_{23}H_{39}NO_4$ $[M+H]^+$ 394.29519, Δ 0.49).

*Andrognathine B (**4.2**):* amorphous solid; ^{1}H NMR (600 MHz, d_6-DMSO) δ 5.47 (d, *J* = 9.7, CH, H-11), 5.38 (d, *J* = 9.7, CH, H-10), 5.11 (s, CH_2, H-14b), 5.05 (s, CH_2, H-14a), 2.9 (m, CH_2, H-5b), 2.88 (m, CH_2, H-4b), 2.27 (m, CH_2, H-16b), 2.27 (m, CH_2, H-20b), 2.21 (m, CH_2, H-16a), 2.21 (m, CH_2, H-20a), 2.02 (m, CH_2, H-7b), 1.91 (m, CH_2, H-5a), 1.79 (m, CH_2, H-4a), 1.71 (s, CH_3, H-13), 1.68 (m, CH, H-8), 1.63 (m, CH_2, H-6), 1.58 (m, CH_2, H-3b), 1.51 (m, CH_2, H-7a), 1.51 (m, CH_2, H-17), 1.51 (m, CH_2, H-21), 1.20 (m, CH, H-2), 1.20 (m, CH_2, H-3a), 1.12 (m, CH,

H-9), 1.01 (d, J = 5.2, CH_3, H-1), 0.87 (m, CH_3, H-18), 0.87 (m, CH_3, H-22); ^{13}C NMR (125 MHz, d_6-DMSO) δ 171.8 (C, C-15), 171.8 (C, C-19), 140.0 (C, C-12), 118.1 (CH_2, C-14a), 118.1 (CH_2, C-14b), 75.9 (CH, C-11), 70.1 (CH, C-10), 64.1 (CH, C-8), 53.2 (CH_2, C-5a), 53.2 (CH_2, C-5b), 51.8 (CH_2, C-4a), 51.8 (CH_2, C-4b), 47.1 (CH, C-9), 35.2 (CH_2, C-16a), 35.2 (CH_2, C-16b), 35.2 (CH_2, C-20a), 35.2 (CH_2, C-20b), 34.2 (CH_2, C-3a), 34.2 (CH_2, C-3b), 32.5 (CH, C-2), 29.7 (CH_2, C-7a), 29.7 (CH_2, C-7b), 20.4 (CH_2, C-6), 19.7 (CH_3, C-1), 17.7 (CH_2, C-17), 17.7 (CH_2, C-21), 17.5 (CH_3, C-13), 13.2 (CH_3, C-18), 13.2 (CH_3, C-22; ESI MS/MS (q-TOF) *m/z* 380.28009 ($C_{22}H_{37}NO_4$), 292.22739 ($C_{18}H_{29}NO_2$), 222.18581 ($C_{14}H_{23}NO$), 204.1752 ($C_{14}H_{21}N$), 138.12822 ($C_9H_{15}N$); HRESIMS $[M+H]^+$ *m/z* 380.28009 (calcd. $C_{22}H_{37}NO_4$ $[M+H]^+$ 380.27954, Δ 1.46).

*Andrognathine C (**4.3**):* amorphous solid; $[\alpha]^{23}_D$ +4.67 (c 0.015, MeOH); ^1H NMR (600 MHz, d_6-DMSO) 5.47 (d, J = 8.4, CH, H-11), 5.37 (d, J = 8.4, CH, H-10), 5.10 (s, CH_2, H-14b), 5.04 (s, CH_2, H-14a), 2.90 (m, CH_2, H-5b), 2.87 (m, CH_2, H-4b), 2.30 (m, CH_2, H-16b), 2.26 (m, CH_2, H-16a), 2.26 (m, CH_2, H-20), 2.02 (m, CH_2, H-7b), 1.90 (m, CH_2, H-5a), 1.79 (m, CH_2, H-4a), 1.71 (s, CH_3, H-13), 1.68 (m, CH, H-8), 1.64 (m, CH_2, H-6), 1.57 (m, CH_2, H-3b), 1.51 (m, CH_2, H-7a), 1.51 (m, CH_2, H-22), 1.45 (m, CH_2, H-21), 1.20 (m, CH, H-2), 1.20 (m, CH_2, H-3a), 1.12 (t, J = 9.3, CH, H-9), 1.02 (m, CH_3, H-17), 1.00 (m, CH_3, H-1). ^{13}C NMR (125 MHz, d_6-DMSO) δ 173.2 (C, C-15), 171.9 (C, C-19), 140.0 (C, C-12), 118.1 (CH_2, C-14b), 118.1 (CH_2, C-14a), 75.9 (CH, C-11), 70.1 (CH, C-10), 64.1 (CH, C-8), 53.2 (CH_2, C-5b), 53.2 (CH_2, C-5a), 51.7 (CH_2, C-4b), 51.7 (CH_2, C-4a), 47.1 (CH, C-9), 34.1 (CH_2, C-3b), 34.1 (CH_2, C-3a), 33.1 (CH_2, C-20), 32.4 (CH, C-2), 29.6 (CH_2, C-7b), 29.6 (CH_2, C-7a), 26.7 (CH_2, C-16b), 26.7 (CH_2, C-16a), 26.3 (CH_2, C-21), 20.4 (CH_2, C-6), 19.6 (CH_3, C-1), 17.7 (CH_2, C-22), 17.5 (CH_3, C-13), 13.3 (CH_3, C-23), 8.8 (CH_3, C-17); ESI MS/MS (q-TOF) *m/z* 380.28061 ($C_{22}H_{37}NO_4$), 306.24353 ($C_{19}H_{31}NO_2$),

278.21259 ($C_{17}H_{27}NO_2$), 222.18591 ($C_{14}H_{23}NO$), 204.17563 ($C_{14}H_{21}N$), 138.12837 ($C_9H_{15}N$); HRESIMS $[M+H]^+$ *m/z* 380.28061 (calcd. $C_{22}H_{37}NO_4$ $[M+H]^+$ 380.27954, Δ 2.83).

*Andrognathine D (**4.4**):* amorphous solid; ^{1}H NMR (600 MHz, d_6-DMSO) δ 5.46 (d, *J* = 9.0, CH, H-11), 5.37 (d, *J* = 9.0, CH, H-10), 5.10 (s, CH_2, H-14b), 5.04 (s, CH_2, H-14a), 2.90 (m, CH_2, H-5a), 2.87 (m, CH_2, H-4a), 2.27 (m, CH_2, H-20b), 2.26 (m, CH_2, H-16b), 2.23 (m, CH_2, H-16a), 2.22 (m, CH_2, H-20a), 1.92 (m, CH_2, H-5b), 1.80 (m, CH_2, H-4b), 1.71 (s, CH_3, H-13), 1.67 (m, CH, H-8), 1.63 (m, CH_2, H-6), 1.57 (m, CH_2, H-3), 1.52 (m, CH_2, H-7), 1.52 (q, *J* = 7.1, CH_2, H-17), 1.46 (t, *J* = 7.7, CH_2, H-21), 1.27 (m, CH_2, H-22), 1.20 (m, CH, H-2), 1.13 (m, CH, H-9), 1.01 (m, CH_3, H-1), 0.87 (m, CH_3, H-18), 0.85 (m, CH_3, H-23); ^{13}C NMR (600 MHz, d_6-DMSO) δ 172.2 (C, C-15), 171.8 (C, C-19), 140.4 (C, C-12), 117.9 (CH_2, C-14b), 117.9 (CH_2, C-14a), 75.9 (CH, C-11), 70.3 (CH, C-10), 64.1 (CH, C-8), 53.1 (CH_2, C-5a), 53.1 (CH_2, C-5b), 51.8 (CH_2, C-4a), 51.8 (CH_2, C-4b), 47.1 (CH, C-9), 35.4 (CH_2, C-16b), 35.4 (CH_2, C-16a), 34.3 (CH_2, C-3), 33.2 (CH_2, C-20b), 33.2 (CH_2, C-20a), 32.5 (CH, C-2), 26.3 (CH_2, C-7), 26.2 (CH_2, C-21), 21.7 (CH_3, C-18), 21.2 (CH_2, C-22), 20.5 (CH_2, C-6), 19.6 (CH_3, C-1), 17.6 (CH_3, C-13), 17.5 (CH_2, C-17), 13.1 (CH_3, C-23); ESI MS/MS (q-TOF) *m/z* 394.29605 ($C_{23}H_{39}NO_4$), 306.24365 ($C_{19}H_{31}NO_2$), 292.22827 ($C_{18}H_{29}NO_2$), 222.18607 ($C_{14}H_{23}NO$), 204.17554 ($C_{14}H_{21}N$), 138.12833 ($C_9H_{15}N$); HRESIMS $[M+H]^+$ *m/z* 394.29605 (calcd. $C_{23}H_{39}NO_4$ $[M+H]^+$ 394.29519, Δ 2.20).

*Andrognathine E (**4.5**):* amorphous solid; ^{1}H NMR (600 MHz, d_6-DMSO) δ 5.46 (d, *J* = 9.2, CH, H-11), 5.38 (d, *J* = 9.2, CH, H-10), 5.10 (s, CH_2, H-14b), 5.04 (s, CH_2, H-14a), 2.90 (m, CH_2, H-5b), 2.87 (m, CH_2, H-4b), 2.27 (m, CH_2, H-16a), 2.22 (m, CH_2, H-16b), 2.15 (m, CH_2, H-20b), 2.11 (m, CH_2, H-20a), 1.90 (m, CH_2, H-5a), 1.79 (t, *J* = 10.9, CH_2, H-4a), 1.70 (s, CH_3, H-13), 1.68 (m, CH, H-8), 1.62 (m, CH_2, H-6), 1.57 (d, *J* = 9.1, CH_2, H-3b), 1.52 (m, CH_2, H-7), 1.52 (m, CH_2, H-17), 1.21 (m, CH_2, H-3a), 1.20 (m, CH, H-2), 1.13 (m, CH, H-9), 1.01 (d, *J* = 5.4, CH_3, H-

1), 0.88 (m, CH_3, H-18), 0.88 (m, CH_3, H-21); ^{13}C NMR (125 MHz, d_6-DMSO) δ 172.2 (C, C-19), 171.2 (C, C-15), 139.9 (C, C-12), 118.1 (CH_2, C-14b), 118.1 (CH_2, C-14a), 76.1 (CH, C-11), 70.3 (CH, C-10), 64.3 (CH, C-8), 53.3 (CH_2, C-5b), 53.3 (CH_2, C-5a), 51.9 (CH_2, C-4b), 51.9 (CH_2, C-4a), 47.3 (CH, C-9), 42.6 (CH_2, C-20b), 42.6 (CH_2, C-20a), 35.4 (CH_2, C-16a), 35.4 (CH_2, C-16b), 34.3 (CH_2, C-3b), 34.3 (CH_2, C-3a), 32.6 (CH, C-2), 21.5 (CH_3, C-21), 20.5 (CH_2, C-6), 19.8 (CH_3, C-1), 17.9 (CH_2, C-7), 17.6 (CH_3, C-13), 17.6 (CH_2, C-17), 13.5 (CH_3, C-18); ESI MS/MS (q-TOF) *m/z* 366.26437 ($C_{21}H_{35}NO_4$), 292.22791 ($C_{18}H_{29}NO_2$), 278.21185 ($C_{17}H_{27}NO_2$), 222.18581 ($C_{14}H_{23}NO$), 204.1752 ($C_{14}H_{21}N$), 138.12834 ($C_9H_{15}N$); HRESIMS $[M+H]^+$ *m/z* 366.26437 (calcd. $C_{21}H_{35}NO_4$ $[M+H]^+$ 366.26389, Δ 1.34).

*Andrognathine F (***4.6***):* amorphous solid; ^1H NMR (600 MHz, d_6-DMSO) δ 5.47 (m, CH, H-11), 5.36 (m, CH, H-10), 5.11 (s, CH_2, H-14b), 5.05 (s, CH_2, H-14a), 2.90 (m, CH_2, H-5b), 2.87 (m, CH_2, H-4b), 2.27 (m, CH_2, H-16), 2.27 (m, CH_2, H-19b), 2.20 (m, CH_2, H-19a), 2.02 (m, CH_2, H-7b), 1.91 (m, CH_2, H-5a), 1.80 (m, CH_2, H-4a), 1.70 (s, CH_3, H-13), 1.68 (m, CH, H-8), 1.63 (m, CH_2, H-6), 1.57 (m, CH_2, H-3b), 1.50 (m, CH_2, H-7a), 1.50 (m, CH_2, H-20), 1.20 (m, CH, H-2), 1.20 (m, CH_2, H-3a), 1.12 (m, CH, H-9), 1.01 (m, CH_3, H-1), 1.01 (m, CH_3, H-17), 0.85 (m, CH_3, H-21); ^{13}C NMR (125 MHz, d_6-DMSO) δ 173.1 (C, C-15), 171.7 (C, C-18), 139.9 (C, C-12), 118.1 (CH_2, C-14a), 118.1 (CH_2, C-14b), 76.1 (CH, C-11), 70.3 (CH, C-10), 64.1 (CH, C-8), 53.2 (CH_2, C-5a), 53.2 (CH_2, C-5b), 52.0 (CH_2, C-4a), 52.0 (CH_2, C-4b), 47.3 (CH, C-9), 35.3 (CH_2, C-19a), 35.3 (CH_2, C-19b), 34.4 (CH_2, C-3a), 34.4 (CH_2, C-3b), 32.5 (CH, C-2), 29.9 (CH_2, C-7a), 29.9 (CH_2, C-7b), 26.9 (CH_2, C-16), 20.5 (CH_2, C-6), 19.8 (CH_3, C-1), 17.9 (CH_2, C-20), 17.7 (CH_3, C-13), 13.5 (CH_3, C-21), 9.1 (CH_3, C-17); ESI MS/MS (q-TOF) *m/z* 366.26544 ($C_{21}H_{35}NO_4$), 292.22799 ($C_{18}H_{29}NO_2$), 278.21147 ($C_{17}H_{27}NO_2$), 222.18539 ($C_{14}H_{23}NO$), 204.17459 ($C_{14}H_{21}N$),

138.12834 ($C_9H_{15}N$); HRESIMS $[M+H]^+$ *m/z* 366.26544 (calcd. $C_{21}H_{35}NO_4$ $[M+H]^+$ 366.26389, Δ 4.26).

*Andrognathanol A (***4.9***):* amorphous solid; $[\alpha]^{23}_D$ +31.7 (*c* 0.015, MeOH); ^{1}H NMR (600 MHz, *d*$_6$-DMSO) δ 4.92 (s, CH, H-6), 4.60 (d, *J* = 4.4, CH, H-11), 4.01 (sext, *J* = 6.4, CH, H-21), 3.60 (d, *J* = 5.5, CH, H-1), 2.94 (d, *J* = 10.7, CH_2, H-3b), 2.55 (d, *J* = 12.0, CH_2, H-4b), 2.37 (m, CH_2, H-20), 2.29 (q, *J* = 7.3, CH_2, H-17), 2.15 (m, CH_2, H-3a), 2.13 (m, CH_2, H-4a), 2.01 (q, *J* = 4.3, CH, H-10), 1.90 (m, CH, H-8), 1.90 (m, CH_2, H-14b), 1.73 (m, CH_2, H-13b), 1.70 (m, CH, H-2), 1.66 (m, CH_2, H-5b), 1.53 (m, CH_2, H-7b), 1.49 (m, CH, H-9), 1.43 (m, CH_2, H-7a), 1.30 (pent, *J* = 6.7, CH_2, H-14a), 1.23 (m, CH_2, H-5a), 1.14 (dd, *J* = 8.6 and 12.5, CH_2, H-13a), 1.10 (d, *J* = 6.0, CH_3, H-22), 1.01 (t, *J* = 7.4, CH_3, H-18), 0.78 (s, CH_3, H-15); ^{13}C NMR (125 MHz, *d*$_6$-DMSO) δ 172.9 (C, H-16), 171.1 (C, H-19), 78.0 (CH, H-11), 75.4 (CH, H-1), 67.7 (CH, H-6), 63.2 (CH, H-21), 57.6 (CH, H-8), 55.4 (CH_2, H-3a), 55.4 (CH_2, H-3b), 49.5 (CH_2, H-4a), 49.5 (CH_2, H-4b), 44.1 (CH_2, H-20), 43.4 (CH, H-2), 42.6 (C, H-12), 40.8 (CH, H-10), 32.0 (CH_2, H-7a), 32.0 (CH_2, H-7b), 30.6 (CH_2, H-13a), 30.6 (CH_2, H-13b), 30.3 (CH, H-9), 28.8 (CH_2, H-5a), 28.8 (CH_2, H-5b), 26.9 (CH_2, H-17), 23.2 (CH_3, H-22), 19.4 (CH_3, H-15), 16.9 (CH_2, H-14a), 16.9 (CH_2, H-14b), 8.8 (CH_3, H-18); ESI MS/MS (q-TOF) *m/z* 410.25436 ($C_{22}H_{35}NO_6$), 366.2283 ($C_{20}H_{31}NO_5$), 336.21802 ($C_{19}H_{29}NO_4$), 306.27502 ($C_{18}H_{27}NO_4$), 292.19098 ($C_{17}H_{25}NO_3$), 250.18091 ($C_{14}H_{23}NO_2$), 232.1711 ($C_{15}H_{21}NO$); HRESIMS $[M+H]^+$ *m/z* 410.25436 (calcd. $C_{22}H_{35}NO_6$ $[M+H]^+$ 410.25371, Δ 1.59).

*Andrognathanol B (***4.10***):* amorphous solid; $[\alpha]^{23}_D$ +19.2 (*c* 0.015, MeOH); ^{1}H NMR (600 MHz, *d*$_6$-DMSO) δ 4.91 (s, CH, H-6), 4.60 (d, *J* = 4.6, CH, H-11), 3.76 (m, CH, H-21), 3.60 (d, *J* = 5.7, CH, H-1), 2.94 (d, *J* = 12.4, CH_2, H-3b), 2.56 (m, CH_2, H-4b), 2.41 (d, *J* = 5.6, CH_2, H-20b), 2.31 (m, CH_2, H-20a), 2.28 (m, CH_2, H-17), 2.16 (m, CH_2, H-3a), 2.14 (m, CH_2, H-4a), 2.02 (m, CH,

H-10), 1.91 (m, CH, H-8), 1.89 (m, CH_2, H-14b), 1.72 (m, CH_2, H-13b), 1.70 (m, CH, H-2), 1.66 (m, CH_2, H-5), 1.54 (m, CH_2, H-7b), 1.50 (m, CH, H-9), 1.43 (m, CH_2, H-7a), 1.36 (m, CH_2, H-22), 1.29 (m, CH_2, H-14a), 1.14 (m, CH_2, H-13a), 1.01 (t, J = 7.4, CH_3, H-18), 0.85 (t, J = 7.4, CH_3, H-23), 0.78 (s, CH_3, H-15); ^{13}C NMR (125 MHz, d_6-DMSO) δ 172.9 (C, C-16), 171.3 (C, C-19), 78.1 (CH, C-11), 75.5 (CH, C-1), 68.3 (CH, C-21), 67.4 (CH, C-6), 57.7 (CH, C-8), 55.4 (CH_2, C-3a), 55.4 (CH_2, C-3b), 49.6 (CH_2, C-4a), 49.6 (CH_2, C-4b), 43.5 (CH, C-2), 42.4 (C, C-12), 42.1 (CH_2, C-20a), 42.1 (CH_2, C-20b), 40.8 (CH, C-10), 32.1 (CH_2, C-7a), 32.1 (CH_2, C-7b), 30.6 (CH_2, C-13a), 30.6 (CH_2, C-13b), 30.3 (CH, C-9), 29.5 (CH_2, C-22), 28.8 (CH_2, C-5), 26.9 (CH_2, C-17), 19.4 (CH_3, C-15), 16.9 (CH_2, C-14a), 16.9 (CH_2, C-14b), 9.6 (CH_3, C-23), 8.8 (CH_3, C-18); ESI MS/MS (q-TOF) *m/z* 424.26984 ($C_{23}H_{37}NO_6$), 366.22775 ($C_{20}H_{31}NO_5$), 350.23306 ($C_{20}H_{31}NO_4$), 324.21756 ($C_{18}H_{29}NO_4$), 306.20706 ($C_{18}H_{27}NO_4$), 292.19104 ($C_{17}H_{25}NO_3$), 250.18045 ($C_{14}H_{23}NO_2$), 232.16995 ($C_{15}H_{21}NO$); HRESIMS $[M+H]^+$ *m/z* 424.30545 (calcd. $C_{23}H_{37}NO_6$ $[M+H]^+$ 424.26936, Δ 0.77 ppm).

*Andrognathanol C (***4.11***):* amorphous solid; $[\alpha]^{23}_D$ +19.2 (*c* 0.015, MeOH); ^{1}H NMR (600 MHz, d_6-DMSO) δ 4.91 (s, CH, H-6), 4.63 (d, J = 4.7, CH, H-11), 3.60 (d, J = 5.9, CH, H-1), 2.92 (d, J = 12.1, CH_2, H-3b), 2.54 (m, CH_2, H-4b), 2.29 (q, J = 7.5, CH_2, H-21), 2.21 (m, CH_2, H-17), 2.15 (m, CH_2, H-3a), 2.13 (m, CH_2, H-4a), 2.02 (m, CH, H-10), 1.97 (m, CH, H-18), 1.91 (m, CH_2, H-14b), 1.90 (m, CH, H-8), 1.71 (m, CH_2, H-13b), 1.70 (m, CH, H-2), 1.67 (m, CH_2, H-5b), 1.54 (m, CH_2, H-7b), 1.46 (m, CH, H-9), 1.43 (m, CH, H-7a), 1.30 (m, CH_2, H-14a), 1.23 (m, CH_2, H-5a), 1.15 (m, CH_2, H-13a), 1.01 (t, J = 7.5, CH_3, H-22), 0.91 (d, J = 6.6, CH_3, H-19), 0.78 (s, CH_3, H-15); ^{13}C NMR (125 MHz, d_6-DMSO) δ 172.9 (C, C-20), 172.1 (C, C-16), 78.1 (CH, C-11), 75.5 (CH, C-1), 67.4 (CH, C-6), 57.6 (CH, C-8), 55.4 (CH_2, C-3b), 55.4 (CH_2, C-3a), 49.5 (CH_2, C-4b), 49.5 (CH_2, C-4a), 43.6 (CH, C-2), 42.7 (CH_2, C-17), 42.4 (C, C-12), 40.9 (CH, C-10), 32.1 (CH_2,

C-7b), 32.1 (CH, C-7a), 30.6 (CH_2, C-13b), 30.6 (CH_2, C-13a), 30.5 (CH, C-9), 28.7 (CH_2, C-5b), 28.7 (CH_2, C-5a), 26.9 (CH_2, C-21), 25.1 (CH, C-18), 21.9 (CH_3, C-19), 19.5 (CH_3, C-15), 16.9 (CH_2, C-14b), 16.9 (CH_2, C-14a), 8.8 (CH_3, C-22); ESI MS/MS (q-TOF) *m/z* 408.2746 ($C_{23}H_{37}NO_5$), 334.23767 ($C_{20}H_{31}NO_3$), 306.20627 ($C_{18}H_{27}NO_4$), 250.17923 ($C_{14}H_{23}NO_2$), 232.1687 ($C_{15}H_{21}NO$); HRESIMS $[M+H]^+$ *m/z* 408.2746 (calcd. $C_{23}H_{37}NO_5$ $[M+H]^+$ 408.27445, Δ 0.36).

*Andrognathanol D (***4.12***):* amorphous solid; $[\alpha]^{23}_D$ +19.2 (*c* 0.015, MeOH); ^{1}H NMR (600 MHz, *d*$_6$-DMSO) NMR (600 MHz, *d*$_6$-DMSO) δ 4.91 (s, CH, H-6), 4.62 (d, *J* = 4.6, CH, H-11), 3.60 (d, *J* = 6.1, CH, H-1), 2.92 (d, *J* = 11.7, CH_2, H-3b), 2.55 (m, CH_2, H-4b), 2.29 (q, *J* = 7.7, CH_2, H-17), 2.21 (dd, *J* = 4.5 and 2.4, CH_2, H-20), 2.16 (m, CH_2, H-3a), 2.13 (m, CH_2, H-4a), 2.01 (m, CH, H-10), 1.99 (m, CH, H-21), 1.91 (m, CH, H-8), 1.91 (m, CH_2, H-14b), 1.70 (m, CH, H-2), 1.70 (m, CH_2, H-13b), 1.66 (m, CH_2, H-5b), 1.52 (m, CH_2, H-7b), 1.45 (m, CH, H-9), 1.43 (m, CH_2, H-7a), 1.30 (m, CH_2, H-14a), 1.22 (m, CH_2, H-5a), 1.15 (m, CH_2, H-13a), 1.01 (t, *J* = 7.7, CH, H-18), 0.90 (d, *J* = 6.8, CH_3, H-22), 0.78 (s, CH_3, H-15); ^{13}C NMR (125 MHz, *d*$_6$-DMSO) δ 172.9 (C, C-16), 172.2 (C, C-19), 78.2 (CH, C-11), 75.6 (CH, C-1), 67.5 (CH, C-6), 57.8 (CH, C-8), 55.6 (CH_2, C-3b), 55.6 (CH_2, C-3a), 49.6 (CH_2, C-4b), 49.6 (CH_2, C-4a), 43.6 (CH, C-2), 42.9 (CH_2, C-20), 42.4 (C, C-12), 41.0 (CH, C-10), 32.2 (CH_2, C-7b), 32.2 (CH_2, C-7a), 30.7 (CH_2, C-13b), 30.7 (CH, C-9), 30.7 (CH_2, C-13a), 28.8 (CH_2, C-5b), 28.8 (CH_2, C-5a), 27.0 (CH_2, C-17), 25.2 (CH, C-21), 22.0 (CH_3, C-22), 19.6 (CH_3, C-15), 17.0 (CH_2, C-14b), 17.0 (CH_2, C-14a), 9.0 (CH, C-18); ESI MS/MS (q-TOF) *m/z* 408.27481 ($C_{23}H_{37}NO_5$), 334.23822 ($C_{20}H_{31}NO_3$), 306.20439 ($C_{18}H_{27}NO_4$), 250.17923 ($C_{14}H_{23}NO_2$), 232.16912 ($C_{15}H_{21}NO$); HRESIMS $[M+H]^+$ *m/z* 408.27466 (calcd. $C_{23}H_{37}NO_5$ $[M+H]^+$ 408.27445, Δ 0.51 ppm).

*Andrognathine G (**4.13**):* ESI MS/MS (q-TOF) *m/z* 240.19685 ($C_{14}H_{25}NO_2$), 184.13312 ($C_{10}H_{17}NO_2$), 168.13872 ($C_{10}H_{17}NO$); HRESIMS $[M+H]^+$ *m/z* 240.19685 (calcd. $C_{14}H_{25}NO_2$ $[M+H]^+$ 240.19581, Δ 4.38).

*Andrognathine H (**4.14**):* ESI MS/MS (q-TOF) *m/z* 352.24725 ($C_{20}H_{33}NO_4$), 292.22632 ($C_{18}H_{29}NO_2$), 264.19669 ($C_{16}H_{25}NO_2$), 222.18658 ($C_{14}H_{23}NO$), 204.17494 ($C_{14}H_{21}N$); HRESIMS $[M+H]^+$ *m/z* 352.24725 (calcd. $C_{20}H_{33}NO_4$ $[M+H]^+$ 352.24824, Δ 2.79).

*Andrognathine I (**4.15**):* ESI MS/MS (q-TOF) *m/z* 352.2486 ($C_{20}H_{33}NO_4$), 292.22632 ($C_{18}H_{29}NO_2$), 264.19757 ($C_{16}H_{25}NO_2$), 222.18607 ($C_{14}H_{23}NO$), 204.17494 ($C_{14}H_{21}N$); HRESIMS $[M+H]^+$ *m/z* 352.2486 (calcd. $C_{20}H_{33}NO_4$ $[M+H]^+$ 352.24824, Δ 1.03).

*Andrognathaine J (**4.16**):* ESI MS/MS (q-TOF) *m/z* 380.28046 ($C_{22}H_{37}NO_4$), 306.24454 ($C_{19}H_{31}NO_2$), 278.21234 ($C_{17}H_{27}NO_2$), 222.18643 ($C_{14}H_{23}NO$), 204.17543 ($C_{14}H_{21}N$), 138.12837 ($C_9H_{15}N$); HRESIMS $[M+H]^+$ *m/z* 380.28046 (calcd. $C_{22}H_{37}NO_4$ $[M+H]^+$ 380.27954, Δ 2.43).

*Andrognathaine K (**4.17**):* ESI MS/MS (q-TOF) *m/z* 352.24896 ($C_{20}H_{33}NO_4$), 278.21033 ($C_{17}H_{27}NO_2$), 222.18517 ($C_{14}H_{23}NO$), 204.17523 ($C_{14}H_{21}N$); HRESIMS $[M+H]^+$ *m/z* 352.24896 (calcd. $C_{20}H_{33}NO_4$ $[M+H]^+$ 352.24824, Δ 2.07).

*Andrognathaine L (**4.18**):* ESI MS/MS (q-TOF) *m/z* 408.31137 ($C_{24}H_{41}NO_4$), 306.24292 ($C_{19}H_{31}NO_2$), 222.18581 ($C_{14}H_{23}NO$), 204.17517 ($C_{14}H_{21}N$); HRESIMS $[M+H]^+$ *m/z* 408.31137 (calcd. $C_{24}H_{41}NO_4$ $[M+H]^+$ 408.31084, Δ 1.31),

*Andrognathanol E (**4.19**):* ESI MS/MS (q-TOF) *m/z* 410.25534 ($C_{22}H_{35}NO_6$), 366.22906 ($C_{20}H_{31}NO_5$), 336.2178 ($C_{19}H_{29}NO_4$), 306.20502 ($C_{18}H_{27}NO_4$), 292.19177 ($C_{17}H_{25}NO_3$), 250.17987 ($C_{14}H_{23}NO_2$), 232.16859 ($C_{15}H_{21}NO$); HRESIMS $[M+H]^+$ *m/z* 410.25534 (calcd. $C_{22}H_{35}NO_6$ $[M+H]^+$ 410.25371, Δ 3.97).

*Andrognathanol F (**4.20**):* ESI MS/MS (q-TOF) *m/z* 424.27097 ($C_{23}H_{37}NO_6$), 366.22751 ($C_{20}H_{31}NO_5$), 350.23404 ($C_{20}H_{31}NO_4$), 324.21906 ($C_{18}H_{29}NO_4$), 306.07608 ($C_{18}H_{27}NO_4$), 292.19171 ($C_{17}H_{25}NO_3$), 250.18159 ($C_{14}H_{23}NO_2$), 232.16801 ($C_{15}H_{21}NO$); HRESIMS $[M+H]^+$ *m/z* 424.27097 (calcd. $C_{23}H_{37}NO_6$ $[M+H]^+$ 424.26936, Δ 3.78).

4.7.4. Hydrogenation and Hydrolysis of Crude Millipede Extract.

An aliquot of the *A. corticarius* (10 mg) crude extract was hydrogenated using 10% Pd/C (23 mg, 0.022 mmol) in EtOAc (2 mL) under H_2 (g) and left stirring at rt for 16 h. The mixture was then filtered through a celite glass plug and dried down under vacuum. This mixture was then resuspended in 1 N NaOH (3 mL), heated to 40° C in an oil bath and left stirring for 48 h. The reaction mixture was quenched by treatment with 1 N HCl *(aq)*. The solution was then extracted with EtOAc (2 mL x3) The organic layer and aqueous layer were dried down separately under vacuum. The dried aqueous material was resuspended in 50% MeCN/H_2O at 5 mg/mL and the hydrolysis products were purified by HPLC equipped with a Phenomenex Luna 5 µm Phenyl-Hexyl (250 × 10 mm) column under the following conditions: holding 0% MeCN + 0.1% FA/100% H_2O + 0.1% FA for 10 min followed by a linear gradient to 50% MeCN/H_2O over 10 min with a flow rate of 3 mL/min. This yielded pure hydrogenated hydrolyzed andrognathine backbone (10.1 min, 0.40 mg, 2.1 µmol) and hydrolyzed andrognathanol backbone (18.7 min, 1.4 mg, 5.2 µmol).

4.7.5. Acetonide Protection of Andrognathine Core (4.7)

An aliquot of the hydrogenated hydrolyzed andrognathine backbone (0.40 mg, 2.1 µmol) was reacted with *p*-toluenesulfonic acid (26 mg, 0.15 mmol) and 2,2-dimethoxypropane (0.20 mL, 1.6 mmol) at rt under N_2 (g) for 16 h. The reaction was quenched by addition of 1 N NaOH. The solution was extracted with EtOAc (3 mL x3) and the organic layer was extracted with brine (4 x 3 mL). The organic layer was dried under vacuum and the acetonide product (**4.7**) was isolated by

HPLC equipped with a Phenomenex 4 µm Hydro column (250 × 10 mm) under the following conditions: holding10% MeCN + 0.1% FA/90% H_2O + 0.1% FA for 5 min followed by a linear gradient to 55% MeCN + 0.1% FA/45% H_2O + 0.1% FA over 15 min with a flow rate of 3 mL/min. This yielded pure **4.7** (17.0 min).

4.7.6. Andrognathine Benzoate (4.8) for ECD

An aliquot of the millipede crude extract (300 µL) was reacted with 0.5 N NaOH (300 µL), heated to 40° C in an oil bath, and left stirring overnight. The reaction mixture was quenched by treatment with 1 N HCl *(aq)*. The solution was then extracted with EtOAc (1 mL x3), and the aqueous layer was dried under vacuum. The crude mixture was then resuspended in THF (5 mL) and treated with bromobenzoyl chloride (30 mg, 0.13 mmol), and DMAP (10 mg, 0.08 mmol). The mixture was left stirring under N_2 for 48 h. The solution was then extracted with EtOAc (1 mL x3) and washed with brine (1 mL). The combined organic layer was dried under vacuum. The dried organic material was resuspended in 50% MeCN/50% H_2O and the esterified products were purified by HPLC equipped with a Phenomenex 4 µm Hydro column (250 × 10 mm) column under the following conditions: holding 45% MeCN + 0.1% FA/55% H_2O + 0.1% FA for 15 min followed by a linear gradient to 100% MeCN + 0.1% FA over 15 min with a flow rate of 3 mL/min. This yielded pure **4.8** (28.6 min).

4.7.7. GCMS Analysis of Fatty Acid Composition in *A. corticarius* Crude Extract

The organic layer from the hydrolysis reaction described above was suspended in EtOAc (1.5 mL) followed by addition of (trimethylsilyl)diazomethane in hexane (6 drops, 0.6 M). The reaction mixture stirred at rt for 15 min then dried under N_2 (*g*). The product, along with commercial standards of methyl-3*R*-hydroxypentanoate and methyl-3*S*-hydroxypentanoate were analyzed by chiral GCMS equipped with a Cyclosil B column (Agilent Technologies J&W

Scientific, 30 m × 0.25 mm) under the following conditions: the initial oven temp was 64 °C, kept for 20 min, followed by a ramp to 85 °C, at a rate of 1.5 °C, followed by a ramp to 200 °C, at a rate of 10 °C/min, kept for 5 min. The authentic standards eluted at: methyl-3*S*-hydroxybutanoate (21.3 min), methyl-3*R*-hydroxybutanoate (21.8 min), methyl-3*S*-hydroxypentanoate (33.1 min) and methyl-3*R*-hydroxypentanoate (34.3 min). The derivatized hydrolysis product exhibited four peaks at 21.3, 21.8, 33.1, and 34.3 min.

4.7.8. GCMS Analysis of Fatty Acid Composition in Andrognathanol A (4.9**) and B (**4.10**)**

Similarly, an aliquot of pure **4.9** (200 µg, 0.49 µmol) and **4.10** (200 µg, 0.47 µmol) were resuspended in MeOH (100 µL) then treated with 0.5 N NaOH (100 µL) at rt for 2 d. The reaction mixture was quenched by the addition of 0.5 N HCl (100 µL) then the reaction mixture was extracted with EtOAc (1 mL x3). The combined organic layers were dried over $MgSO_4$, filtered through celite and dried under N_2. The crude product along with standards for (3*S*)-hydroxybutanoate, and (3*R*)-hydroxybutanoate were methylated by resuspension in EtOAc (1 mL) followed by addition of (trimethylsilyl)diazomethane in hexane (4 drops, 0.6 M). The reaction mixtures were stirred at rt for 15 min then dried under N_2 (g). The products were analyzed by chiral GCMS using the method described above. The derivatized hydrolysis product of **4.9** exhibited two peaks at 21.3 and 21.8 min, while the derivatized hydrolysis product for **4.10** exhibited a single peak at 33.1 min.

4.7.9. Density Functional Theory (DFT) Calculation of ^{1}H and ^{13}C NMR

For NMR chemical shift prediction analysis of **4.7**, MMFF94 energy-minimized in Chem3D and a sparse systematic conformational search was performed using MMFF force field in the Spartan '24 software package. Geometry and energies of the selected conformers were further optimized in Spartan '24 at the HF/3-21G and wB97X-D/6-31G* levels of theory, with a

final energy calculation for Boltzmann weighting at wB97X-V/6-311+G(2df,2p)[6-311G*] level of theory. Chemical shift predictions were performed in Gaussian09 with ^{13}C chemical shift predictions performed at the PCM-ωB97X-D/def2-SVP//PCM-B3LYP-D3/6-311G(d,p) level of theory, and ^{1}H chemical shift predictions were performed at the PCM-WP04/6-311++G(2d,p)//PCM-B3LYP-D3/6-311G(d,p) level of theory, both of which utilized an integral equation formalism (IEF) polarizable continuum model (PCM) for DMSO. Linear scaling factors include a slope of -1.0099 and intercept of 196.0386 for ^{13}C, and a slope of -1.0080 and intercept of 32.0998 for ^{1}H. Predicted chemical shifts were Boltzmann-weighted based on the total Gibbs free energy of each conformer. No imaginary frequencies were present within the frequency calculation results. Relative mean standard deviation (RMSD) of chemical shifts were compared to both possible configurations for **4.7**.

4.7.10. LCMS Quantification of Andrognathanols and Andrognathines

Thirty individual *A. corticarius* were collected and placed in 1.5 mL Eppendorf tubes. Each of the millipedes were measured and then preserved in 0.5 mL of MeOH. A small aliquot (5 µL) was taken from each millipede and run on LR-LCMS (LTQ) using a Kinetex 5µm EVO C18 (100 x 3.0 mm) column using the following solvent gradient system: holding 10% MeCN + 0.1% FA/90% H_2O + 0.1% FA for 3 min followed by a gradient to 40% MeCN + 0.1% FA/60% H_2O + 0.1% FA over 63 min with a flow rate of 0.3 mL/min. The raw files were converted to mzML using MSConvert (Version 3.0.20337) and the data was subsequently processed in MzMine3 (Version 3.9.0). Mass detections were conducted with a noise threshold for MS1 of 6.0E2, for MS2 1.0E2. The ADAP chromatogram builder used a minimum group size of 5, a group intensity threshold of 6.0E2, minimum height intensity of 2.0E3 and *m/z* tolerance was 0.50. The local minimum resolver utilized the following settings: Chromatographic threshold: 90%, Search minimum in RT range

(min)=0.20, minimum relative height=1%, minimum absolute height = 1.6E3 minimum ratio or peak top/edge=1, minimum number of data points=3 and peak duration range (min) = 0.0–2.0. The ^{13}C isotope filler had an *m/z* tolerance of 0.50 *m/z*, retention time tolerance of 0.30, maximum charge of 3 and representative isotope of most intense. Finally, the join aligner had an *m/z* tolerance of 0.50 *m/z*, a weight for *m/z* of 75, retention time tolerance of 0.30 min, and weight for RT of 25. The .csv file was then exported, the peak areas for extracted ion chromatograms corresponding to the $[M+H]^+$ for each andrognathine and andrognathanol [352, 366, 380, 394, 408, 410 and 424], were averaged and plotted against the length of each millipede using Prism (Version 10.2.0).

4.7.11. Sigma-1 and Sigma-2 Receptor Assay Procedure from Psychoactive Drug Screening Program (PDSP)

HEKT cell lines were used to make membrane pallets for binding assays. In the primary binding assays, compounds were tested at a single concentration (10 µM) and in quadruplicate in 96-well plates. Compounds showing a minimum of 50% inhibition at 10 µM were tagged for secondary radioligand binding assays to determine equilibrium binding affinity at specific targets. In secondary binding assays, compounds were tested at 11 concentrations (0.1, 0.3, 1, 3, 10, 30, 100, 300, 1,000, 3,000, and 10,000 nM) and in triplicate (3 sets of 96-well plates). Both primary and secondary radioligand binding assays were carried out in a final volume of 125 µL per well in appropriate binding buffers (50 mM Tris HCl, pH 8.0, rt). Pentazocine was used as a radioligand and the hot ligand concentration was determined close to its K_i. Total binding and nonspecific binding were determined in the absence and presence of 10 µM of haloperidol, the reference compound. Plates were incubated at room temperature and in the dark for 90 min. Reactions were stopped by vacuum filtration onto 0.3% polyethyleneimine (PEI) soaked 96-well filter mats using a 96-well Filtermate harvester, followed by three washes with cold wash buffers (50 mM Tris HCl,

pH 7.4). Scintillation cocktail was then melted onto the microwave-dried filters on a hot plate and radioactivity was counted in a Microbeta counter. K_i values for [3H]-(+)-pentazocine (σ_1R: 6.70 nM), (σ_2R: 14.50) were determined via separate homologous competitive binding experiments. K_i values were determined from at least three independent experiments and are reported as mean ± SEM.

4.8. References

(1) Wong, V. L.; Hennen, D. A.; Macias, A. M.; Brewer, M. S.; Kasson, M. T.; Marek, P. Natural history of the social millipede Brachycybe lecontii Wood, 1864. *Biodiversity Data Journal* **2020**, *8*, e50770. DOI: 10.3897/BDJ.8.e50770.

(2) Gardner, M. R. Revision of the millipede family Andrognathidae in the Nearctic Region (Diplopoda: Platydesmida). *Memoirs of the Pacific Coast Entomological Society* **1974**, *5*, 1-61.

(3) Shorter, P. L.; Hennen, D. A.; Marek, P. E. Cryptic diversity in Andrognathus corticarius Cope, 1869 and description of a new Andrognathus species from New Mexico (Diplopoda, Platydesmida, Andrognathidae). *Zookeys* **2018**, (786), 19-41. DOI: 10.3897/zookeys.786.27631.

(4) Meinwald, J.; Eisner, T.; Meinwald, J.; Eisner, T. The chemistry of phyletic dominance. *Proceedings of the National Academy of Sciences* **1995**, *92* (1). DOI: 10.1073/pnas.92.1.14.

(5) Meinwald, J.; Smolanoff, J.; McPhail, A. T.; Miller, R. W.; Eisner, T.; Hicks, K. Nitropolyzonamine: A spirocyclic nitro compound from the defensive glands of a milliped (polyzonium rosalbum). *Tetrahedron Letters* **1975**, *16* (28). DOI: 10.1016/0040-4039(75)80013-X.

(6) Wood, W. F.; Hanke, F. J.; Kubo, I.; Carroll, J. A.; Crews, P. Buzonamine, a new alkaloid from the defensive secretion of the millipede, Buzonium crassipes. *Biochemical Systematics and Ecology* **2000**, *28* (4), 305-312. DOI: 10.1016/S0305-1978(99)00068-X.

(7) Kuwahara, Y.; Mori, N. M. N.; Tanabe, T. Detection of a neotropical frog alkaloid spiropyrrolizidine 236 from a Japanese polyzoniid millipede Kiusiozonium okai as a major defense component together with polyzonimine and nitropolyzonamine. *Japanese Journal of Environmental Entomology and Zoology* **2007**, *18* (2). DOI: 10.11257/jjeez.18.91.

(8) Shear, W. A. The chemical defenses of millipedes (diplopoda): Biochemistry, physiology and ecology. *Biochemical Systematics and Ecology* **2015**, *61*, 78-117. DOI: 10.1016/j.bse.2015.04.033.

(9) Menegatti, C.; Wood, J. S.; Banks, P.; Knott, K.; Briganti, J. S.; Briganti, A. J.; McNally, S. V. G.; Marek, P. E.; Brown, A. M.; Jones, T. H.; et al. Neuromodulating Alkaloids from Millipede Defensive Secretions. *Journal of Natural Products* **2024**. DOI: 10.1021/acs.jnatprod.4c01162.

(10) Banks, P.; Funkhouser, E. M.; Macias, A. M.; Lovett, B.; Meador, S.; Hatch, A.; Garraffo, H. M.; Cartwright, K. C.; Kasson, M. T.; Marek, P. E.; et al. The Chemistry of the Defensive Secretions of Three Species of Millipedes in the Genus Brachycybe. *Journal of Chemical Ecology* **2024**, *50* (9), 478-488. DOI: 10.1007/s10886-024-01518-6.

(11) Jones, T. H.; Harrison, D. P.; Menegatti, C.; Mevers, E.; Knott, K.; Marek, P.; Hennen, D. A.; Kasson, M. T.; Macias, A. M.; Lovett, B.; et al. Deoxybuzonamine Isomers from the Millipede Brachycybe lecontii (Platydesmida: Andrognathidae). *Journal of Natural Products* **2022**, *85* (4), 1134-1140. DOI: 10.1021/acs.jnatprod.2c00077.

(12) Banks, P.; Menegatti, C.; Knott, K.; Marek, P.; Mevers, E. Chemical Diversity of Millipede Defensive Alkaloids Provides Insights into their Evolutionary History. **2025**. DOI: 10.26434/chemrxiv-2025-tdt3n.

(13) Menegatti, C.; Wood, J. S.; Banks, P.; Knott, K.; Briganti, J. S.; Briganti, A. J.; McNally, S. V. G.; Marek, P. E.; Brown, A. M.; Jones, T. H.; et al. Neuromodulating Alkaloids from Millipede

Defensive Secretions. *Journal of Natural Products* **2025**, *88* (1), 110-118. DOI: 10.1021/acs.jnatprod.4c01162.

(14) Rodriguez, J.; Jones, T. H.; Sierwald, P.; Marek, P. E.; Shear, W. A.; Brewer, M. S.; Kocot, K. M.; Bond, J. E. Step-wise evolution of complex chemical defenses in millipedes: a phylogenomic approach. *Scientific Reports* **2018**, *8* (1), 3209. DOI: 10.1038/s41598-018-19996-6.

(15) Lancaster, J.; Khrimian, A.; Young, S.; Lehner, B.; Luck, K.; Wallingford, A.; Ghosh, S. K. B.; Zerbe, P.; Muchlinski, A.; Marek, P. E.; et al. De novo formation of an aggregation pheromone precursor by an isoprenyl diphosphate synthase-related terpene synthase in the harlequin bug. *Proceedings of the National Academy of Sciences* **2018**, *115* (37). DOI: 10.1073/pnas.1800008115.

(16) Marek, P. E.; Buzatto, B. A.; Shear, W. A.; Means, J. C.; Black, D. G.; Harvey, M. S.; Rodriguez, J. The first true millipede—1306 legs long. *Scientific Reports* **2021**, *11* (1), 23126. DOI: 10.1038/s41598-021-02447-0.

(17) Shear, W.; Jones, T.; Wesener, T. Glomerin and homoglomerin from the North American pill millipede Onomeris sinuata (Loomis, 1943) (Diplopoda, Pentazonia, Glomeridae). *International Journal of Myriapodology* **2011**, *4*. DOI: 10.3897/ijm.4.1105.

(18) Eisner, T.; Alsop, D.; Hicks, K.; Meinwald, J. Defensive Secretions of Millipeds. In *Arthropod Venoms*, Bettini, S. Ed.; Springer Berlin Heidelberg, 1978; pp 41-72.

(19) Hash, J. M.; Millar, J. G.; Heraty, J. M.; Harwood, J. F.; Brown, B. V. Millipede Defensive Compounds Are a Double-Edged Sword: Natural History of the Millipede-Parasitic Genus Myriophora Brown (Diptera: Phoridae). *Journal of Chemical Ecology* **2017**, *43* (2), 198-206. DOI: 10.1007/s10886-016-0815-7.

(20) Carrel, J. E.; Eisner, T.; Carrel, J. E.; Eisner, T. Spider sedation induced by defensive chemicals of milliped prey. *Proceedings of the National Academy of Sciences* **1984**, *81* (3). DOI: 10.1073/pnas.81.3.806.

(21) Badio, B.; Shi, D.; Shin, Y.; Hutchinson, K.; Padgett, W.; Daly, J. Spiropyrrolizidines: a new class of blockers of nicotinic receptors. *Biochemical pharmacology* **1996**, *52* (6). DOI: 10.1016/0006-2952(96)00464-9.

(22) Clark, V. C.; Raxworthy, C. J.; Rakotomalala, V.; Sierwald, P.; Fisher, B. L. Convergent evolution of chemical defense in poison frogs and arthropod prey between Madagascar and the Neotropics. *Proceedings of the National Academy of Sciences* **2005**, *102* (33), 11617-11622. DOI: 10.1073/pnas.0503502102.

(23) Brewer, M. S.; Spruill, C. L.; Rao, N. S.; Bond, J. E. Phylogenetics of the millipede genus Brachycybe Wood, 1864 (Diplopoda: Platydesmida: Andrognathidae): Patterns of deep evolutionary history and recent speciation. *Molecular Phylogenetics and Evolution* **2012**, *64* (1). DOI: 10.1016/j.ympev.2012.04.003.

(24) Moritz, L.; Wesener, T. The first known fossils of the Platydesmida—an extant American genus in Cretaceous amber from Myanmar (Diplopoda: Platydesmida: Andrognathidae). *Organisms Diversity and Evolution* **2019**, *19* (3), 423-433. DOI: 10.1007/s13127-019-00408-0.

(25) Bock, M.; Buntin, K.; Muller, R.; Kirschning, A. Stereochemical determination of thuggacins A-C, highly active antibiotics from the myxobacterium Sorangium cellulosum. *Angewandte Chemie International Edition* **2008**, *47* (12), 2308-2311. DOI: 10.1002/anie.200704897.

(26) Vazquez, J. T.; Chang, M.; Nakanishi, K.; Manta, E.; Perez, C.; Martin, J. D. Structure of Hydroazulenoid Diterpenes from a Marine Alga and Their Absolute-Configuration Based on

Circular-Dichroism. *Journal of Organic Chemistry* **1988**, *53* (20), 4797-4800. DOI: DOI 10.1021/jo00255a025.

(27) Gusovsky, F.; Rossignol, D. P.; McNeal, E. T.; Daly, J. W. Pumiliotoxin B binds to a site on the voltage-dependent sodium channel that is allosterically coupled to other binding sites. *Proceedings of the National Academy of Sciences* **1988**, *85* (4), 1272-1276. DOI: doi:10.1073/pnas.85.4.1272.

(28) Marek, P. E.; Shear, W. A. Myriapods. *Current Biology* **2022**, *32* (23). DOI: 10.1016/j.cub.2022.09.058.

4.9. Appendix Figures

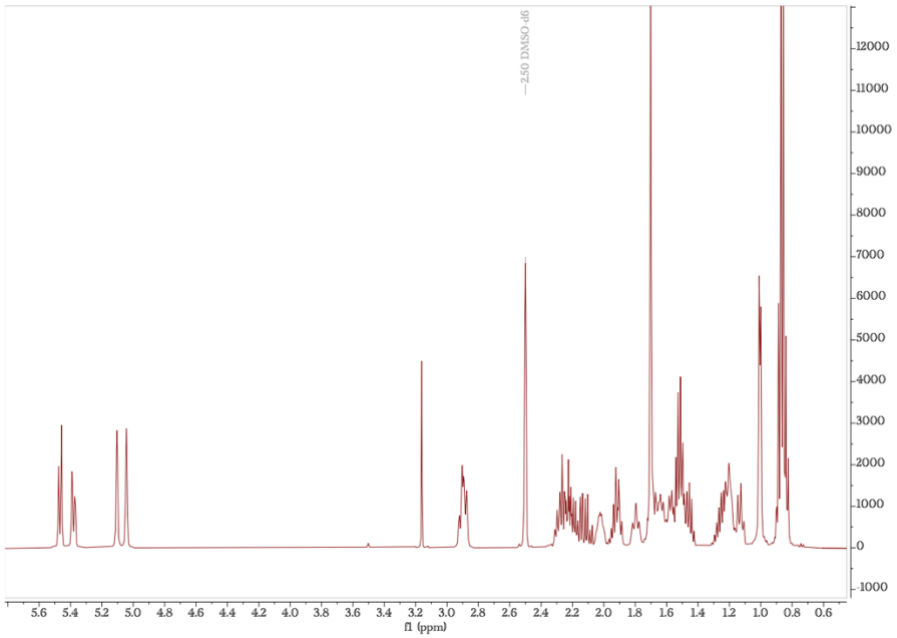

Figure 4.9.1. ^{1}H NMR spectra for andrognathine A (**4.1**) (600Hz, *d6*-DMSO) 64 scans.

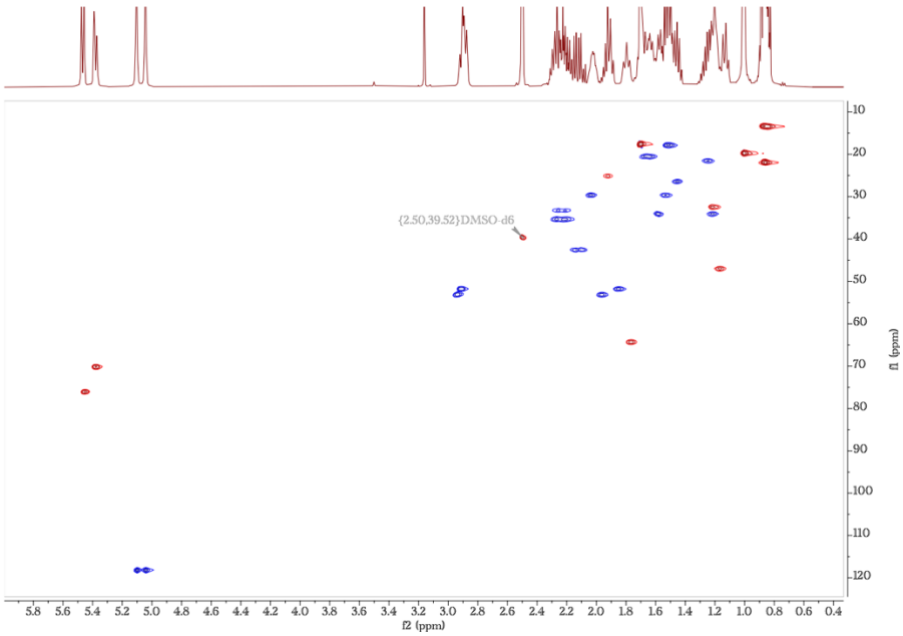

Figure 4.9.2. gHSQC NMR spectra for andrognathine A (**4.1**) (600 MHz, *d6*-DMSO) 64 scans, NUS25 and 400 increments.

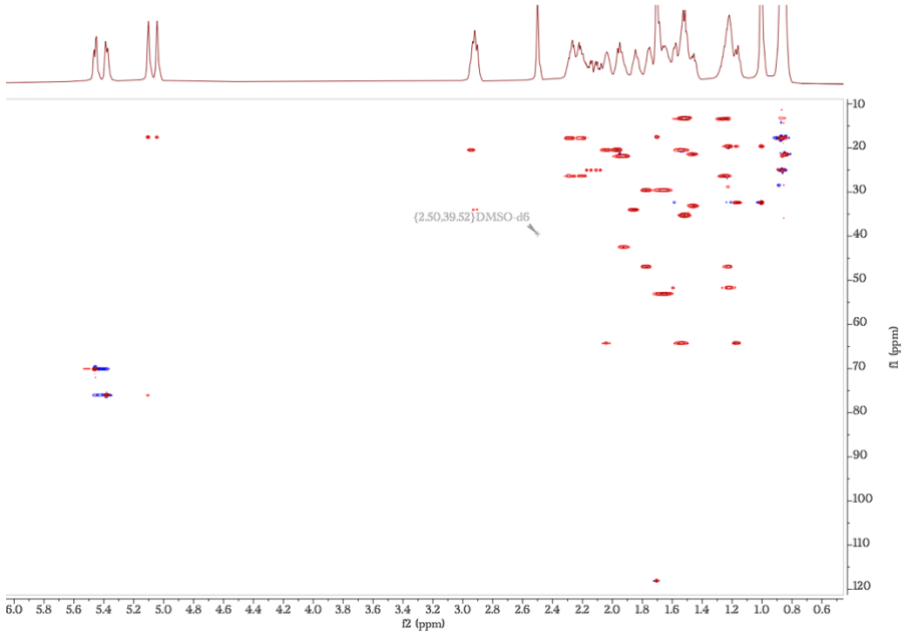

Figure 4.9.3. H2BC NMR spectra for andrognathine A (**4.1**) (600 MHz, d_6-DMSO) 64 scans, NUS50 and 400 increments.

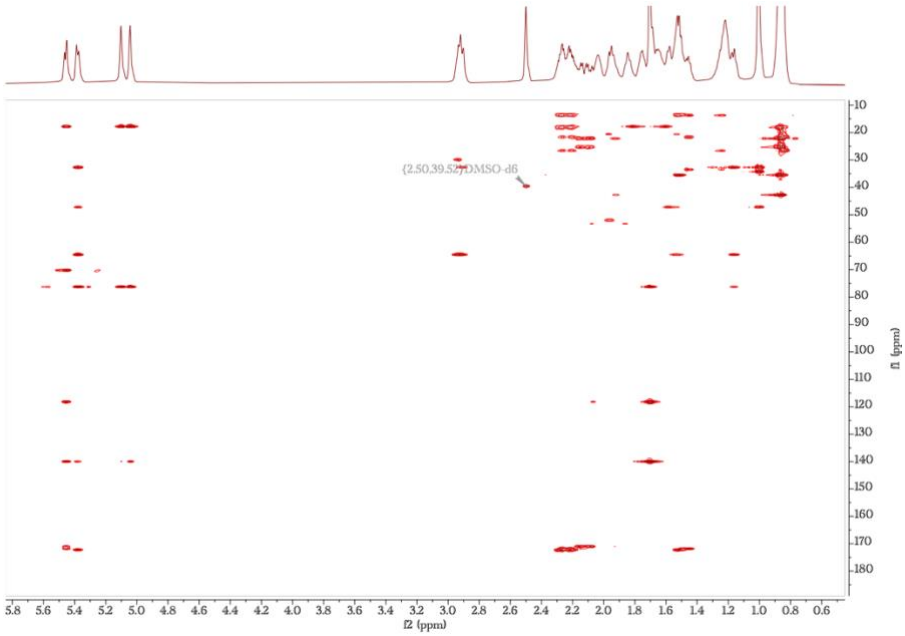

Figure 4.9.4. HMBC NMR spectra for andrognathine A (**4.1**) (600 MHz, d_6-DMSO) 64 scans, NUS50 and 512 increments.

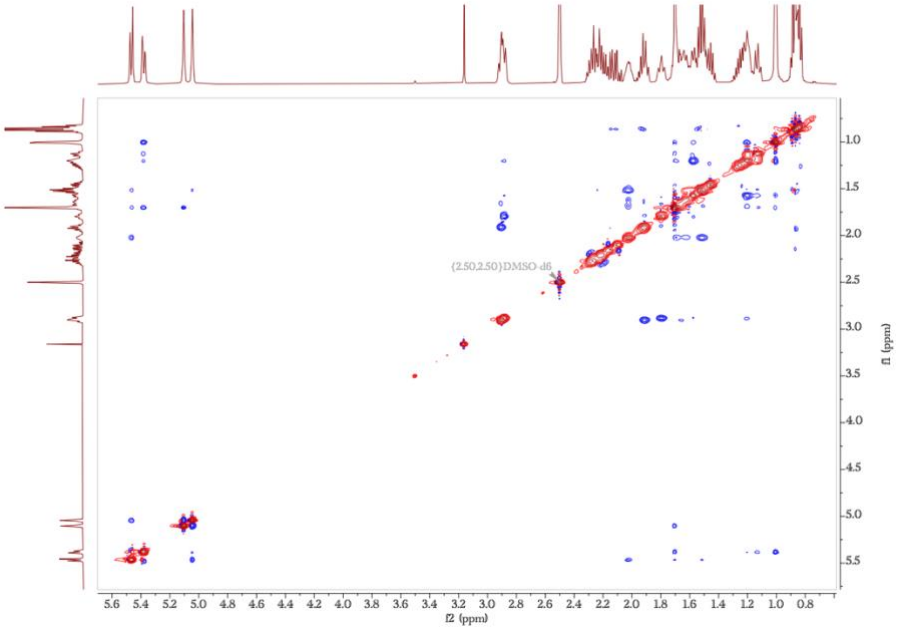

Figure 4.9.5. easyROESY NMR spectra for andrognathine A (**4.1**) (600 MHz, *d*6-DMSO) 32 scans, NUS50 and 400 increments.

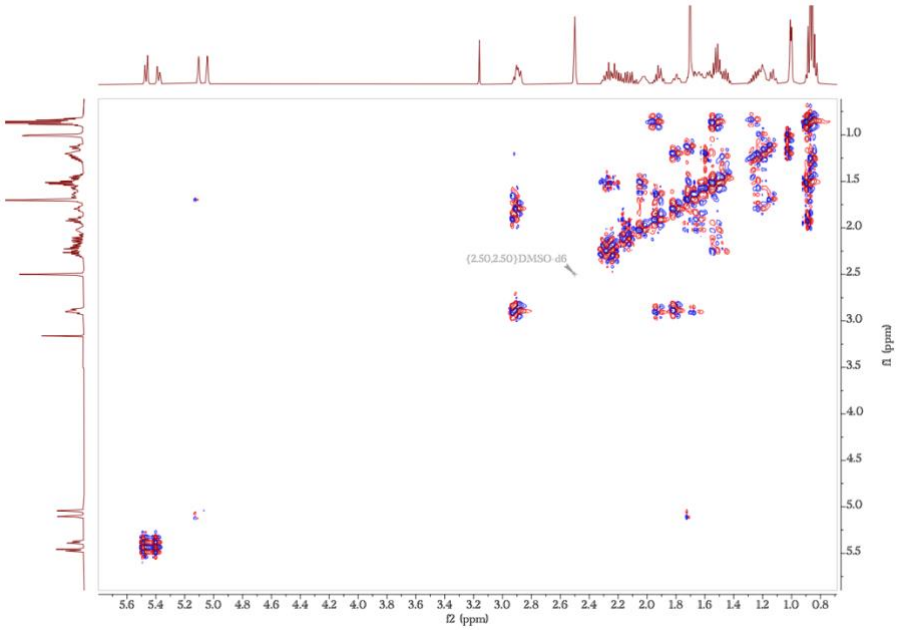

Figure 4.9.6. dqfCOSY NMR spectra for andrognathine A (**4.1**) (600 MHz, *d*6-DMSO) 32 scans, NUS50 and 256 increments.

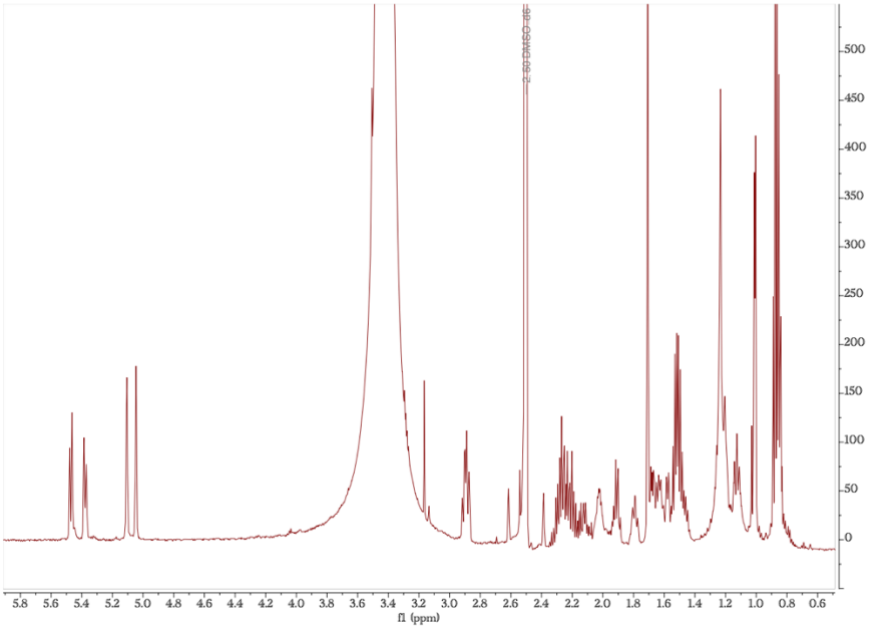

Figure 4.9.7. ^{1}H NMR spectra for andrognathine B (**4.2**) (600 MHz, *d6*-DMSO) 64 scans.

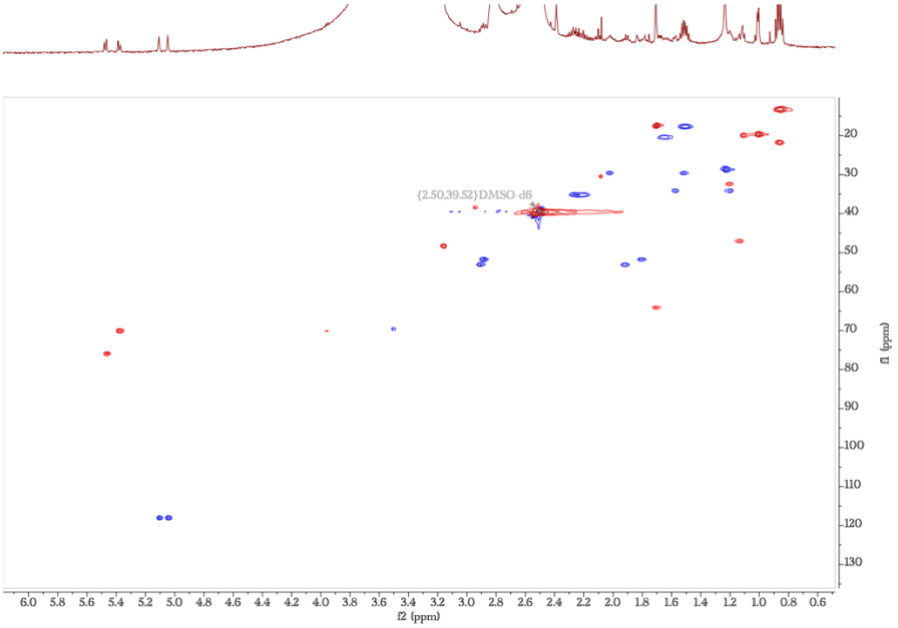

Figure 4.9.8. gHSQC NMR spectra for andrognathine B (**4.2**) (600 MHz, *d6*-DMSO) 64 scans, NUS25 and 400 increments.

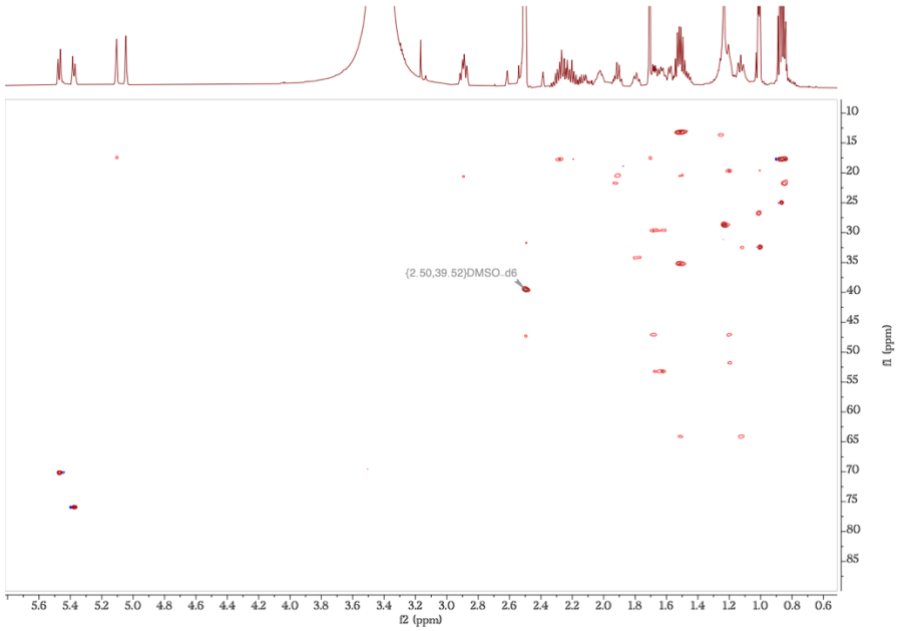

Figure 4.9.9. H2BC NMR spectra for andrognathine B (**4.2**) (600 MHz, *d6*-DMSO) 64 scans, NUS50 and 400 increments.

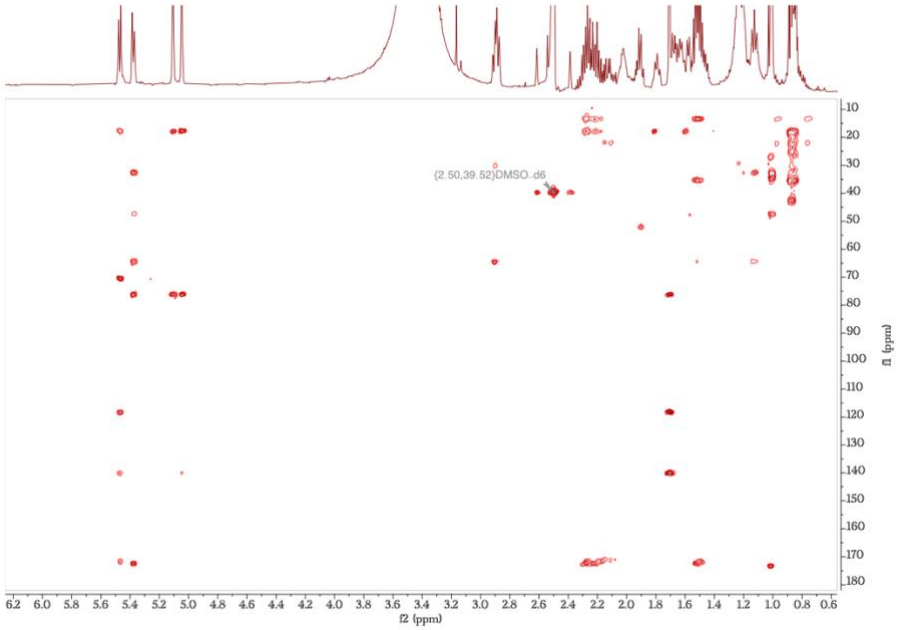

Figure 4.9.10. HMBC NMR spectra for andrognathine B (**4.2**) (600 MHz, *d6*-DMSO) 64 scans, NUS50 and 256 increments.

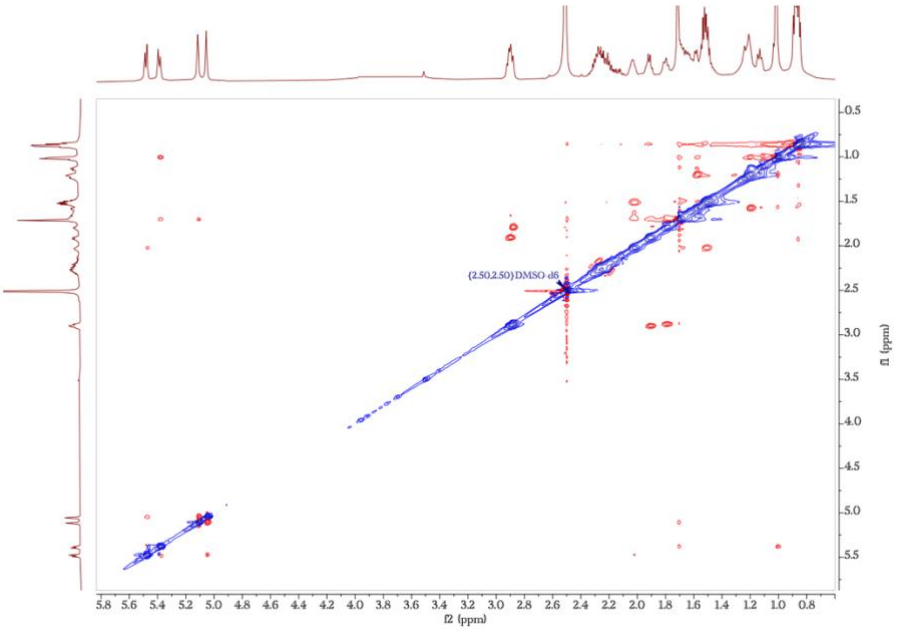

Figure 4.9.11. easyROESY NMR spectra for andrognathine B (**4.2**) (600 MHz, *d*$_6$-DMSO) 16 scans, NUS50 and 400 increments.

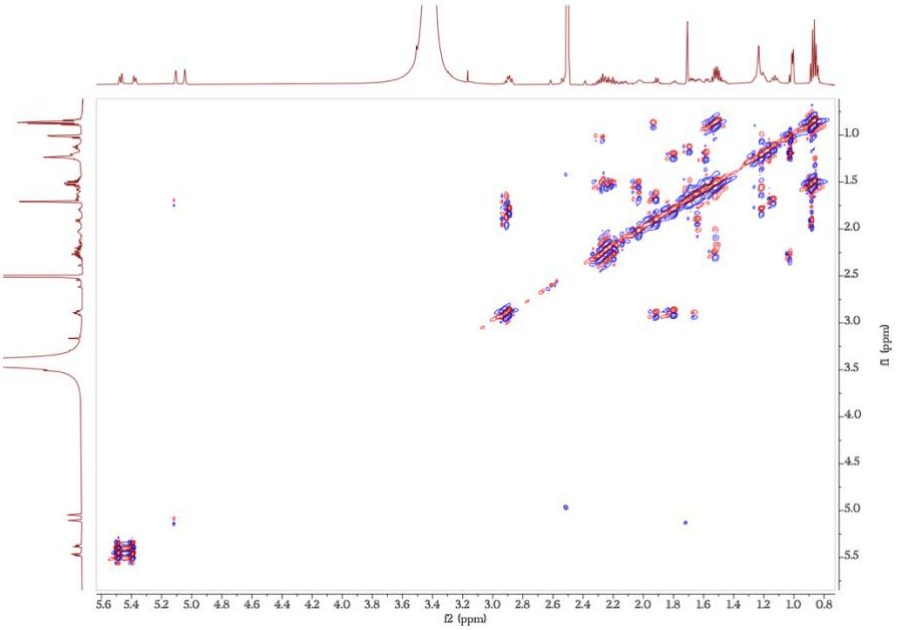

Figure 4.9.12. dqfCOSY NMR spectra for andrognathine B (**4.2**) (600 MHz, *d*$_6$-DMSO) 16 scans, NUS50 and 256 increments.

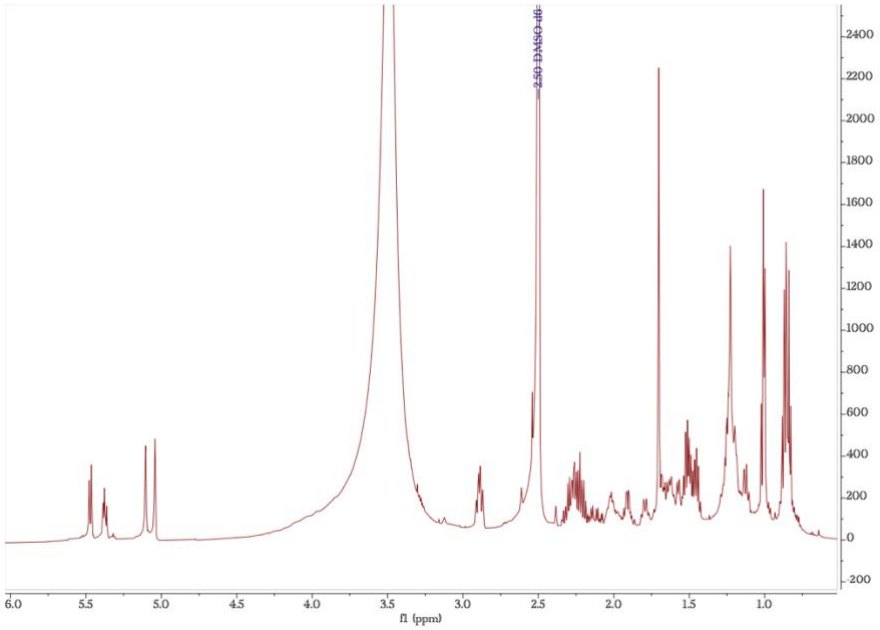

Figure 4.9.13. ^{1}H NMR spectra for andrognathine C (**4.3**) (600 MHz, *d6*-DMSO) 128 scans.

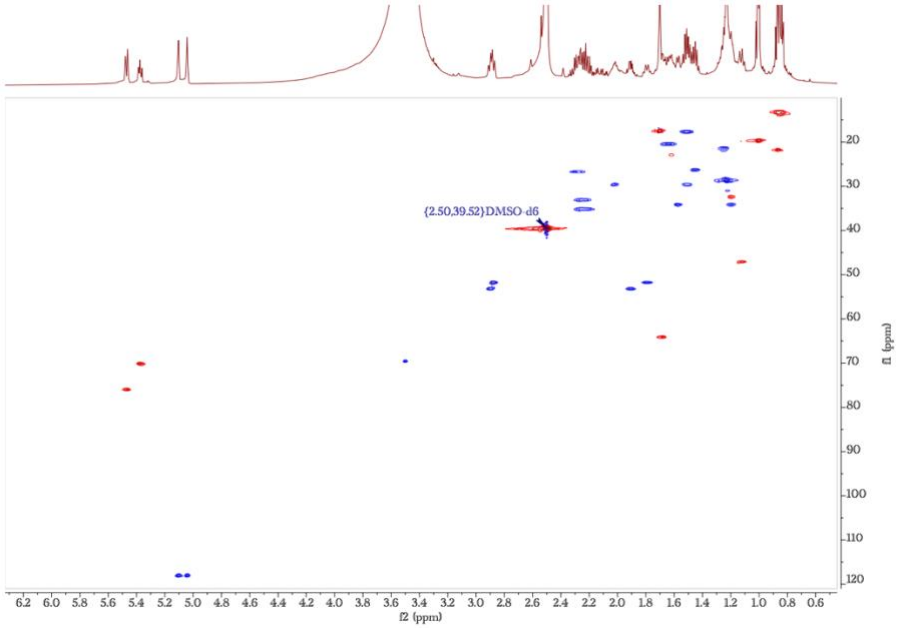

Figure 4.9.14. gHSQC NMR spectra for andrognathine C (**4.3**) (600 MHz, *d6*-DMSO) 64 scans, NUS25 and 400 increments.

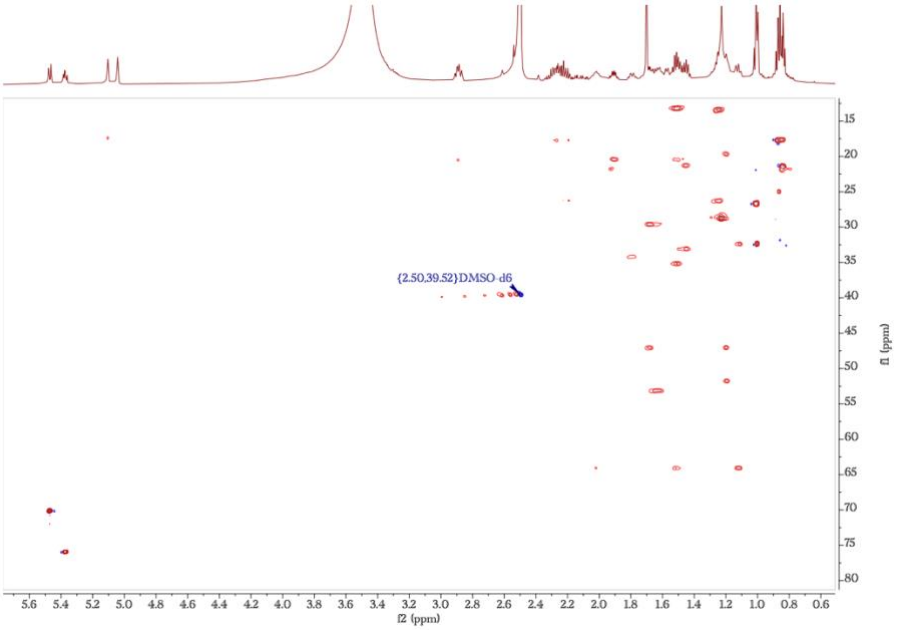

Figure 4.9.15. H2BC NMR spectra for andrognathine C (**4.3**) (600 MHz, *d6*-DMSO) 48 scans, NUS50 and 400 increments.

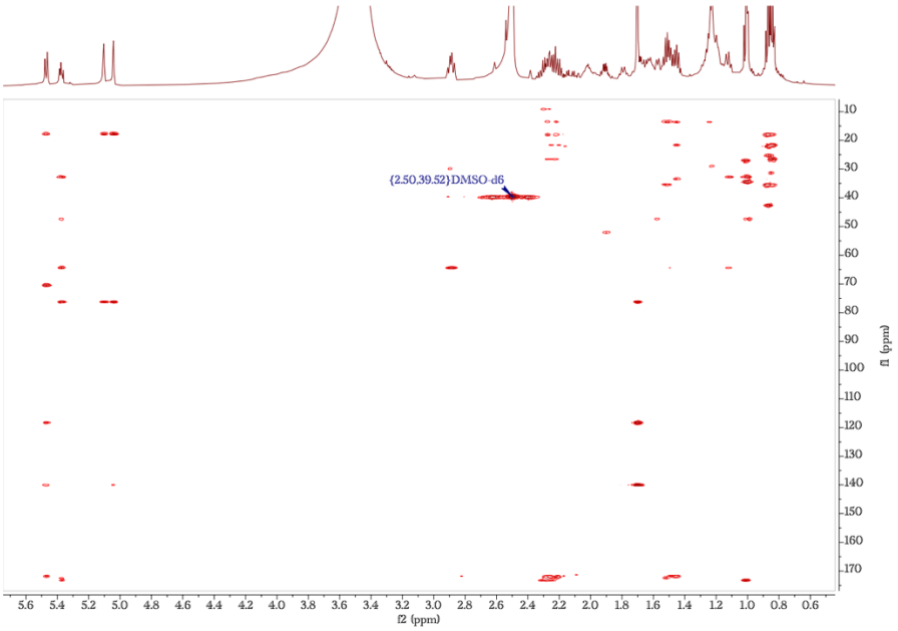

Figure 4.9.16. HMBC NMR spectra for andrognathine C (**4.3**) (600 MHz, *d6*-DMSO) 48 scans, NUS50 and 400 increments.

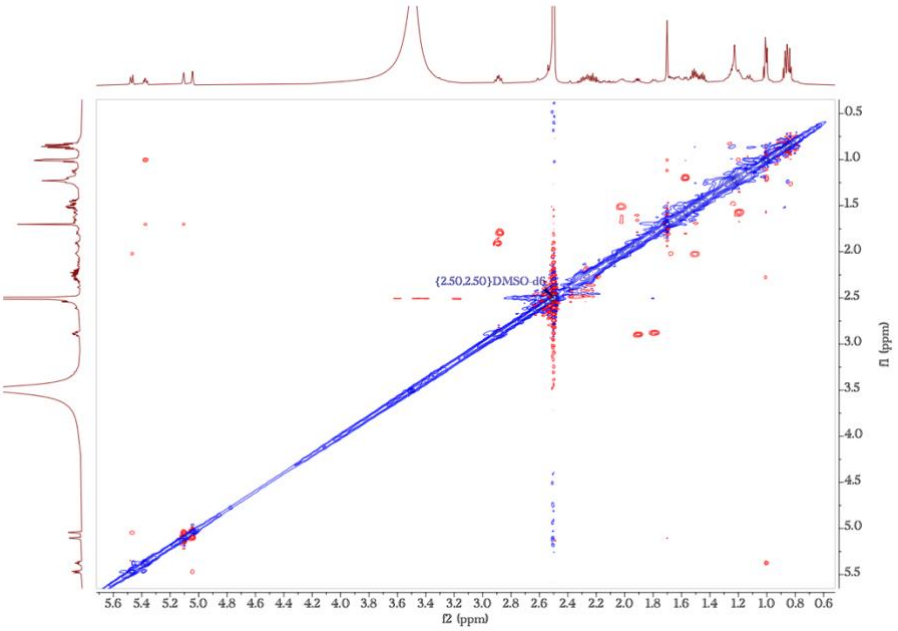

Figure 4.9.17. easyROESY NMR spectra for andrognathine C (**4.3**) (600 MHz, *d6*-DMSO) 32 scans, NUS50 and 400 increments.

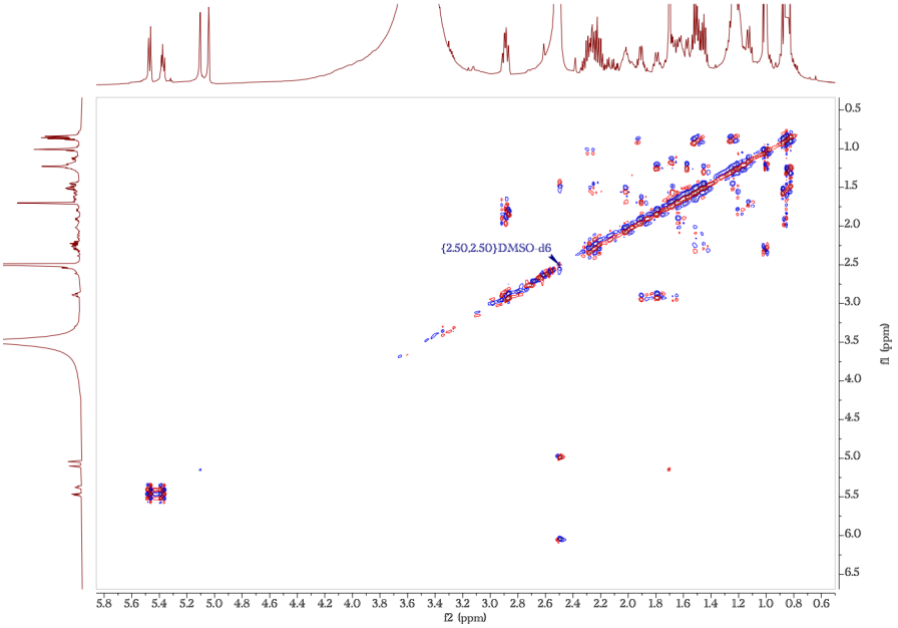

Figure 4.9.18. dqfCOSY NMR spectra for andrognathine C (**4.3**) (600 MHz, *d6*-DMSO) 32 scans, NUS50 and 256 increments.

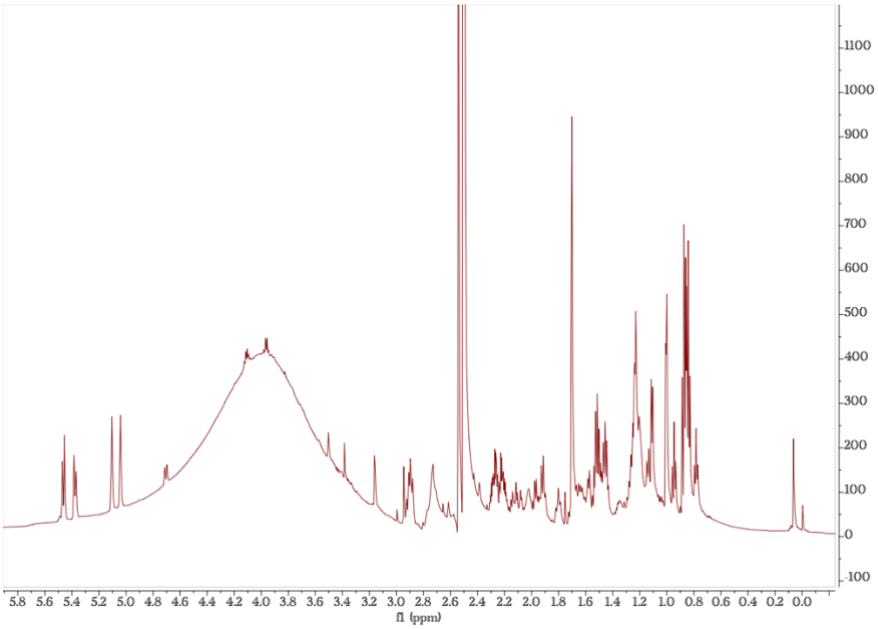

Figure 4.9.19. ^{1}H NMR spectra for andrognathine D (**4.4**) (600 MHz, *d*$_6$-DMSO) 128 scans.

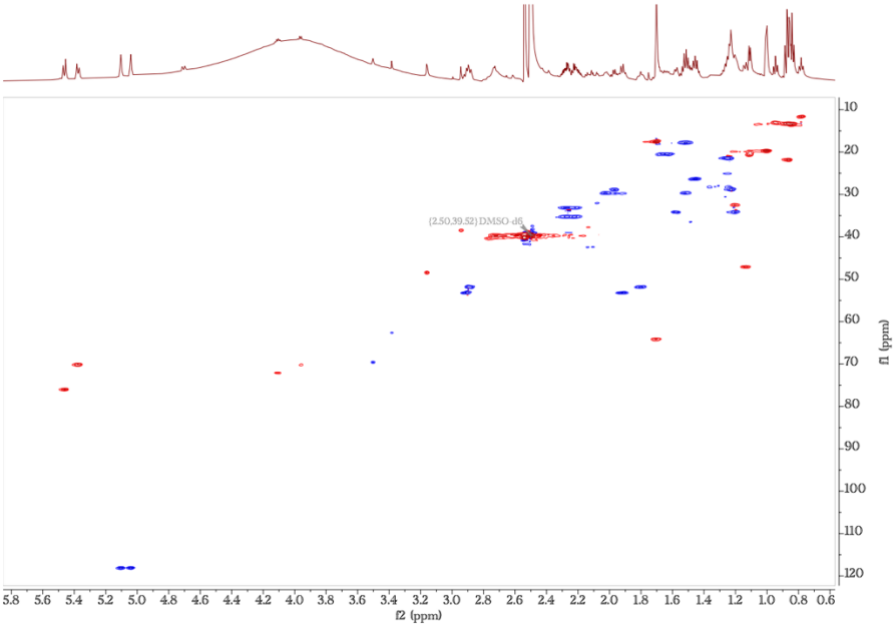

Figure 4.9.20. gHSQC NMR spectra for andrognathine D (**4.4**) (600 MHz, *d*$_6$-DMSO) 64 scans, NUS25 and 400 increments.

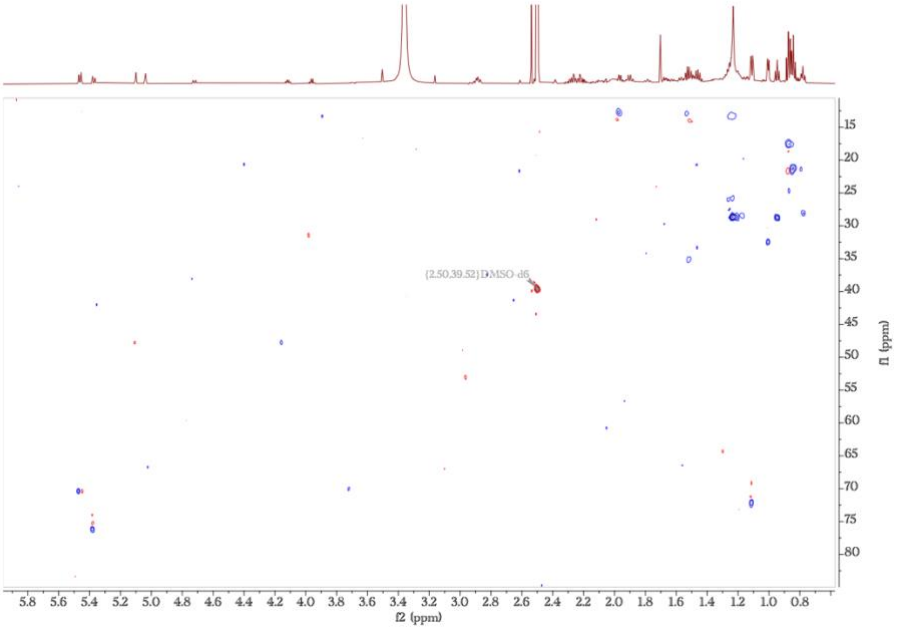

Figure 4.9.21. H2BC NMR spectra for andrognathine D (**4.4**) (600 MHz, *d*$_6$-DMSO) 128 scans, NUS50 and 256 increments.

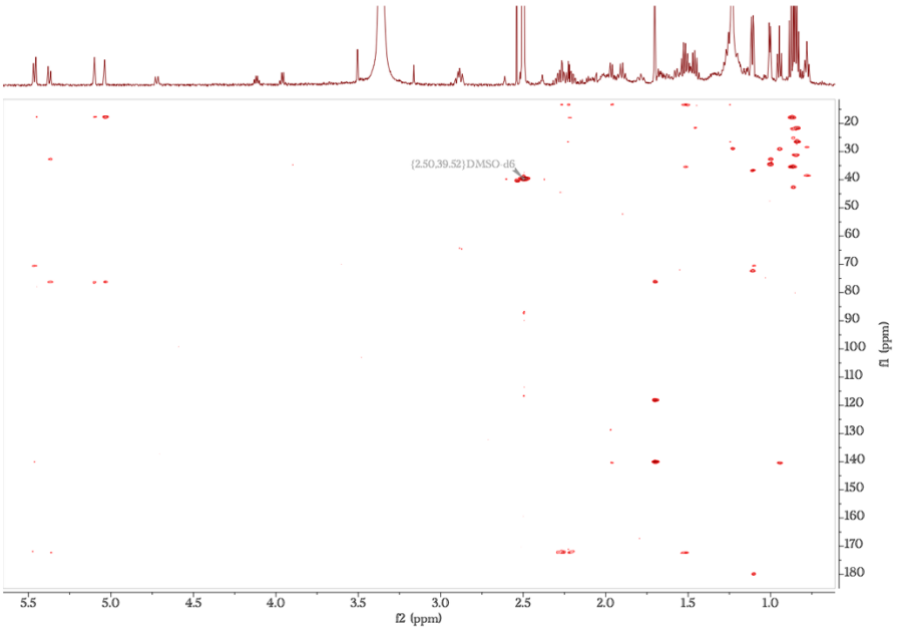

Figure 4.9.22. HMBC NMR spectra for andrognathine D (**4.4**) (600 MHz, *d*$_6$-DMSO) 96 scans, NUS50 and 256 increments.

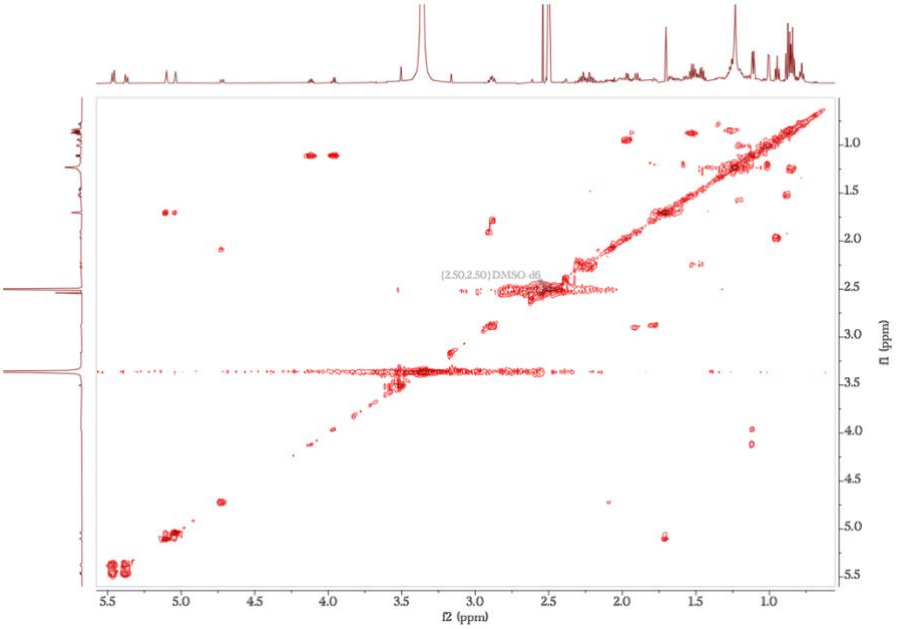

Figure 4.9.23. COSY NMR spectra for andrognathine D (**4.4**) (600 MHz, *d6*-DMSO) 4 scans, NUS50 and 320 increments.

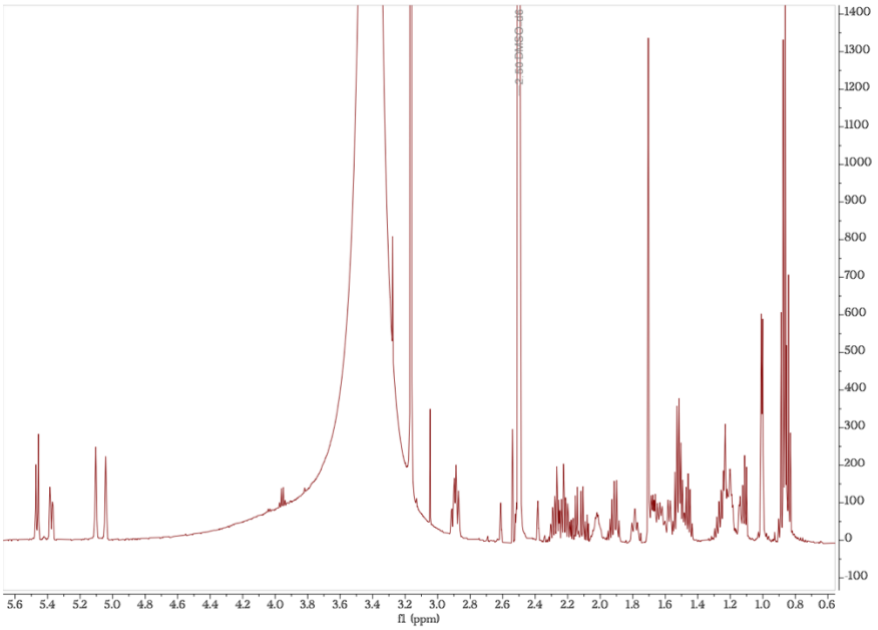

Figure 4.9.24. ^{1}H NMR spectra for andrognathine E (**4.5**) (600 MHz, *d6*-DMSO) 128 scans.

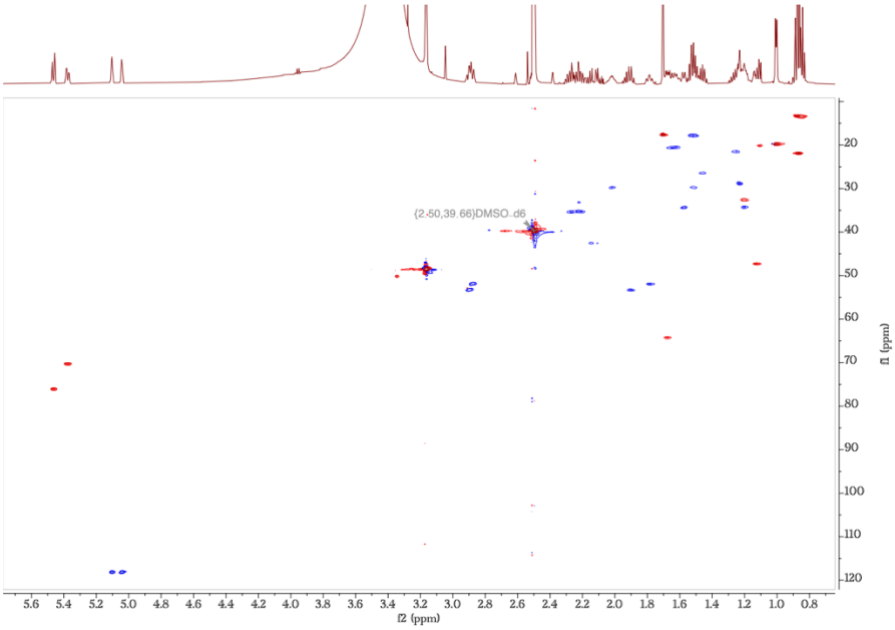

Figure 4.9.25. gHSQC NMR spectra for andrognathine E (**4.5**) (600 MHz, *d*6-DMSO) 64 scans, NUS25 and 400 increments.

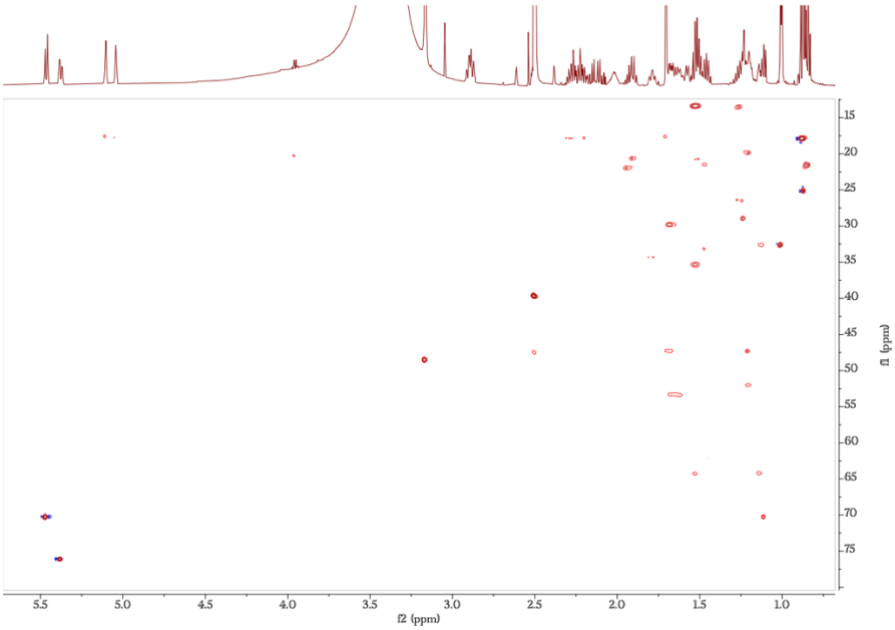

Figure 4.9.26. H2BC NMR spectra for andrognathine E (**4.5**) (600 MHz, *d*6-DMSO) 64 scans, NUS50 and 400 increments.

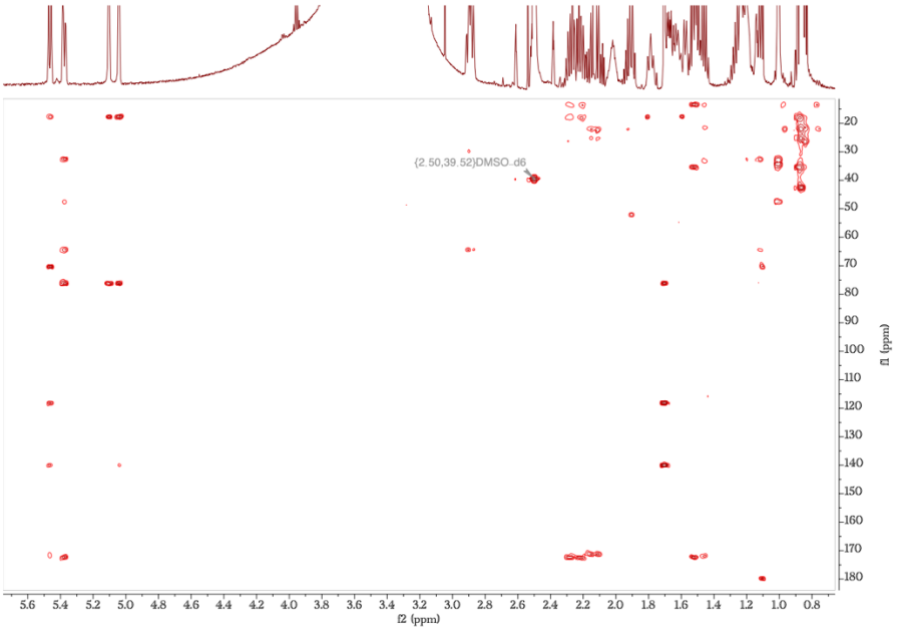

Figure 4.9.27. HMBC NMR spectra for andrognathine E (**4.5**) (600 MHz, *d6*-DMSO) 64 scans, NUS50 and 256 increments.

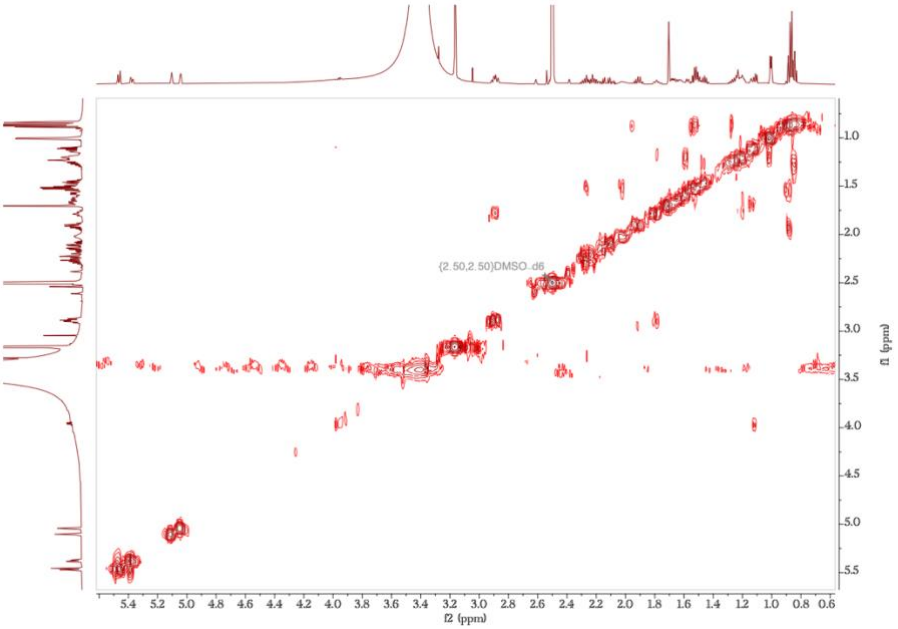

Figure 4.9.28. COSY NMR spectra for andrognathine E (**4.5**) (600 MHz, *d6*-DMSO) 128 scans, NUS50 and 128 increments.

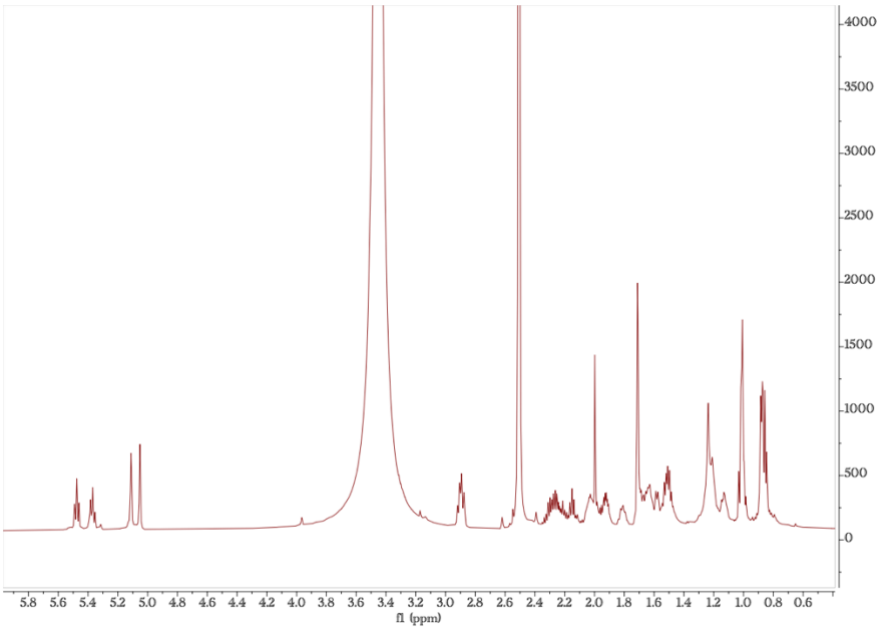

Figure 4.9.29. ^{1}H NMR spectra for andrognathine F (**4.6**) (600 MHz, *d6*-DMSO) 128 scans.

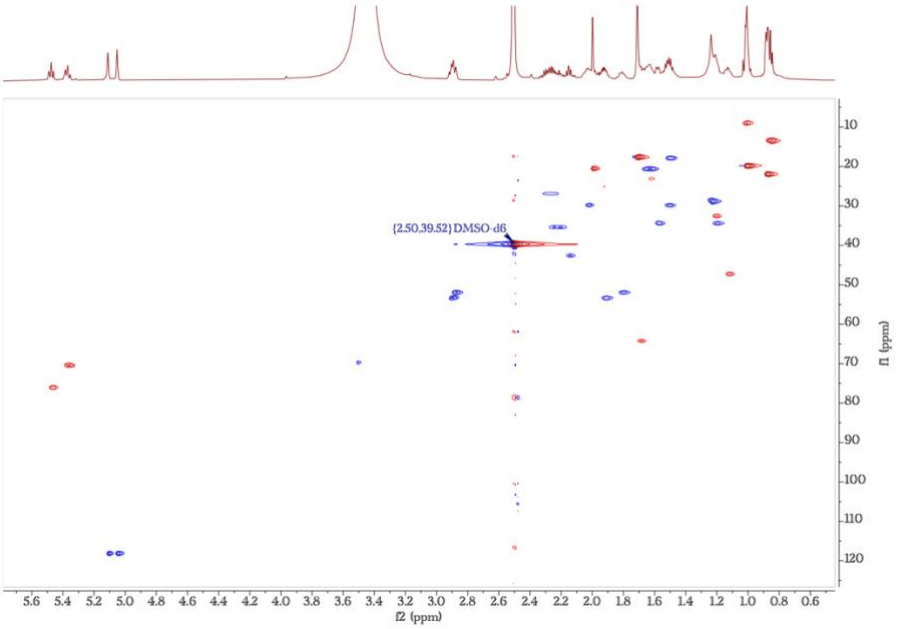

Figure 4.9.30. gHSQC NMR spectra for andrognathine F (**4.6**) (600 MHz, *d6*-DMSO) 64 scans, NUS25 and 400 increments.

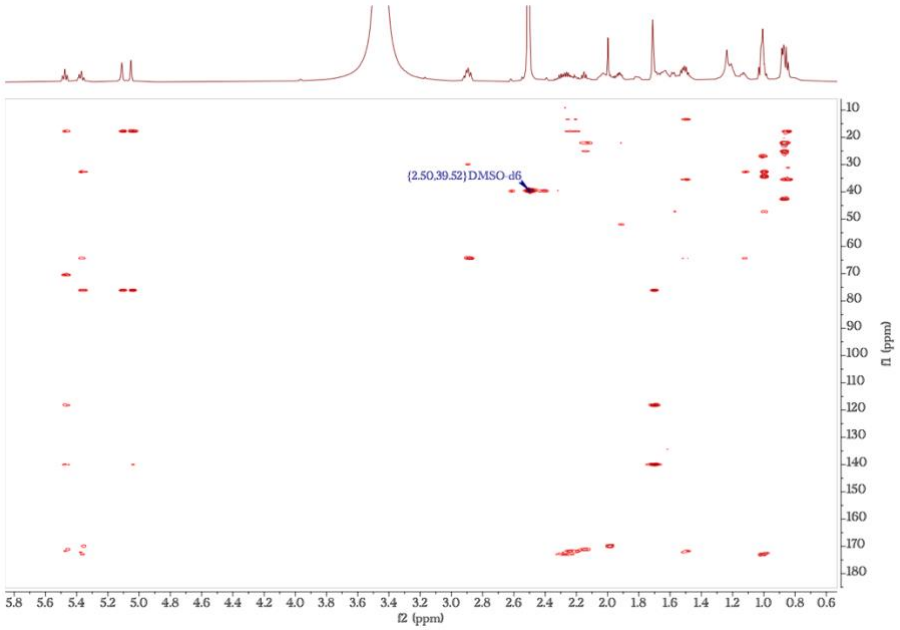

Figure 4.9.31. HMBC NMR spectra for andrognathine F (**4.6**) (600 MHz, *d6*-DMSO) 32 scans, NUS50 and 512 increments.

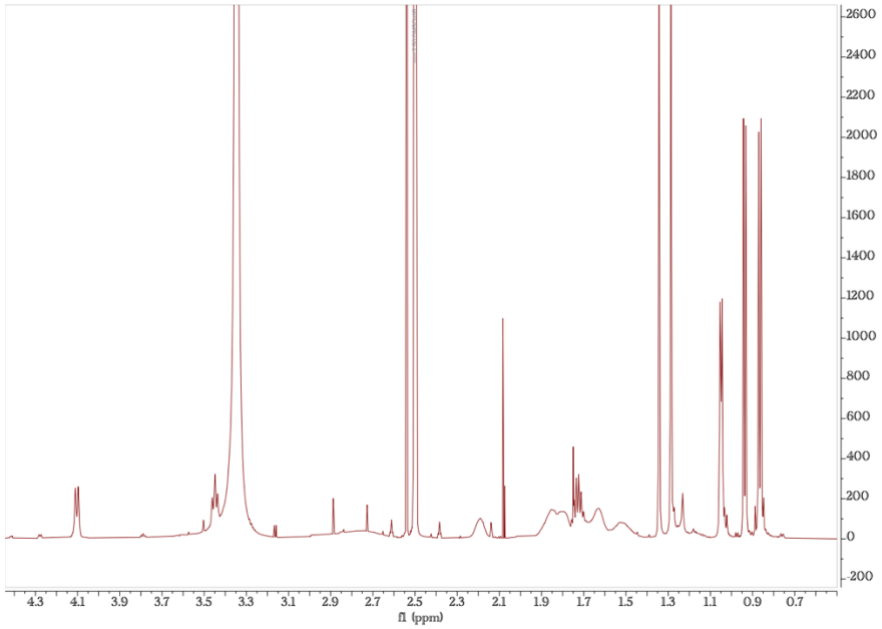

Figure 4.9.32. ^{1}H NMR spectra for andrognathine acetonide (**4.7**) (600 MHz, *d6*-DMSO) 256 scans.

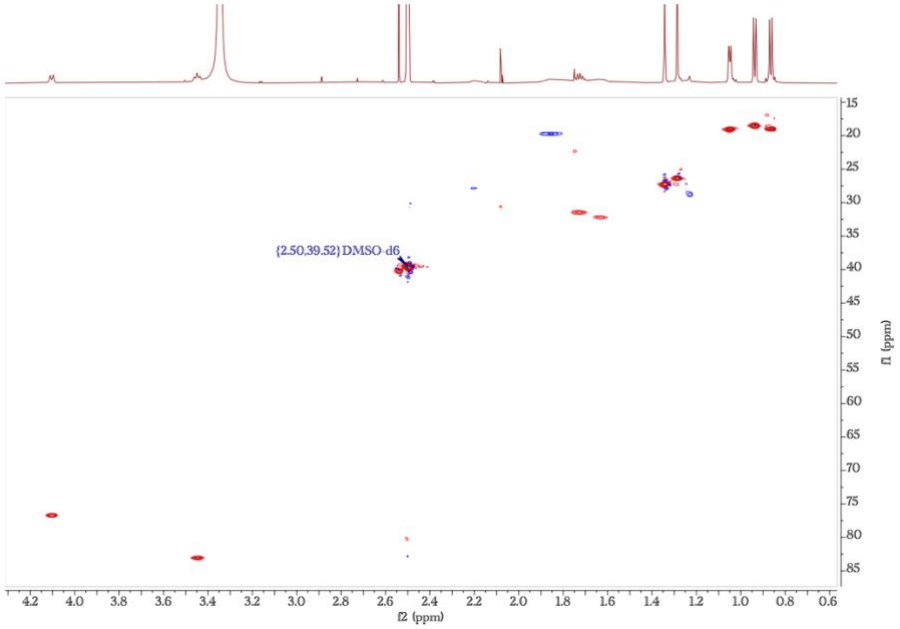

Figure 4.9.33. gHSQC NMR spectra for andrognathine acetonide (**4.7**) (600 MHz, *d*$_6$-DMSO) 512 scans, NUS25 and 400 increments.

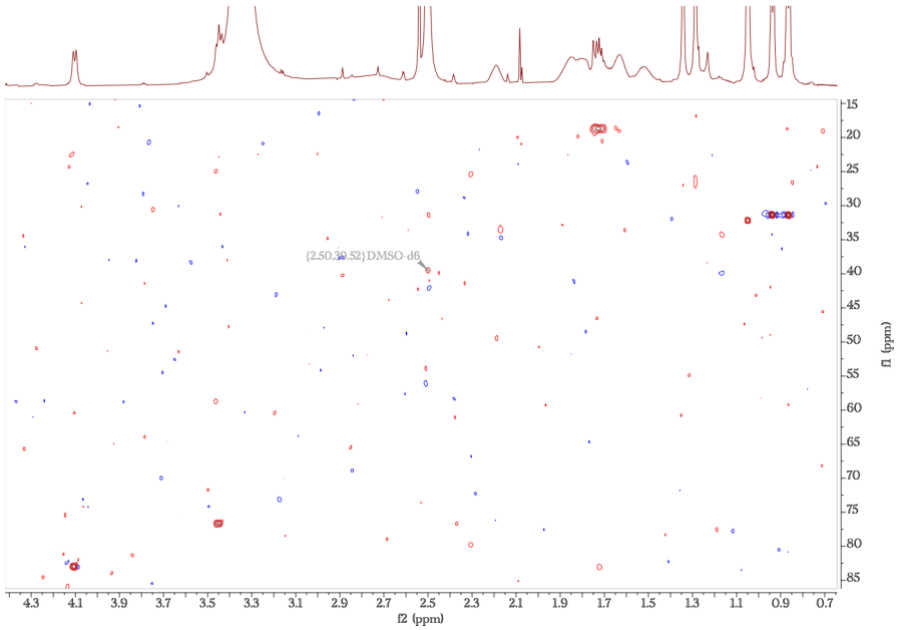

Figure 4.9.34. H2BC NMR spectra for andrognathine acetonide (**4.7**) (600 MHz, *d*$_6$-DMSO) 128 scans, NUS50 and 256 increments.

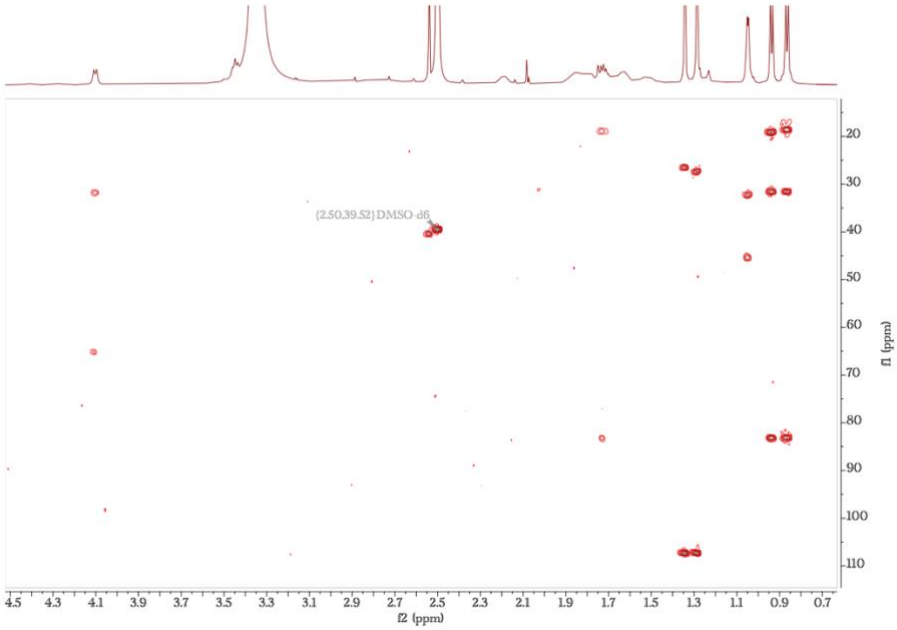

Figure 4.9.35. HMBC NMR spectra for andrognathine acetonide (**4.7)** (600 MHz, *d6*-DMSO) 128 scans, NUS50 and 256 increments.

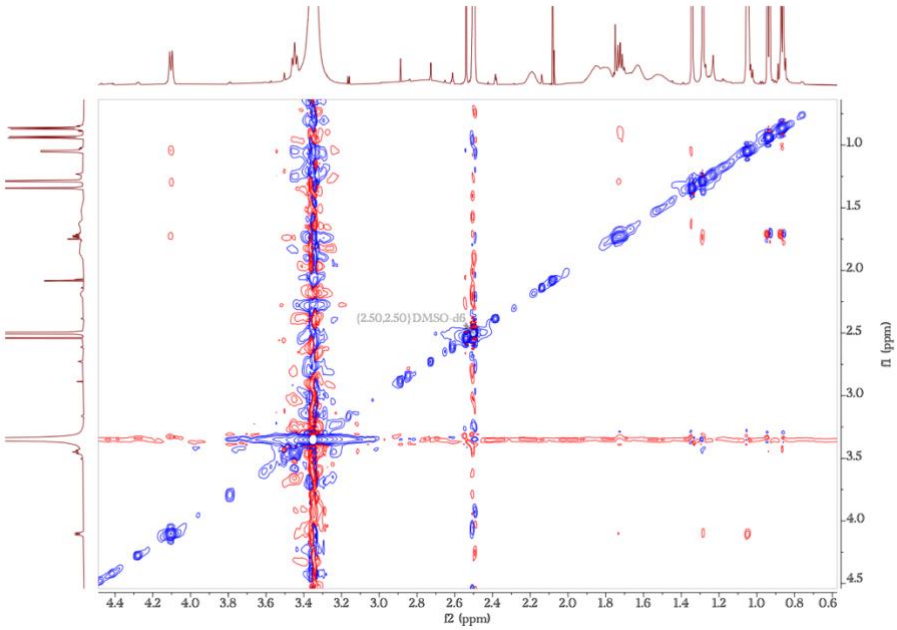

Figure 4.9.36. easyROESY NMR spectra for andrognathine acetonide (**4.7**) (600 MHz, *d6*-DMSO) 128 scans, NUS50 and 256 increments.

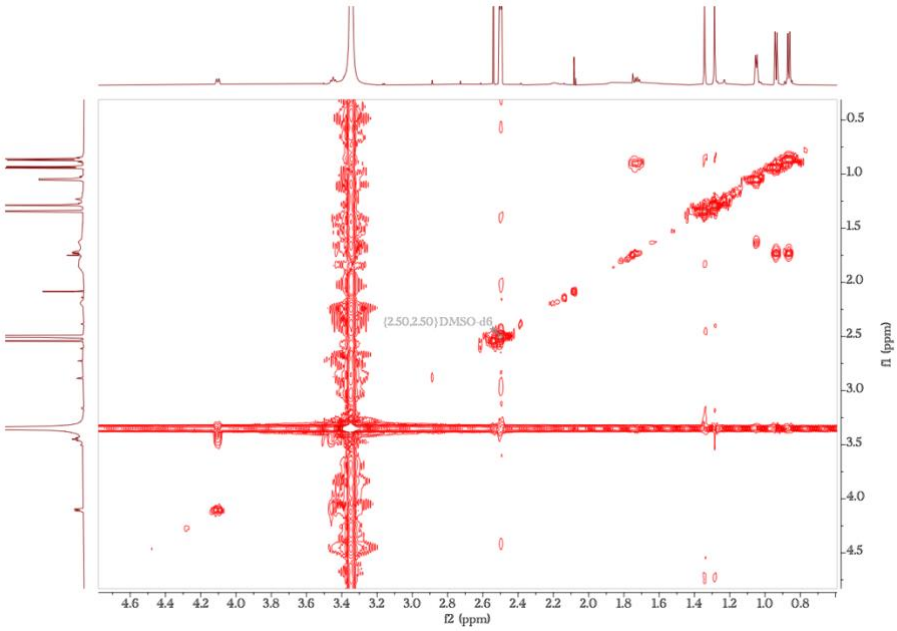

Figure 4.9.37. COSY NMR spectra for andrognathine acetonide (**4.7**) (600 MHz, *d6*-DMSO) 64 scans, NUS50 and 256 increments.

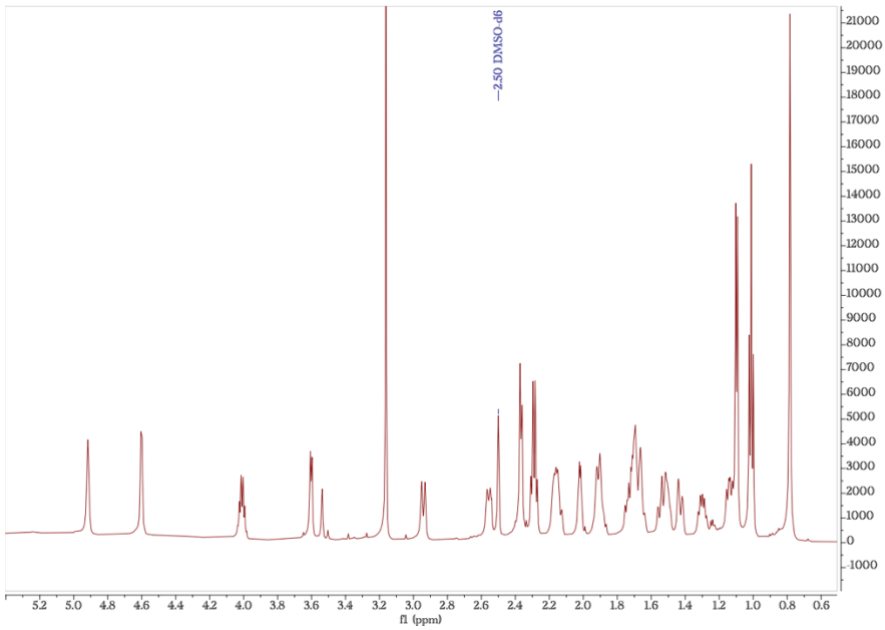

Figure 4.9.38. ^{1}H NMR spectra for andrognathanol A (**4.9**) (600 MHz, *d6*-DMSO) 128 scans.

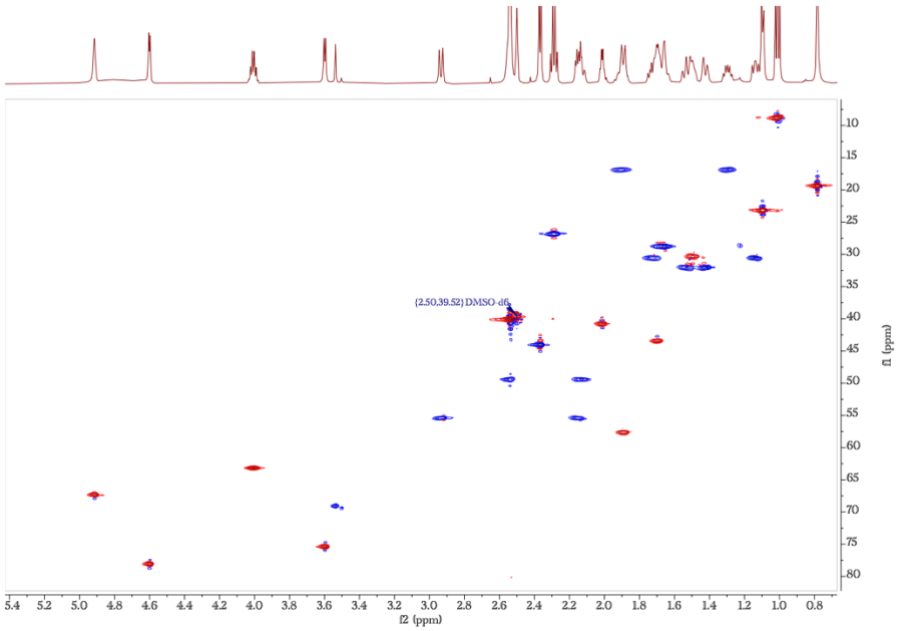

Figure 4.9.39. gHSQC NMR spectra for andrognathanol A (**4.9**) (600 MHz, d_6-DMSO) 64 scans, NUS25 and 400 increments.

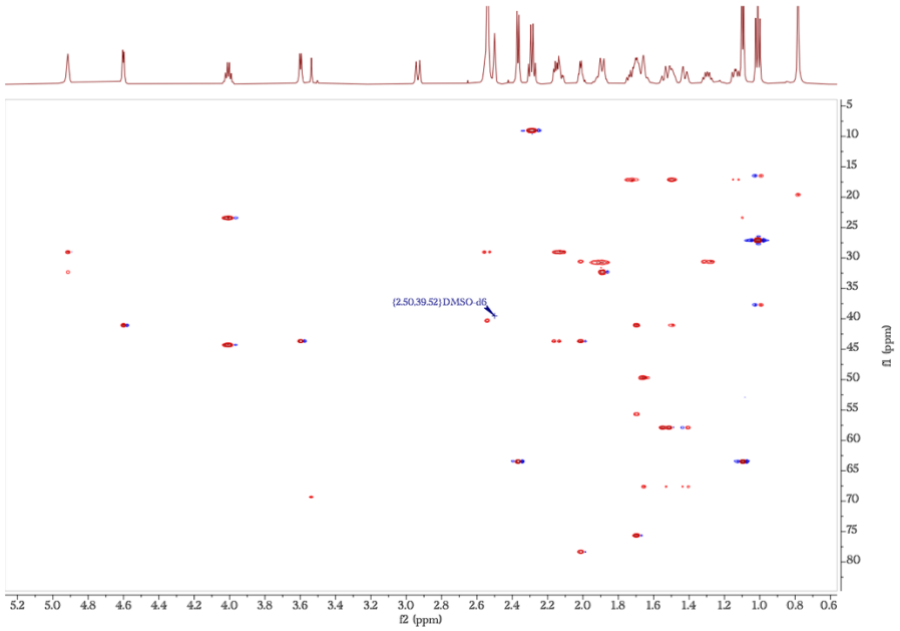

Figure 4.9.40. H2BC NMR spectra for andrognathanol A (**4.9**) (600 MHz, d_6-DMSO) 64 scans, NUS50 and 400 increments.

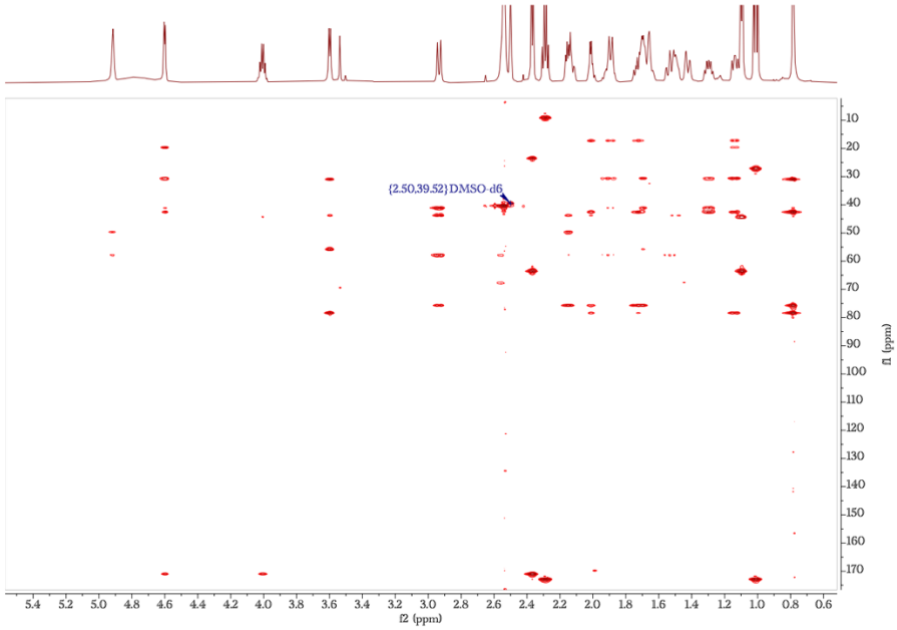

Figure 4.9.41. HMBC NMR spectra for andrognathanol A (**4.9**) (600 MHz, *d6*-DMSO) 64 scans, NUS50 and 292 increments.

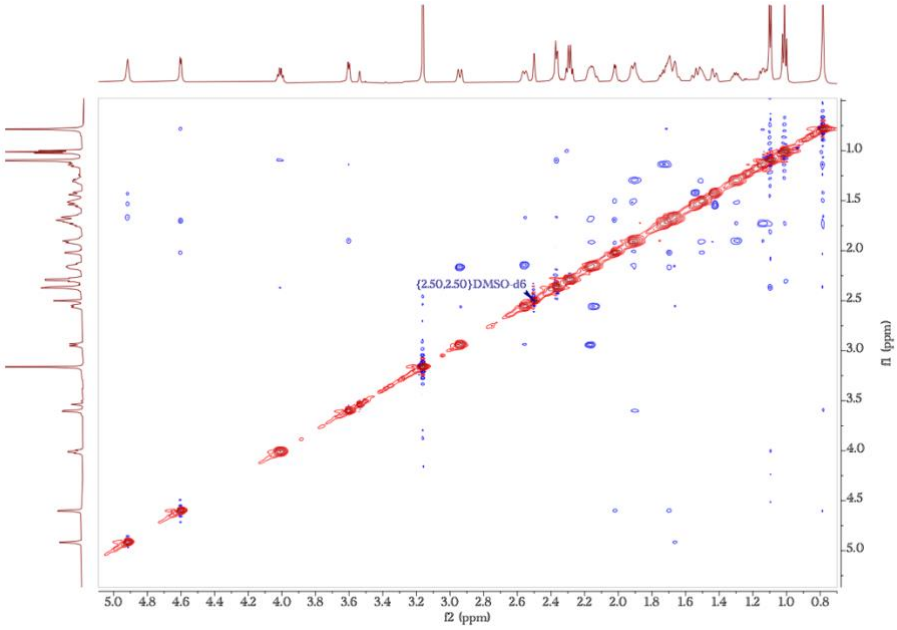

Figure 4.9.42. easyROESY NMR spectra for andrognathanol A (**4.9**) (600 MHz, *d6*-DMSO) 64 scans, NUS50 and 356 increments.

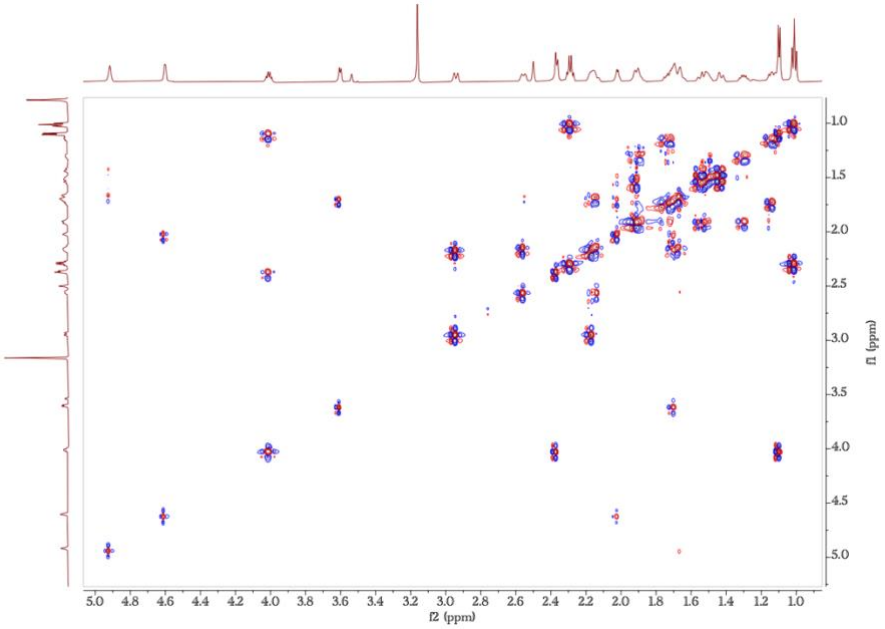

Figure 4.9.43. dqfCOSY NMR spectra for andrognathanol A (**4.9**) (600 MHz, *d6*-DMSO) 48 scans, NUS50 and 256 increments.

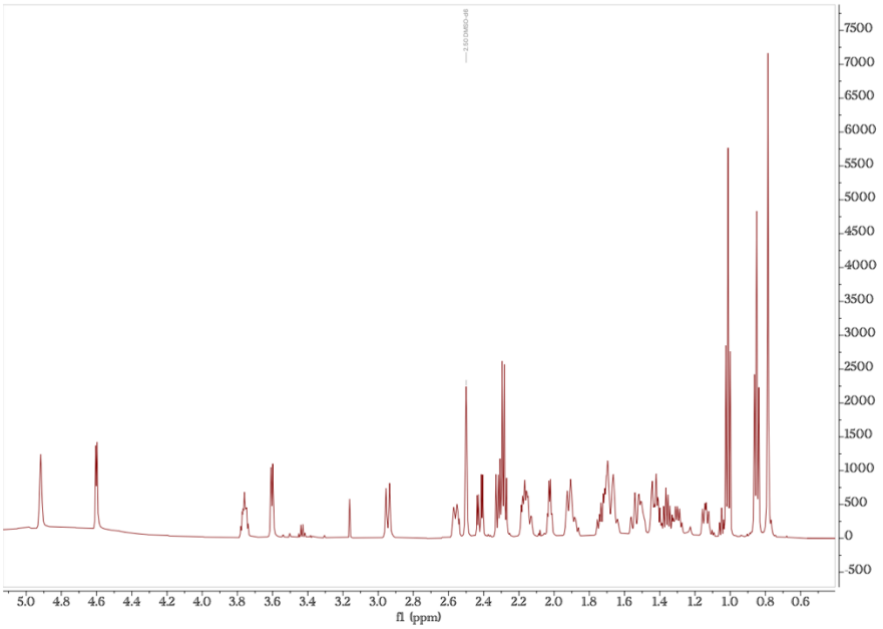

Figure 4.9.44. ^{1}H NMR spectra for andrognathanol B (**4.10**) (600 MHz, *d6*-DMSO) 128 scans.

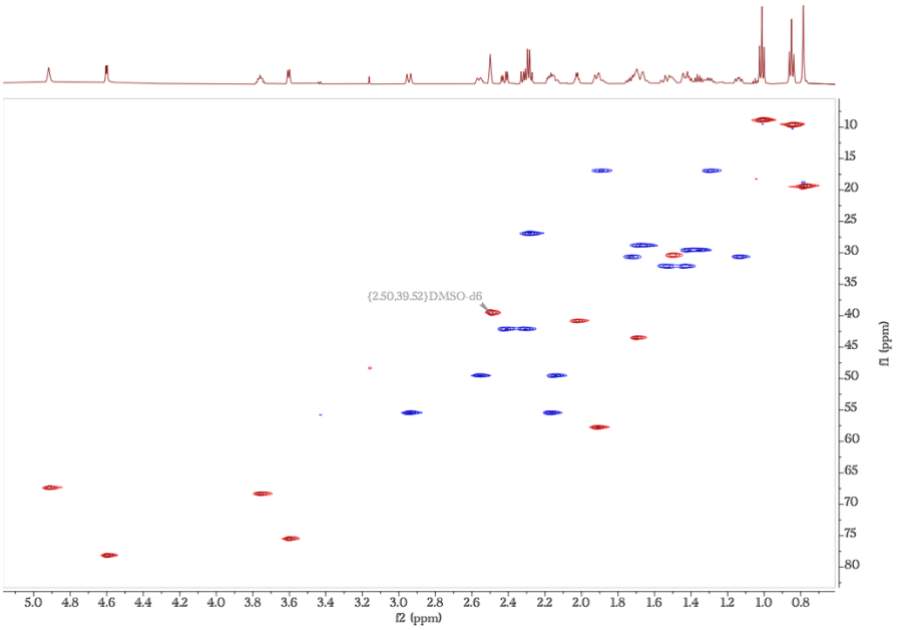

Figure 4.9.45. gHSQC NMR spectra for andrognathanol B (**4.10**) (600 MHz, *d6*-DMSO) 32 scans, NUS25 and 400 increments.

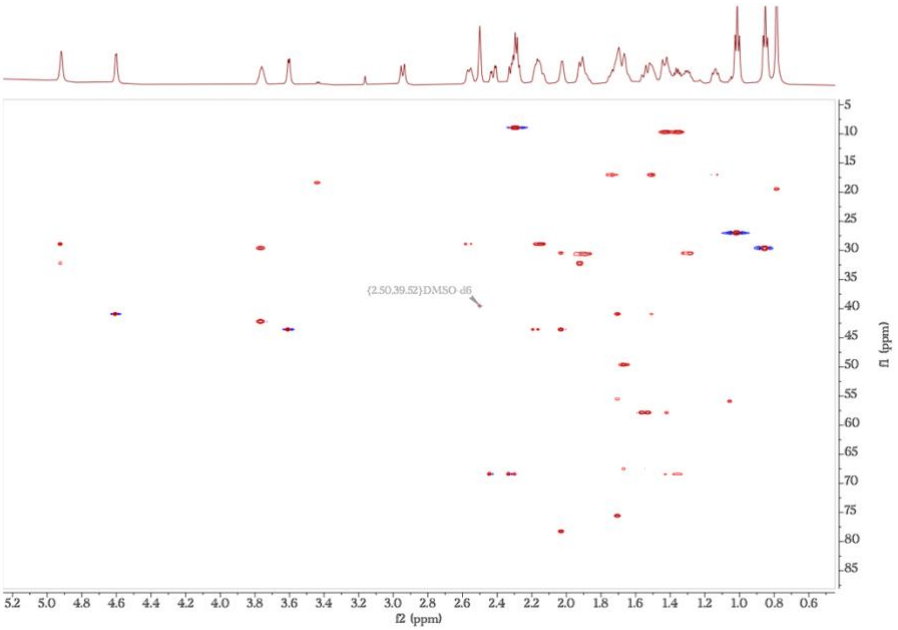

Figure 4.9.46. H2BC NMR spectra for andrognathanol B (**4.10**) (600 MHz, *d6*-DMSO) 32 scans, NUS50 and 400 increments.

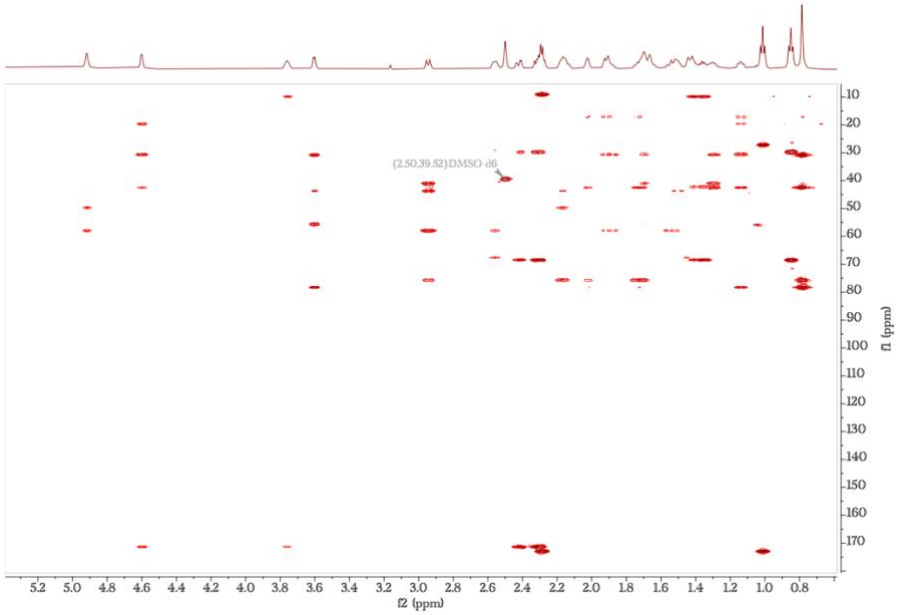

Figure 4.9.47. HMBC NMR spectra for andrognathanol B (**4.10**) (600 MHz, *d6*-DMSO) 32 scans, NUS50 and 512 increments.

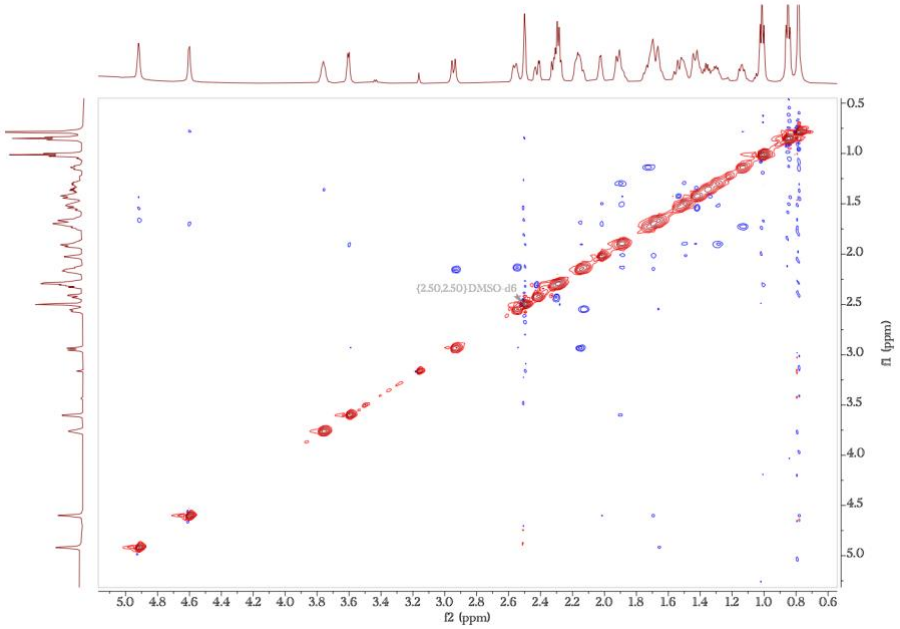

Figure 4.9.48. easyROESY NMR spectra for andrognathanol B (**4.10**) (600 MHz, *d6*-DMSO) 32 scans, NUS50 and 400 increments.

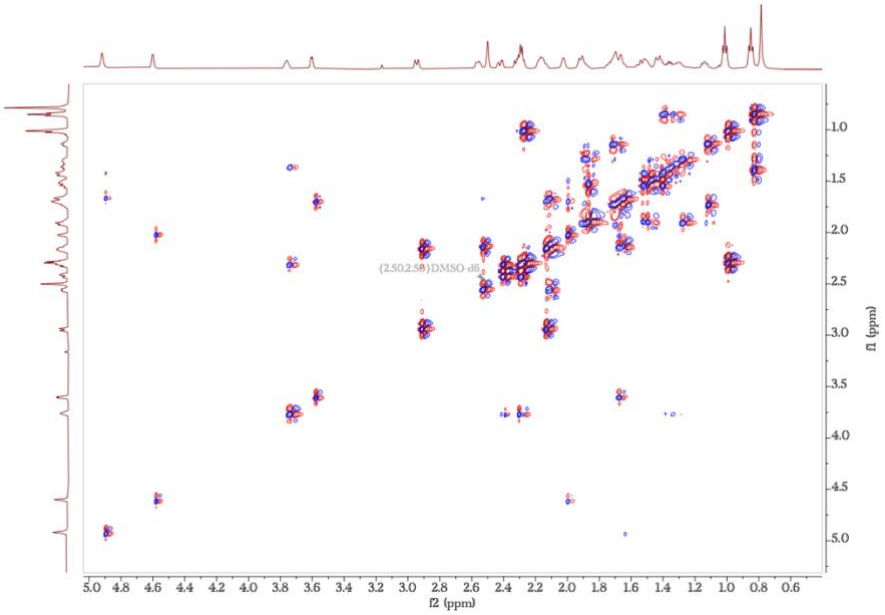

Figure 4.9.49. dqfCOSY NMR spectra for andrognathanol B (**4.10**) (600 MHz, *d6*-DMSO) 16 scans, NUS50 and 256 increments.

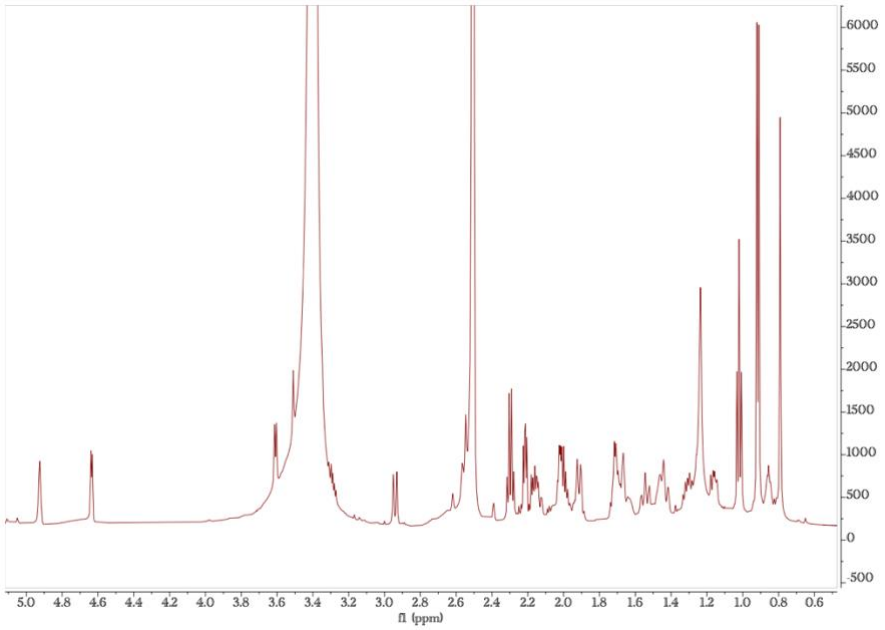

Figure 4.9.50. ^{1}H NMR spectra for andrognathanol C (**4.11**) (600 MHz, *d6*-DMSO) 256 scans.

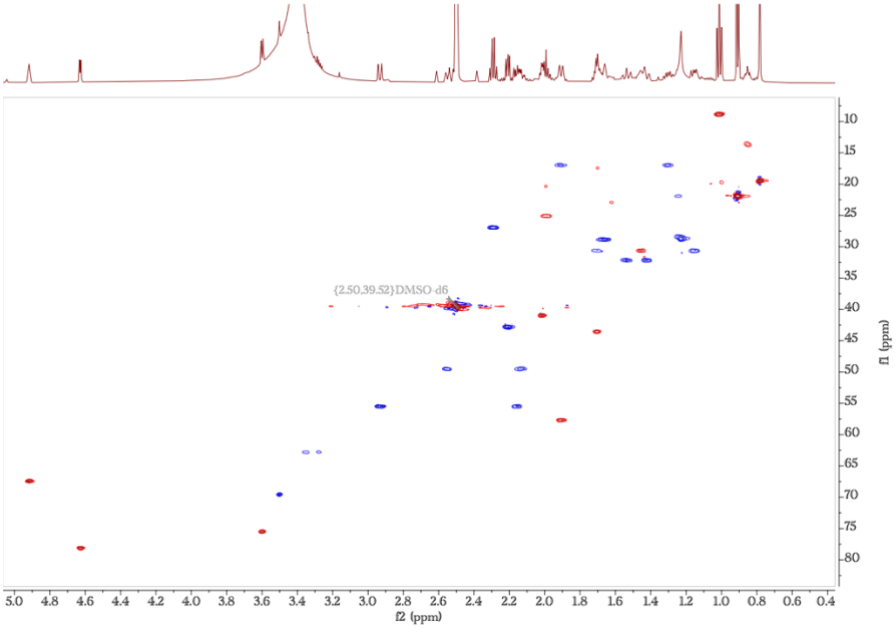

Figure 4.9.51. gHSQC NMR spectra for andrognathanol C (**4.11**) (600 MHz, *d*$_6$-DMSO) 64 scans, NUS25 and 400 increments.

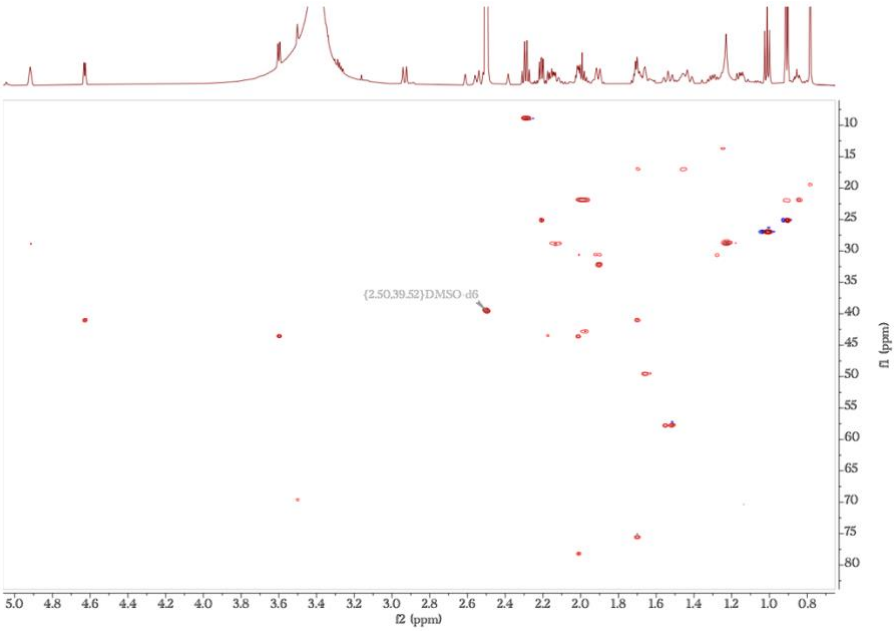

Figure 4.9.52. H2BC NMR spectra for andrognathanol C (**4.11**) (600 MHz, *d*$_6$-DMSO) 64 scans, NUS50 and 400 increments.

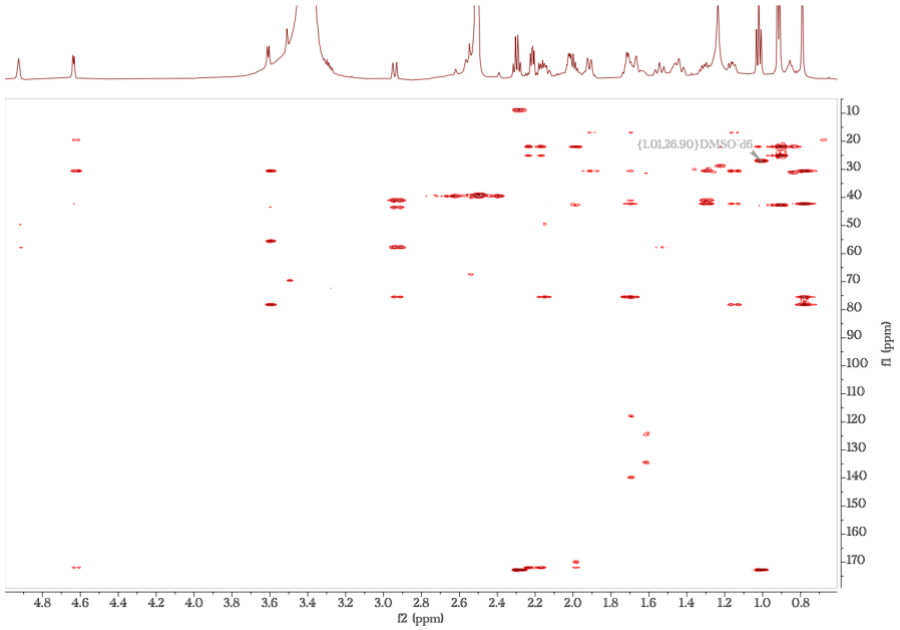

Figure 4.9.53. HMBC NMR spectra for andrognathanol C (**4.11**) (600 MHz, *d6*-DMSO) 256 scans, NUS50 and 512 increments.

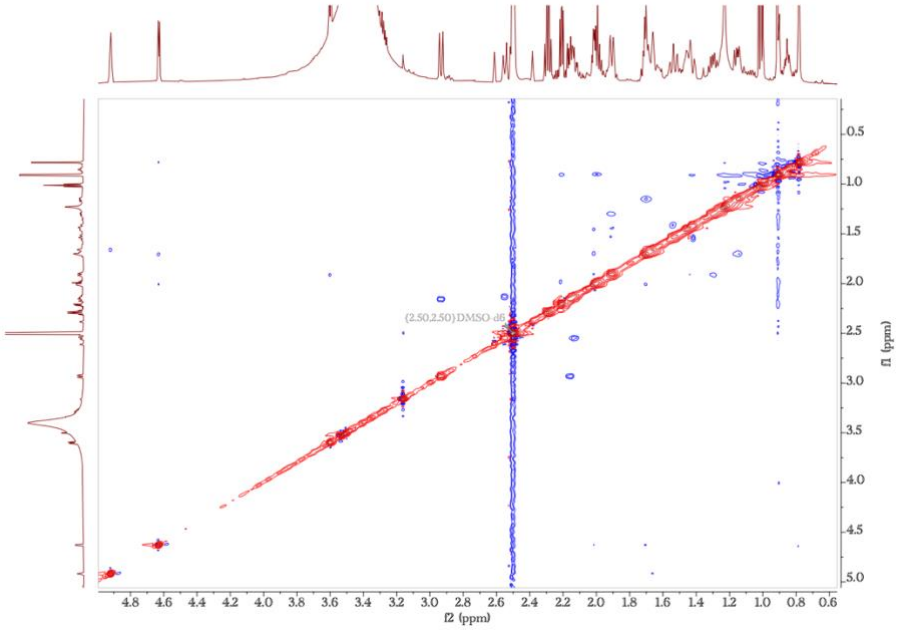

Figure 4.9.54. easyROESY NMR spectra for andrognathanol C (**4.11**) (600 MHz, *d6*-DMSO) 64 scans, NUS50 and 400 increments.

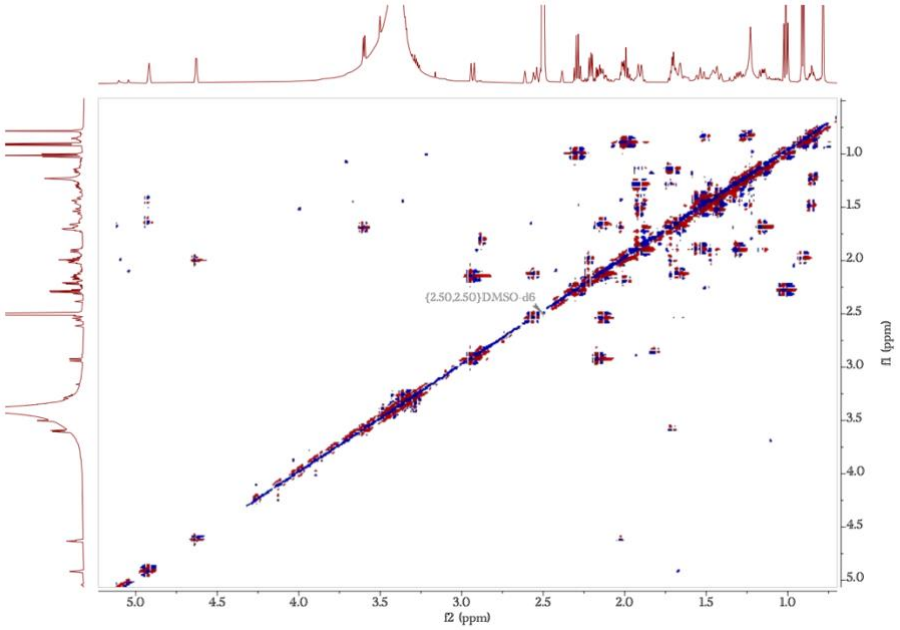

Figure 4.9.55. dqfCOSY NMR spectra for andrognathanol C (**4.11**) (600 MHz, *d6*-DMSO) 64 scans, NUS50 and 400 increments.

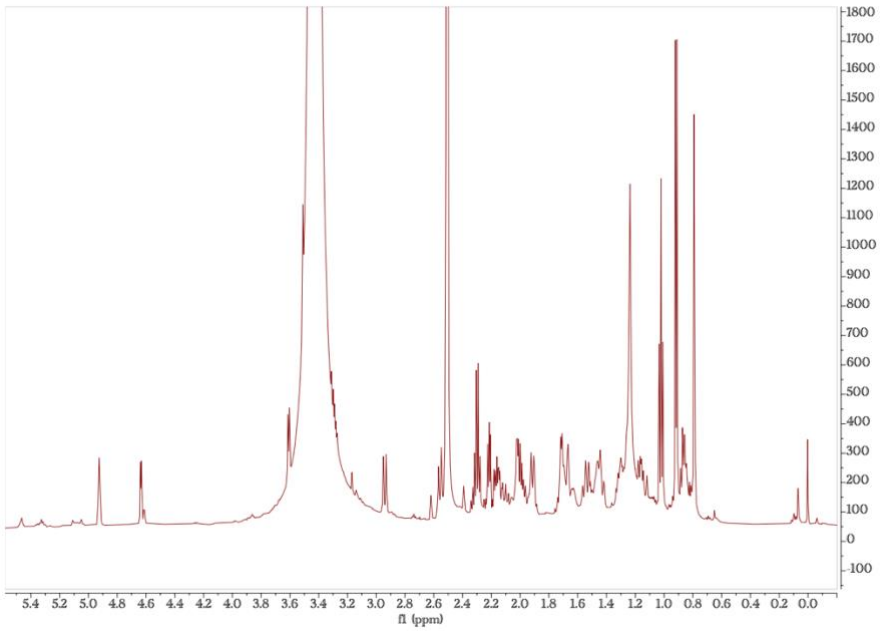

Figure 4.9.56. ^{1}H NMR spectra for andrognathanol D (**4.12**) (600 MHz, *d6*-DMSO) 128 scans.

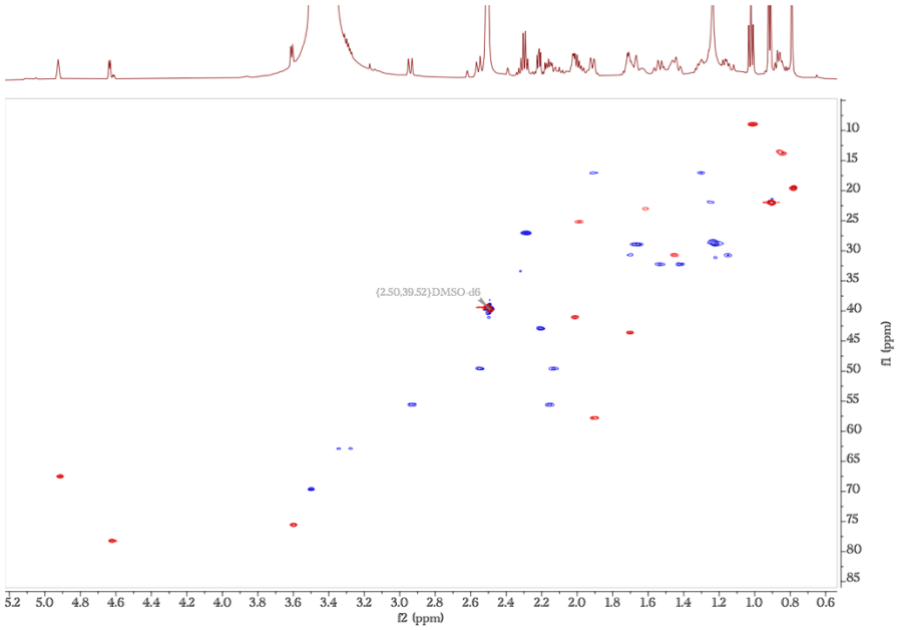

Figure 4.9.57. gHSQC NMR spectra for andrognathanol D (**4.12**) (600 MHz, d_6-DMSO) 64 scans, NUS25 and 400 increments.

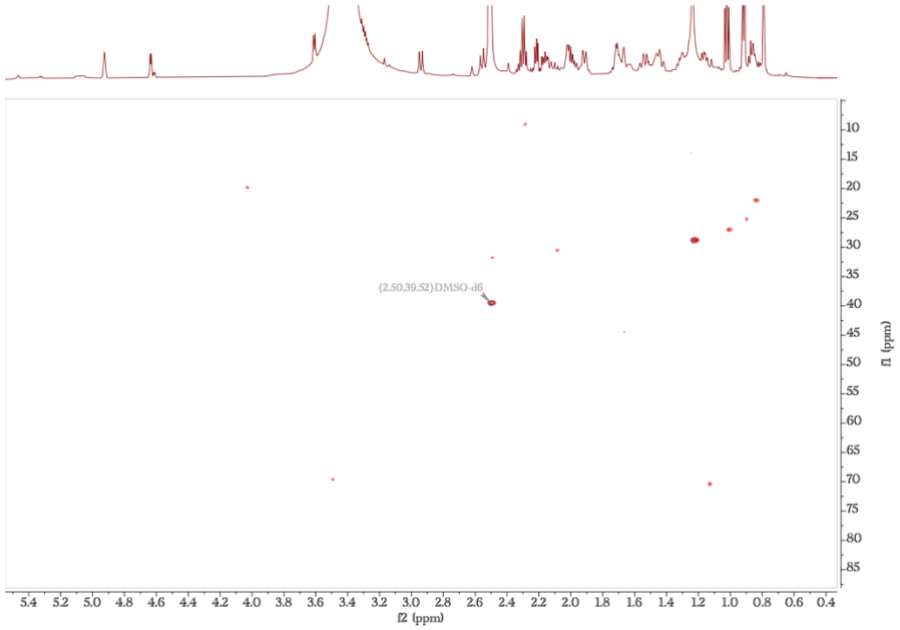

Figure 4.9.58. H2BC NMR spectra for andrognathanol D (**4.12**) (600 MHz, d_6-DMSO) 64 scans, NUS50 and 400 increments.

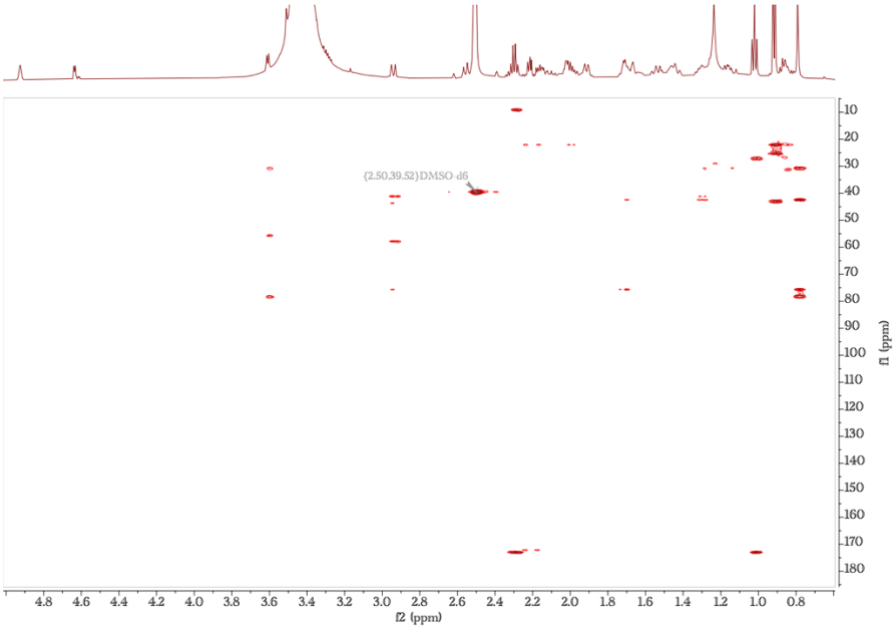

Figure 4.9.59. HMBC NMR spectra for andrognathanol D (**4.12**) (600MHz, d_6-DMSO) 32 scans, NUS50 and 512 increments.

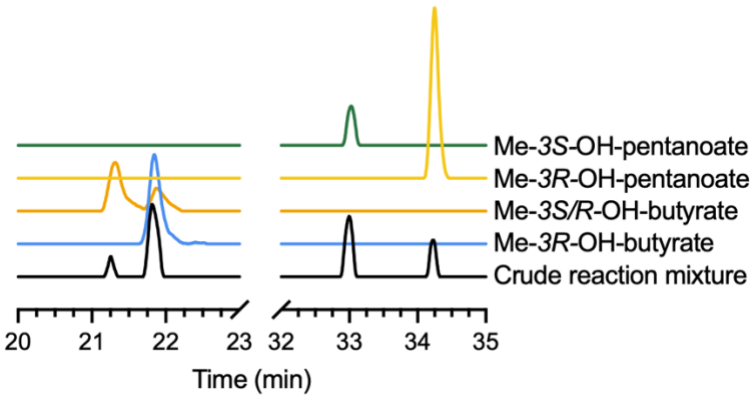

Figure 4.9.60. Ester side chain reactions. Stacked chromatograms of the methylated hydrolysate of crude extract along with Me-OH-pentanoate and Me-OH-butyrate standards, confirming the incorporation of both (*R*)- and (*S*)-Me-OH-pentanoate and (*R*)- and (*S*)-Me-OH-butyrate.

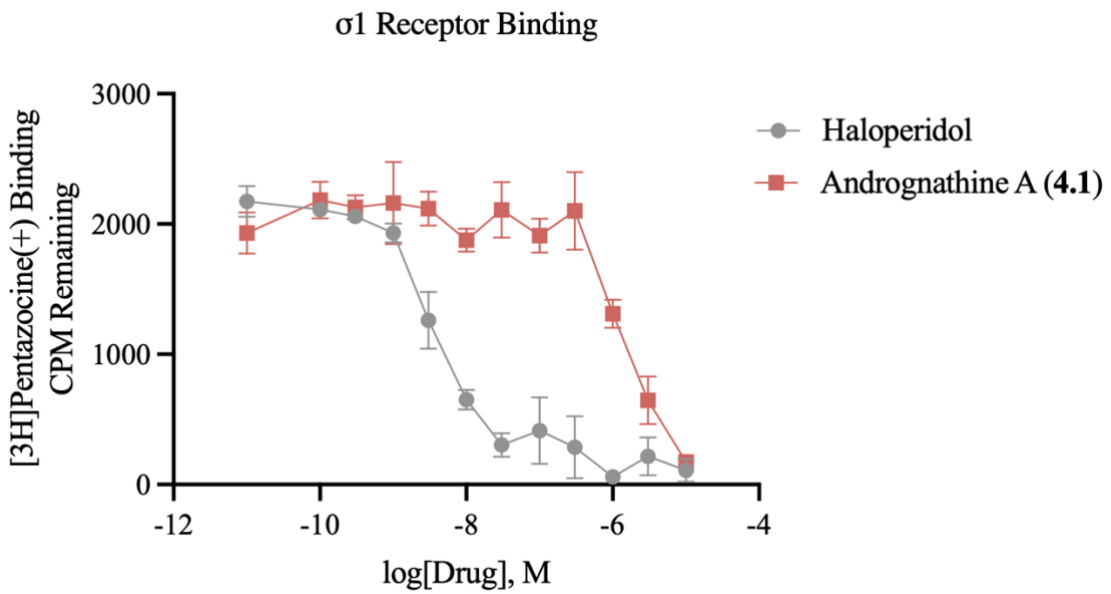

Figure 4.9.61. σ_1R Binding. Secondary screening of andrognathine A (**4.1**), and positive control Haloperidol.

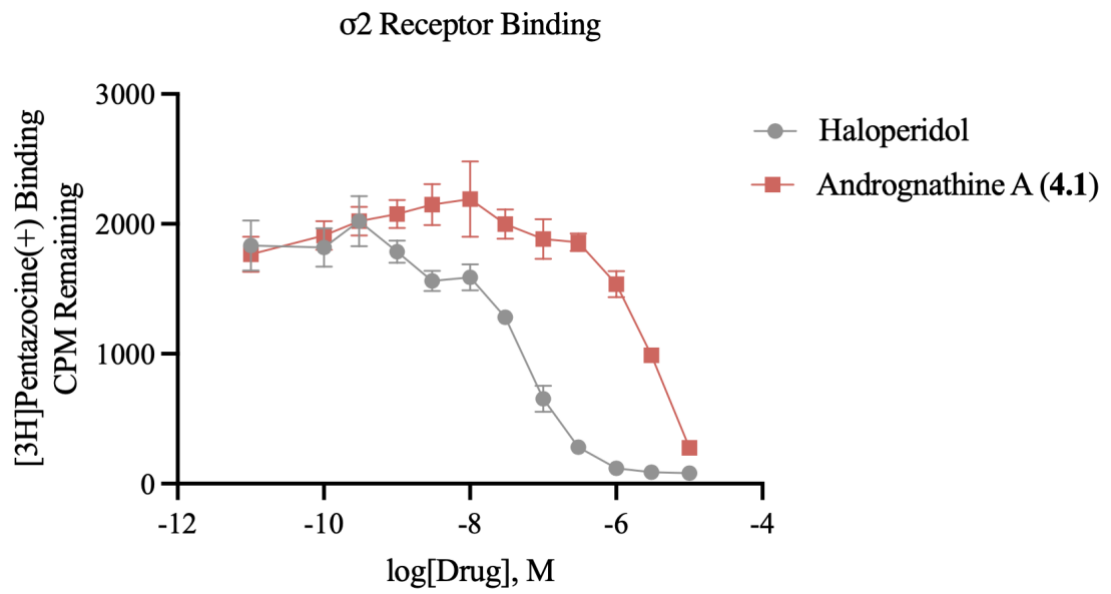

Figure 4.9.62. σ_2R Binding. Secondary screening of Andrognathine A (**4.1**), and positive control Haloperidol.

4.10. Appendix Tables

Table 4.10.29. NMR Spectroscopy Data for Andrognathine A (**4.1**)
(600 MHz, d_6-DMSO, 25 °C)

Position	δ_C, type[a]	δ_H (J in Hz)	H2BC	HMBC	COSY	ROESY
1	19.8, CH_3	1.00, d, 5.2	2	2, 3, 9	2	3b, 10
2	32.5, CH	1.21, m	1, 9		1	9, 4b
3a	34.1, CH_2	1.21, m	4	4, 9	4	
3b		1.58, m				1
4a	51.8, CH_2	1.85, m	3	2, 8	3, 8	
4b		2.91, m				2, 8
5a	53.1, CH_2	1.96, m	6	4, 6, 7, 8	6	
5b		2.94, m				
6	20.5, CH_2	1.65, m	5, 7		5	
7a	29.7, CH_2	1.53, m	6, 8	6, 8		
7b		2.03, m				11
8	64.3, CH	1.76, t, 10.2	7, 9	4	4, 9	4b
9	47.1, CH	1.16, m	2, 8	2, 8, 10	8	2, 10, 13
10	70.1, CH	5.38, d, 9.3	11	2, 8, 9, 11, 12, 15		1, 9, 13
11	76.1, CH_2	5.45, d, 9.3	10	10, 12, 13, 14, 20		7b, 13
12	139.9, C					
13	17.5, CH_3	1.70, s		11, 12, 14	14	9, 11
14a	118.1,	5.04, s		11, 12, 13	13	
14b	CH_2	5.10, s				
15	172.3, C					
16a	33.2, CH_2	2.21, m	17	15, 17, 18, 19		
16b		2.25, m				
17	26.5, CH_2	1.45, m	16, 18	16, 18, 19	18	18
18	21.6, CH_2	1.24, m	17, 19	16, 17, 19	17, 19	17
19	13.3, CH_3	0.87, m	18	17, 18	18	
20	171.8, C					
21a	35.3, CH_2	2.22, m	22	20, 22, 23		
21b		2.27, m				
22	17.9, CH_2	1.53, m	23	20, 21, 23	23	
23	21.9, CH_3	0.86, m	22	21, 22	22	

[a]δ_C obtained indirectly through gHSQC and gHMBC data.

Table 4.10.30. NMR Spectroscopy Data for Andrognathine B (**4.2**)
(600 MHz, d_6-DMSO, 25 °C)

Position	δ_C, type[a]	δ_H (J in Hz)	H2BC	HMBC	COSY	ROESY
1	19.7, CH_3	1.01, d, 5.2	2	9		10, 13
2	32.5, CH	1.20, m	1, 9			9
3a	34.2, CH_2	1.20, m	4	1		
3b		1.58, m				
4a	51.8, CH_2	1.79, m		1		
4b		2.88, m				
5a	53.2, CH_2	1.91, m		4, 8		
5b		2.90, m	6			
6	20.4, CH_2	1.63, m	5, 7			
7a	29.7, CH_2	1.51, m	6	8		11
7b		2.02, m				
8	64.1, CH	1.68, m	9		9	
9	47.1, CH	1.12, m	2	2, 8	8	2, 10, 11, 13
10	70.1, CH	5.38, d, 9.7	11	2, 8, 9, 11, 15	11	1, 9, 13
11	75.9, CH	5.47, d, 9.7	10	10, 12, 13, 14, 19	10	7a, 9, 13
12	140.0, C					
13	17.5, CH_3	1.71, s		11, 12, 14	14	1, 9, 10, 11, 22
14a	118.1,	5.05, s		13, 11	13	
14b	CH_2	5.11, s				
15	171.8, C					
16a	35.2, CH_2	2.21, m	17	15, 17	17	
16b		2.27, m				
17	17.7, CH_2	1.51, m	16, 18	15, 16	16, 18	
18	13.2, CH_3	0.87, m	17	15, 16, 17	17	
19	171.8, C					
20a	35.2, CH_2	2.21, m	21	19, 21	21	
20b		2.27, m				
21	17.7, CH_2	1.51, m	20, 22	19, 20	20, 22	
22	13.2, CH_3	0.87, m	21	15, 20. 21	21	13

[a]δ_C obtained indirectly through gHSQC and gHMBC data.

Table 4.10.31. NMR Spectroscopy Data for Andrognathine C (**4.3**) (600 MHz, d_6-DMSO, 25 °C)

Position	δ_C, type[a]	δ_H (J in Hz)	H2BC	HMBC	COSY	ROESY
1	19.6, CH_3	1.00, m	2	2, 3, 9		3b, 10
2	32.4, CH	1.20, m	1, 9			
3a	34.1, CH_2	1.20, m	4	9	4	
3b		1.57, m				1
4a	51.7, CH_2	1.79, m	3		3, 5	
4b		2.87, m				
5a	53.2, CH_2	1.90, m	6	7, 8	4, 6	
5b		2.90, m				
6	20.4, CH_2	1.64, m	5		5	
7a	29.6, CH_2	1.51, m	6, 8	8		11
7b		2.02, m				
8	64.1, CH	1.68, m	7, 9		9	9
9	47.1, CH	1.12, t, 9.3	2, 8	2, 8	8	8, 10
10	70.1, CH	5.37, d, 8.4	11	2, 9, 11, 15		1, 9, 13
11	75.9, CH	5.47, d, 8.4	10	10, 12, 13, 14, 19		7a, 13
12	140.0, C					
13	17.5, CH_3	1.71, s		11, 12, 14		10, 11
14a	118.1, CH_2	5.04, s		11, 12, 13		
14b		5.10, s				
15	173.2, C					
16a	26.7, CH_2	2.26, m	17	15, 17		
16b		2.30, m				
17	8.8, CH_3	1.02, m	16	15, 16		
19	171.9, C					
20	33.1, CH_2	2.26, m	21	19, 21, 22, 23	21	
21	26.3, CH_2	1.45, m	20, 22	19, 20, 22, 23	20, 22	
22	17.7, CH_2	1.51, m	21, 23	20, 23	21, 23	
23	13.3, CH_3	0.85, m	22	21, 22	22	

[a]δ_C obtained indirectly through gHSQC and gHMBC data.

Table 4.10.32. NMR Spectroscopy Data for Andrognathine D (**4.4**) (600 MHz, d_6-DMSO, 25 °C)

Position	δ_C, type[a]	δ_H (J in Hz)	H2BC	HMBC	COSY
1	19.6, CH_3	1.01, m	2	2, 3	2
2	32.5, CH	1.20, m			1
3	34.3, CH_2	1.57, m			4
4a	51.8, CH_2	2.87, m		8	3
4b		1.80, m			
5a	53.1, CH_2	2.90, m		4	
5b		1.92, m			
6	20.5, CH_2	1.63, m			
7	26.3, CH_2	1.52, m			8
8	64.1, CH	1.67, m			7, 9
9	47.1, CH	1.13, m			8
10	70.3, CH	5.37, d, 9.0	11	11 15, 16	
11	75.9, CH	5.46, d, 9.0	10	10, 13, 19	
12	140.4, C				
13	17.6, CH_3	1.71, s		11	
14a	117.9, CH_2	5.04, s		12, 13, 14	
14b		5.10, s			
15	172.2, C				
16a	35.4, CH_2	2.23, m		15, 17	
16b		2.26, m			
17	17.5, CH_2	1.52, q, 7.1	16	16, 18	18
18	21.7, CH_3	0.87, m	17	16, 17	17
19	171.8, C				
20a	33.2, CH_2	2.22, m		19, 23, 21	
20b		2.27, m			
21	26.2, CH_2	1.46, t, 7.7	20		22
22	21.2, CH_2	1.27, m	21, 23	23	21, 23
23	13.1, CH_3	0.85, m	22	21, 22	22

[a]δ_C obtained indirectly through gHSQC and gHMBC data.

Table 4.10.33. NMR Spectroscopy Data for Andrognathine E (**4.5**) (600 MHz, d_6-DMSO, 25 °C)

Position	δ_C, type[a]	δ_H (J in Hz)	H2BC	HMBC	COSY
1	19.8, CH_3	1.01, d, 5.4	2	3, 9	2
2	32.6, CH	1.20, m	1, 9		1
3a	34.3, CH_2	1.21, m	4		
3b		1.57, d, 9.1			
4a	51.9, CH_2	1.79, t, 10.9	5		3, 5
4b		2.87, m			
5a	53.3, CH_2	1.90, m	6	4	4
5b		2.90, m			
6	20.5, CH_2	1.62, m	5	7	
7	17.9, CH_2	1.52, m	6		
8	64.3, CH	1.68, m	9		9
9	47.3, CH	1.13, m	2, 10	2, 10	8
10	70.3, CH	5.38, d, 9.2	11	2, 8, 9, 11, 15	
11	76.1, CH	5.46, d, 9.2	10	10, 12, 13, 14, 19	
12	139.9, C				
13	17.6, CH_3	1.70, s		11, 12, 14	
14a	118.1, CH_2	5.04, s		11, 12, 13	
14b		5.10, s			
15	171.2, C				
16a	35.4, CH_2	2.27, m	17	15, 16, 18	17
16b		2.22, m			
17	17.6, CH_2	1.52, m	16, 18	15, 16, 18	16, 18
18	13.5, CH_3	0.88, m	17	17	17
19	172.2, C				
20a	42.6, CH_2	2.11, m		19, 21	
20b		2.15, m			
21	21.5, CH_3	0.88, m		20	

[a]δ_C obtained indirectly through gHSQC and gHMBC data.

Table 4.10.34. NMR Spectroscopy Data for Andrognathine F (**4.6**) (600 MHz, d_6-DMSO, 25 °C)

Position	δ_C, type[a]	δ_H (J in Hz)	HMBC
1	19.8, CH_3	1.01, m	2
2	32.5, CH	1.20, m	
3a	34.4, CH_2	1.20, m	9
3b		1.57, m	
4a	52.0, CH_2	1.80, m	2, 3, 8
4b		2.87, m	
5a	53.2, CH_2	1.91, m	4, 7
5b		2.90, m	
6	20.5, CH_2	1.63, m	
7a	29.9, CH_2	1.50, m	8
7b		2.02, m	
8	64.1, CH	1.68, m	
9	47.3, CH	1.12, m	2, 9
10	70.3, CH	5.36, m	8, 11
11	76.1, CH	5.47, m	10, 12, 13, 14
12	139.9, C		
13	17.7, CH_3	1.70, s	11, 12, 14
14a	118.1, CH_2	5.05, s	11, 12, 13
14b		5.11, s	
15	173.1, C		
16	26.9, CH_2	2.27, m	17
17	9.1, CH_3	1.01, m	10, 16
18	171.7, C		
19a	35.3, CH_2	2.20, m	18, 20, 21
19b		2.27, m	
20	17.9, CH_2	1.50, m	19, 21
21	13.5, CH_3	0.85, m	19, 20

[a] δ_C obtained indirectly through gHSQC and gHMBC data.

Table 4.10.35. NMR Spectroscopy Data for Andrognathine Acetonide (**4.7**)
(600 MHz, d_6-DMSO, 25 °C)

Position	δ_C, type[a]	δ_H (J in Hz)	H2BC	HMBC	COSY	ROESY
1	18.9, CH_3	1.05, d, 5.7	2	2, 9	2	11
2	32.0, CH	1.62, m			1	
3	28.6, CH_2	1.23, m				
4	ND[b]					
5	ND[b]					
6	19.6, CH_2	1.84, m				
7	27.8, CH_2	2.21, m				
8	65.9, CH	ND[b]				
9	45.2, CH	1.65, m				
10	74.7, CH	4.10, d, 8.2	11	2, 8		1, 12, 16
11	83.2, CH	3.44, t, 7.5	10, 12			
12	31.3, CH	1.73, m	13, 14	11, 14	13, 14	10, 13, 14, 16
13	18.4, CH_3	0.94, d, 6,7	12	11, 12, 14	12	12
14	18.9, CH_3	0.86, d, 6.7		11, 12, 13	12	12
15	107.3, C					
16	27.2, CH_3	1.33, s		15, 17		10, 12
17	26.3, CH_2	1.29, s		15, 16		

[a]δ_C obtained indirectly through gHSQC and gHMBC data. [b]ND: Not detected. Significant peak broadening occurred in signals near the tertiary amine. This led to weak and/or missing signals.

Table 4.10.36. Comparison of Experimental and Calculated Chemical Shifts for **4.7**

Position	δ_C[a]	4.7a	4.7b	δ_H	4.7a	4.7b
1	18.9	19.9	20.8	1.05	1.37	1.37
2	32.0	36.7	35.0	1.62	1.74	1.78
3a	28.6	28.7	30.9	1.23	1.18	1.37
3b				ND[b]	2.53	1.96
4a	ND[b]	52.4	52.4	ND[b]	3.11	3.05
4b				ND[b]	2.15	2.07
5	ND[b]	67.9	65.9	ND[b]	2.28	2.39
6a	19.6	24.8	23.3	1.84	1.93	1.89
6b				ND[b]	1.64	1.60
7a	27.8	27.8	26.3	2.2	1.72	2.12
7b				ND[b]	1.64	1.74
8	65.9	67.9	65.9	ND[b]	2.28	2.39
9	45.2	41.4	40.5	1.65	1.67	2.19
10	74.7	77.5	77.8	4.10	4.37	4.54
11	83.2	85.4	82.8	3.44	4.04	4.33
12	31.3	27.9	27.5	1.73	1.80	3.12
13	18.4	16.1	15.7	0.94	1.05	1.03
14	18.9	21.4	21.4	0.86	1.16	1.09
15	107.3	109.9	108.3			
16	27.2	28.2	28.1	1.33	1.46	1.46
17	26.3	26.9	27.2	1.29	1.32	1.29
RMSD		2.50	2.47		0.22	0.50

[a]δ_C obtained indirectly from gHSQC and gHMBC experiments. [b]ND: Not detected. Significant peak broadening occurred in signals near the tertiary amine. This led to weak and/or missing signals.

Table 4.10.37. NMR Spectroscopy Data for Andrognathanol A (**4.9**)
(600 MHz, d_6-DMSO, 25 °C)

Position	δ_C, type[a]	δ_H (J in Hz)	H2BC	HMBC	COSY	ROESY
1	75.4, CH	3.60, d, 5.5	2	2, 3, 11,13	2	14b
2	43.4, CH	1.70, m	1, 3, 10	9, 10	1, 3	3b, 10, 11
3a	55.4, CH_2	2.15, m	2	1, 2, 4, 8, 10	2, 4	
3b		2.94, d, 10.7				2, 4b
4a	49.5, CH_2	2.13, m	5		3, 5	
4b		2.55, d, 12.0				3b
5a	28.8, CH_2	1.23, m	4, 6		4, 6	
5b		1.66, m				6
6	67.7, CH	4.92, s	5, 7	4, 8	5, 7	5b, 6b
7a	32.0, CH_2	1.43, m	6, 8	8	6	8
7b		1.53, m				6
8	57.6, CH	1.90, m	7, 9		9, 14	7a, 9a, 14
9	30.3, CH	1.49, m	10, 14		8	8, 10
10	40.8, CH	2.01, q, 4.3	2, 9, 11	1, 11, 12, 14	11	2, 9, 11
11	78.0, CH	4.60, d, 4.4	10	9, 12, 15, 19	10	2, 10
12	42.6, C					
13a	30.6, CH_2	1.14, dd, 8.6, 12.5	14	1, 11, 12, 14	14	
13b		1.73, m				
14a	16.9, CH_2	1.30, pent, 6.7	13	10, 12, 13	9, 13	8
14b		1.90, m				1
15	19.4, CH_3	0.78, s				
16	172.9, C					
17	26.9, CH_2	2.29, q, 7.3	18	16, 18	18	18
18	8.8, CH_3	1.01, t, 7.4	17	16, 17	17	17
19	171.1, C					
20	44.1, CH_2	2.37, m	21	19, 21, 22	21	22
21	63.2, CH	4.01, sext, 6.4	20, 22	19, 20	22	
22	23.2, CH_3	1.10, d, 6.0	21	20, 21	21	20

[a] δ_C obtained indirectly from gHSQC and gHMBC experiments.

Table 4.10.38. NMR Spectroscopy Data for Andrognathanol B (**4.10**)
(600 MHz, d_6-DMSO, 25 °C)

Position	δ_C, type[a]	δ_H (J in Hz)	H2BC	HMBC	COSY	ROESY
1	75.5, CH	3.60, d, 5.7	2	2, 3, 11, 13	2	
2	43.5, CH	1.70, m	1, 3, 10	1, 9, 10, 12	1	10
3a	55.4, CH_2	2.16, m	2	1, 2, 4, 8, 10		
3b		2.94, d, 12.4				
4a	49.6, CH_2	2.14, m	5	6, 8	5	
4b		2.56, m				
5	28.8, CH_2	1.66, m	4, 6		4, 6	6
6	67.4, CH	4.91, s	5, 7	4, 8	5	5, 7b
7a	32.1, CH_2	1.43, m	6, 8			8
7b		1.54, m				6
8	57.7, CH	1.91, m	7	9, 14	7	7a, 9, 10
9	30.3, CH	1.50, m	8, 10, 14			8, 10
10	40.8, CH	2.02, m	2, 9, 11	1, 12	11	2, 8, 9, 11
11	78.1, CH	4.60, d, 4.6	10	12, 13, 15	10	10, 15
12	42.4, C					
13a	30.6, CH_2	1.14, m	14	11, 12, 14		15
13b		1.72, m				
14a	16.9, CH_2	1.29, m	13	8, 10, 13		
14b		1.89, m				
15	19.4, CH_3	0.78, s		1, 11, 12, 13		11, 13a
16	172.9, C					
17	26.9, CH_2	2.28, m	18	16, 17	18	
18	8.8, CH_3	1.01, t, 7.4	17	16, 17	17	
19	171.3, C					
20a	42.1, CH_2	2.31, m	21	19, 21, 22	21	
20b		2.41, d, 5.6				
21	68.3, CH	3.76, m	20, 22	19, 23	20	
22	29.5, CH_2	1.36, m	21, 23	20, 21, 23	23	
23	9.6, CH_3	0.85, t, 7.4	22	21, 22	22	

[a]δ_C obtained indirectly through gHSQC and gHMBC data.

Table 4.10.39. NMR Spectroscopy Data for Andrognathanol C (**4.11**)
(600 MHz, d_6-DMSO, 25 °C)

Position	δ_C, type[a]	δ_H (J in Hz)	H2BC	HMBC	COSY	ROESY
1	75.5, CH	3.60, d, 5.9	2	2, 3, 11, 13	2	8, 13a
2	43.6, CH	1.70, m	1, 3, 10	1, 10	1, 3	3a, 10, 11
3a	55.4, CH_2	2.15, m	2	1, 2, 4	2	2
3b		2.92, d, 12.1				4b
4a	49.5, CH_2	2.13, m	5	6, 8	5	
4b		2.54, m				3b, 5b
5a	28.7, CH_2	1.23, m	4, 6		4, 6	
5b		1.67, m				6
6	67.4, CH	4.91, s	5	4, 8	5, 7	5b, 7b
7a	32.1, CH	1.43, m		6, 8	6, 8	
7b		1.54, m				6
8	57.6, CH	1.90, m	7, 9	9, 14	7	1
9	30.5, CH	1.46, m	14			10
10	40.9, CH	2.02, m	2, 9, 11	1, 11, 12, 14	11	2, 9, 11
11	78.1, CH	4.63, d, 4.7	10	9, 12, 15	10	2, 10, 15
12	42.4 C					
13a	30.6, CH_2	1.15, m	14	11, 12, 14, 15	14	1
13b		1.71, m				
14a	16.9, CH_2	1.30, m	9, 13	9, 10, 12, 13	13	
14b		1.91, m				
15	19.5, CH_3	0.78, s		1, 11, 12, 13		11
16	172.1, C					
17	42.7, CH_2	2.21, m		16, 17	18	
18	25.1, CH	1.97, m	17, 18	17, 19	17, 19	
19	21.9, CH_3	0.91, d, 6.6	18	17, 18	18	
20	172.9, C					
21	26.9, CH_2	2.29, q, 7.5	22		22	
22	8.8, CH_3	1.01, t, 7.5	21	20, 21	21	

[a]δ_C obtained indirectly through gHSQC and gHMBC data.

Table 4.10.40. NMR Spectroscopy Data for Andrognathanol D (**4.12**)
(600 MHz, d_6-DMSO, 25 °C)

Position	δ_C, type[a]	δ_H (J in Hz)	H2BC	HMBC
1	75.6, CH	3.60, d, 6.1		3, 11, 13
2	43.6, CH	1.70, m		1, 12
3a	55.6, CH_2	2.16, m		1, 2, 8, 10
3b		2.92, d, 11.7		
4a	49.6, CH_2	2.13, m		
4b		2.55, m		
5a	28.8, CH_2	1.22, m		
5b		1.66, m		
6	67.5, CH	4.91, s		
7a	32.2, CH_2	1.43, m		
7b		1.52, m		
8	57.8, CH	1.91, m		
9	30.7, CH	1.45, m		
10	41.0, CH	2.01, m		
11	78.2, CH	4.62, d, 4.6		9
12	42.4, C			
13a	30.7, CH_2	1.15, m		
13b		1.70, m		
14a	17.0, CH_2	1.30, m		10, 12, 13
14b		1.91, m		
15	19.6, CH_3	0.78, s		1, 11, 12, 13
16	172.9, C			
17	27.0, CH_2	2.29, q, 7.7	18	16, 18
18	9.0, CH	1.01, t, 7.7	17	16, 17
19	172.2, C			
20	42.9, CH_2	2.21, dd, 4.5, 2.4		19, 21, 22
21	25.2, CH	1.99, m		
22	22.0, CH_3	0.90, d, 6.8	21	20, 21

[a] δ_c obtained indirectly through gHSQC and gHMBC data.

Table 4.10.41. *A. corticarius* Length Versus Average Peak Area Study

Length (cm)	Average Peak Area
0.7	2.51E+05
2.2	1.38E+06
1.8	3.00E+05
2.0	9.22E+05
0.8	4.08E+05
1.0	6.54E+05
1.7	1.73E+06
0.8	5.17E+05
0.7	9.31E+05
1.6	7.49E+05
0.7	1.59E+05
1.0	4.41E+05
0.9	2.77E+05
0.5	5.21E+04
1.2	5.37E+05
0.6	6.48E+05
1.0	7.66E+05
0.6	5.26E+05
0.6	6.89E+05
0.3	3.95E+04
0.8	8.54E+05
1.0	4.67E+05
0.9	3.12E+05
0.8	2.37E+05
1.1	4.00E+05
0.8	3.06E+05
0.9	1.07E+06
1.0	8.83E+05
1.1	7.06E+05
1.3	9.37E+05
1.0	1.00E+06

Table 4.10.42. σ_1R Binding

	Haloperidol			Andrognathine A (4.1)		
log[Drug], M	Trial 1	Trial 2	Trial 3	Trial 1	Trial 2	Trial 3
-11	2100	2100	2300	1800	2100	1800
-10	2100	2100	2100	2000	2300	2200
-9.52	2100	2000	2100	2000	2100	2200
-9	1900	1900	2000	1800	2400	2200
-8.52	1100	1500	1200	2000	2300	2100
-8	600	700	600	1800	1900	1900
-7.52	200	400	300	1900	2200	2300
-7	200	400	700	1800	1900	2100
-6.52	90	600	200	1900	2000	2400
-6	60	60	50	1200	1400	1300
-5.52	50	300	300	400	800	700
-5	10	100	200	100	200	200

Table 4.10.43. σ_2R Binding

	Haloperidol			Andrognathine A (4.1)		
log[Drug], M	Trial 1	Trial 2	Trial 3	Trial 1	Trial 2	Trial 3
-11	1700	1800	2000	1900	1700	1700
-10	1800	1700	2000	1800	1900	2000
-9.52	2200	1800	2100	1900	2100	2100
-9	1800	1800	1700	2200	2000	2000
-8.52	1600	1500	1600	2000	2300	2200
-8	1500	1700	1600	2500	1900	2200
-7.52	1300	1300	1300	2000	2100	1900
-7	800	600	600	2100	1800	1800
-6.52	270	200	300	1900	1800	1900
-6	140	110	110	1400	1600	1600
-5.52	90	100	80	900	1000	1000
-5	130	40	70	200	300	300

Table 4.10.44. Nav1.5 Human Sodium Ion Channel Cell Based APC LeadHunter Assay

Compound	Concentration (µM)	Pulse 2	Pulse 1
0.3% DMSO		4.89	-16.6
Andrognathanol A (4.9)	0.03	6.71	-17.9
	0.1	15.3	-7.21
	0.3	6.91	-16.5
	1	8.93	-4.26
	3	3.43	-15.7
	10	4.33	-19.9
Andrognathine A (4.1)	0.03	2.20	-21.8
	0.1	3.87	-18.5
	0.3	-2.87	-24.6
	1	5.70	-15.8
	3	4.27	-16.9
	10	7.73	-17.4

Assay completed by Eurofins Discovery Services

Table 4.10.45. Nav1.8 Human Sodium Ion Channel Cell Based APC LeadHunter Assay

Compound	Concentration (µM)	Pulse 2	Pulse 1
0.3% DMSO		-2.65	5.09
Andrognathanol A (4.9)	0.03	-9.18	0.02
	0.1	-1.86	-10.0
	0.3	-11.0	-21.7
	1	-3.96	-8.35
	3	-22.8	-15.7
	10	-6.62	-5.76
Andrognathine A (4.1)	0.03	-0.12	-7.02
	0.1	-5.71	-3.99
	0.3	-4.29	2.00
	1	5.12	10.0
	3	-13.7	-7.71
	10	-11.8	-6.70

Assay completed by Eurofins Discovery Services

Chapter 5.

Future Pathways: Integrating Phylogenetics, Biosynthesis, and Ecology in Millipede Research

5.1. Introduction

Millipedes are among the earliest land animals, with fossil records dating back over 400 mya.[1] They are also incredibly diverse with 12,000 species described; however, some reports suggest that the vast majority of the species have yet to be described with some estimates suggesting >80,000 species worldwide.[2] Colobognathan millipedes, a distinct subterclass, evolved 99 mya and possess unique characteristics, including their reduced mouthparts, small bodies and social aggregation behaviors.[3] Colobognatha consist of four orders (Platydesmida, Siphonocryptida, Siphonophorida, and Polyzoniida).[3] They are most commonly found on the underside of decaying logs, feeding on fungus, and often times forming large aggregations (>100 millipedes).[4] This coupled with the fact they are slow moving and nocturnal leads to them being classified a cryptic subterclass. Like most millipedes, Colobognatha, produce chemical defenses that are secreted upon disturbance through ozopores. However, Colobognatha are the only millipedes to produce terpenoid alkaloids, the most structurally intriguing of all the defensive secretions.[5]

As a whole, the Colobognatha subterclass has been historically understudied, with chemical studies into only a single order prior to 2020.[6] Since 2020, there have been a total of 33 new alkaloids characterized from the defensive secretions, many of these represent new structural classes.[7-11] This dissertation accounts for the discovery of nearly three quarters of the newly reported alkaloids (25), yet there is still much work remaining to be done. The discoveries described within clearly demonstrates novel chemistry exists; however, only ~10% of the

described Colobognatha millipedes have been chemically investigated. Future work on Colobognatha is vast with many questions left to be answered, such as: What is the true chemical potential of other orders? How are these molecules biosynthesized? What are their ecological roles, i.e. do they serve a defensive role, are they used to identify self as a pheromone, or do they potentially serve both functions? How does the structural diversity relate to the molecular phylogeny of this subterclass? In addition, continued studies into millipedes terpenoid alkaloids are needed to fully evaluate their medicinal potential. In **Chapter 3**, we discovered a subset of the alkaloids potently binds to neuroreceptors; however, we could not fully evaluate this activity due to limited isolation quantities.[9] Future studies involving total syntheses and/or chemical investigations into understudied millipedes to discovery additional classes chemistry could provide useful information into structure activity relationships (SAR) and provide material for *in vivo* evaluation. The former is essential to fully understand the pharmaceutical potential of these intriguing classes of natural products. The interdisciplinary nature of this work makes it unique and allows for more questions to be answered through collaboration.

5.2. Summary of Findings and Their Significance

5.2.1. Our Current Understanding of the Chemical Diversity Within Colobognatha Defensive Secretions

The work presented in this dissertation has greatly expanded the depth of knowledge surrounding the defensive compounds produced by Colobognatha. Prior to this work, 13 alkaloids had been described within Colobognatha; however, this dissertation describes the discovery of 25 new alkaloids all from the order Platydesmida (**Table 5.3, Figure 5.14**).[7-9] In addition, other groups have reported three new alkaloids, all from genera within Polyzoniida.[10] These recent discoveries represent the most structurally interesting alkaloids discovered from millipedes to date, as they are

predicted to require significant post-modifications (e.g, ligation, oxidation, cyclization), and have played an integral role in our current understanding of how they could potentially be biosynthesized.[7] To date, nearly all studies into distinct Platydesmida genera has led to the discovery of novel chemistry. For example, the gosodesmines are primarily produced by *Brachycybe* species, the ischnocybines are only produced by *I. plicata*, and the andrognathanols are only produced by *Andrognathus corticarius*.[7-9,11] Structurally, the andrognathanols are remarkable natural products, possessing an unprecedented 6,6,6,5-fused heterocycle with seven continuous stereogenic centers.[7] No other millipede order's defensive secretions have this level of structural diversity and complexity amongst its defensive secretions. The closest order is likely Julida, which produce a wealth of benzoquinones and straight chain fatty acids.[5] However, the structural diversity is much more modest, such as changes in the position of a double bond or methyl group, but not inclusion in various functional groups.[12]

Table 5.3. Millipede subterclass Colobognatha Chemistry

Order	Millipede	Compound	Source
Siphonocryptida	*Hirudicryptus canariensis*	O-methyloxime 236 (**5.1**)	Shear (2015)
Siphonophorida	*Siphonophorus* spp.	α-pinene (**5.2**), β-pinene (**5.3**)	Shear (2015)
Polyzoniida	*Rhinotus purpureus*	O-methyloxime 236 (**5.1**)	Saporito, *et al.* (2003)
	Buzonium crassipes	Buzonamine (**5.4**), β-pinene **5.3**, limonene (**5.5**)	Wood, *et al.* (2000)
	Polyzonium rosalbum	Polyzonimine (**5.6**), nitropolyzonamine(**5.7**)	Meinwald, *et al.* (1975); Smolanoff, *et al.* (1975)
	Petaserpes cryptocephalus	Polyzonimine (**5.6**), nitropolyzonamine (**5.7**)	Meinwald, *et al.* (1975); Shear (2015)

	Polyzonium germanicum	Polyzonimine (**5.6**), nitropolyzonamine (**5.7**), acetylated 3-hydroxy-nitro-polyzonamine (5.**8**) and two isomers (**5.9**, **5.10**)	Kunert, *et al.* (2023)
	Kiusiozonium okai	Polyzonimine (**5.6**), nitropolyzonamine (**5.7**), O-methyloxime 236 (**5.1**)	Kuwahara, *et al.* (2007)
Platydesmida	*Gosodesmus claremontus*	Gosodesmine (**5.11**)	Hassler, *et al.* (2020)
	Brachycybe lecontii	Deoxybuzonamine isomers (**5.12**)	Jones, *et al.* (2022)
	B. rosea	Deoxybuzonamine (**5.12**)	Banks, *et al.* (2024) (**Chapter 2**)
	B. petasata	Gosodesmine (**5.11**), homogosodesmine (5.**13**), hydrogosodesmine (**5.14**), homo-hydrogosodesmine (**5.15**)	Banks, *et al.* (2024) (**Chapter 2**)
	Platydesmus sp.	Deoxybuzonamine (**5.12**)	Shear (2015)
	B. producta	Gosodesmine (**5.11**), homogosodesmine (5.**13**), hydrogosodesmine (**5.14**), homo-hydrogosodesmine (**5.15**)	Banks, *et al.* (2024) (**Chapter 2**)
	I. plicata	Ischnocybine A-C(**5.16**, **5.17**, **5.18**) Ischnocybinone (**5.19**)	Menegatti, *et al.* (2024) (**Chapter 3**)
	A. corticarius	Andrognathine A-L (**5.20**), Andrognathanol A-F (**5.21**)	Banks, *et al.* (2025) (**Chapter 4**)

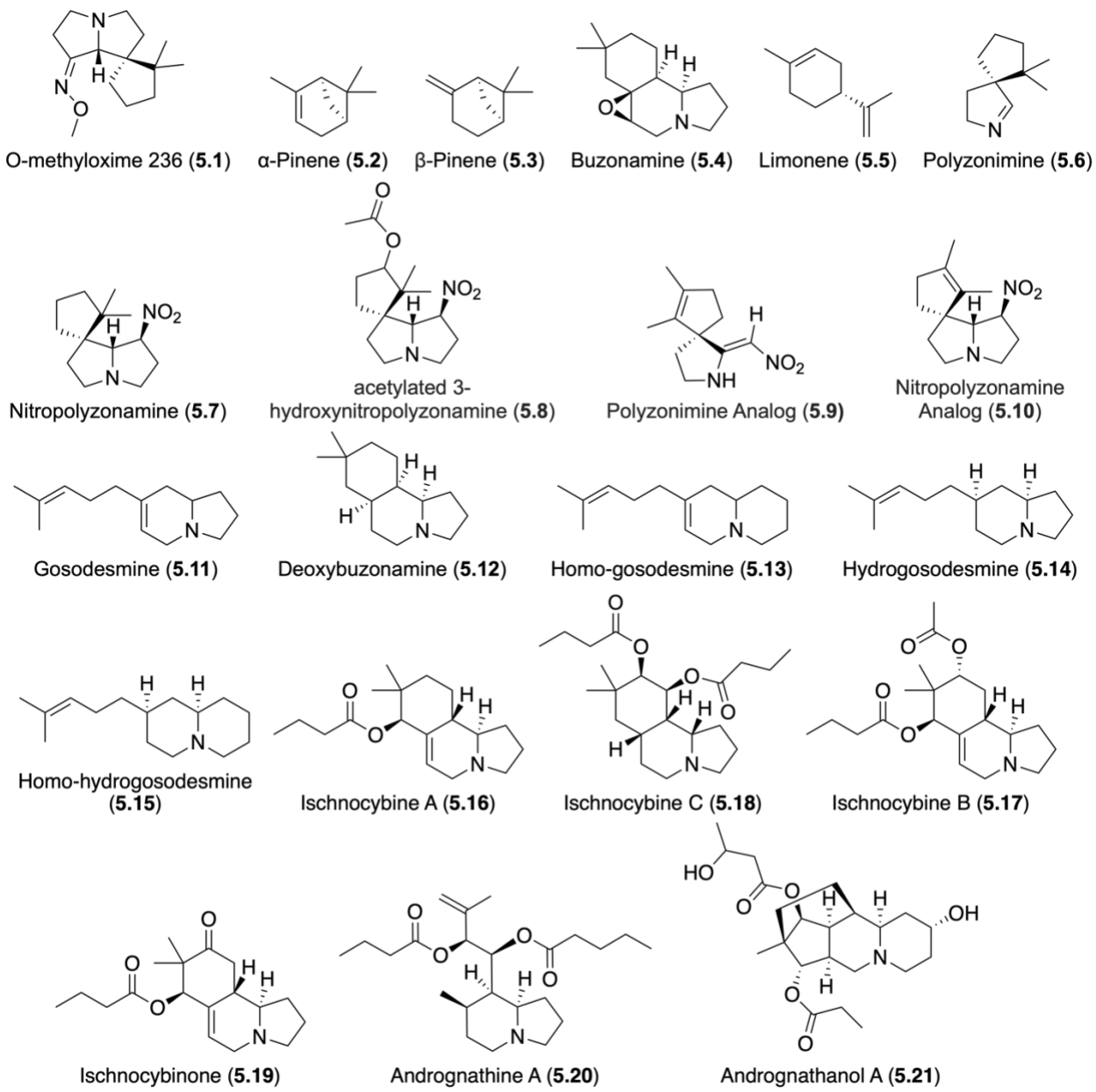

Figure 5.14. Structures coming from Colobognathan millipedes

5.2.2. Insights into the Biosynthetic Pathway Leading to all Platydesmida Terpenoid Alkaloids

All Platydesmida alkaloids are hypothesized to consist of a monoterpene coupled with either a pyrrolidine or pyrrole ring (**Figure 5.15**). This core intermediate is predicted to undergo diversification during cyclization, followed by additional post-modifications. The ischnocybines

(**5.16**–**5.19**), deoxybuzonamine (**5.12**), andrognathines (**5.20**), and andrognathanols (**5.21**) are predicted to follow a similar cyclization route, beginning with iso-geranyl pyrrolidine (**5.22**) or iso-geranyl pyrrole. Conversely, the gosodesmines likely derive from a structural isomer **5.23**, in which the C-10 methyl is incorporated into the indolizidine/quinolizidine core (**Figure 5.15**). These precursors are hypothesized to undergo cyclization through carbocation propagation as is common amongst terpenoid natural products. The timing and mechanism of carbocation quenching during cyclization of **5.22** is what drives some of the observed structural diversity. Further modifications by oxidases and ligases are predicted to lead to the formation of **5.16**–**5.19**, **5.12** and **5.20**. The final ring in the **5.21** is predicted to derive from functionalization of the *gem*-dimethyl moiety in **5.12**, followed by an additional cyclization step. The tetracyclic scaffold then undergoes further decoration to form the **5.21**. Currently this proposal is supported by the fact that many of the predicted intermediates have been characterized (those in boxes).

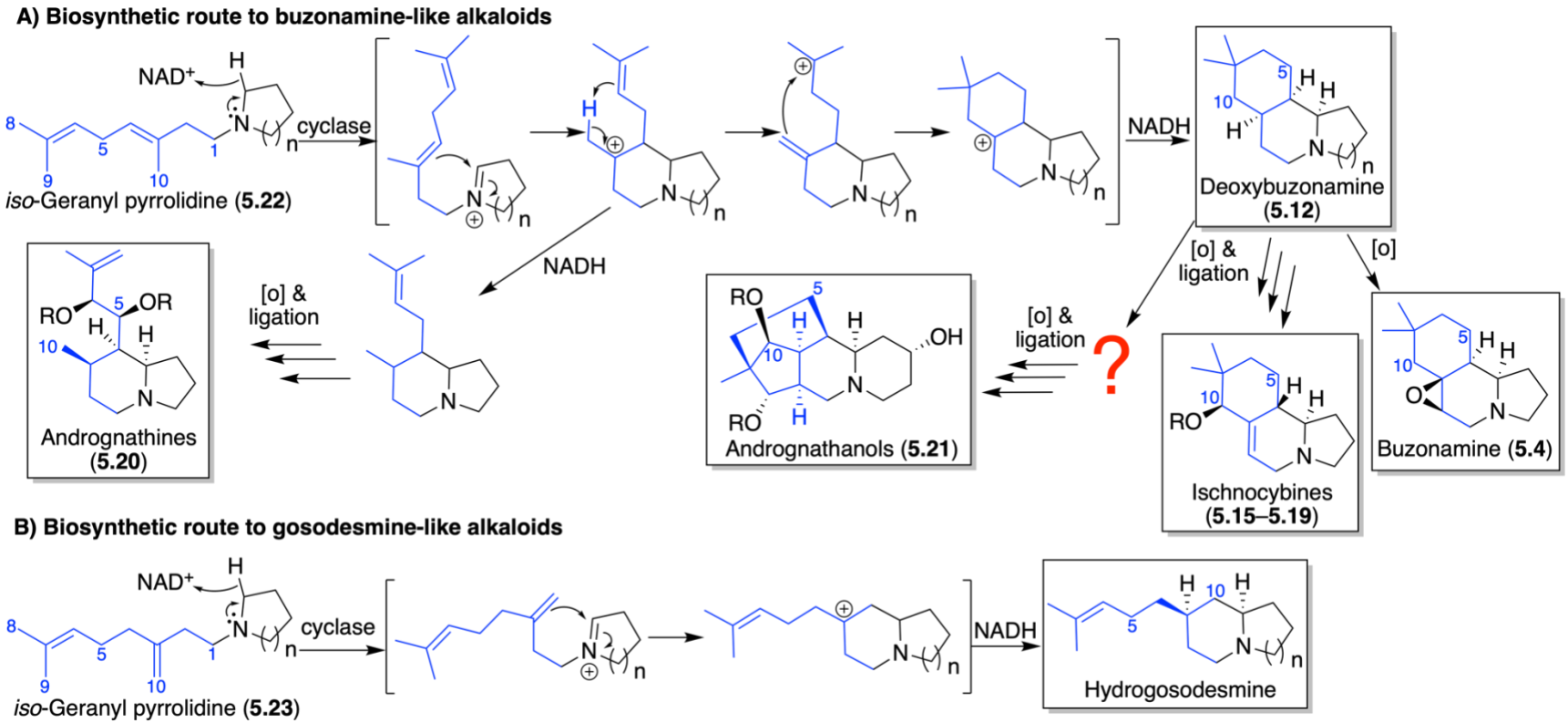

Figure 5.15. Potential biosynthetic route for production of defense compounds from Platydesmida

To gain experimental confirmation of this proposed biosynthetic route, we are attempting heavy isotope feeding studies and through crude protein assays. For the heavy isotope feeding studies, we synthesized ^{13}C labeled *iso*-geranyl pyrrolidine (**5.22**) and have been attempting to get the isotopes to incorporate into the final products. We also made a deuterium labeled **5.22**, but is not ideal for this study as during the predicted cyclization, a deuterium will need to be removed, and this might not be possible due to known isotope issues. However, we could not easily change the substrate used so we moved forward. First, we are doping millipede food with the substrate to directly feed the substrate to living millipedes. We then are extracting the defensive secretions and analyzing it by LCMS to determine if the labeled substrate was incorporated into any intermediates or final products. There is some concern as to whether the millipedes are consuming the food and how much, so we are also attempting inject the labeled substrate directly into the millipedes. However, we have yet to see the isotope incorporate into any of the alkaloids. We do not believe this failure suggests that our predicted precursor is incorrect, but rather that we are not able to deliver the substrate to the right location in high enough concentrations to detect incorporation into a final product. In addition to the feeding studies, we tested to see if a crude protein extraction from millipedes could use the proposed common precursor as a substrate to form any of the intermediates. Crude protein extracts were generated from whole millipedes, and then the substrate was added along with various protein cofactors, such as NAD^+. The results of these experiments were inconclusive and need to be troubleshooted more.

Another option to confirm the proposed biosynthetic pathway is by leveraging modern genomic tools. One possibility is to sequence and assemble millipede genomes to begin to identify key genes used in the biosynthesis of the alkaloids. For example, we could attempt to identify cytochrome P450s and terpene cyclases using bioinformatic tools. Targeted genes could be

purchased, and gene functions confirmed through heterologous expression. Another option is to use transcriptomics to identify highly expressed genes in body parts containing the glands (e.g., body) compared to glandless body parts (e.g., head). The alkaloids are produced in high quantities (>50 μg/millipede) therefore it is predicted that the genes involved in their biosynthesis should be highly expressed in the bodies. Finally, all approaches mentioned above could be simplified if they were run on the glands alone, thus improving dissection techniques should improve success rates.

5.2.3. Evolution of Terpenoid Alkaloids Biosynthetic Pathway in Platydesmida

It has long been known that millipede defensive secretions clades with phylogeny. Analysis of all orders of millipedes begins to highlight patterns. For example, the order Julida produces benzoquinones and straight chain fatty acids while Glomerida produce glomerin and homoglomerin, which are quinazolinone alkaloids.[19] This trend continues throughout all chemically described orders of millipedes, where they all produce related compounds to one another, if not the same compound.[5,20] Similar analysis of within Colobognatha shows similar trends, where all four orders are known to produce monoterpenes.[5] However, the spirocyclic alkaloids (e.g., **5.6** and **5.7**) have only been described from genera within Polyzoniida and Siphonocryptida. While fused and bridged heterocycles (e.g., **5.11**, **5.12**, and **5.16**–**5.21**) have only been described from the secretions of genera representing Platydesmida.[9] Only simple monoterpenes (e.g., **5.2** and **5.3**) have been described from Siphonophorida, although only one genera has truly been investigated.[5] Previous studies into correlations between secretion compositions and molecular phylogeny are sparse, with none specifically focused on the millipede-derived terpenoid alkaloids. Rodriguez*, et al.* (2018) reported that oxidized aromatics evolve through a stepwise diversification within the superfamily Juliformia, with increasing complexity of the defensive secretions as a derived trait. They proposed that phenol was the ancestral defensive

agent, which evolved into benzoquinone, then methoxy-benzoquinone, and so on, with many of the observed modifications involving oxidations and alkylation. Recognizing that phenols are not directly involved in the production of quinazolinone nor terpenoid alkaloids, Rodriguez*, et al.* (2018) stated that these other compounds originated as defenses in Colobognatha and Glomerida, respectively, independent from the evolution of chemical defenses in Juliformia. Although phenol likely preceded benzoquinone defenses in juliform millipedes, the ancestral defense compound of alkaloid producing millipedes is uncertain.

All orders of Colobognatha are known to produce terpenes with the Siphonophorida known to produce only monoterpenes based on studies into a single species.[5] On the other hand, Platydesmida has multiple studies into diverse genera, allowing for a fuller analysis.[8,9,11,18] Compounds **5.11** and **5.12** are structurally the simplest of the terpenoid alkaloids produced by Platydesmida genera, as they lack evidence of the post-modifications seen in other alkaloids; their biosynthesis is predicted to involve around three genes.[11,18] Gosodesmines are known to be produced by only two *Brachycybe* sister species, *B. producta* and *B. petasata*; while compound **5.12** are produced by another set of *Brachycybe* sisters, *B. lecontii* and *B. rosea*.[8,11] Recent molecular phylogeny of *Brachycybe* species suggests that the genus diverged ~50 mya with *B. producta* and *B. petasata* more recently (~18 mya) compared to *B. lecontii* and *B. rosea*.[21] Conversely, **5.21** represents the most structurally complex alkaloids, followed by the compounds **5.16**–**5.19**, with their biosynthetic pathways estimated to require 7–9 and 5–7 genes (including oxidases and ligases), respectively.[9] Compound **5.21** is only produced by *Andrognathus corticarius*. *Andrognathus* is evolutionary sister to all other Platydesmida and presumed oldest genus within the order.[3] Similarly, compounds **5.16**–**5.19** are only produced by *Ischnocybe plicata*. Although *I. plicata* has not been analyzed within a phylogenetic context, the species is classified

in the subfamily Dolisteninae (with *Gosodesmus claremontus*), which based on its narrow body shape, is likely a closer relative of *Andrognathus* than to *Brachycybe*. This supports the hypothesis that terpenoid alkaloids in Platydesmida evolved toward simplicity, rather than the complexity seen in Juliformia.[20] Although evolution to simplicity through loss or reduced functionality has not previously been reported in animal defensive secretions, it has been documented in anatomical development and bacterial natural products (e.g., glycoproteins)[22] and in the presumed secondary loss of cyanogenics in some Polydesmida.[20,23]

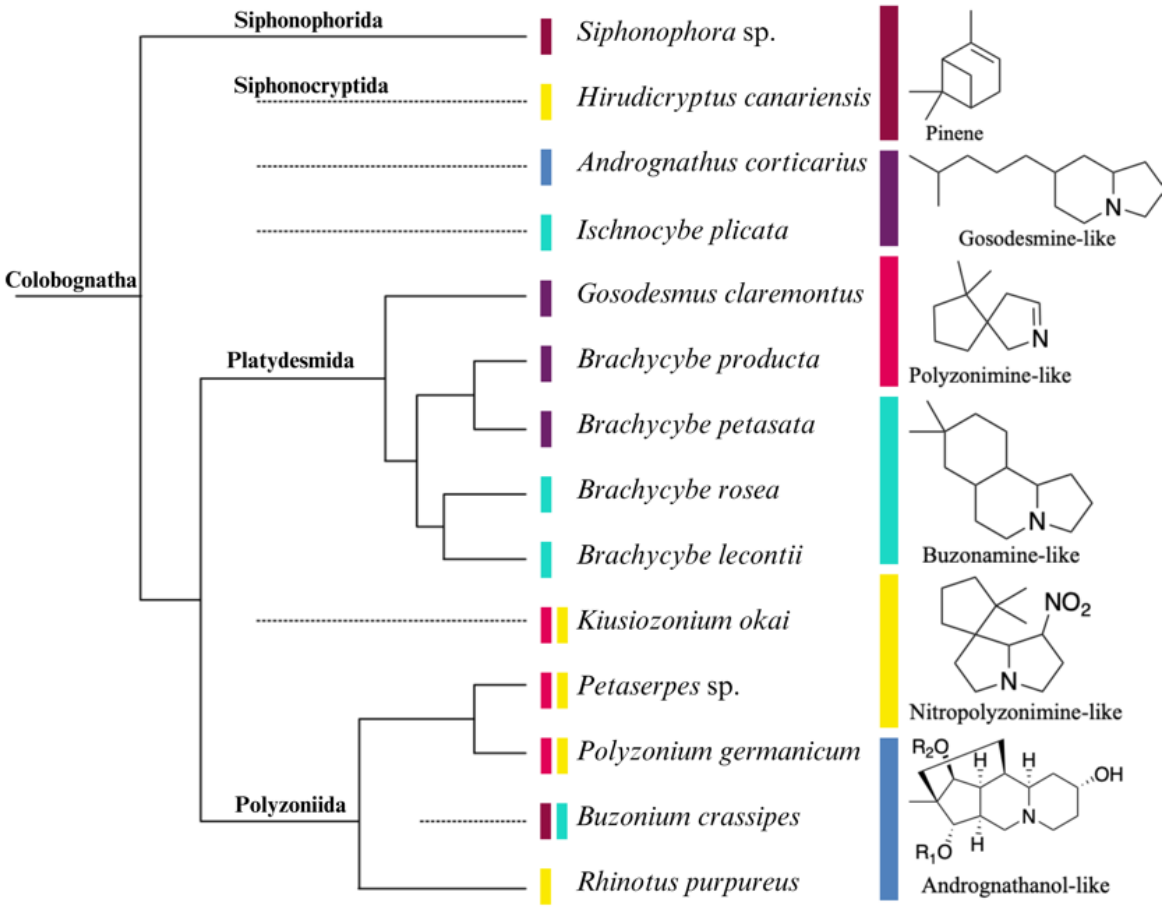

Figure 5.16. Millipede phylogenetic tree for subterclass colobognath. The types of compounds produced by each millipede are shown. [Figure adapted from Menegatti, *et al.* (2024)]

5.2.4. Ecological and Biomedical Implications of Millipede Terpenoid Alkaloids

The ecological and biomedical roles of the terpenoid alkaloids have yet to be fully explored. Their defensive roles are relatively well established; however, it has been noted that even though Colobognatha lack eyes they are capable of forming large aggregations on the underside of decaying logs.[3,24] Thus, indicating there must be some pheromones present to attract them to one another.[5] In addition, we observed in the field that if we remove all visible millipedes from a log and then return to that same log, more millipedes will appear in the exact same spot of the log. We have hypothesized these secretions may have a dual purpose, to provide defense from predators and be a signaling molecule, used to warn other millipedes of danger and used to attract them to one another, depending on the dose. This would also provide a potential rationale for the large structural diversity within the Platydesmida.

To begin to test these hypotheses, we conducted some simple ecological assays with *I. plicata* and *A. corticarius*. First, we screened *I. plicata* secretions in some predator assays where they clearly deterred ants (**Chapter 3**).[9] The ants stayed as far away from the paper disc as they could, and if they did approach the disc, they would preen their antennae, indicating a potential neurological target. This led us to explore the pharmacological potential of the alkaloids coming from millipedes. Ischnocybine A (**5.16**) was first to be shown to potently (K_i 14 nM) and selectively (>100-fold) bind to σ_1R over σ_2R, two orphan neuroreceptors that have been implicated in the treatment of a variety of neurodegenerative diseases, such as Alzheimer's, Parkinson's and pain management.[25] Interestingly, there is a natural SAR within the four described ischnocybines and other terpenoid alkaloids. Both ischnocybine B (**5.17**) and ischnocybine C (**5.18**) are about 30-fold less active than **5.16** with K_i of 380 and 380 nM, respectively, while ischnocybinone (**5.19**) is 100-fold less active with a K_i of 1500 nM.[9] The andrognathines (**5.20**) were found to be much less

active against σ_1R (K_i 840 nM).[7] The andrognathanols (**5.21**) were completely inactive against both receptors. The hydrate of homo-hydrogosodesmine shows inverse selectivity binding to σ_2R (K_i 260 nM) over σ_1R (K_i 840 nM) (unpublished). A subset of the new alkaloids was evaluated against two sodium channels, Nav1.8 and Nav1.5 but all were inactive. Further testing should be completed on each of the terpenoid alkaloids to determining other potential targets and drug applications.

To test potential pheromone roles, we transitioned to using *A. corticarius*, a millipede native to Appalachia region. As *I. plicata* is native to the Pacific Northwest, we were not able to do any studies with live millipedes. Using a Y-tube assay, one millipede was placed at the bottom of the Y, and another millipede was placed at the top of one of the arms in a vial and was physically prevented from leaving the vial by a Kimwipe (**Figure 5.17**). The other arm the was an empty vial, but a Kimwipe was similarly placed at the tip. During the assay, the millipede was given time to move around the Y tube apparatus, but once at the junction, it had to choose to go either in the direction of the other millipede or toward the empty vial. Preliminary attempts at this assay suggest that the millipede initially prefers to move toward the other millipede but then crawl back and forth between the two arms, along with returning to the bottom of the Y. However, not enough replicates were completed to confidently conclude. Further studies will be needed to conclusively indicate whether these alkaloids are in fact behaving as pheromones.

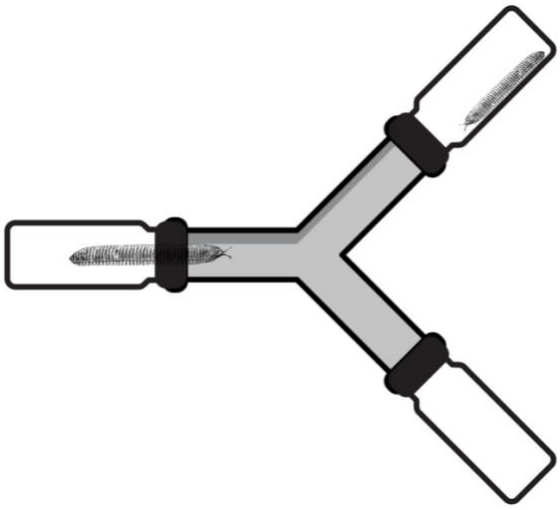

Figure 5.17. *A. corticarius* Y-tube choice assays. This assay was used to determine if millipedes were attracted to each other.

5.3. Future Directions

5.3.1. Advancing Millipede Phylogeny Through Sequencing

Millipede phylogeny is still not well understood, primarily due to a lack in sequencing depth of diverse genera. Much of the established phylogeny reported in this dissertation is dependent of key millipede characteristics, such as size, shape, and gonopod development.[26] However, this is not the most reliable method and struggles to decipher between closely related species. The gold standard to identify relationships between organisms is through DNA sequencing. Millipede phylogeny would benefit greatly from more thorough sequencing efforts, as only a handful of Colobognatha millipedes have been sequenced.[21] It is also possible to use DNA barcoding, which involves comparing a smaller, well conserved region of the genome. This technique a faster, cheaper way to quickly establish relationships and has been used to establish molecular phylogeny within other arthropods, such as, Korean leptonetid spiders.[27] Others have begun to sequence the genomes of Platydesmida, to establish molecular phylogeny, particularly amongst the *Brachycybe* genera. This study only involved five millipede species, which were then

compared to six other Andrognathidae genomes available in public databases.[4,6,28,29] Through this, a new species in the genera *Dolistenus* was described. However, a much greater sample size is necessary to understand the cryptic diversity present.

5.3.2. Expanding Our Understanding of the Ecological Role of the Millipede Alkaloids

Ecological studies into the role of the terpenoid alkaloids will provide great insights in to how their importance and potential applications. As mentioned above and throughout this dissertation, many of the alkaloids cause disorientation in various insects, which led to discovery that a subset of the alkaloids potently binds σ_1R—an orphan neuroreceptor.[25] This is an important finding as it indicates that these compounds may have useful pharmaceutical properties in the treatment of various neurological disorders.[25] In addition, gaining a better understand of the pheromone properties of these compounds could potentially indicate their use as insecticides. To determine this, Y-tube choice assay should be performed. This assay quantifies the propensity for a millipede to choose between alkaloids and an empty tube. These choice assays can be used to understand if specific species of millipedes prefers its own secretions (pheromone), repels another species secretions, or if the alkaloids attract or deter other arthropods. Furthermore, additional predator-prey assays should be performed using diverse suite of potential predators of the millipedes, such as spiders, beetles, salamanders, and birds. Thus far, all predator assays have focused on predators that are easily to acquire, not necessarily true predators. Expanding these studies will provide useful information into the true potential of the alkaloids to serve as insecticides and/or their pharmaceutical potential.

5.3.3. Conservation Implications

The need for biodiversity conservation is crucial or we will lose critical species prior to any scientific studies. For example, little is known about the geographic reaches of Colobognatha. Species have been found in the Americas, parts of Europe and Asia; however, there has been a significant lack of studies into other geographical reaches, such as in Africa, remote parts of Asia and Eastern Europe. Current sampling is biased or is completely lacking.[6] With the current losses in biodiversity due to a multitude of issues, it is likely that some species will be lost before any studies into them can occur. This is even more urgent if the terpenoid alkaloid pathway is evolving simplicity.[3] Nature has played a key role in the development of the majority of our current therapies and is still one of our most promising sources to repopulate the drug pipeline.[30] This is why the time is now to be looking at nature for the future of medicine, prior to losing their diversity.[31] Ecosystems rich in diversity, namely rain forests, are also home to millipedes, and these ecosystems are at the highest risk of being destroyed, risking loss of this critical chemical diversity. Conservation efforts are worldwide endeavors and need to a priority for everyone.[32]

5.4. Conclusion

Within this dissertation, the depth of knowledge of the chemical diversity millipede defense compounds has been greatly increased. This wealth of knowledge includes the description of 25 new terpenoid alkaloids, many of which represent new classes of natural products. However, this is just the beginning of the work to be accomplished, as raised more questions than it answered. Only 10% of the described millipedes have been chemically investigated, and there are estimates that an additional 60,000 species unclassified. The chemistry in this dissertation is sure to be just the tip of the iceberg of what remains to be discovered. Future studies will certainly make significant contribution to our knowledge pertaining to animal biosynthesis, assist with

establishing molecular phylogeny within Colobognatha, provide insights into the ecological role these alkaloids serve, and may provide new drug candidates for the treatment of various neurological diseases.

5.5. References

(1) Wilson, H. M. Juliformian millipedes from the lower devonian of euramerica: implications for the timing of millipede cladogenesis in the paleozoic. *Journal of Paleontology* **2006**, *80* (4). DOI: 10.1666/0022-3360(2006)80.

(2) Golovatch, S.; Kime, R. Millipede (Diplopoda) distributions: a review. *Soil Organisms* **2009**, *81*.

(3) Moritz, L.; Wesener, T. The first known fossils of the Platydesmida—an extant American genus in Cretaceous amber from Myanmar (Diplopoda: Platydesmida: Andrognathidae). *Organisms Diversity and Evolution* **2019**, *19* (3), 423-433. DOI: 10.1007/s13127-019-00408-0.

(4) Shorter, P. L.; Hennen, D. A.; Marek, P. E. Cryptic diversity in Andrognathus corticarius Cope, 1869 and description of a new Andrognathus species from New Mexico (Diplopoda, Platydesmida, Andrognathidae). *Zookeys* **2018**, (786), 19-41. DOI: 10.3897/zookeys.786.27631.

(5) Shear, W. A. The chemical defenses of millipedes (diplopoda): Biochemistry, physiology and ecology. *Biochemical Systematics and Ecology* **2015**, *61*, 78-117. DOI: 10.1016/j.bse.2015.04.033.

(6) Recuero, E.; Rodriguez-Flores, P. C. A new Mediterranean species of Dolistenus (Diplopoda, Platydesmida, Andrognathidae), with an updated key for the genus and the first contribution for a barcode database of European Platydesmida. *Zootaxa* **2020**, *4718* (1). DOI: 10.11646/zootaxa.4718.1.10.

(7) Banks, P.; Menegatti, C.; Knott, K.; Marek, P.; Mevers, E. Chemical Diversity of Millipede Defensive Alkaloids Provides Insights into their Evolutionary History. **2025**. DOI: 10.26434/chemrxiv-2025-tdt3n.

(8) Banks, P.; Funkhouser, E. M.; Macias, A. M.; Lovett, B.; Meador, S.; Hatch, A.; Garraffo, H. M.; Cartwright, K. C.; Kasson, M. T.; Marek, P. E.; et al. The Chemistry of the Defensive Secretions of Three Species of Millipedes in the Genus Brachycybe. *Journal of Chemical Ecology* **2024**, *50* (9), 478-488. DOI: 10.1007/s10886-024-01518-6.

(9) Menegatti, C.; Wood, J. S.; Banks, P.; Knott, K.; Briganti, J. S.; Briganti, A. J.; McNally, S. V. G.; Marek, P. E.; Brown, A. M.; Jones, T. H.; et al. Neuromodulating Alkaloids from Millipede Defensive Secretions. *Journal of Natural Products* **2024**. DOI: 10.1021/acs.jnatprod.4c01162.

(10) Kunert, O.; Pferschy-Wenzig, E. M.; Orthaber, A.; Raspotnig, G.; Bodner, M. Alkaloids from millipedes: a re-evaluation of defensive exudates from Polyzonium germanicum. *Frontiers in Ecology and Evolution* **2023**, *11*. DOI: 10.3389/fevo.2023.1212452.

(11) Hassler, M. F.; Harrison, D. P.; Jones, T. H.; Richart, C. H.; Saporito, R. A. Gosodesmine, a 7-Substituted Hexahydroindolizine from the Millipede Gosodesmus claremontus. *Journal of Natural Products* **2020**, *83* (9). DOI: 10.1021/acs.jnatprod.0c00722.

(12) Weatherston, J.; Tyrrell, D.; Percy, J. E. Long chain alcohol acetates in the defensive secretion of the millipede Blaniulus guttulatus. *Chemistry and Physics of Lipids* **1971**, *7* (1), 98-100. DOI: 10.1016/0009-3084(71)90023-5.

(13) Saporito, R. A.; Donnelly, M. A.; Hoffman, R. L.; Garraffo, H. M.; Daly, J. W. A Siphonotid Millipede (Rhinotus) as the Source of Spiropyrrolizidine Oximes of Dendrobatid Frogs. *Journal of Chemical Ecology* **2003**, *29* (12). DOI: 10.1023/B:JOEC.0000008065.28364.a0.

(14) Wood, W. F.; Hanke, F. J.; Kubo, I.; Carroll, J. A.; Crews, P. Buzonamine, a new alkaloid from the defensive secretion of the millipede, Buzonium crassipes. *Biochemical Systematics and Ecology* **2000**, *28* (4), 305-312. DOI: 10.1016/S0305-1978(99)00068-X.

(15) Meinwald, J.; Smolanoff, J.; McPhail, A. T.; Miller, R. W.; Eisner, T.; Hicks, K. Nitropolyzonamine: A spirocyclic nitro compound from the defensive glands of a milliped (polyzonium rosalbum). *Tetrahedron Letters* **1975**, *16* (28). DOI: 10.1016/0040-4039(75)80013-X.

(16) Smolanoff, J.; Kluge, A. F.; Meinwald, J.; McPhail, A.; Miller, R. W.; Hicks, K.; Eisner, T. Polyzonimine: A Novel Terpenoid Insect Repellent Produced by a Milliped. *Science* **1975**, *188* (4189), 734-736. DOI: doi:10.1126/science.1124395.

(17) Kuwahara, Y.; Mori, N. M. N.; Tanabe, T. Detection of a neotropical frog alkaloid spiropyrrolizidine 236 from a Japanese polyzoniid millipede Kiusiozonium okai as a major defense component together with polyzonimine and nitropolyzonamine. *Japanese Journal of Environmental Entomology and Zoology* **2007**, *18* (2). DOI: 10.11257/jjeez.18.91.

(18) Jones, T. H.; Harrison, D. P.; Menegatti, C.; Mevers, E.; Knott, K.; Marek, P.; Hennen, D. A.; Kasson, M. T.; Macias, A. M.; Lovett, B.; et al. Deoxybuzonamine Isomers from the Millipede Brachycybe lecontii (Platydesmida: Andrognathidae). *Journal of Natural Products* **2022**, *85* (4), 1134-1140. DOI: 10.1021/acs.jnatprod.2c00077.

(19) Shear, W.; Jones, T.; Wesener, T. Glomerin and homoglomerin from the North American pill millipede Onomeris sinuata (Loomis, 1943) (Diplopoda, Pentazonia, Glomeridae). *International Journal of Myriapodology* **2011**, *4*. DOI: 10.3897/ijm.4.1105.

(20) Rodriguez, J.; Jones, T. H.; Sierwald, P.; Marek, P. E.; Shear, W. A.; Brewer, M. S.; Kocot, K. M.; Bond, J. E. Step-wise evolution of complex chemical defenses in millipedes: a

phylogenomic approach. *Scientific Reports* **2018**, *8* (1), 3209. DOI: 10.1038/s41598-018-19996-6.

(21) Brewer, M. S.; Spruill, C. L.; Rao, N. S.; Bond, J. E. Phylogenetics of the millipede genus Brachycybe Wood, 1864 (Diplopoda: Platydesmida: Andrognathidae): Patterns of deep evolutionary history and recent speciation. *Molecular Phylogenetics and Evolution* **2012**, *64* (1). DOI: 10.1016/j.ympev.2012.04.003.

(22) Gagneux, P.; Panin, V.; Hennet, T.; Aebi, M.; Varki, A. Evolution of Glycan Diversity. 2022.

(23) Kuwahara, Y.; Ichiki, Y.; Morita, M.; Tanabe, T.; Asano, Y. Chemical Polymorphism in Defense Secretions during Ontogenetic Development of the Millipede Niponia nodulosa. *Journal of Chemical Ecology* **2014**, *41* (1). DOI: 10.1007/s10886-014-0536-8.

(24) Macias, A. M.; Marek, P. E.; Morrissey, E. M.; Brewer, M. S.; Short, D. P. G.; Stauder, C. M.; Wickert, K. L.; Berger, M. C.; Metheny, A. M.; Stajich, J. E.; et al. Diversity and function of fungi associated with the fungivorous millipede, Brachycybe lecontii. *Fungal Ecology* **2019**, *41*, 187-197. DOI: 10.1016/j.funeco.2019.06.006.

(25) Nguyen, L.; Lucke-Wolds, B. P.; Mookerjee, S.; Kaushal, N.; Matsumoto, R. R. Sigma-1 Receptors and Neurodegenerative Diseases: Towards a Hypothesis of Sigma-1 Receptors as Amplifiers of Neurodegeneration and Neuroprotection. *Advances in experimental medicine and biology* **2017**, *964*. DOI: 10.1007/978-3-319-50174-1_10.

(26) Gardner, M. R. Revision of the millipede family Andrognathidae in the Nearctic Region (Diplopoda: Platydesmida). *Memoirs of the Pacific Coast Entomological Society* **1974**, *5*, 1-61.

(27) Oh, J.-H.; Kim, S.; Lee, S. DNA barcodes reveal population-dependent cryptic diversity and various cases of sympatry of Korean leptonetid spiders (Araneae: Leptonetidae). *Scientific Reports* **2022**, *12* (1), 15528. DOI: 10.1038/s41598-022-18666-y.

(28) Marek, P.; Shear, W.; Bond, J. A redescription of the leggiest animal, the millipede Illacme plenipes, with notes on its natural history and biogeography (Diplopoda, Siphonophorida, Siphonorhinidae). *Zookeys* **2012**, *241*. DOI: 10.3897/zookeys.241.3831.

(29) Brewer, M. S.; Swafford, L.; Spruill, C. L.; Bond, J. E. Arthropod phylogenetics in light of three novel millipede (myriapoda: diplopoda) mitochondrial genomes with comments on the appropriateness of mitochondrial genome sequence data for inferring deep level relationships. *Public Library of Science One* **2013**, *8* (7), e68005. DOI: 10.1371/journal.pone.0068005.

(30) Stratton, C. F.; Newman, D. J.; Tan, D. S. Cheminformatic comparison of approved drugs from natural product versus synthetic origins. *Bioorganic and Medicinal Chemistry Letters* **2015**, *25* (21), 4802-4807. DOI: 10.1016/j.bmcl.2015.07.014.

(31) Shin, Y. J.; Midgley, G. F.; Archer, E. R. M.; Arneth, A.; Barnes, D. K. A.; Chan, L.; Hashimoto, S.; Hoegh-Guldberg, O.; Insarov, G.; Leadley, P.; et al. Actions to halt biodiversity loss generally benefit the climate. *Global Change Biology* **2022**, *28* (9), 2846-2874. DOI: 10.1111/gcb.16109.

(32) de Lange, E.; Sze, J. S.; Allan, J.; Atkinson, S.; Booth, H.; Fletcher, R.; Khanyari, M.; Saif, O. A global conservation basic income to safeguard biodiversity. *Nature Sustainability* **2023**, *6* (8), 1016-1023. DOI: 10.1038/s41893-023-01115-7.